Behavioral and pharmacological validation of genetic zebrafish models for ADHD

-

Pharmakologische und verhaltensbasierte Validierung genetischer Zebrafischmodelle für ADHS

Doctoral Thesis for a Doctoral Degree
at the Graduate School of Life Sciences,
Julius-Maximilians Universität Würzburg,
Section: Neuroscience

submitted by

Teresa Magdalena Lüffe

from
Weingarten

Würzburg 2021

Submitted on: _____

Date of Public Defense: _____

Date of Receipt of Certificates: _____

Members of the Thesis Committee:

Chairperson: Prof. Dr. Manfred Gessler
Department of Developmental Biochemistry
Biocenter
University of Würzburg

Primary Supervisor: Prof. Dr. Marcel Romanos
Department of Child and Adolescent Psychiatry
Center of Mental Health
University Hospital of Würzburg

2nd supervisor: Prof. Dr. Christian Wegener
Department of Neurobiology and Genetics
Biocenter
University of Würzburg

3rd supervisor: PD Dr. Christina Lillesaar
Department of Child and Adolescent Psychiatry
Center of Mental Health
University Hospital of Würzburg

4th supervisor: Dr. Carsten Drepper
Department of Child and Adolescent Psychiatry
Center of Mental Health
University Hospital of Würzburg

Contents

At the time of thesis submission, a considerable part of the here presented results were either prepared for publication in Lueffe et al. (2021b) or accepted for publication in Lueffe et al. (2021a) in the peer-reviewed journal Translational Psychiatry.

Summary

Attention-deficit/hyperactivity disorder (ADHD) is the most prevalent neurodevelopmental disorder described in psychiatry today. ADHD arises during early childhood and is characterized by an age-inappropriate level of inattention, hyperactivity, impulsivity, and partially emotional dysregulation. Besides, substantial psychiatric comorbidity further broadens the symptomatic spectrum. Despite advances in ADHD research by genetic- and imaging studies, the etiopathogenesis of ADHD remains largely unclear. Twin studies suggest a heritability of 70-80 % that, based on genome-wide investigations, is assumed to be polygenic and a mixed composite of small and large, common and rare genetic variants. In recent years the number of genetic risk candidates is continuously increased. However, for most, a biological link to neuropathology and symptomatology of the patient is still missing. Uncovering this link is vital for a better understanding of the disorder, the identification of new treatment targets, and therefore the development of a more targeted and possibly personalized therapy.

The present thesis addresses the issue for the ADHD risk candidates GRM8, FOXP2, and GAD1. By establishing loss of function zebrafish models, using CRISPR/Cas9 derived mutagenesis and antisense oligonucleotides, and studying them for morphological, functional, and behavioral alterations, it provides novel insights into the candidate's contribution to neuropathology and ADHD associated phenotypes. Using locomotor activity as behavioral read-out, the present work identified a genetic and functional implication of Grm8a, Grm8b, Foxp2, and Gad1b in ADHD associated hyperactivity. Further, it provides substantial evidence that the function of Grm8a, Grm8b, Foxp2, and Gad1b in activity regulation involves GABAergic signaling. Preliminary indications suggest that the three candidates interfere with GABAergic signaling in the ventral forebrain/striatum. However, according to present and previous data, via different biological mechanisms such as GABA synthesis, transmitter release regulation, synapse formation and/or transcriptional regulation of synaptic components. Intriguingly, this work further demonstrates that the activity regulating circuit, affected upon Foxp2 and Gad1b loss of function, is involved in the therapeutic effect mechanism of methylphenidate. Altogether, the present thesis identified altered GABAergic signaling in activity regulating circuits in, presumably, the ventral forebrain as neuropathological underpinning of ADHD associated hyper-

activity. Further, it demonstrates altered GABAergic signaling as mechanistic link between the genetic disruption of Grm8a, Grm8b, Foxp2, and Gad1b and ADHD symptomatology like hyperactivity. Thus, this thesis highlights GABAergic signaling in activity regulating circuits and, in this context, Grm8a, Grm8b, Foxp2, and Gad1b as exciting targets for future investigations on ADHD etiopathogenesis and the development of novel therapeutic interventions for ADHD related hyperactivity. Additionally, thigmotaxis measurements suggest Grm8a, Grm8b, and Gad1b as interesting candidates for prospective studies on comorbid anxiety in ADHD. Furthermore, expression analysis in *foxp2* mutants demonstrates Foxp2 as regulator of ADHD associated gene sets and neurodevelopmental disorder (NDD) overarching genetic and functional networks with possible implications for ADHD polygenicity and comorbidity. Finally, with the characterization of gene expression patterns and the generation and validation of genetic zebrafish models for Grm8a, Grm8b, Foxp2, and Gad1b, the present thesis laid the groundwork for future research efforts, for instance, the identification of the functional circuit(s) and biological mechanism(s) by which Grm8a, Grm8b, Foxp2, and Gad1b loss of function interfere with GABAergic signaling and ultimately induce hyperactivity.

Zusammenfassung

Aufmerksamkeitsdefizit-/Hyperaktivitätsstörung (ADHS) ist mit einer weltweiten Prävalenz von rund 5 % die am häufigsten vorkommende Neuroentwicklungsstörung. Das Krankheitsbild, das zumeist im Kindesalter auftritt und bis ins Erwachsenenalter bestehen kann, zeigt sich im Wesentlichen durch eine Beeinträchtigung der Aufmerksamkeit, der Aktivität, der Impulskontrolle und zum Teil durch emotionale Dysregulation. Darüber hinaus führt das vermehrte Auftreten von psychischen Begleiterkrankungen (so genannte Komorbiditäten) zu einer komplexen Symptomatik vieler Betroffener, die über die klassischen Merkmale von ADHS hinausgeht. Während das Krankheitsbild vielfach beschrieben wurde, ist die Ätiopathogenese trotz intensiver wissenschaftlicher Bemühungen bis heute weitestgehend ungeklärt. Zwillingsstudien weisen darauf hin, dass ADHS zu 70-80 % erblich bedingt ist. Aufgrund mehrerer Genom-Studien wird vermutet, dass es sich dabei um eine polygene Vererbbarkeit handelt und sowohl kleine (SNPs), verhältnismäßig häufig auftretende, als auch große (CNVs) verhältnismäßig seltene Genpolymorphismen beteiligt sind. Die Anzahl der potenziellen Risikogene für ADHS ist in den letzten Jahren kontinuierlich gestiegen, jedoch ist es nach wie vor unklar, inwiefern und durch welche biologischen Prozesse die meisten zur Neuropathologie und Symptomatik von ADHS Patienten beitragen. Diese Prozesse zu identifizieren ist von zentraler Bedeutung für ein besseres Verständnis der Erkrankung, der Identifizierung neuer Angriffsziele und somit, der Entwicklung gezielterer und möglicherweise personalisierter Behandlungsmöglichkeiten.

Die vorliegende Arbeit befasst sich mit diesen Prozessen am Beispiel der potenziellen Risikogene *GRM8*, *FOXP2* und *GAD1*. Durch die Etablierung und Validierung entsprechender (genetischer) Knockout und Knockdown Zebrafischmodelle und der anschließenden Untersuchung auf Verhaltens-, morphologische und funktionelle Veränderungen liefert die vorliegende Dissertation wichtige Erkenntnisse über die funktionelle Relevanz der einzelnen Kandidaten für die Neuropathologie und die Symptomatik von ADHS. Beispielsweise zeigen die erfassten Aktivitätsdaten von Knockdown und Knockout Larven, dass Grm8a, Grm8b, Foxp2 und Gad1b an der Regulation von Bewegungsaktivität beteiligt sind und dass dies, die korrekte Funktion GABAerger Prozesse bedarf. Des Weiteren liefert die Arbeit Hinweise, dass der Effekt im Subpallium/Striatum verankert ist. Jedoch ist aufgrund vorliegender und bereits publizierter

Daten anzunehmen, dass im Falle der einzelnen Kandidaten, zum Teil unterschiedliche Mechanismen wie die Transmittersynthese, die Transmitterfreisetzung, die Synapsenbildung und die Expression synaptischer Komponenten betroffen sind. Interessanterweise scheinen die durch die Kandidaten betroffenen Signalwege außerdem, laut erhobener Daten, am Wirkmechanismus von Methylphenidat beteiligt zu sein. Kurzum, die vorliegende Dissertation identifiziert die Beeinträchtigung GABAerger Signalübertragung eines, mutmaßlich subpallialen/striatalen aktivitäts-regulierenden neuronalen Netzwerks als neurobiologische Grundlage ADHS-assoziierter Hyperaktivität. Gleichzeitig präsentiert die Arbeit diese Prozesse als funktionelles Bindeglied zwischen der genetischen Veränderung von *GRM8*, *FOXP2* und *GAD1* und Hyperaktivität in ADHS. Folglich sind die entwicklungs- und neurobiologischen Mechanismen rund um die GABAerge Übertragung in diesem Netzwerk, und in diesem Zusammenhang die Funktion von Grm8a, (Grm8b), Foxp2 und Gad1b, spannende Ziele für zukünftige Projekte zur Erforschung der Ätiopathogenese und der Entwicklung neuer Therapien von Hyperaktivität in ADHS. Neben der Rolle in ADHS-assoziierter Hyperaktivität, präsentieren die erhobenen Verhaltensdaten Grm8a, Grm8b und Gad1b außerdem, als interessante Kandidaten für die Erforschung komorbider Angststörung in ADHS. Foxp2 dagegen, wurde mit Hilfe einer Genexpressionsanalyse als Regulator zahlreicher ADHS Risikogene und Entwicklungsstörungsübergreifenden genetischen und funktionellen Netzwerken, mit möglicher Relevanz für die Polygenie und Komorbidität von ADHS, identifiziert. Im Allgemeinen schafft die vorliegende Dissertation mit der Bestimmung der Genexpressionsmuster und Etablierung und Validierung der (genetischen) Zebrafischmodelle für Grm8a, Grm8b, Foxp2 und Gad1b die Grundlage, diese und weitere Aspekte in zukünftigen Forschungsprojekten zu untersuchen. Beispielsweise die Identifizierung der Netzwerke und Mechanismen, mit dessen Hilfe Grm8a, (Grm8b), Foxp2 und Gad1b in die GABAerge Signalübertragung eingreifen und so letztlich die Aktivität beeinflussen.

1 Introduction

1.1   Attention-deficit/hyperactivity disorder (ADHD)

Attention-deficit/hyperactivity disorder (ADHD) is the most common neurodevelopmental disorder (NDD), with a prevalence of 11.4 % in school-aged children, 8.0 % in adolescents, and 5.0 % in adults worldwide (Willcutt 2012). With 143 – 266 billion US dollar "excess costs" per year (Doshi et al. 2012), ADHD represents a significant economic burden to healthcare and society, which stresses the importance of a detailed understanding of cause(s) and pathology to develop goal-directed treatment strategies.

1.1.1   Historical investigations and conceptualization of ADHD

The first description of ADHD symptomatology is traced back to the physicians Melchior Adam Weikard and Alexander Crichton, who reported independent observations of children and adults with an increased level of inattention, distractibility, impulsivity, and overactivity in the late 18th century (Palmer and Finger 2003, Lange et al. 2010, Barkley and Peters 2012). However, predominantly cited across the literature is the pediatrician George Frederic Still (Barkley and Peters 2012). Besides his detailed investigation of 43 children showing severe problems with sustained attention among other phenotypes, he was first to describe a gender bias and early childhood onset as characteristic hallmarks of the observed condition. According to Still, observed symptoms result from a "major defect in moral control over the behavior" which appears in children with and without mental retardation and makes them more prone to aggression, alcoholism, and affective disorders such as depression and suicide (Still 2006, Lange et al. 2010, Barkley 2014). Remarkably, recent investigations substantiated genetic comorbidity between major depressive disorder (MDD), substance use disorder (SUD) and ADHD (Rice et al. 2019,Cross-Disorder Group of the Psychiatric Genomics Consortium 2019, Vilar-Ribó et al. 2020). Further, Still assumed that observed behavioral alterations could go back to poor childrearing but are more likely the outcome of a biological predisposition. In line with today's assumption on a genetic and neuropathological component in ADHD etiology,

he speculated that heritability and pre- and postnatal injuries, following incomplete curing of numerous brain diseases, contribute to such predisposition (Still 2006, summarized by Lange et al. 2010 and Barkley 2014).

Brain injury as primary explanation for cognitive and behavioral impairments in children received most attention between 1930 and 1960. The striking similarity between observed hyperactivity in children and behavioral alterations in brain-injured soldiers, children diagnosed with postencephalitic behavioral disorder, and primates with frontal lobe ablations introduced the theory of the "brain-injured child" (Levin 1938, Goldstein 1942, Strauss and Lehtinen 1947). Later, this theory gave rise to the persistent concept of minimal brain damage/ minimal cerebral injury (MBD, Gesell and Amatruda 1941 cited by Schain 1975). Following the criticism of behavior as diagnostic indicator for anatomical injuries (Meyer 1957), MBD evolved into "minimal brain dysfunction" (Clements and Peters 1962, 1966) before it was replaced by more descriptive terms on children's deficits like "hyperactivity" or "learning disability" (Lange et al. 2010, Barkley 2014). However, what remained was the significance of neurological impairments over environmental factors such as poor childrearing for future concepts on ADHD etiology.

One of the first known attempts to localize neurological defects underlying hyperactivity in children was published by Laufer and colleagues in 1957 (Laufer et al. 1957). Using a drug-based stimulation assay, Laufer et al. (1957) revealed a significantly lower stimulation threshold, attributed to the thalamic area, for impatient children with displayed hyperactivity. They hypothesized that a lower stimulation threshold results in poor filtering, excess stimulation of the brain, and subsequently in observed hyperactivity (Laufer et al. 1957). Two years later, this concept known as "hyperkinetic impulse disorder" (Eisenberg 1957, Laufer et al. 1957) was substantiated by Knobel et al. (1959), who suggested that imbalanced cortical and subcortical activity negatively affects sensory filtering. Like Laufer et al. (1957), they hypothesized that poor filtering results in an overstimulation of the cortex expressed as hyperactivity by the patient (Knobel et al. 1959). Notably, the hypothesis of a functional disturbance rather than a damage of the central nervous system (CNS) still reflects today's assumption of ADHD neuropathology.

In 1960, scientific interest switched focus from cause to symptom triggered by the considerable criticism of MBD. In this era, Chess (1960) introduced the "hyperactive behavior syndrome" with the description of 36 children with physiological hyperactivity. In the same context, they emphasized the necessity of objective proof beyond reported symptoms by parents or teachers (Barkley 2014). This suggestion should later lead to the definition of hyperactivity in the section for "reactions of hyperkinetic childhood disorders" in the 2nd edition of the Diagnostic and Statistical Manual of Mental Disorders (DSM-II) released in 1968 (American Psychiatric Association (APA) 1968).

In 1972, attention deficit was emphasized as the primary characteristic of the disorder initiated by the psychologist Virginia I. Douglas (Douglas 1972). Douglas and colleagues demonstrated that hyperactive children show some of their greatest deficits during the assessment of sustained attention and vigilance (Douglas 1972, Sykes et al. 1973). These observations were so influential that by the publication of the DSM-III in 1980 (APA 1980), the disorder was renamed attention-deficit disorder (ADD) that can appear with and without hyperactivity (ADD+H / ADD-H). Additionally, observations reporting a persistence of symptoms into adulthood (Menkes et al. 1967, Mendelson et al. 1971) refuted the prevailing opinion of ADHD as a pure childhood disorder.

Lack of experimental support for two independent subtypes (ADD+H/ADD-H) and ongoing discussions about the importance of hyperactivity in ADD (Barkley 2014) induced a further reconceptualization in the revised version of the DSM-III (DSM-III-R) (APA 1987) such that ADD with hyperactivity was renamed to Attention-deficit/hyperactivity disorder (ADHD) while ADD without hyperactivity changed into undifferentiated ADD (APA 1987).

During the 1990s, research invested tremendous energy in the identification of neurological and genetic alterations underlying ADHD. With the emergence of new imaging tools, variations in brain size and metabolic activity (Hynd et al. 1990, Zametkin et al. 1990) were uncovered and corroborated the previously assumed developmental and/or functional deficit in the ADHD brain. Furthermore, adoption- (1970s), twin-, and family-aggregation studies suggested a heritable component in ADHD etiology (Morrison and Stewart 1973, Cantwell 1975, Biederman et al. 1990, 1992, Levy et al. 1997) and together with the identification of the first putative risk

gene (Comings et al. 1991), paved the way for the extensive genome-wide-association studies carried out today (Demontis et al. 2019).

The publication of the 4th edition of the DSM and its text revised version (DSM-IV/DSM-IV-TR) in 1994/2000 (APA 1994, 2000) was the last reconceptualization before its latest version DSM-V (APA 2013). Unlike DSM-III-R and previous editions, the classification in DSM-IV and DSM-V comprises three presentations: predominantly inattentive (ADHD-PI), predominantly hyperactive-impulsive (ADHD-HI), and a combined presentation (ADHD-C), whereas the ICD-10 defines two additional types: the "other type" and the "unspecified type" (World Health Organization (WHO) 2004).

1.1.2   Symptoms

ADHD is a heterogeneous disorder regarding symptoms, etiology, treatment response, and outcome. The three major behavioral characteristics are inattention, hyperactivity, and impulsivity, as indicated by the DSM-IV/DSM-V classification described above. In addition, executive dysfunction and deficient emotional self-regulation are possible, although not central (Willcutt et al. 2005, Anastopoulos et al. 2011, Shaw et al. 2014). According to DSM-V, patients suffering from the inattentive presentation show major problems during the organization and/or execution of activities or tasks due to increased distractibility, elevated forgetfulness, and the inability to keep focus, provide attention to details, follow instructions, or listen when spoken to. In contrast, patients diagnosed with hyperactivity-impulsivity are often described as "on the go". They appear fidgety or restless, stand up, run, or climb when it's not appropriate, and often have difficulties carrying out activities quietly. The impulsive character is expressed through excessive talking, the interruption of others, blurting out answers hastily and difficulties waiting their turn (APA 2013). Moreover, the increased risk to develop any listed comorbid disorder during lifetime (like mood disorders, SUD, communication disorder, intellectual disability, learning disabilities, disruptive behavior disorders, tic disorders, autism spectrum disorder, anxiety disorders, and sleep disorders (Kessler et al. 2006, Ghanizadeh 2009, Kraut et al. 2013, Jensen and Steinhausen 2015, Tung et al. 2016) further broadens the symptomatic spectrum of ADHD.

In ADHD, symptoms are often presented in multiple settings, including social, academic, occupational, and emotional functioning (APA 2013), in which long-term problems are likely. Accordingly, ADHD is associated with an increased long-term risk for an adverse academic outcome, unemployment, SUDs, criminality, parental and family conflict, social rejection, vehicular accidents, suicide, and therefore also greater mortality (Bagwell et al. 2001, Hoza et al. 2005, Lee et al. 2011, Mrug et al. 2012, Barbaresi et al. 2013, Dalsgaard et al. 2015, Erskine et al. 2016, Barkley and Fischer 2018). Interestingly, there is substantial evidence that symptom expression and severity show temporal and contextual variations (Zagar and Bowers 1983, Pelham et al. 2001, Pedersen et al. 2020). Contextual variations, often referred to as "school- or home-specific ADHD" (Ho et al. 1996), are hypothesized to be related to differences in social or cognitive demands, whereas a correlation between drug effects and temporal variations is still heavily discussed (Pedersen et al. 2020). In contrast to the contextual presentation, the more frequently described pervasiveness to multiple settings is considered as early indicator for a chronic course of ADHD (Bunte et al. 2014).

Symptoms are diagnosed, at the earliest, by the age of four, whereas the highest prevalence is reported for children between the ages of 6 to 12 followed by 13 to 17 years old adolescents (Chien et al. 2012, Willcutt 2012, Hire et al. 2018, Pérez-Crespo et al. 2020). Although follow-up studies showed that symptoms and functional alterations persist into adulthood in 40-65 % of the cases (Faraone et al. 2006a, Caye et al. 2016), there is strong evidence that both symptom expression and experience change, resulting in a generally stronger symptom internalization (Franke et al. 2018). For instance, hyperactivity in adult patients might no longer be expressed as excessive running or climbing but rather perceived as internal restlessness (APA 1994, Weyandt et al. 2003). In addition, follow-up studies claimed a persistence primarily for the inattentive than for the hyperactive-impulsive presentation (Hart et al. 1995, Biederman et al. 2000, Todd et al. 2008, Arnold et al. 2014, Semeijn et al. 2016).

Besides age, gender plays a crucial role in the prevalence and presentation of ADHD. Males are shown to be three times more likely to develop ADHD than females, although the ratio greatly varies between 3:1 and 16:1 depending on country and study design (Nøvik et al. 2006). Fur-

ther, a gender imbalance has been claimed for presentation, symptomatology, and family history, however, with partially conflicting results. Female patients are more frequently diagnosed with the inattentive (3:1 gender ratio males to females) than with the hyperactive-impulsive (7:1) or combined presentation (5:1) (Nøvik et al. 2006, Hinshaw et al. 2006, Ramtekkar et al. 2010). Besides, they are alleged to be less symptomatic with a generally lower level of externalizing behavior, rule-breaking, comorbidity with CD/ODD, and poor school-functioning (Gaub and Carlson 1997, Newcorn et al. 2001, Graetz et al. 2005, Mowlem et al. 2019). By contrast, they show more parent-related emotional symptoms, prosocial behavior (Nøvik et al. 2006) and, in the long run, suffer more often from anxiety, depression, and peer-rejection than males (Rucklidge and Tannock 2001, Cortese et al. 2016). Furthermore, positive family history was reported to be more frequent in female patients with higher relevance for the combined over the inattentive presentation (Nøvik et al. 2006, Stawicki et al. 2006).

1.1.3   Diagnosis

The absence of biomarkers and limited knowledge about the etiology of ADHD still restricts diagnosis to the evaluation of self-anamnesis and interviews of persons involved. Two diagnostic handbooks are applied during this process: the 10th revision of the International Statistical Classification of Diseases and Related Health Problems (ICD-10) published by the World Health Organization (World Health Organization (WHO) 2004) and the 5th edition of the Diagnostic and Statistical Manual of Mental Disorders (DSM-V) released by the American Psychiatric Association (APA 2013). While the DSM criteria are predominantly applied in North America and mainly enjoy popularity within the scientific community, the ICD-10 is primarily used by international clinicians (Mezzich 2002, Reed et al. 2011).

According to DSM-V, a person suffers from ADHD as soon as its behavior met at least six out of nine symptoms for inattention (predominantly inattentive) and/or hyperactivity-impulsivity (combined / predominantly hyperactive-impulsive) over the past six months. If the adolescent or adult individual reaches or exceeds the age of seventeen, the number of required symptoms is reduced to a minimum of five. The DSM-V further specifies that several inattentive or hyperactive-impulsive symptoms must have been present before the age of twelve. In addition

to general diagnostic criteria, the DSM-V provides guidelines for the specification of severity level (mild, moderate, or severe) and remission of the disorder (APA 2013).

The diagnosis of a "hyperkinetic disorder with a disturbance of activity and attention" based on ICD-10 criteria requires the expression of at least six symptoms related to inattention, three to hyperactivity, and one to impulsivity over at least six months. In contrast to the DSM-V criteria, the first symptoms must have been present before the age of seven (World Health Organization (WHO) 2004).

According to ICD-10 and DSM-V, symptoms have to be present in at least two settings, significantly interfere with social, academic, or occupational functioning and consequently, result in a significant impairment of daily life. At the same time, observed disruptions must not fulfill diagnostic criteria of other psychiatric disorders such as schizophrenia (DSM-V, APA 2013) or pervasive developmental disorders (ICD-10, World Health Organization (WHO) 2004).

Both DSM and ICD provide guidelines for categorizing ADHD that are appreciated for their applicability in clinical diagnosis and health service (Reed et al. 2011). However, unlike medical issues induced by a single cause, ADHD etiology appears to be multifactorial (see 1.1.6). Accordingly, patients differ substantially in behavioral characteristics, severity, and dimension (see 1.1.2), which blurs the boundaries between psychiatric disorders that have previously been claimed to be distinct. Consequently, about two-thirds of ADHD patients meet the criteria of more than one psychiatric disorder (Elia et al. 2008), defined as increased comorbidity in ADHD (Jensen and Steinhausen 2015, Tung et al. 2016).

It has been repeatedly argued that the diagnostic categorization of heterogeneous disorders like ADHD doesn't properly reflect underlying dysfunctions. According to the critics, this impedes the identification of etiology and underlying neuropathology and therefore, the development of targeted therapies and the formulation of characterization guidelines that fully reflect the multidimensionality considering gene, circuit, and behavior (Insel et al. 2010, Cuthbert and Insel 2013). To address this issue, in 2009, the US National Institute of Mental Health launched the Research Domain Criteria (RDoC) initiative for a systematic research-based investigation of

mental health issues (Insel et al. 2010). In contrast to DSM and ICD, RDoC represents a translational research framework that incorporates research-based information of several domains of human functioning, studied from multiple perspectives (gene, molecule, cell, circuit, physiology, behavior, self-report, paradigms). The main objective is to understand mental disorders on multiple levels and differentiate and treat them based on their full complexity (Cuthbert and Insel 2013, Lupien et al. 2017, Mittal and Wakschlag 2017).

1.1.4   Neuropathology

The neuropathology of ADHD appears as complex as its behavioral presentation. For a long time, ADHD is hypothesized to be a disorder of the prefrontal cortex (PFC) and connected circuits due to frequently altered functions controlled by dorsal fronto-striatal (cognitive control), orbitofronto-striatal (reward processing), and fronto-cerebellar circuits (response control/responsiveness) in ADHD (Barkley 1997 cited by Ivanov et al. 2014). Several imaging studies using sMRI, DTI, fMRI, SPECT, PET, and others partially supported this assumption by revealing several structural, functional, and neurochemical alterations in particularly these areas in patients with ADHD (see below).

1.1.4.1   Structural alterations

Brain imaging in ADHD patients revealed a reduced total cerebral and grey matter volume (Valera et al. 2007, Narr et al. 2009, Nakao et al. 2011, Greven et al. 2015, Silk et al. 2016, Ambrosino et al. 2017, Hoogman et al. 2017) as well as region-specific alterations of cortical thickness or grey matter volume in frontal, prefrontal, occipital, parietal and temporoparietal regions, the cerebellum, basal ganglia (BG), insula, amygdala, hippocampus, thalamus, anterior cingulate cortex (ACC) and the splenium of the corpus callosum (CC) (Plessen et al. 2006, Mackie et al. 2007, Shaw et al. 2007, Valera et al. 2007, Ellison-Wright et al. 2008, Narr et al. 2009, Almeida et al. 2010, Ivanov et al. 2010, Frodl and Skokauskas 2012, Hoekzema et al. 2011, Lopez-Larson et al. 2012, Greven et al. 2015, Norman et al. 2016, Silk et al. 2016, Hoogman et al. 2017). In contrast, volumetric alterations of white matter are inconsistent (Valera et al. 2007, Narr et al. 2009, Greven et al. 2015). Since findings on gyrification

and intrinsic curvature are contradictory (Wolosin et al. 2009, Shaw et al. 2012, Mous et al. 2014, Ambrosino et al. 2017, Forde et al. 2017), it remains unclear whether volumetric differences are related to (region-specific) alterations in surface, thickness, or both (Silk et al. 2016, Ambrosino et al. 2017). Besides volumetric differences, it was demonstrated that structural alterations also affect inter-regional connectivity through abnormalities in white matter fiber tracts of, in particular, prefrontal- and striatal connections (Hong et al. 2014).

In order to provide a more comprehensive picture of structural alterations in ADHD, the following sections will focus on the PFC, the cerebellum, and the BG, which till now have provided the most coherent data on brain structural alterations in ADHD (Fig. 1).

Prefrontal cortex

Alterations in the PFC are claimed to be central in the neuropathology of ADHD for several reasons. First, the PFC is extremely sensitive to neurochemical variations (Robbins 2005) and thus especially vulnerable to genetic risk variants affecting regulatory components of brain neurochemistry (see 1.1.6.2). Second, due to its extensive connections with other brain regions, the PFC regulates a broad spectrum of behavioral output (Arnsten 2009). And third, behavioral alterations following PFC lesions in human patients and animal models closely resemble ADHD symptomatology (Kennard et al. 1941, French 1959, Gross 1963, Petrides 1986, Woods and Knight 1986, Chao and Knight 1995, Godefroy and Rousseaux 1996, Manes et al. 2002).

Frequently documented alterations of the PFC in ADHD individuals comprise reduced cortical volume, thickness, and surface area (Sowell et al. 2003, Makris et al. 2007, Valera et al. 2007, Biederman et al. 2008, Shaw et al. 2012). Structural alterations were most frequently observed for the dorso-lateral (DLPFC) and lateral orbitofrontal prefrontal cortex (OFC) with roughly the same frequency of bilateral or hemisphere-specific defects (Hesslinger et al. 2002, Seidman et al. 2006, Makris et al. 2007, Seidman et al. 2011). Observed volumetric reductions appear to be gender independent and equally affect grey and white matter of both PFC hemispheres (Mostofsky et al. 2002, Kates et al. 2002, Seidman et al. 2011). Furthermore, disorganized white matter fiber tracts in the PFC suggest weaker functional connectivity between PFC and brain regions like the striatum (Casey et al. 2007, Hong et al. 2014).

According to a supposed developmental background of structural alterations in the PFC, the cortical maturation of ADHD patients was shown to be delayed by approximately three and up to five years (Shaw et al. 2007, Shaw et al. 2012). However, longitudinal studies demonstrate that although cortical thickness peaks earlier and higher in healthy compared to ADHD-affected individuals, both trajectories converge by the age of twelve due to an equally delayed entering point into cortical thinning in ADHD patients (Shaw et al. 2009). The normalization of cortical maturation is in line with partial or total remission of symptoms in some patients (Biederman et al. 2000, Faraone et al. 2006a, Karam et al. 2015). Notably, delayed cortical maturation of surface area and thickness (Shaw et al. 2007, 2012) seems specific to ADHD, since other NDDs (dyslexia or autism) display maturation alterations in just one of both parameters (Frye et al. 2010, Raznahan et al. 2010, Smith et al. 2016).

Cerebellum

The cerebellum represents an interesting brain region for ADHD pathology due to its protracted development, sexual dimorphism, and pronounced susceptibility to external factors (Bledsoe et al. 2009, Tiemeier et al. 2010, Hoekzema et al. 2011). ADHD associated alterations in the cerebellum are diverse, comprising volumetric changes for the entire cerebellar volume, the vermis, the hemispheres, and more specifically, the crus and the right cerebellar cortex (Mackie et al. 2007, Biederman et al. 2008, Ivanov et al. 2014). Of all reported alterations, the volumetric reduction of vermal structures is the most frequent. It affects both the entire vermis and specifically, the (anterior) superior vermis and primarily the posterior inferior vermis (Mackie et al. 2007, Valera et al. 2007, Bledsoe al. 2009, Ivanov et al. 2014). A volumetric reduction of the anterior superior vermis or the posterior inferior hemispheres correlates with progressive symptom severity or clinical outcome in ADHD patients, respectively (Mackie et al. 2007, Ivanov et al. 2014). Overall, ADHD associated alterations in the cerebellum appear to be plastic with respect to age, pharmacological and cognitive therapy. Volumetric measurements revealed an age-dependent normalization in the left anterior hemisphere (Mackie et al. 2007) and a significantly increased volume of the posterior inferior cerebellum in response to stimulant treatment or cognitive training in ADHD patients (Bledsoe et al. 2009, Hoekzema et al. 2011). Likewise, altered cerebellar activity, observed in ADHD affected individuals, is

normalized by an acute methylphenidate therapy (Rubia et al. 2009).

Basal ganglia

The most consistent reduction of grey matter across studies was reported for structures of the BG like the caudate nucleus, the putamen, the globus pallidus, and the nucleus accumbens (NAc) (Valera et al. 2007, Ellison-Wright et al. 2008, Qiu et al. 2009, Frodl and Skokauskas 2012, Nakao et al. 2011, Norman et al. 2016, Hoogman et al. 2017). Particularly alterations of the striatum were strongly associated with the expression of ADHD-like symptoms. Closed head injuries and stroke lesions in the putamen and volumetric differences in the caudate nucleus induce or correlate with the expression or severity of ADHD-like symptoms (Mataró et al. 1997, Herskovits et al. 1999, Max et al. 2002, Millichap 2002, Onnink et al. 2014). Notably, volumetric alterations of the striatum appear to normalize by age or in response to stimulant medication (Frodl and Skokauskas 2012, Nakao et al. 2011). Accordingly, longitudinal investigations revealed a steeper age-related decline in caudate volume for healthy compared to ADHD affected individuals that result in similar caudate volumes by late adolescence (Castellanos et al. 2002). Similarly, DTI demonstrated an aberrant developmental trajectory of the caudate microstructural organization in ADHD patients that is presumed to normalize by mid- or late adolescence (Silk et al. 2009). As discussed for the PFC, striatal normalization goes in parallel with full or partial remission of ADHD symptomatology (Biederman et al. 2000, Faraone et al. 2006a, Karam et al. 2015).

1.1.4.2   Functional alterations

Structural alterations in various brain regions that equally display aberrant activity during task performance (Ernst et al. 2003, Ströhle et al. 2008, Hart et al. 2012, 2013, Plichta and Scheres 2014) suggest that instead of a discrete neural correlate, impaired inter-regional connectivity may underly functional deficits in ADHD.
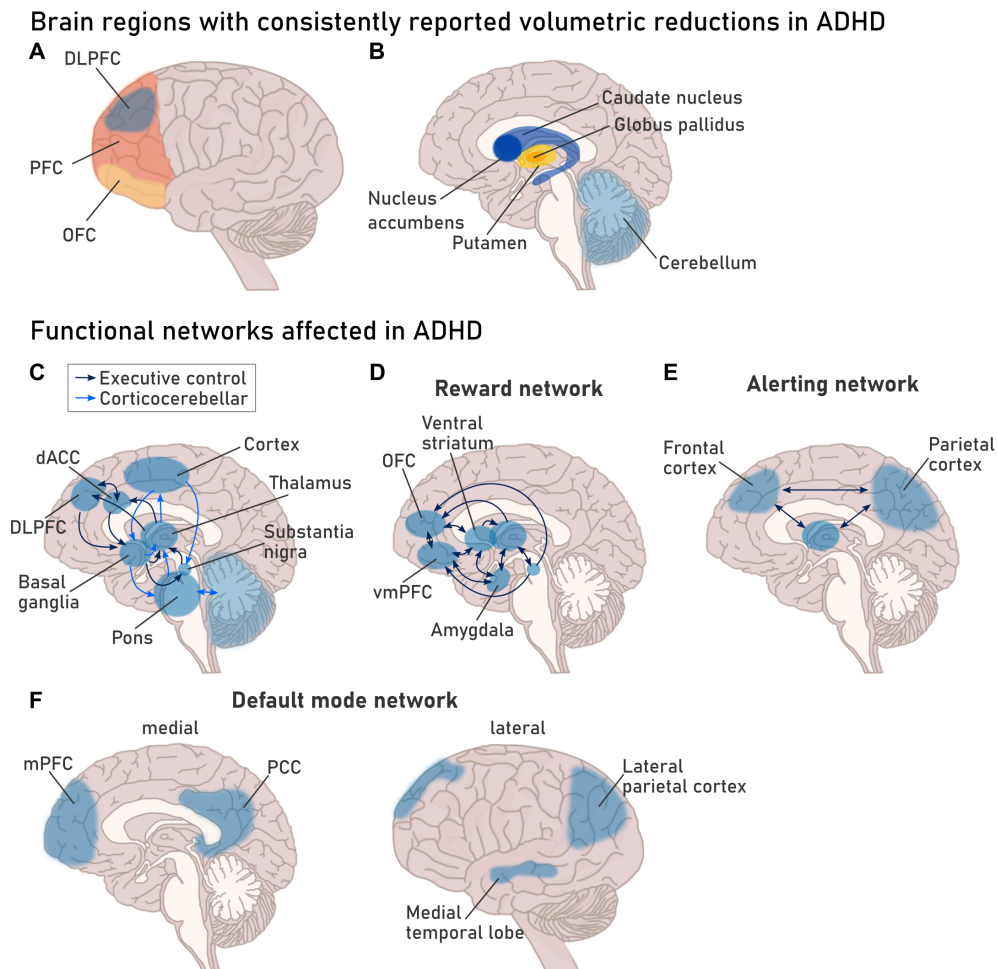
Figure 1: **Schematic illustrating brain regions and neuronal networks affected by structural and functional alterations in ADHD.** (A, B) Cortical (A) and subcortical (B) brain regions with confirmed volumetric reduction in ADHD patients. DLPFC: dorso-lateral prefrontal cortex; PFC: prefrontal cortex; OFC: orbitofrontal prefrontal cortex. (C-F) Functional networks affected by altered brain activity and/or connectivity in ADHD patients. dACC: dorsal anterior cingulate cortex; vmPFC: ventromedial prefrontal cortex; mPFC: medial prefrontal cortex; PCC: posterior cingulate cortex. Based on Faraone et al. 2015.

Beyond a repeatedly reported alteration of network activity and/or connectivity for the default mode network (DMN) and the fronto-striatal, fronto-parietal, fronto-cerebellar and mesocorticolimbic circuit (Vaidya et al. 2005, Dickstein et al. 2006, Scheres et al. 2007, Durston et al. 2007, Castellanos et al. 2008, Ströhle et al. 2008) (Fig. 1), meta-analyses indicate impaired

connectivity of large-scale neuronal networks in ADHD (Cortese 2012, Gao et al. 2019). Functional imaging points towards a modified triple network dysfunction (Menon 2011) underlying aberrant functional connectivity in the ADHD brain (Gao et al. 2019). Data derived from ADHD patients, suggests the fronto-parietal network (FPN) as the key regulator (core network) in a triple network with DMN and ventral attention network (VAN) which together are assumed to account for the symptoms of inattention. Further, according to functional data, the triple network is supplemented by altered connectivity with the dorsal attention network (DAN) and the somatosensory- (SSN) and the affective network (AN) of which the latter were suggested to be involved in the hyperactive and impulsive expression, respectively (Gao et al. 2019) (Fig. 2).
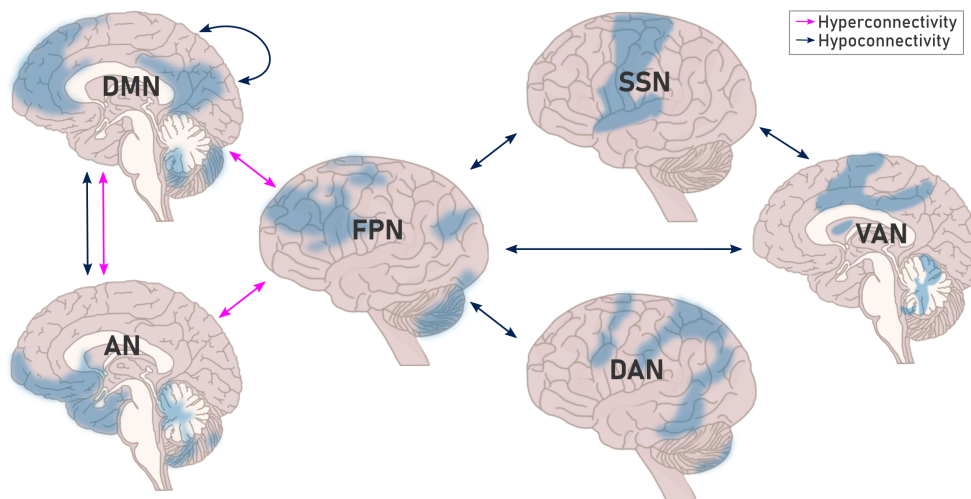
Figure 2: **Schematic illustrating large-scale network alterations in ADHD.** Functional imaging data suggests a triple network dysfunction of fronto-parietal (FPN), default mode (DMN), and ventral attention network (VAN). Further, altered connectivity between the triple network and dorsal attention (DAN), somatosensory (SSN), and affective network (AN) is assumed. Based on Gao et al. 2019.

Under healthy conditions, the DMN and FPN/VAN are anticorrelated. During stimulus-driven cognitive performance, FPN and/or VAN are engaged, whereas the DMN (which partially mediates mind wandering (Weissman et al. 2006)) is disengaged (Douw et al. 2016, Long et al. 2016). In ADHD, fMRI indicates hypoconnectivity within (Castellanos et al. 2008) and hyperconnectivity between DMN and FPN (Gao et al. 2019). This suggests that the anticorrelation of DMN and FPN is impaired (Castellanos et al. 2008, Sun et al. 2012, Lin and Gau 2015) and in response causes more attentional lapses/ poor attention in ADHD patients (Castellanos et al. 2008). Similarly, observed hypoconnectivity between FPN and insula (VAN) was assumed

to be involved in attentional deficits (Gao et al. 2019) due to reported insula hypoactivation during attention tasks in ADHD patients (Hart et al. 2013). In addition, hypoactivation of the putamen (VAN) during inhibitory control tasks (Norman et al. 2016) indicates that beyond inattention (FPN-insula), hypoconnectivity between FPN and VAN may also underly impaired inhibitory control (Hart et al. 2013, Gao et al. 2019). Notably, Sripada and colleagues (2014) revealed a maturational lag for connections within the DMN and between DMN and FPN or VAN, suggesting that besides structural alterations, delayed maturation may underly impaired large-scale network connectivity in the ADHD brain.

Altered FPN connectivity was also observed beyond the triple network of FPN DMN and VAN. One example is the revealed hypoconnectivity between FPN and SSN (precentral gyrus (PG), Gao et al. 2019). Altered FPN-PG connectivity was associated with impaired inhibitory motor control in ADHD due to a previously demonstrated engagement of the PG in executive functions (Dibbets et al. 2010, Lei et al. 2015) and PG hypoactivation in the context of impaired motor/response inhibition in ADHD patients (Mulligan et al. 2011, Hart et al. 2013). Additionally, hyperconnectivity between AN (NAc, superior temporal gyrus, orbitofrontal cortex) and FPN or DMN (anterior prefrontal cortex, middle frontal gyrus) was suggested to be associated with greater impulsivity in ADHD patients (Costa Dias et al. 2013, Gao et al. 2019).

To summarize, the great variety of structurally and functionally altered brain regions and small- and large-scale network connectivity (Fig. 1, Fig. 2) once again reflects the substantial heterogeneity of ADHD neuropathology. Further, it shows that contrary to previous assumptions, ADHD is not solely a disorder of the PFC or BG. Instead, it represents a manifestation of closely linked structural and functional alterations that result in a highly individual and context-dependent set of behavioral impairments. In addition, longitudinal studies support the notion of a maturational delay underlying structural and functional alterations in the ADHD affected brain.

1.1.4.3   Neurochemical alterations

Evidence from imaging, animal models, and pharmacotherapy suggests that altered neuro-transmission plays a crucial role in the neuropathology of ADHD. Especially catecholamines, target of stimulant and non-stimulant therapy, are considered most relevant, whereas, in recent years, serotonin, acetylcholine, glutamate, and GABA also gained in importance.

Catecholamines

The significant improvement of ADHD symptoms following stimulant and non-stimulant treatment indicates that deficient dopamine and norepinephrine signaling plays a central role in ADHD pathology. Accordingly, findings from animal models demonstrate that alteration of norepinephrine or dopamine transmission through changes in the transmitter level, transporter or receptor activity or availability significantly affect ADHD associated behavioral conditions like attention, locomotor activity, and response inhibition (Li and Mei 1994, Giros et al. 1996, Zhuang et al. 2001, Archer et al. 2002, Zhang et al. 2002, Ma et al. 2005, Diaz Heijtz and Castellanos 2006, Bouchatta et al. 2018).

In ADHD patients, imaging studies revealed that metabolism and release of dopamine are significantly reduced (Ernst et al. 1998, Forssberg et al. 2006, Ludolph et al. 2008) attributed to altered dopamine transporter (DAT) levels in the ADHD brain. In fact, some studies discovered DAT bindings that are raised by up to 70 % (Dougherty et al. 1999, Dresel et al. 2000, Cheon et al. 2003, Spencer et al. 2005, la Fougère et al. 2006, Spencer et al. 2007), whereas others suggest that striatal DAT availability is reduced but increase in response to stimulant treatment (Volkow et al. 2007a, Wang et al. 2009, Fusar-Poli et al. 2012, Chu et al. 2018). Besides DAT, the dopamine receptors D_2 and/or D_3 availability was shown to be reduced (in the midbrain, BG, and hypothalamus) and correlate with the severity of inattention in ADHD patients (Volkow et al. 2007b, 2009). If alteration of DAT or D_2/D_3 receptor availability underly ADHD pathology or rather reflects an adaption to disrupted dopamine release is unknown. However, together with the reported increase in extracellular dopamine and DAT inhibition in the BG upon stimulant treatment (Volkow et al. 2001, 2005), these findings provide strong evidence for a general deficiency in dopamine-mediated signaling in subcortical regions like the BG of

ADHD patients. Further, they confirm structural and functional alterations, which, likewise, suggested a significant impairment of the BG in ADHD (see 1.1.4.1 and 1.1.4.2).

Unlike DAT, investigations on norepinephrine transporter (NET) availability in the brain of ADHD patients are limited. Recent findings suggest a reduction of NET availability in the right-fronto-parietal-thalamic-cerebellar regions of unmedicated adult patients (Ulke et al. 2019) that negatively correlates with symptom severity and (omission) error rate during attention tasks (Ulke et al. 2019). Notably, regions with altered NET availability showed stimulant-induced normalization of brain activity and behavioral improvement in ADHD patients in a former investigation (Kowalczyk et al. 2019). Thus, preliminary findings support the notion of deficient dopamine and norepinephrine signaling in the ADHD brain.

Experimental evidence suggests it is unlikely that catecholamines alone account for the entire set and severity of functional and behavioral alterations observed in ADHD (del Campo et al. 2013). Instead, mostly dopamine might fail to modulate glutamatergic or GABAergic signal transmission appropriately through mesocortical, mesolimbic, or nigrostriatal branches (Sagvolden et al. 2005, Carrey et al. 2007). Others, conversely, speculate that dopaminergic dysfunction may partially derive from impaired glutamatergic transmission (Carlsson et al. 1999, 2001, Russell 2003, Perlov et al. 2007).

Glutamate and GABA and a possible excitatory/inhibitory (E/I) imbalance in ADHD

In recent years, glutamate and GABA, as the primary excitatory and inhibitory neurotransmitter of the mammalian CNS, received considerable attention in the context of ADHD pathology due to the significant importance in fronto-striatal signaling. Fronto-striatal signaling, as previously mentioned, is involved in many behavioral functions implicated in ADHD symptomatology, and its development and proper functioning highly depend on balanced GABA and glutamate levels (Wu and Sun 2015, Naaijen et al. 2017). Neurophysiological investigations on GABA levels in ADHD patients revealed a significant reduction in the striatum, primary somatosensory, and motor cortex of children (Edden et al. 2012, Puts et al. 2020) and increased (BG) as well as decreased (ACC) levels in adult individuals (Bollmann et al. 2015, Ende et al. 2016).

In contrast, glutamate and/or its precursor glutamine were reported to be increased in the frontal lobe, right PFC, ACC, and left BG of ADHD affected children or adolescents (MacMaster et al. 2003, Courvoisie et al. 2004, Moore et al. 2006, Carrey et al. 2007, Ferreira et al. 2009, Hammerness et al. 2010, Bollmann et al. 2015) whereas adult patients displayed both increased (BG, left cerebellar hemisphere (Ferreira et al. 2009, Perlov et al. 2010)) as well as decreased (right ACC, left midfrontal area, BG (Perlov et al. 2007, Dramsdahl et al. 2011, Maltezos et al. 2014) glutamate and/or glutamine levels. Notably, increased striatal glutamate/glutamine levels are reduced in response to stimulant treatment (Carrey et al. 2003). Further, both GABA and glutamate levels correlate with symptom severity of adult ADHD patients (Bollmann et al. 2015, Ende et al. 2016). Although there is substantial variation across studies, the existing data consistently indicates a significant alteration of glutamate-mediated excitation and GABA-mediated inhibition in fronto-striatal circuits of ADHD affected individuals. Thus, providing evidence for an E/I imbalance in ADHD pathology. Further, the observed correlation between subcortical GABA or glutamate and the age of examined ADHD individuals supports evidence from structural and functional investigations indicating a developmental component in ADHD pathology (Bollmann et al. 2015, Puts et al. 2020).

Although structural, functional, and neurochemical studies are both consistent and contradictory, the increasing amount of data in these fields insistently emphasizes that ADHD is a disorder of the brain and not, as the prevailing stigma suggests, the result of bad parenting or familial environment. This means not only great relief to patients and relatives but also provides important recognition for future scientific investigations on the cause(s), pathology, and even treatment opportunities in the field of ADHD research.

1.1.5   Treatment

The treatment strategies for ADHD are multimodal, comprising dietary modification, neu-
rofeedback, cognitive, behavioral, and predominantly pharmacological therapy (Caye et al.
2019). In pharmacotherapy, stimulant and non-stimulant medication are most accepted (Catalá-
López et al. 2017). Although responsiveness and treatment outcome strongly vary across indi-
viduals (Elia et al. 1991), psychostimulants still achieve an improvement in 70 % of the cases,
and with moderate to high effect sizes (Spencer et al. 1996, Schachter et al. 2001, Faraone et al.
2004, 2006b, Mészáros et al. 2009, Castells et al. 2011) represent one of the most effective
treatment strategies in psychiatry (Schachter et al. 2001, Leucht et al. 2012). In ADHD, psy-
chostimulants are still considered as first-line medication, whereas non-stimulants are typically
applied when psychostimulants induce no response, are contraindicated, not tolerated, or due
to comorbidities may increase the risk for mood destabilization, substance abuse, or Tourette
syndrome (Pliszka and AACAP Work Group on Quality Issues 2007, Caye et al. 2019). The most
common psychostimulants prescribed in ADHD are methylphenidate (MPH) (methylphenidate,
dexmethylphenidate) and amphetamines (AMP) (dextroamphetamine, methamphetamine, lis-
dexamphetamine, and mixed amphetamine salts). MPH and AMP function as catecholamine/
monoamine reuptake inhibitors, whereas AMP also facilitates the release (via VMAT2) and
inhibits the metabolization (via MAO-A) (Faraone 2018, Ferrucci et al. 2019). Consequently,
predominantly DA or NE accumulate in the extracellular space with repeatedly reported impact
on striatal and/or PFC activity (Vaidya et al. 1998, Volkow et al. 2001, Bymaster et al. 2002,
Volkow et al. 2002, 2005, Wilens 2008).

Besides monoamines, preclinical and clinical data suggest the GABAergic system as a possible
target of psychostimulants (Freese et al. 2012, Goitia et al. 2013, Solleveld et al. 2017). In
ADHD patients, the acute application of MPH was reported to cause a considerable increase
in prefrontal GABA (Solleveld et al. 2017). Likewise, preclinical studies in rodents revealed a
significant alteration of prefrontal and striatal GAD mRNA levels (Freese et al. 2012) besides a
considerable increase in GABAergic transmission following MPH treatment (Goitia et al. 2013).
Although the reported findings indicate a direct impact of MPH on the GABAergic system of

humans and mice, the effects were equally suggested to be induced by the aforementioned alterations in DA transmission (Solleveld et al. 2017).

Since psychostimulants induce subtle but detectable alterations of dopamine levels in subcortical regions involved in mediating drug abuse behavior (NAc) (Segal and Kuczenski 1999, Kuczenski and Segal 2002, Berridge et al. 2006), non-stimulants, targeting the PFC (Bymaster et al. 2002), are applied as valuable substitutions with less potential for drug abuse or dependence. Two non-stimulants are currently approved for ADHD pharmacotherapy, the NET reuptake inhibitor atomoxetine (EMA decision number: P/0095/2013) and the alpha-2 receptor agonist guanfacine (P/0265/2013). Additionally, several substances are tested and applied for off-label use, comprising the alpha-2 receptor agonist clonidine (Connor et al. 1999, Hirota et al. 2014), the DA/NE reuptake inhibitors bupropion (Verbeeck et al. 2017) and modafinil (Wang et al. 2017), and the serotonin/DA/NE reuptake inhibitors tricyclic anti-depressants (Otasowie et al. 2014). Like stimulants, non-stimulants aim to increase DA and NE and, as such, new drug developments that currently undergo clinical testing (centanafadine, dasotraline, viloxazine (non-stimulants), HLD200, mazindol (stimulants)(Konofal et al. 2014, Koblan et al. 2015, Wigal et al. 2018, Findling et al. 2019, Childress et al. 2020, Nasser et al. 2020a, 2020b)). But also treatment strategies beyond DA and NE are considered for future interventions comprising, for instance, the sodium channel blocker amiloride (Caye et al. 2019), the GABA modulator metadoxine (Manor et al. 2012), the serotonin reuptake inhibitor vortioxetine (Biederman et al. 2019), and the metabotropic glutamate receptor agonist fasoracetam (Caye et al. 2019, Nageye and Cortese 2019). However, although these substances appear to follow new treatment strategies, they likely interfere with similar pathways but downstream of DA and NE.

Pharmacological interventions in ADHD predominantly purpose a non-specific increase in the synaptic availability of catecholamines, although structural, functional, neurochemical, and genetic observations indicate a more complex clinical picture. Hence, future drug developments require a better understanding of ADHD etiopathogenesis to establish more specific treatment strategies that consider the entire complexity of an individual's genetic, neurolog-

ical, and behavioral alterations to increase responsiveness, reduce side effects , and curtail adverse long-term outcomes.

1.1.6 Etiology

Unlike environmental or single-gene diseases, ADHD cannot be attributed to one single cause. Instead, current data suggest a contribution of genetic (Larsson et al. 2004, Faraone et al. 2005, Schultz et al. 2006, van den Berg et al. 2006, Larsson et al. 2014) and environmental factors (Kahn et al. 2003, Laucht et al. 2007, Grizenko et al. 2012) to the overall risk, severity, and heterogeneity of the disorder that, by themselves, are neither necessary nor sufficient to account for the complex presentation of ADHD. Further, the interplay of both, known as gene-environment interaction, was speculated to account for the 50 % mismatch between estimates on ADHD heritability and the contribution of identified risk loci (Posner et al. 2020). Accordingly, studies found that the polymorphisms of *DRD4* or *DAT1* increase the risk and severity of ADHD, especially in connection with maternal smoking, alcohol consumption, or stress during pregnancy (Kahn et al. 2003, Brookes et al. 2006b, Neuman et al. 2007, Grizenko et al. 2012).

1.1.6.1 Environment

Environmental risk factors associated with ADHD predominantly affect the pre- and perinatal phase, but also postnatal effects correlate occasionally. However, a causal relationship has not been proven for any risk factor yet, suggesting that environmental impact alone does not induce ADHD.

Prematurity represents the most consistent risk factor across studies. Except for post-term deliveries, the corresponding data indicate a negative correlation between ADHD risk and gestational age (Halmøy et al. 2012, Silva et al. 2014, Henriksen et al. 2015). In addition, some studies suspected birthweight and, due to the risk for ischemic hypoxic events, neonatal, pregnancy, labor, and delivery complications as potential risk factors in ADHD (Halmøy et al. 2012, Getahun et al. 2013, Class et al. 2014, Silva et al. 2014, Henriksen et al. 2015). However, inconsistent or partially attenuated effects after further adjustments still question a true relationship (Silva et al. 2014, Clements et al. 2015).

Besides prematurity, maternal smoking and nicotine replacements were repeatedly associated with the risk (Silva et al. 2014) and severity of ADHD (Thakur et al. 2013). However, sibling comparison and a similar but weaker correlation with paternal smoking indicate that genetic factors may drive the effect (Langley et al. 2012, Skoglund et al. 2014, Zhu et al. 2014). Similarly, sibling comparison suggests that genetic factors underly the correlation between maternal age, prenatal anti-depressant exposure, and ADHD (Laugesen et al. 2013, Chang et al. 2014). In contrast, the positive relationship between maternal alcohol consumption, diagnosed parental alcohol disorder, paracetamol (acetaminophen) usage and the risk to develop ADHD was not controlled for genetic confounding (Langley et al. 2012, Liew et al. 2014, Sundquist et al. 2014, Thompson et al. 2014).

To differentiate between genetic predisposition and environmental contribution in ADHD etiology is particularly challenging for risk factors related to maternal physical and mental health. Some (maternal major depressive disorder, epilepsy, hyperthyroidism, urinary tract infection, obesity, and stress) (Halmøy et al. 2012, Andersen et al. 2014, Chen et al. 2014, Park et al. 2014, Silva et al. 2014, Clements et al. 2015), are suspected to be genetically predisposed by themselves or show attenuated effects following sibling comparison (Chen et al. 2014). This equally applies to psychosocial adversity, which was repeatedly associated with ADHD risk and partially suggested to be influenced by genetic factors (Biederman et al. 1995b, 1995a, Lasky-Su et al. 2007, Hjern et al. 2010, Russell et al. 2015).

Besides various parental, social, and gestational factors, studies also assessed the impact of environmental toxins and artificial food additives. Corresponding data indicate no association with manganese and perfluoroalkyl substances (Ode et al. 2014, 2015, Liew et al. 2015), little evidence for mercury (Yoshimasu et al. 2014) and artificial food additives (McCann et al. 2007), and an increased prevalence when exposed to higher levels of selenium (Ode et al. 2015), lead (Nigg et al. 2008, Cho et al. 2010, Nicolescu et al. 2010, Nigg et al. 2010), and artificial water fluoridation (Malin and Till 2015). However, inconsistent results suggest that the reported correlations should be interpreted with caution.

How environmental risk factors contribute to ADHD pathology is largely unknown. A global research trend focusing on the microbial composition and its influence on the CNS, known as the microbiota-gut-brain axis, demonstrated a correlation between environmental risk factors in ADHD and the gut microbial composition (Barrett et al. 2013, Jašarević et al. 2015). Further, the normalization of the microbiome appeared effective in preventing mental health issues (Pärtty et al. 2015), indicating that this field holds great potential for identifying viable biomarkers and innovative prevention strategies for future clinical application. Furthermore, epigenetics was repeatedly assumed as a direct link between genetic predisposition and environmental risk in ADHD. Accordingly, ADHD risk genes were reported to be more sensitive to epigenetic regulation (Shumay et al. 2010), are differentially methylated in ADHD patients (Park et al. 2015, Xu et al. 2015, Walton et al. 2017), or contribute to epigenetic modulation themselves (Nagarajan et al. 2006 Oct-Dec, Gokcen et al. 2011). Further, there is evidence that ADHD-affected individuals show dysregulated miRNA levels (Kandemir et al. 2014), short non-coding RNAs involved in post-transcriptional regulation.

1.1.6.2 Genetics

According to family-linkage analysis, first-degree relatives show a four- to ninefold (depending on diagnostic criteria) risk for ADHD compared to unrelated individuals indicating a genetic liability of ADHD (Biederman et al. 1990, Faraone et al. 2000, Brookes et al. 2006a, Chen et al. 2008, 2017). Twin studies corroborate the assumption reporting a higher monozygotic than dizygotic concordance rate and a heritability estimate of 70-80 % (Sherman et al. 1997, Faraone et al. 2005, Nikolas and Burt 2010, Larsson et al. 2014, Chen et al. 2017). Accordingly, adoption studies demonstrate a greater transmission to biological than adoptive relatives (Alberts-Corush et al. 1986, Epstein et al. 2000, Sprich et al. 2000). Thus, shared environmental impact seems negligible in ADHD etiology, whereas genetic factors appear primarily responsible for the variance in ADHD (Burt 2009, Larsson et al. 2014). Moreover, shared inherited factors were suggested to account for the considerable comorbidity between ADHD and other neurodevelopmental and psychiatric conditions (Ronald et al. 2008, Lichtenstein et al. 2010, Rommelse et al. 2010, Demontis et al. 2019), eventually supported by several pleiotropic loci

with impact across different disorders (Cross-Disorder Group of the Psychiatric Genomics Consortium et al. 2013, 2019, Brainstorm Consortium et al. 2018).

Candidate-gene-association studies

Hypothesis-driven candidate-gene-association studies first identified a relationship between individual gene variants and ADHD susceptibility (Cook et al. 1995, LaHoste et al. 1996, Daly et al. 1999). Most candidate genes were selected on account of their role in catecholaminergic neurotransmission. However, only ten candidate genes (listed in Table 1) survived reaffirmation (by meta-analysis, GWAS, large-scale linkage studies, and animal models), whereas others (listed in Table 2) failed to reach significance during meta-analyses or miss profound experimental support (Gizer et al. 2009, Bonvicini et al. 2016).

Table 1: **List of potential ADHD risk genes derived from hypothesis-driven candidate-gene-association studies and confirmed by meta-analyses, GWAS, large-scale linkage studies, or animal models.** [1] Cook et al. (1995), [2] LaHoste et al. (1996), [3] Daly et al. (1999), [4] Manor et al. (2001), [5] Brophy et al. (2002), [6] Hawi et al. (2002), [7] de Silva et al. (2003), [8] Lowe et al. (2004), [9] Li et al. (2006), [10] Lasky-Su et al. (2008), [11] Gizer et al. (2009), [12] Reif et al. (2009), [13] Mick et al. (2010), [14] Arcos-Burgos et al. (2010), [15] Ribasés et al. (2011), [16] Won et al. (2011).

Gene name	Gene symbol	Reference
adhesion G protein-coupled receptor L3	ADGRL3/LPHN3	[14] [15]
D(4) dopamine receptor	DRD4	[2] [9] [11]
D(5) dopamine receptor	DRD5	[3] [8] [9] [11]
ARF GTPase-activating protein GIT1	GIT1	[16]
5-hydroxytryptamine receptor 1B	HTR1B	[6] [11]
nitric oxide synthase	NOS1	[12]
sodium-dependent dopamine transporter	SLC6A3/DAT1	[1] [11]
sodium-dependent serotonin transporter	SLC6A4/HTT/SERT	[4] [11]
sodium/hydrogen exchanger 9	SLC9A9	[7] [10] [13]
synaptosomal-associated protein 25	SNAP25	[5] [11]

Table 2: **Potential ADHD risk genes that miss or failed reaffirmation.**

Gene name	Gene symbol
alpha-2a/2C/1C adrenergic receptor	ADRA2A,2C,1C
brain-derived neurotrophic factor	BDNF
neuronal acetylcholine receptor subtype alpha-4	CHRNA4
catechol-O-methyltransferase	COMT
dopamine beta-hydroxylase	DBH
D(2) dopamine receptor	DRD2
D(3) dopamine receptor	DRD3
ionotropic glutamate receptor NMDA 2A	GRIN2A
5-hydroxytryptamine receptor 2A	HTR2A
amine oxidase [flavin-containing] A	MAOA
sodium-dependent noradrenaline transporter	SLC6A2/NET1
tryptophan 5-hydroxylase 1	TPH1
tryptophan 5-hydroxylase 2	TPH2

Low reproducibility across candidate gene studies caused major criticism of the approach (Duncan et al. 2019). Heterogeneity in study design (by study population or phenotype definition), underpowered studies (for detecting low impact variations), and the selection of non-causal polymorphisms were suspected to be responsible for the variation (Ioannidis et al. 2001 , Tabor et al. 2002, Faraone et al. 2005). Therefore, subsequent investigations switched to large-scale hypothesis-free whole genome-association studies that are claimed to be more reliable, more sensitive, and, in addition, more suitable for the identification of new biological pathways involved in disorder etiology (Duncan et al. 2019).

Genome-wide-association studies based on SNPs

Genome-wide association studies (GWAS) are a powerful tool to identify common (> 1 % of the population) gene variants that contribute individually with low penetrance but cumulative for a substantial proportion (h^2_{SNP} = 0.22-0.28) of the overall genetic predisposition in ADHD (Cross-Disorder Group of the Psychiatric Genomics Consortium et al. 2013, Demontis et al. 2019). In 2019, a GWAS study, based on single nucleotide polymorphisms (SNPs), identified 304 gene variants in 12 loci that exceeded genome-wide significance ($p < 5x10^{-8}$) in the ADHD sample (Demontis et al. 2019). A detailed investigation determined the identified loci as a mixture of evolutionary constraint regions, loss-off function intolerant genes, and CNS-expressed regulatory elements with a particular focus on genes involved in neurodevelopmental processes (Demontis et al. 2019). However, none of the identified risk loci coincided with candidate genes studied earlier, indicating that former candidate gene approaches were substantially biased and concealed the full complexity of genetic contribution in ADHD (Demontis et al. 2019). In addition, observed effect sizes of individual SNPs and calculated polygenic risk scores across different GWAS study designs support the notion of a polygenic etiology in ADHD (Demontis et al. 2019).

Genome-wide copy number variation studies

Common variants like SNPs only account for about 22-32 % of the overall heritability of ADHD (Cross-Disorder Group of the Psychiatric Genomics Consortium et al. 2013, Demontis et al. 2019), which implies that unlike the common disease-common variant hypothesis (Cargill

et al. 1999) suggests, rare (< 1 %) chromosomal structural abnormalities also play a substantial role in the genetic predisposition of ADHD (Demontis et al. 2016). Rare structural variants are of particular interest since, on account of their low frequency, they are assumed to contribute with moderate to large effect size (Williams et al. 2012). Further, due to the size (1kb to several megabases), they are assumed to affect single and multiple genes, causing loss or overexpression, as well as functional properties through excision or duplication of functional domains (Williams et al. 2012).

Studies, focusing on the relevance of rare genetic variants in ADHD etiology, report an association between chromosomal microdeletion syndromes (like 22q11), subtle chromosomal alterations (like deletions, duplications, triplications, or translocations) and ADHD prevalence (Niklasson et al. 2009 Jul-Aug, Elia et al. 2010, 2012, Williams et al. 2010, Williams et al. 2012). Although smaller chromosomal deletions or duplications, known as copy number variations (CNVs), are present in each genome, they were reported to be more frequent in ADHD affected individuals (Williams et al. 2010, Yang et al. 2013b, Ramos-Quiroga et al. 2014). Especially duplications at chromosomal location 16p13.11 and 15q11-13 were significantly associated with ADHD susceptibility by former studies (Williams et al. 2010, Williams et al. 2012). Since Elia and colleagues published the first genome-wide CNV study for ADHD in 2010 (Elia et al. 2010), the number of gene sets associated with inherited CNVs in ADHD affected individuals has continuously increased (Williams et al. 2010, Lesch et al. 2011, Williams et al. 2012, Lionel et al. 2011, Elia et al. 2012, Jarick et al. 2014). Many comprise risk candidates of other neuropsychiatric disorders (schizophrenia, epilepsy, Tourette syndrome, and autism) and genes involved in neurodevelopmental signaling, neuron projection, or neurotransmission (Elia et al. 2010, Lionel et al. 2011, Elia et al. 2012, Williams et al. 2012, Yang et al. 2013b).

Although the effect size of CNVs in ADHD ranges from moderate to large, ADHD patients with and without elevated CNV rates appear similar in most aspects of their clinical presentation (Langley et al. 2011). Since some regions enriched for common variants (like SNPs) significantly overlap with genomic areas spanned by rare CNVs, both potentially affect the same genes and biological pathways (Stergiakouli et al. 2012).

Based on current knowledge, ADHD etiology is shaped by a synergistic effect of environmental and genetic risk factors. Together with gene-environment interactions like epigenetic alterations, they are suggested to account for the full heritability estimated by former twin studies. The genetic risk in ADHD is polygenic and a mixed composite of common and rare genetic variants that contribute with minor to moderate effect size in an additive manner. Thus far, several gene variants and environmental risk factors were associated with ADHD prevalence. However, the biological mechanisms linking genetic or environmental predisposition and neuropathological and behavioral alterations remain to be investigated. To study these mechanisms despite the complexity of ADHD etiology, the present work focuses on three potential ADHD risk genes, *GRM8*, *FOXP2*, and *GAD1*, identified by CNV, GWAS, and candidate-gene association study, respectively. (Elia et al. 2012, Bruxel et al. 2016, Demontis et al. 2019).

1.2   GRM8/Grm8 – Metabotropic glutamate receptor 8

Glutamate, the main excitatory neurotransmitter in the vertebrate CNS, acts via two distinct receptor classes: ionotropic (AMPA, NMDA, and kainate receptor) and metabotropic glutamate receptors (GRM1-8). GRM8 belongs to the latter and is encoded by the eponymous human gene *GRM8*. The gene, which was mapped to the human chromosome 7q(31) (Scherer et al. 1996), comprises eleven exons (nine coding exons) over about 1000 kb, representing the largest among the eight *GRM* genes described today (Yates et al. 2020, Howe et al. 2021).
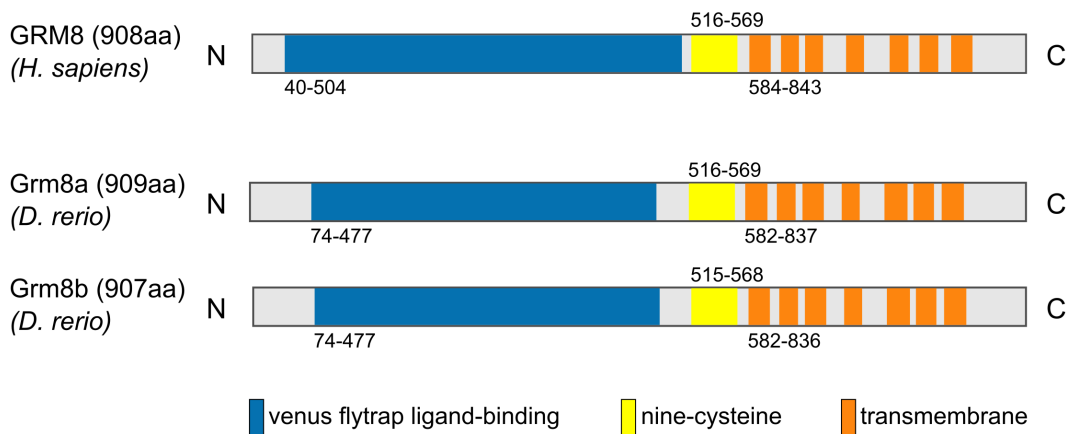
Figure 3: **Schematic illustrating and comparing functional domains of human GRM8 and Grm8a and Grm8b in zebrafish (*Danio rerio*).**

Like other metabotropic glutamate receptors, GRM8 belongs to the heterogeneous class C family (Inoue et al. 2004) of G-protein-coupled receptors, which exerts its long-lasting action through G-protein activation and modulation of intracellular signaling cascades. The heptahelical receptor protein contains seven transmembrane domains for localization, an intracellular C-terminus for G-protein coupling and, extracellularly, a nine-cysteine domain for dimerization and signal propagation and large N-terminal domain termed venus flytrap domain (VFD) for ligand-binding (Conn and Pin 1997, Muto et al. 2007, Chun et al. 2012) (Fig. 3). The ligand, mostly glutamate, is bound in the cleft between both VFD lobes that sit on top of each other (Kunishima et al. 2000, Tsuchiya et al. 2002, Muto et al. 2007). Metabotropic glutamate receptors occur as constitutive dimers linked by disulfide-bridges in proximity to the VFD (Romano et al. 1996, Robbins et al. 1999, Lee et al. 2020). Both the extracellular VFD and the transmembrane domains show high sequence homology across all eight receptor subtypes, whereas

the C-terminus is subtype-specific and, due to alternative splicing, exists as different subtype variants (for *GRM8/mGluR8*: *mGluR8a*, *mGluR8b* and *mGluR8c* (Pin and Duvoisin 1995, Malherbe et al. 1999, Willard and Koochekpour 2013)).

Based on sequence homology, intracellular signal transduction mechanism, and agonist selectivity, metabotropic glutamate receptors are subdivided into three main receptor families: type I, type II, and type III (Nakanishi 1992, Schoepp et al. 1999). Together with GRM4, GRM6, and GRM7, GRM8 belongs to the latter type III family. Type III metabotropic glutamate receptors (mGluRs III) are characterized by a potent reactivity to the mGluR agonists L-AP4 and L-SOP, a signal transduction through adenyl cyclase inhibition and subsequent reduction of intracellular cAMP levels, and a predominant localization in or near the presynaptic active zone (Shigemoto et al. 1996, Kinoshita et al. 1996, Shigemoto et al. 1997, Schoepp et al. 1999, Corti et al. 2002, Somogyi et al. 2003). Functional investigations revealed that GRM8 stands out from other mGluR III by a distinct pharmacological profile with shared characteristics of mGluR II and mGluR III (Saugstad et al. 1997) and signal transduction properties that go beyond the classical repression of cAMP. Besides a negative coupling to adenyl cyclase and direct modulation of potassium channel activity, GRM8 was suggested to regulate intracellular Ca^{2+} levels and/or Ca^{2+} sensitivity to modulate presynaptic transmitter release (Koulen et al. 1999, Koulen et al. 2005, Erdmann et al. 2012). Accordingly, experimental data show that GRM8 induces both facilitation and inhibition of presynaptic glutamate release and release inhibition of the main inhibitory neurotransmitter GABA (Marabese et al. 2005, Erdmann et al. 2012). Thus, there is substantial evidence that GRM8, as well as other presynaptic mGluRs, represent crucial regulatory entities for the homeostasis of excitatory and inhibitory neurotransmission in the CNS (Nakanishi et al. 1994, Shigemoto et al. 1997, Koerner and Cotman 1981, Cartmell and Schoepp 2000, Evans et al. 2000, Isaacson 2000, Schoepp 2001).

Imbalanced excitation and inhibition is assumed to be implicated in various mental disorders (Rubenstein and Merzenich 2003, Yizhar et al. 2011, Rivero et al. 2015, Kang et al. 2019, Wang et al. 2019, Yoon et al. 2020) that were likewise associated with genetic variants of *GRM8* (Serajee et al. 2003, Takaki et al. 2004, Terracciano et al. 2010, Prasad et al. 2012, Zhang et al.

2014, Li et al. 2016, Sangu et al. 2017, Tavakkoly-Bazzaz et al. 2018). Accordingly, a genome-wide CNV study identified a locus on chromosome 7 which harbors a copy number deletion in proximity to *GRM8* with significant replication in ADHD compared to non-ADHD cases (eight vs. no case(s) (Elia et al. 2012)).

Currently, little is known about the functional role of GRM8. Based on expression data, studies suggest that GRM8 exerts its function in the thalamic reticular nucleus (TRN), hippocampus, BG, cerebral cortex, cerebellum, hindbrain, pons, olfactory bulb, and retina (Duvoisin et al. 1995, Kinoshita et al. 1996, Saugstad et al. 1997, Shigemoto et al. 1997, Corti et al. 1998, Messenger et al. 2002, Ferraguti et al. 2005). Notably, most of these regions show structural and functional alterations in ADHD affected individuals (see 1.1.4.1 and 1.1.4.2). Further, TRN dysfunction, a region with the densest *Grm8* expression observed (Messenger et al. 2002), was associated with attention-deficit, increased distractibility, and hyperactivity in mice (Wells et al. 2016). To uncover the physiological role of GRM8, individual knockout lines were generated in the past. However, while an anxiogenic effect upon GRM8 loss of function was observed across studies (Linden et al. 2002, 2003, Duvoisin et al. 2005, Robbins et al. 2007, Duvoisin et al. 2010, 2011, Fendt et al. 2010, 2013), alterations regarding locomotor activity or cognitive performance in *Grm8* mutants were contradictory (Gerlai et al. 2002, Linden et al. 2002, Duvoisin et al. 2005, Robbins et al. 2007, Fendt et al. 2010). Therefore, more comprehensive investigations are required to better understand the functional relevance of GRM8 in order to unravel molecular mechanisms and neuronal circuit(s) that may link GRM8 deficiency and ADHD pathology.

1.3   FOXP2/Foxp2 – Forkhead-box transcription factor P2

FOX transcription factors belong to the family of winged-helix DNA binding proteins and are subdivided into nineteen subfamilies (FOXA-FOXS) based on phylogenetic analysis (Jackson et al. 2010). Together with FOXP1, FOXP3, and FOXP4, FOXP2 belongs to the P-subfamily (Brunkow et al. 2001, Shu et al. 2001, Lu et al. 2002, Teufel et al. 2003) and is characterized by several functional domains, including the eponymous C-terminal DNA-binding motif termed winged helix or forkhead domain, a highly conserved C2H2 zinc-finger domain, a leucine-zipper domain, several nuclear localization signals, an N-terminal glutamine (Gln)-rich region and the C-terminal binding protein 1 (CtBP1) binding domain (Fig. 4) which is exclusively shared by FOXP2 and FOXP1 (Li et al. 2004). The regulatory properties of FOXP2 as transcriptional repressor and activator are modulated through a context-dependent interaction with different cofactors and the formation of homo- and heterodimers with FOXP1 and FOXP4 (Li et al. 2004, Deriziotis et al. 2014, Sin et al. 2015, Mendoza and Scharff 2017, Estruch et al. 2018, Hickey et al. 2019).
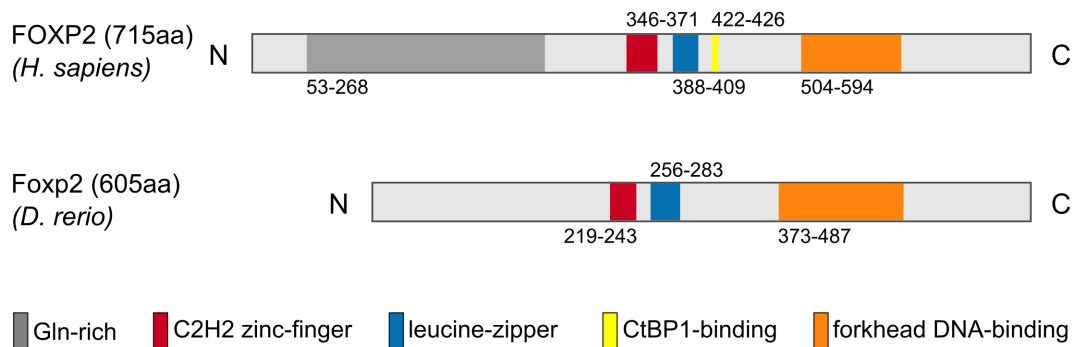
Figure 4: **Schematic illustrating and comparing functional domains of human FOXP2 and Foxp2 in zebrafish (*Danio rerio*).** Based on Kim et al. 2019.

Like *GRM8*, *FOXP2* is located on chromosome 7q(31) in the human genome (Fisher et al. 1998, Lai et al. 2000). Comparative sequence analysis across species revealed a substantial sequence homology that puts FOXP2 among the 5 % most-conserved proteins of human-rodent gene pairs (Enard et al. 2002). Accordingly, *FOXP2/Foxp2/FoxP2* expression was described in various species, including mammals, birds, reptiles, amphibians, and fish (Ferland et al. 2003, Lai et al. 2003, Takahashi et al. 2003, Haesler et al. 2004, Teramitsu et al. 2004, Bonkowsky and

Chien 2005, Schön et al. 2006, Itakura et al. 2008, Takahashi et al. 2008, Campbell et al. 2009, Harvey-Girard et al. 2012, Chen et al. 2013, Kato et al. 2014, Mendoza et al. 2015, Pengra et al. 2018, Rodenas-Cuadrado et al. 2018). In line with its genetic conservation, concordant spatio-temporal expression patterns in motor function-associated brain regions of different species also suggest functional conservation (Ferland et al. 2003, Lai et al. 2003, Campbell et al. 2009, Chen et al. 2013, Kato et al. 2014).

The most studied function of FOXP2 represents its possible involvement in speech development and language formation, triggered by the identification of an arginine-to-histidine substitution (R553H) in the FOXP2 forkhead domain found in a multigenerational pedigree (known as KE family) with severe childhood apraxia of speech (Lai et al. 2001). Animal models support a functional role in vocalization (development and/or execution) but also point out a general involvement in motor learning and/or motor execution with a yet unknown molecular background (Shu et al. 2005, Haesler et al. 2007, Fujita et al. 2008, Groszer et al. 2008, Kurt et al. 2012, Bowers et al. 2013, Law and Sargent 2014, Mendoza et al. 2014, Castellucci et al. 2016, Chabout et al. 2016, Castells-Nobau et al. 2019, Day et al. 2019, French et al. 2019). Gene ontology of FOXP2 transcription targets and expression analysis suggests that FOXP2 exerts its function predominantly on synaptic transmission and (neuro)-developmental processes (Vernes et al. 2011, Co et al. 2019). Accordingly, FOXP2 loss of function results in imbalanced excitatory/-inhibitory neurotransmission, aberrant neural firing rate, delayed development, impaired thalamic patterning, and alterations in cell migration and differentiation, neurogenesis, neurite outgrowth, dendrite morphogenesis, synaptogenesis, synaptic organization, and plasticity (Shu et al. 2005, Fujita et al. 2008, Groszer et al. 2008, Enard et al. 2009, French et al. 2012, Tsui et al. 2013, Chiu et al. 2014, Chen et al. 2016, Ebisu et al. 2017, van Rhijn et al. 2018, Castells-Nobau et al. 2019, Druart et al. 2020).

Notably, many processes altered upon *Foxp2* interference or with assumed relevance for FOXP2 function (Spiteri et al. 2007, 2011) are hypothesized to be involved in the pathophysiology of various neurodevelopmental disorders (NDDs). Accordingly, several studies suggest FOXP2 as a potential risk candidate in NDDs, such as ADHD and autism (Gong et al. 2004, Li et al. 2005,

Laroche et al. 2008, Casey et al. 2012, Ribasés et al. 2012, Demontis et al. 2019, Satterstrom et al. 2020). In addition, various NDD risk candidates are supposed transcriptional targets of FOXP2 (Spiteri et al. 2007, Vernes et al. 2008, Konopka et al. 2009, Mukamel et al. 2011, Vernes et al. 2011, Bowers and Konopka 2012). Hence, according to genetic and functional data, FOXP2 represents an interesting candidate to study developmental and/or neuro-functional processes underlying ADHD pathology as well as shared etiopathogenesis of different psychiatric disorders.

1.4 GAD1(GAD67)/Gad1 – Glutamate decarboxylase 1

Glutamate decarboxylases (GAD) comprise a class of enzymes that, as the name suggests, catalyzes L-glutamate decarboxylation to synthesize the main inhibitory neurotransmitter gamma-Aminobutyric acid (GABA) (Awapara et al. 1950, Roberts and Frankel 1950, 1951). In the CNS, two GAD isozymes are proven and named according to the molecular weight: GAD65 (65 kDa, GAD2) and GAD67 (67kDa, GAD1) (Erlander et al. 1991). In humans, GAD67/GAD1 is encoded by the gene *GAD1* on chromosome 2q(31) (Bu et al. 1992).
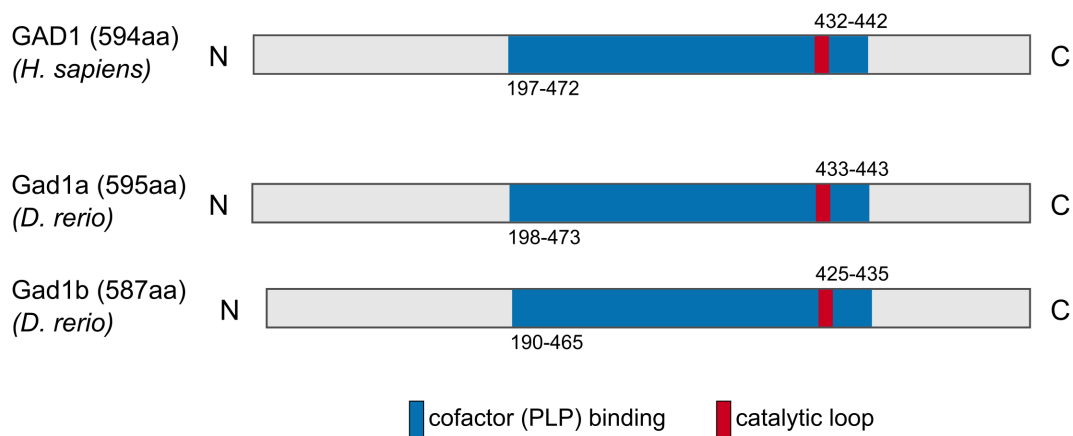
Figure 5: **Schematic illustrating and comparing functional domains of human GAD1/GAD67 and Gad1a and Gad1b in zebrafish (*Danio rerio*).** Based on Fenalti et al. 2007.

Both GAD isoforms (GAD1/GAD2) contain a highly homologous C-terminal and cofactor-binding domain and a more distinct N-terminal domain that confers properties crucial for subcellular targeting, membrane association, and heteromeric interaction to each isoform (Erlander et al. 1991, Bu and Tobin 1994). Accordingly, the N-terminal membrane anchoring signal allows the soluble and hydrophilic GAD1 protein to traffic to nerve terminals and associate with membrane compartments independent of heterodimerization with the hydrophobic GAD2 (Kanaani et al. 1999). Consequently, GAD1 as homo- and heterodimer is present in soluble and membrane-associated form in cell bodies and proximal dendrites and to a lower extent in nerve terminals and the Golgi complex region (Kaufman et al. 1991, Esclapez et al. 1994, Dirkx et al. 1995). The catalytic domain of GAD1 is harbored by the cofactor-binding domain (Fig. 5), which interacts with the vital cofactor PLP (pyridoxal phosphate). Divergent residues in the catalytic domain and associated regions are crucial for the conformation, sta-

bility and thus activity of the active site. The majority of GAD1 occurs in the active holo form and produces over 90 % of basal GABA, comprising the cytoplasmic and, to a large extent, also the vesicular pool (Kaufman et al. 1991, Martin et al. 1991, Asada et al. 1997, Battaglioli et al. 2003, Lau and Murthy 2012).

Due to its key function in GABA synthesis, GAD1 is crucial for the homeostasis of excitation and inhibition in the CNS. Alterations or even a conditional loss of GAD1 result in reduced inhibitory synaptic transmission and behavioral impairments associated with different psychiatric disorders (Lau and Murthy 2012, Sandhu et al. 2014, Brown et al. 2015, Fujihara et al. 2015, Lazarus et al. 2015, Kolata et al. 2018, Smith 2018, Miyata et al. 2019, 2021). Notably, many of these disorders were linked to genetic or quantitative alterations of *GAD1*/GAD1 and are assumed to hold a deficiency in balanced neurotransmission (Guidotti et al. 2000, Heckers et al. 2002, Hashimoto et al. 2003, Courvoisie et al. 2004, Addington et al. 2005, Fatemi et al. 2005, Lundorf et al. 2005, Straub et al. 2007, Yip et al. 2007, Du et al. 2008, Gao and Penzes 2015, Bruxel et al. 2016, Giacopuzzi et al. 2017). ADHD, which was genetically linked to *GAD1* polymorphisms for the hyperactive/impulsive domain (Bruxel et al. 2016), is characterized by several behavioral alterations such as timing-deficit, hyperactivity, and impulsivity, which are hypothesized to derive from impaired inhibitory control caused by inappropriate modulation of glutamatergic and/or GABAergic neurotransmission (MacMaster et al. 2003, Courvoisie et al. 2004, Boy et al. 2010, 2011, Edden et al. 2012, Silveri et al. 2013, Bollmann et al. 2015, Naaijen et al. 2017). Functional investigations in heteroallelic *Gad1* knockout mice partially support this link, reporting a significant reduction of GABA and a hyperactive phenotype (Smith 2018).

Beyond its well-known function as an inhibitory neurotransmitter, GABA is involved in regulating early developmental processes such as proliferation, migration, differentiation, neurite growth, and synapse formation (Wolff et al. 1978, Behar et al. 2000, Haydar et al. 2000, Maric et al. 2001). Accordingly, patients carrying a biallelic mutation of *GAD1* exhibit a severe developmental delay among other symptoms (Neuray et al. 2020), while *Gad1* knockout mice die shortly after birth (Asada et al. 1997, Condie et al. 1997). Notably, in mice, first *GAD1* expres-

sion is detected during prenatal development (Trifonov et al. 2014) and coincides with brain regions (frontal cortex, striatum, and cerebellum) that, according to structural and functional data, are delayed in maturation in ADHD patients (see 1.1.4.1 and 1.1.4.2). Thus, on account of its central role in neurodevelopmental and neurosignaling processes, GAD1 represents a valuable risk candidate to study biological mechanisms that underly ADHD etiopathogenesis.

1.5 Zebrafish as a model organism in ADHD research

Several genetic variants were associated with ADHD risk in the past. However, the pathophysiological mechanism(s) linking genetic risk and behavioral alteration are still unknown in most cases. Even though animal models cannot entirely reflect the complex etiopathogenesis seen in ADHD patients, they can provide important insights into the underlying mechanisms that cannot be studied in the patient itself.

In the past, rodent models like the spontaneously hypertensive rat (Okamoto and Aoki 1963) and others were successfully applied to model behavioral characteristics of ADHD like hyperactivity, impulsivity, and attention-deficit (Shaywitz et al. 1978, Luthman et al. 1989, Sagvolden 2000, Viggiano et al. 2002). Further, multiple candidate genes were screened by the generation of corresponding mutant lines (Giros et al. 1996, Rubinstein et al. 1997, Gainetdinov et al. 1999, Ralph et al. 2001, Helms et al. 2008, Young et al. 2011, Papaleo et al. 2008, 2012, Yamashita et al. 2013). The application of rodent models in psychiatric research follows a long tradition. The high genetic similarity to humans (∼99 % homology), cutting-edge genetic tools, and the availability of standardized behavioral and neurobiological techniques to investigate multiple complex behaviors are only a few out of many advantages that make rodents valuable in ADHD research. However, expensive housing, *in utero* embryonic development, and a comparably low number of offsprings limit the investigation of early neurodevelopmental alterations and the implementation of high-throughput screens.

In contrast, the teleost zebrafish (*Danio rerio*) is a relatively cheap vertebrate model organism that generates a comparably large number of offspring, making it well-suited for high-throughput screens and multi-conditional experiments. In particular, the combination of behavior-based phenotyping and large-scale drug screening provides an excellent approach to dissect unknown pathogenesis and promote new drug discoveries in translational research (Kokel and Peterson 2008, Ali et al. 2012, Hoffman et al. 2016). Further, the possibility to reach high sample sizes enables the detection and investigation of (behavioral) alterations induced by genetic variants of merely low individual penetrance as suggested for ADHD etiology (see 1.1.6.2).

Behavioral studies in zebrafish are important complementations to behavioral assessments in rodents. Free-swimming, behaving larvae from 3 dpf (days post fertilization) onwards allow investigations on early behavioral alterations and underlying molecular mechanisms (Wolman and Granato 2012) that are inaccessible in (*in utero*) developing rodents. Zebrafish show a great variety of simple and complex behavior (Kalueff et al. 2013), such that several behavioral correlates of ADHD associated phenotypes can be studied in larval and/or adult zebrafish (Ellis et al. 2012, Lange et al. 2012, Parker et al. 2013). Behavioral assays to extract pathological phenotypes range from simple motion tracking experiments to the more complex 5-Choice Serial Reaction Time Task to assess visuospatial attention and motor impulsivity (Robbins 2002, Parker et al. 2013).

Unlike rodents, fertilization and development occur *ex utero*, providing accessibility for genetic manipulation and pharmacological treatment. Consequently, the generation of various mutant lines (using microinjections) together with behavioral phenocopy, rescue, or drug monitoring experiments (Lange et al. 2012, Spulber et al. 2014, Hoffman et al. 2016, Thyme et al. 2019) allow developmental and neurobiological investigations of gene-phenotype relationships. In parallel, early developmental and anatomical alterations can be detected in the intact embryo due to embryonic transparency.

Zebrafish show substantial genetic and physiological similarity to humans and other vertebrates. In fact, ~70 % of human genes are present in the zebrafish (Howe et al. 2013), show a substantial similarity (*grm8a/grm8b*: 93 %, *foxp2*: 83 %, *gad1b*: 94 %), and can be targeted by an extensive collection of established tools, including CRISPR/Cas9, TALEN, zinc-finger nucleases, viral vector-mediated insertional mutagenesis, morpholino antisense-oligonucleotides, and optogenetics (Amsterdam et al. 1999, Nasevicius and Ekker 2000, Meng et al. 2008, Foley et al. 2009, Huang et al. 2011, Hruscha and Schmid 2015, Simone et al. 2018, Antinucci et al. 2020). However, due to a whole-genome duplication event ~440 million years ago (Meyer and Schartl 1999, Taylor et al. 2003), some gene duplicates in zebrafish are redundant and challenge the generation of gene-targeted disease models by phenotypic buffering (Peng 2019). Nevertheless, studies have shown in the past that ADHD risk candidates can be successfully

studied using mutant zebrafish lines (Lange et al. 2012, Yang et al. 2018). Besides genetic similarity, zebrafish show physiological similarity in brain structures comprising gene expression patterns, neurochemical identity, and regional connectivity (Mueller and Wullimann 2009, Kozol et al. 2016). Likewise, the major mammalian transmitter systems are conserved in zebrafish (Higashijima et al. 2004, Panula et al. 2010, Mueller and Wullimann 2015). Thus, despite reduced complexity, topographical differences, and the absence of the cerebral cortex, the conserved neuroanatomy, neurochemistry, and well-described neurodevelopmental processes in zebrafish provide a crucial framework to study biological mechanisms that underly alterations in maturation, neuroanatomy, and neurotransmission in ADHD.

To summarize, the zebrafish represents a valuable model organism to study NDDs like ADHD due to its substantial homology in genetics, anatomy, and functional biology and the well-established collection of tools and techniques. Furthermore, the comparably large batch size, the external development, larval transparency, and the opportunity for early behavioral assessments are specific advantages that allow important complementation to insights derived from mice or rats. Concerning future research strategies, it also holds great potential to functionally screen the multitude of identified risk candidates for various psychiatric disorders due to its greater compliance with resource economization and bioethical considerations.

2 Aims of the thesis

The aim of the present thesis was to generate (genetic) zebrafish models for the ADHD risk gene paralogs *grm8a*, *grm8b*, *foxp2*, and *gad1b* and validate and investigate them based on expression, morphology, and behavior. With the collected data, this work intends to contribute to a better understanding of the molecular mechanism(s) that link genetic susceptibility and pathophysiology in ADHD.

The strong heritability of ADHD is a widely accepted condition, and substantial progress has been made in the identification of risk loci associated with ADHD susceptibility. However, in contrast to the continuously growing list of potential risk genes, the number of studies providing a mechanistic link between a proposed risk gene and observed ADHD pathophysiology remains limited.

With the generation of genetic zebrafish models for the three risk candidates GRM8, FOXP2, and GAD1, the present work intends to provide a framework to study these mechanism(s) *in vivo*. Further, by investigating different paralogs under comparable conditions, the project aims to unravel similarities across mechanisms that may help understanding how different gene variants converge onto common behaviorally relevant deficiencies.

3 Materials and Methods

Fish husbandry and embryo preparation

Animal handling followed the official regulations for animal welfare of the District Government of Lower Franconia, Germany. If not stated differently, experiments were carried out on the AB/AB wildtype strain (zfin id.: ZDB-GENO-960809-7). *foxp2* and *grm8a* expression in monoaminergic cells were localized in the enhancer trap line Tg(Etvmat2:GFP) (Wen et al. 2008). Larvae were raised at 28 °C for five days and at 25 °C afterward, both with a light/dark cycle of 14/10 h. Larvae were raised in Danieau's solution (recipe according to Cold Spring Harb. Protoc., 2011) containing 0.1 % methylene blue for twenty-four hours and in Danieau's solution without methylene blue for the following four days. During this period, Danieau's solution was replaced once per day, and larvae were closely monitored for anatomical malformations and signs of increased cell death. The number of larvae raised per petri dish was comparable across experimental days and never exceeded seventy individuals.

Embryos for whole-mount RNA *in situ* hybridization (ISH) and immunohistochemistry (IHC) were raised in Danieau's solution with 0.2 mM 1-phenyl-2-thiourea (Merck KGaA, Darmstadt, HE, Germany) to suppress pigmentation. After the developmental stage was determined based on Kimmel et al. (1995), embryos were manually dechorionated and prepared for the following staining procedure. Unless specified differently, embryos were fixed in 4 % paraformaldehyde (PFA) (Carl Roth GmbH & Co. KG, Karlsruhe, BW, Germany) in 1x phosphate-buffered saline (PBS) overnight at 4 °C. Then, embryos were extensively washed in PBS containing 0.1 % tween-20 (PBST) (Carl Roth GmbH & Co. KG, Karlsruhe, BW, Germany) before dehydrated through a methanol (MeOH) series with final storage in 100 % MeOH (Merck KGaA, Darmstadt, HE, Germany) at -20 °C. For adult brain preparations, heads derived from euthanized (overdose of MS-222) and decapitated fish were fixed overnight at 4 °C in 4 % PFA, dissected, and post-fixed for additional 4 hours at room temperature (RT).

RNA *in situ* hybridization (ISH) on whole-mounts and adult brain slices

The cDNA template for *grm8a*, *foxp2*, and *ppp1r1b* RNA ISH probe synthesis was generated by PCR target site amplification under optimized PCR primer conditions (for primer sequence and PCR conditions, see Table 3). Subsequently, the PCR amplicon was cleaned using the GenElute PCR Clean-Up Kit (Merck KGaA, Darmstadt, HE, Germany), cloned into pCR®II with the TA Cloning® Kit Dual Promoter (Thermo Fisher Scientific, Waltham, MA, USA), and transformed into the competent *E. coli* strain DH5-alpha (custom-made, original stock derived from New England Biolabs GmbH, Ipswich, MA, USA). Positive clones were selected by ampicillin resistance, and target site incorporation was verified by Sanger sequencing (Eurofins Genomics, Ebersberg, BY, Germany). The isolated and target site-containing plasmid was linearized (for applied restriction enzymes, see Table 4) and purified (GenElute PCR Clean-Up Kit, Merck KGaA, Darmstadt, HE, Germany) before it was *in vitro* transcribed with the SP6/T7 RNA polymerase and DIG RNA Labeling Mix (Merck KGaA, Darmstadt, HE, Germany) into the RNA ISH probe. Finally, the RNA probe was purified twice by LiCl and ethanol precipitation (for detailed protocol, see appendix) and stored at -80 °C.

Table 3: **List of oligonucleotides applied for RNA *in situ* hybridization (RNA ISH) and splice-inhibiting morpholino-derived knockdown.** Amplicon lengths are given for genomic (gDNA) and complementary DNA (cDNA) as PCR template. Coding (exonic) or non-coding regions (intronic) are presented in capital or small letters, respectively. Adjusted from Lueffe et al. 2021a.

Application	Oligo name	Gene symbol	Forward sequence (5'- 3')	Reverse sequence (5'- 3')	Amplicon length (gDNA)	Amplicon length (cDNA)	Ann. Temp. (°C)	Target site (5'- 3')
RNA ISH	*foxp2* exon 18 fwd. / 3'UTR rev.	*foxp2*	GGG TTA TGG GGC AGC TCT TA	CAC TTC AGT TCC GTG AGC CT	9839 bp	695 bp	59.5	
	grm8a exon 8 fwd. / exon 12/3' UTR rev.	*grm8a*	AGC AAC ATC AAT GGG AAA G	TCC TCA TAT GGC GTG ATT G		1434 bp	60	
	ppp1r1b-12 exon 2 fwd. / exon 5 rev.	*ppp1r1b*	CGC CGG CCA CTT TGT TTA AA	CCT CTG GCT ACA TAA TTC GCG	9334 bp	620 bp	64	
	ppp1r1b-13 exon 1 fwd. / exon 3 rev.	*ppp1r1b*	ATA AGA ACA GGC AGG GGA GG	TCG CTT TGG TTT GAG GAT GC		423 bp	64	
	ppp1r1b-123 exon 2 fwd. / exon 3 rev.	*ppp1r1b*	CGC CGG CCA CTT TGT TTA AA	GGG GCT GGT AGA TAT TTG GGT	1668 bp	129 bp	62	
Morpholino	*gad1b* exon 8 / intron 8 morpholino	*gad1b*		TTT GTG ATC AGT TTA CCA GGT GAG A				TCTCACCTGgtaaactgatcacaaa
	gad1b exon 7 fwd. / exon 9 rev.	*gad1b*	ATT GGT CTG GCT GGA GAA TG	ATT TAT ACC GCG CAA CCA TC	500 bp	208 bp	58	
	grm8a exon 4 / intron 4 morpholino	*grm8a*		AAA AAG CAG CCC TAC CCA TTT CTC T				AGAGAAATGGgtagggctgctttt
	grm8a exon 3 fwd. / exon 5 rev.	*grm8a*	AGC CGG ACT CAA TAC CAG TT	CTT GTC AAA TTC CCC AGC CC		771 bp	58.4	
	grm8a intron 4 rev.	*grm8a*	*grm8a* exon 3 fwd.	TCA GCA ACT CTT CCA GAC TG		0 bp	58.4	
	grm8b exon 3 / intron 3 morpholino	*grm8b*		AAT GTT CTC TGG AAA CTT ACC CGT T				AACGGgtaagttccagagaacatt
	grm8b exon 2 fwd. / exon 4 rev.	*grm8b*	GTA CGG ATC CAC TGA CTC CC	TGT CAA ACT CTC CTG GTC GG		717 bp	58.4	
	grm8b intron 3 rev.	*grm8b*	*grm8b* exon 2 fwd.	TCC CTT GAA CAC AAA GCA CT		0 bp	58.4	
	actb1 exon 2/3 fwd. / exon 3 rev.	*actb1*	CCC AGA CAT CAG GGA GTG AT	TCT CTG TTG GCT TTG GGA TT	0 bp	239 bp	53	
	lbx1a exon 1 fwd. / intron 1 rev.	*lbx1a*	TCC ACC TGC TAA CTC AAA CA	TTT AAC GAC CGT TTT CAC GA	353 bp	0 bp	56	

Table 4: **List of restriction enzymes applied for the generation of CRISPR/Cas9 sgRNAs or RNA *in situ* hybridization probes (ISH).** *ppp1r1b* ISH probes are named according to their sensitivity to three transcript versions (named 1, 2, and 3).

Enzyme	Company	Buffer	Purpose :	*foxp2*	*grm8a*	*grm8b*	*gad1a*	*gad1b*	*ppp1r1b-12*	*ppp1r1b-13*	*ppp1r1b-123*
Bsa I	Thermo Fisher Scientific	G		CRISPR/Cas9	CRISPR/Cas9	CRISPR/Cas9					
Dra I	Thermo Fisher Scientific	Tango		CRISPR/Cas9	CRISPR/Cas9	CRISPR/Cas9					
EcoR I	Thermo Fisher Scientific	EcoRI Buffer					ISH, antisense	ISH, antisense			
EcoR V	Thermo Fisher Scientific	R							ISH, antisense	ISH, antisense	ISH, sense
Hind III	Thermo Fisher Scientific	R				ISH, sense					
Kpn I	Thermo Fisher Scientific	KpnI Buffer		ISH, sense	ISH, sense						
Not I	Thermo Fisher Scientific	O		ISH, antisense	ISH, antisense	ISH, antisense					
Spe I	Thermo Fisher Scientific	Tango							ISH, sense	ISH, sense	ISH, antisense

grm8b RNA ISH probe: The *grm8b* cDNA template for RNA *in vitro* transcription was kindly provided by Marion Haug and Stephan Neuhaus (Haug et al. 2013). After the provided plasmid was transformed and amplified in competent *E. coli* DH5-alpha, the *grm8b* RNA ISH probe was generated and precipitated as described above. For better tissue penetration, the RNA ISH probe was hydrolyzed (to reduce probe size) for 20 min at 60 °C and 30 min at -20 °C before it was precipitated by LiCl and ethanol once more.

The procedure for whole-mount RNA ISH follows instructions published by Thisse and Thisse (2008) and was performed in a 24-well plate. Specimens stored in 100 % MeOH were rehydrated in PBST with decreasing concentration of MeOH. After the specimens were permeabilized by Proteinase K in PBST for a stage-dependent period (10 μg/ml, Merck KGaA, Darmstadt, HE, Germany) and post-fixed in 4 % PFA for 20 min at RT, they were extensively washed in PBST. Afterward, the specimens were exposed to hybridization buffer (for recipe see appendix) containing 5 mg/ml torula yeast RNA type VI (Merck KGaA, Darmstadt, HE, Germany) for 1 h at 65 °C, before they were transferred and incubated in hybridization buffer containing recycled RNA ISH probe (1:100) overnight at 65 °C.

On day two, the specimens went through a number of stringent washing steps at 65 °C in decreasing concentration of hybridization buffer diluted with increasing concentration of 2x saline-sodium-citrate (SSC) buffer. After a final washing step in 0.05x SSC in PBST for 1 h at 65 °C and several washes in PBST at RT, unspecific binding sites were blocked by incubation in ISH blocking buffer (for recipe see appendix) for 1 h at RT. Subsequently, the hybridized and digoxigenin (DIG)-labeled RNA ISH probe was immunolabeled for 2 hours (at RT) by incubation in sheep anti-DIG Fab fragments conjugated with Alkaline Phosphatase (AP, anti-DIG-AP, Merck KGaA, Darmstadt, HE, Germany) and diluted in ISH blocking buffer (1:5000).

After extensive washes in PBST at RT and overnight at 4 °C, the specimens were transferred into alkaline tris-buffer (pH 9.5, for recipe, see appendix) for 30 min at RT. Then AP activity was revealed at RT by nitroblue tetrazolium/5-bromo-4-chloro-3-indolylphosphate (NBT/BCIP) (Merck KGaA, Darmstadt, HE, Germany) diluted in alkaline tris-buffer. From now on, speci-

mens were kept in darkness. As soon as the desired staining pattern was fully developed, the enzymatic reaction was stopped by replacing the staining solution with PBST. Afterward, the specimens were extensively washed in PBST at RT and overnight at 4 °C, post-fixed in 4 % PFA for 20 min at RT, and finally stored in 80 % glycerol in PBST in the dark.

Adult brain sections: Procedure for RNA ISH on adult brain sections follows that of whole-mounts with one exception. Before transferring the specimens to ISH blocking buffer, pre-processed brains were embedded in agarose (3 % in PBS) and cut into transverse sections of 80 μm thickness using a vibratome (Vibratome Series 1000 Sectioning System, TPI Lab, London, EN, UK).

Two-color RNA ISH: To generate *gad1a* and *gad1b* fluorescein (FLUO)-labeled RNA ISH probes, pBluescript II (KS+) containing the *gad67a* (*gad1a*) or *gad67b* (*gad1b*) cDNA template (kindly provided by Laure Bally-Cuif) were linearized (for applied restriction enzymes see Table 4) and purified using the GenElute PCR Clean-Up Kit (Merck KGaA, Darmstadt, HE, Germany). Then, the linearized and purified plasmid was transcribed by the T3 RNA polymerase and FLUO RNA Labeling Mix (Merck KGaA, Darmstadt, HE, Germany) and purified twice by LiCl and ethanol precipitation. For hybridization, specimens were exposed to a mix of DIG- and FLUO-labeled RNA ISH probes diluted 1:100 each in hybridization buffer. The hybridized FLUO-labeled probe was immunolabeled first by incubation in sheep anti-FLUO-AP Fab fragments (1:2000) in ISH blocking buffer. Before AP activity was detected by applying SIGMAFAST fast red TR/naphtol AS-MX phosphate (4-chloro-2-methylbenzenediazonium/3-hydroxy-2-naphtoic acid 2,4-dimethylanilide phosphate) tablets in Trizma buffer (Merck KGaA, Darmstadt, HE, Germany), the specimens were washed in tris-buffer (pH 8.2, for recipe, see appendix) for a total of 30 min at RT. When reaching the full staining pattern, the specimens were transferred to PBST to stop AP activity, and the anti-FLUO-AP Fab fragments were detached in PBST for 2 hours at 68 °C. Subsequently, specimens were blocked in ISH blocking buffer and incubated in anti-DIG-AP Fab fragments before AP-activity was revealed as described before.

Cryosections

Specimens stained by RNA ISH and stored in 80 % glycerol (in PBST) were extensively washed in PBST and in PBS before they were incubated in 15 % sucrose solution in PBS overnight at 4 °C for cryoprotection. On the next day, cryoprotected specimens were embedded in 7.5 % gelatine in 15 % sucrose solution and incubated at 4 °C until the gelatine had become solid. Then, gelatine blocks were cut, fixed on cork plates using Tissue-Tek® O.C.T.™ Compound (Thermo Fisher Scientific, Waltham, MA, USA), and immediately snap-frozen in pre-cooled (liquid nitrogen) 2-methylbutane (Carl Roth GmbH & Co. KG, Karlsruhe, BW, Germany). Frozen cryoblocks were stored at -80 °C until they were cut on a Microm microtome cryostat HM 500 OM (Microm International GmbH, Dreieich, HE, Germany) into transverse sections of 20 μm. If not further processed, sections collected on SuperFrostPlus slides (Thermo Fisher Scientific, Waltham, MA, USA) were mounted in 80 % glycerol or 1 % Mowiol 4-88 (Carl Roth GmbH & Co. KG, Karlsruhe, BW, Germany), covered with a 40 mm x 60 mm coverslip (A. Hartenstein GmbH, Würzburg, BY, Germany) and sealed with nail polisher. Mounted sections were stored in the dark at 4 °C until image acquisition.

Injection of splice-inhibiting morpholinos and verification by RT-PCR

Splice-inhibiting morpholino oligonucleotides (GeneTools, Table 3) were designed by the Gene-Tools custom support and selected based on the number of off-targets and expected missplicing effects. Each oligonucleotide was injected in diluted form (nuclease-free water, not DEPC treated, Thermo Fisher Scientific, Waltham, MA, USA) into the animal pole of one-cell stage zebrafish eggs (Fig. 6).
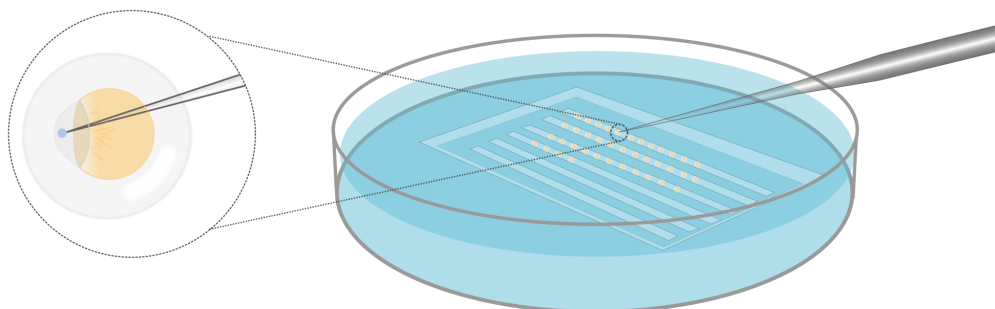
Figure 6: **Schematic illustrating microinjection into the animal pole of a one-cell stage zebrafish egg.**

The appropriate concentration for each splice-inhibiting morpholino (hereinafter referred to as "splice-morpholino" in the main text) was determined before it was applied for functional experiments (for details on volume and concentration, see Table 5). Detectable levels of misssplicing by PCR and minimal side-effects like anatomical malformations or elevated cell death were major criteria. To test for missplicing, the injected eggs were raised until 24 hours post fertilization (hpf) and 5 dpf when total RNA of five splice-morphant (hereinafter referred to as "morphant" in the main text) and five uninjected individuals of either developmental stage was extracted by phenol (TRIZOL)-chloroform precipitation (for detailed protocol, see appendix) and purified by LiCl and ethanol precipitation. Next, extracted RNA was treated with DNase I (Merck KGaA, Darmstadt, HE, Germany) before the samples were used as PCR templates to test for genomic DNA (gDNA) contamination. The applied reverse primer was designed to bind in the intronic region of the *lbx1a* gene (Table 3), such that a PCR-based amplification requires gDNA. gDNA-free RNA samples were transcribed into cDNA by applying the RevertAid First Strand cDNA Synthesis Kit (Thermo Fisher Scientific, Waltham, MA, USA). Successful reverse transcription and morpholino-induced missplicing were confirmed by a beta-actin (*actb1/β-actin*) control PCR and PCR using custom-designed primer pairs (Table 3), respectively. Final confirmation of splicing defects was done by Sanger sequencing (Eurofins Genomics, Ebersberg, BY, Germany) on gel purified (GenElute Gel Extraction Kit, Merck KGaA, Darmstadt, HE, Germany) PCR product.

Table 5: **Injection parameters and induced missplicing effects for applied splice-inhibiting morpholinos.**

Target site	Concentration	Volume	Effect
gad1b exon 8 / intron 8	0.5 mM	0.5 nl	intron retention
grm8a exon 4 / intron 4	0.25 mM	0.5 nl	exon exclusion
grm8b exon 3 / intron 3	0.0625 mM	0.5 nl	exon exclusion

Generation and validation of CRISPR/Cas9 mutant lines

For each candidate gene, two CRISPR/Cas9 target sites (Table 6) were selected based on efficiency scores provided by the online algorithm CHOPCHOP (Labun et al. 2019). Based on each target site, two oligonucleotides were designed (Table 6), which later functioned as template for the spacer sequence (homologous to the selected target region) during single guide RNA (sgRNA) synthesis. Therefore, both oligonucleotides were annealed with a T4 DNA lig-

49

ase (Thermo Fisher Scientific, Waltham, MA, USA) before they were incorporated into the linearized (*Eco31*I/*Bsa*I, Thermo Fisher Scientific, Waltham, MA, USA) and purified (GenElute Gel Extraction Kit, Merck KGaA, Darmstadt, HE, Germany) plasmid pDR274 (kindly provided by Keith Joung and Addgene # 42250, Watertown, MA, USA). The ligated plasmid was transformed into the competent *E. coli* strain DH5-alpha (custom-made, original stock derived from New England Biolabs GmbH, Ipswich, MA, USA) and selectively grown by the introduced kanamycin resistance. Subsequently, a colony PCR (using oligonucleotide 2 (Oligo 2) as forward and M13 uni (-21) as reverse primer, Table 6) was performed to determine positive clones, which were later verified by Sanger sequencing (Eurofins Genomics, Ebersberg, BY, Germany). Amplified and extracted plasmid (containing the annealed oligonucleotides) was linearized (*Dra*I, Thermo Fisher Scientific, Waltham, MA, USA), purified (GenElute Gel Extraction Kit, Merck KGaA, Darmstadt, HE, Germany) and *in vitro* transcribed using a custom-made T7 RNA polymerase (generated and provided by Thomas Ziegenhals and Utz Fischer). Afterward, Roti®-phenol/chloroform/isoamylalcohol (Carl Roth GmbH & Co. KG, Karlsruhe, BW, Germany) RNA precipitation was applied to purify the synthesized sgRNA (for detailed protocol, see appendix). The final sgRNA stock was stored at -80 °C.

Table 6: **Oligonucleotides applied for the generation or verification of CRISPR/Cas9 mutant lines and induced indel mutations.** Oligonucleotides, highlighted in green, were used for the generation of CRISPR/Cas9 mutant lines which were functionally tested in the present work. Protospacer adjacent motifs (PAMs) are underlined. Amplicon length is given for genomic DNA as PCR template. (MO) Oligonucleotides also applied during splice-morpholino verification (Table 3).

Oligo name	Gene symbol	Forward sequence (5'- 3')	Reverse sequence (5'- 3')	Amplicon length	Ann. Temp. (°C)	Target site (5'- 3')
foxp2 exon 6 Oligo 1 / Oligo 2	*foxp2*	TAG GAG ATT TCA GGC CAC TGC C	AAA CGG CAG TGG CCT GAA ATC TCC			GGAGATTTCAGGCCACTGCCTGG
foxp2 intron 5 fwd. / intron 6 rev.	*foxp2*	TTG CGT CTC CTT TTC TCT TCT C	CCA GAA TTA CAT TGC CAA ATC A	232-bp	55	
foxp2 exon 10 Oligo 1 / Oligo 2	*foxp2*	TAG GAC ATG CTG TGA TGA GTG A	AAA CTC ACT CAT CAC AGC ATG TCC			GGACATGCTGTGATGAGTGATGG
foxp2 exon 10 fwd. / intron 10 rev.	*foxp2*	CAA CTT TGG AAA GAC GTC ACT G	TGG GTA TGC GGT AGA ATA AAC C	268-bp	58	
grm8a exon 3 Oligo 1 / Oligo 2	*grm8a*	TAG GAT AAT ATC GCC ATC CAG A	AAA CTC TGG ATG GCG ATA TTA TCC			GGATAATATCGCCATCCAGACGG
grm8a exon 3 rev.	*grm8a*	*grm8a* exon 3 fwd. (MO)	GCA TTG CCT CTA ATC GGT GG	217-bp	58	
grm8a exon 4 Oligo 1 / Oligo 2	*grm8a*	TAG GCC ATG CTG GAT ATA GTG A	AAA CTC ACT ATA TCC AGC ATG GCC			GGCCATGCTGGATATAGTGACGG
grm8a in/ex 3/4 fwd. / exon 4 rev.	*grm8a*	CTT CTT TCG TCT GCA GAT CCT T	TTT CCC CAT AGT TTC CTT CAG A	194-bp	55	
grm8b exon 2 Oligo 1 / Oligo 2	*grm8b*	TAG GCG AAC GGG GTG CTC CTT G	AAA CCA AGG AGC ACC CCG TTC GCC			GGCGAACGGGGTGCTCCTTGTGG
grm8b exon 2 rev.	*grm8b*	*grm8b* exon 2 fwd. (MO)	GTA ACA TTG GGC AGC AGG TC	217-bp	58	
grm8b exon 6 Oligo 1 / Oligo 2	*grm8b*	TAG GAC TCC ACT TAT GAG CAA G	AAA CCT TGC TCA TAA GTG GAG TCC			GGACTCCACTTATGAGCAAGAGG
grm8b intron 5 fwd. / exon 6 rev.	*grm8b*	ATC ATT GCC TCT AAC CCA AGA A	ATC CTG AGC AGA GAT CCC TAT G	271-bp	58	
grm8b intron 5 fwd. / intron 6 rev. [2]	*grm8b*	TTA GCA TTG CAC CCT TCT TTT T	AAC AAC CCA ATT AAA CCG AGA A	290-bp	58	
M13 uni (-21) rev.			CAG GAA ACA GCT ATG AC		58	

The synthesized sgRNA alone or as cocktail with Cas9-NLS protein (300 ng/µl, *S. pyogenes*, New England Biolabs GmbH, Ipswich, MA, USA) was injected (for individual concentration see Table 7) into the animal pole of one-cell stage eggs (Fig. 6). Injected eggs were raised until 3 dpf when gDNA of twenty individuals per group (sgRNA+Cas9, sgRNA only and Cas9

only) was extracted (for detailed protocol, see appendix) and pooled (by four) to screen for insertion/deletion (indel) mutations by PCR (for applied primer pairs, see Table 6). Since indel mutations appear as double bands on the gel and as double traces during sequencing, the amplified PCR product was run on a 3 % high-resolution NuSieve$^\circledR$ 3:1 agarose gel (in 1x tris-borate-EDTA buffer, Lonza Group AG, Basel, BS, Switzerland) and sent for Sanger sequencing (Eurofins Genomics, Ebersberg, BY, Germany) (Fig. 7).

Table 7: **Injection concentrations for CRISPR/Cas9 sgRNAs and co-injected Cas9-NLS protein plus verified status on individual sgRNA functionality.**

Target site	Concentration (sgRNA)	Concentration (Cas9 protein)	Indel mutations
foxp2 exon 6	100 ng/µl	300 ng/µl	yes
foxp2 exon 10	190 ng/µl	300 ng/µl	yes
grm8a exon 3	100 ng/µl	300 ng/µl	yes
grm8a exon 4	100 ng/µl	300 ng/µl	yes
grm8b exon 2	100 ng/µl	300 ng/µl	yes
grm8b exon 6	200, 150, 100 and 50 ng/µl	300 ng/µl	no

Germline transmission in F_0: To test for germline transmission of induced mutations, injected embryos were raised and outcrossed with AB/AB wildtypes. Then, gDNA from several F_1 off-springs was extracted and used for target site amplification by PCR. F_0 individuals with verified germline transmission were outcrossed with AB/AB wildtypes to generate F_1 mutant lines (Fig. 7).

Mutation identification in F_1: Individual F_1 mutants were genotyped by fin biopsies, gDNA extraction, and genotyping PCR. Then, the corresponding PCR product was purified and cloned into pre-linearized pCRII vector (TA Cloning Kit Dual Promotor, Thermo Fisher Scientific, Waltham, MA, USA) before the plasmid was extracted and sent for Sanger sequencing (LGC Genomics GmbH, Berlin, BE, Germany) to precisely characterize the target site mutation. Based on the available sequencing data, six truncation mutations (2x *foxp2*, 2x *grm8a*, and 2x *grm8b*) were selected for further investigations (one each) and/or maintenance. Therefore, previously characterized F_1 mutant individuals were outcrossed with AB/AB wildtypes to breed heterozygous and wildtype F_2 mutant siblings (Fig. 7).

Generation of intercrossed and outcrossed F_3: F_2 generation fish were genotyped as described above. Then, heterozygous F_2 mutants were outcrossed with AB/AB wildtypes to clean the

genetic background from potential off-target mutations. In addition, heterozygous F_2 individuals were intercrossed with heterozygous siblings to generate and investigate heterozygous, homozygous, and wildtype siblings (Fig. 7).

Mutation confirmation in F_3: To confirm the mutation characteristics identified in the corresponding F_1 generation, gDNA of homozygous F_3 mutants were amplified and sent for Sanger sequencing (LGC Genomics GmbH, Berlin, BE, Germany) (Fig. 7).
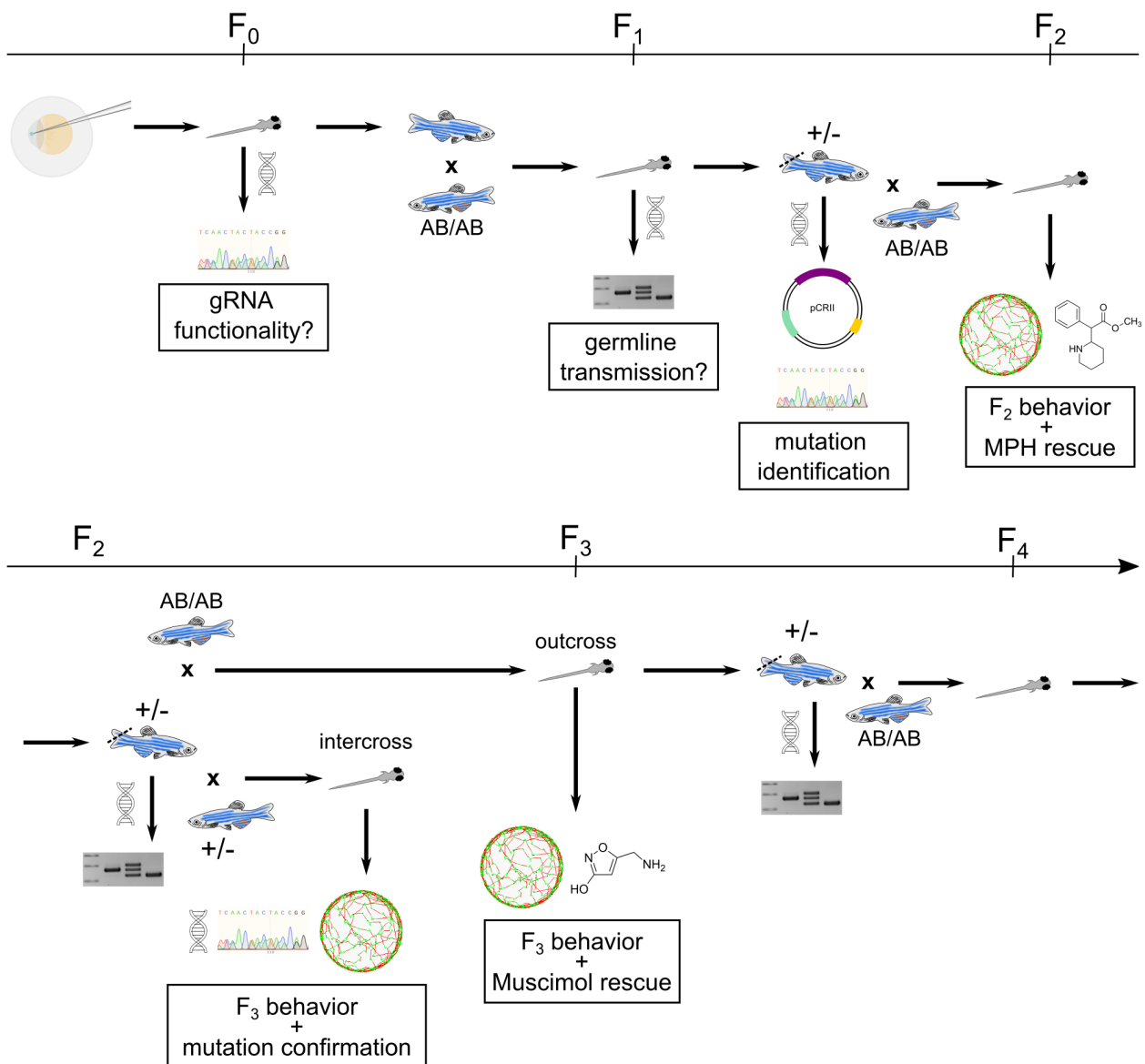

Figure 7: **Schematic illustrating the stepwise generation, genetic and functional verification, and maintenance of described CRISPR/Cas9 mutant lines.**

RNA extraction and real-time quantitative PCR (qPCR)

The genotype of 5 dpf old larvae, tested by quantitative real-time PCR (qPCR), was determined by gDNA extraction and genotyping PCR (primer pairs are listed in Table 6) on a small fraction of tail tissue. After the tail was cut, the remaining embryo was kept in RNAprotect Tissue Reagent (Qiagen N.V., Venlo, LI, Netherlands) for later RNA extraction. Total RNA of ten larvae per genotype was isolated using the RNeasy® Mini Kit (Qiagen N.V., Venlo, LI, Netherlands). Before RNA was extracted according to the manufacturer's instructions, the collected tissue was transferred to a guanidine-thiocyanate-containing lysis buffer mixed with β-mercaptoethanol (10 μg/ml), in which it was homogenized with a TissueLyser II (Qiagen N.V., Venlo, LI, Netherlands). Due to gDNA contamination, DNase I was added to each RNA sample. After the DNase I activity was stopped by EDTA application, the final amount of RNA was measured at the NanoDrop® (Thermo Fisher Scientific, Waltham, MA, USA). Finally, cDNA was synthesized using the SuperScript® IV Reverse Transcriptase Kit (Thermo Fisher Scientific, Waltham, MA, USA).

Table 8: **Oligonucleotides applied for real-time quantitative PCR (qPCR).** Amplicon length is given for complementary DNA (cDNA) as template. From Lueffe et al. 2021a.

Gene symbol	Gene name	Gene ID (Ensembl)	Forward primer sequence (5'- 3')	Reverse primer sequence (5'- 3')	Amplicon length (bp)	Ann. Temp. (°C)
actb1	actin, beta 1	ENSDARG00000037746	GCT GTT TTC CCC TCC ATT GTT	GGG CCT CAT CTC CCA CAT AG	91	62
adgrl3.1	adhesion G protein-coupled receptor L3.1	ENSDARG00000061121	ACT GGG AGA GTC TGC TGT GT	CCC GTG CGT TGT TGA GAA TG	117	62
adgrl3(.2)	adhesion G protein-coupled receptor L3(.2)	ENSDARG00000090624	GAC GAC GCC TTC CTC AAG AA	GCT CAG GAT CAG GCA GAG TG	80	62
cntnap2a	contactin associated protein 2a	ENSDARG00000058969	GCT GAT TTC CCC TTC AAT G	AGA TCA CCA CCG CAA TGA T	80	61
cntnap2b	contactin associated protein 2b	ENSDARG00000074558	AGG AGC GCA TCA GTC GAG AT	CGT GCA GAG GAT GGT GAA GAT	89	63
dusp6	dual specificity phosphatase 6	ENSDARG00000070914	TCT CGG AGG GCT CAG AAT CA	GGC TGC CAT CTG AGT CAG TT	92	62
foxp1a	forkhead box P1a	ENSDARG00000004843	GCT CTC GCC TCT GCC TAC	GTG TCT GGA CTC TGC TGC TC	114	62
foxp1b	forkhead box P1b	ENSDARG00000014181	AGA GGA AAT GAA TGG GGC CA	CTG GGT CCA TTG GCT CCT C	119	62
foxp2	forkhead box P2	ENSDARG00000005453	CCT GGA TAC TCC CCA CAC AC	ACA GTC CTC GTC CTC CAT GTT	78	61
gad1a	glutamate decarboxylase 1a	ENSDARG00000093411	CAG ATG GAG AGG AGA AAC GAC AT	ACC ATT GTT GTC CCG CAC T	85	66
gad1b	glutamate decarboxylase 1b	ENSDARG00000027419	ATG CCG AAC GGA GAC GAG	GCA CTC CAT CAT CAT TGC TTT G	75	63
gad2	glutamate decarboxylase 2	ENSDARG00000015537	GTG GAG AGG ATG AAG CGT CTG	GAC CAT GCG GAA GAA GTT GAC	123	62
gapdh	glyceraldehyde-3-phosphate dehydrogenase	ENSDARG00000043457	CGA TCA CTT TGT CAA GCT GGT	GCT GTA ACC GAA CTC ATT GTC A	89	62
grm3	glutamate receptor, metabotropic 3	ENSDARG00000031712	GAG CGG GCC AAG CAA CTA G	GAA CGT AGT GGG CAC TCA CA	116	63
lrrn1	leucine rich repeat neuronal 1	ENSDARG00000060115	TCC CGT TGC AAG GAA GGA TC	TCG TCT CGT TAC ATC CAC GC	84	62
mef2ca	myocyte enhancer factor 2ca	ENSDARG00000029764	TCA TCT GGG CTC CAT GAC C	GAC GGC AGA GAT AGG GCA GA	114	63
mef2cb	myocyte enhancer factor 2cb	ENSDARG00000009418	GCA GCA CTC TGC ACT CAG TC	CTT GAT GTG CAG GCT TTG AG	100	63
ntrk2b	neurotrophic tyrosine kinase, receptor, type 2b	ENSDARG00000098511	CTT CAC CTA TGG CAA GCA ACC	TAA CAC CCG ACC CTG TGT GAT	79	62
pcdh7a	protocadherin 7a	ENSDARG00000078898	TAG TGG GGT GGA GGA CTC AG	CTA CGC TCC CTT CTG GTG TG	116	64
pcdh7b	protocadherin 7b	ENSDARG00000060610	ACT AGG TGC CCT CCC TCT AC	CCA TAT GCT CTG CCT CAC CG	80	62
ppp1r1b	protein phosphatase 1, regulatory (inhibitor) subunit 1B	ENSDARG00000076280	TGG CTG AAG CTC AAA TGC AG	TTG TGC AGG ATG AGC AGA GC	105	62
sema6d	semaphorin 6D	ENSDARG00000002748	GTG ATG TCA AAT CAG CTG TGG A	AAA CGC TAG CAA CAC ACA CG	116	62
slitrk2	SLIT and NTRK-like family, member 2	ENSDARG00000006636	TCT ACG GGA CCC CCA GAA AA	CCA GCA CTT CGA GGT AGT CC	99	65

For qPCR, each gene was represented by three technical and three biological replicates per genotype. In addition, a no reverse transcriptase control and a no template control served as general controls for external nucleic acid contamination. For each reaction, a mix of SYBR® Select Mastermix for CFX, cDNA (1:20), and individual primer pair (Table 8) was pipetted together. For the qPCR run, a CFX384 Touch Real-Time PCR Detection System (Bio-Rad Labo-

ratories, Inc., Hercules, CA, USA) was used with the annealing temperature set to 60 °C. The final analysis was performed with the CFX Maestro software (Bio-Rad Laboratories, Inc., Hercules, CA, USA) by applying the C_t (2-$\Delta\Delta$Ct) method. Significant differences were calculated by a one-way ANOVA with a significance level of 0.05.

Behavioral assays

Locomotion tracking of 5 dpf old larvae was performed by the semi-automatic system ZebraBox using the commercial software ZebraLab (ViewPoint, Civrieux, ARA, France). Larvae were tracked in a 12-well plate filled with 1 ml of Danieau's solution per well and surrounded by a constant water flow of 28 °C. Each larva occupied one well while swimming behavior was recorded with 30 fps by an integrated infrared-detecting camera. All experiments were carried out in darkness, although with an integrated infrared illumination of 850 nm wavelength. Swimming tracks were recorded with the internal detection threshold set to 11. During tracking, activity was specified by three different levels: inactivity (< 0.2 cm/s), low activity (0.2 cm/s < and < 1 cm/s), and high activity (> 1 cm/s). Tracking was performed for 10 min in total (5 min habituation and a 5 min test period), with "test" data used for final analysis. Alterations in locomotor activity were extracted by analyzing four major parameters: total distance swum, mean velocity (of low or high activity or both (total)), and duration of, and the number of events for each activity level (inactivity, low or high activity).

To test for changes in thigmotaxis behavior, data obtained during locomotion tracking was replayed by the software, after each region of interest/well (ROI) was virtually divided (Fig. 15) into an outer (width of 4 mm, fits one larva entirely) and an inner zone (radius of 7.35 mm). Increased thigmotaxis behavior was defined by an increased percentage of time spent in the outer zone of the well.

Drug treatment

Working solutions were freshly prepared for each experiment (for summarized details on drug treatments, see Table 9).

L-allylglycine: To inhibit glutamate decarboxylase (Gad) activity, 5 dpf old wildtype larvae were treated with 100 mM of the Gad1 antagonist L-allylglycine. Therefore, L-allylglycine powder (Santa Cruz Biotechnology, Dallas, TX, USA) was dissolved in ddH$_2$O to 1000 mM and diluted to a working stock of 200 mM in Danieau's solution. Following locomotion tracking for 10 min (described above) without treatment, 500 μl of 1 ml Danieau's solution (per well) was exchanged by pure Danieau's solution or 200 mM L-allylglycine working stock (100 mM final concentration) in which larvae were then incubated for 1 h in darkness. Subsequently, locomotion was tracked every hour for 10 min over a period of 8 hours.

SR-95531/gabazine hydrobromide: The GABA-A-receptor (GABA-A-R) antagonist SR-95531 /gabazine hydrobromide (Thermo Fisher Scientific, Waltham, MA, USA) was dissolved in nuclease-free water (not DEPC treated) to a final concentration of 10 mM and injected into the yolk of one-cell stage wildtype eggs (Stehr et al. 2006).

CGP-55845 hydrochloride: 0.1 mM of the GABA-B-receptor (GABA-B-R) antagonist CGP-55845 hydrochloride (Hello Bio, Bristol, EN, UK) was dissolved in 0.1 % DMSO (Carl Roth GmbH & Co. KG, Karlsruhe, BW, Germany) in Danieau's solution. Next, 3 dpf old wildtype zebrafish larvae were raised in 25 ml of either 0.1 mM CGP55845 solution or 0.1 % DMSO in Danieau's solution for 48 hours (Song et al. 2017). At 5 dpf, locomotor activity of treated and untreated wildtypes was recorded in pure Danieau's solution as described above.

Muscimol hydrobromide: The GABA-A-R agonist muscimol hydrobromide (Merck KGaA, Darmstadt, HE, Germany) was dissolved in ddH$_2$O to a final stock concentration of 70 mM and stored as aliquots at –20 °C in the dark. 3 dpf old *foxp2* mutants were incubated in 25 ml Danieau's solution with or without 0.05 mM muscimol for 48 hours. After 24 hours, both solutions were replaced by fresh ones. At 5 dpf, locomotor activity of treated and untreated *foxp2* mutants and wildtype siblings was recorded in fresh Danieau's solution as described above.

R-baclofen: The GABA-B-R agonist R-baclofen (Hello Bio, Bristol, EN, UK) was dissolved in nuclease-free water to a stock concentration of 20 mM and stored as aliquots at -20 °C in the dark. 3 dpf old wildtype zebrafish larvae were bathed in 25 ml of 0.025 mM, 0.05 mM, or 0.1 mM baclofen diluted in Danieau's solution or in Danieau's solution only for 48 hours. At 5 dpf, locomotor activity of treated and untreated wildtypes was recorded in pure Danieau's solution as described above.

Methylphenidate hydrochloride: The psychostimulant methylphenidate hydrochloride was dissolved in ddH$_2$O to a stock concentration of 8 mM and stored as aliquots at –80 °C in the dark. To treat 5 dpf old morphant and mutant larvae, the stock solution was further diluted in Danieau's solution to a working concentration of 0.024 mM. Following locomotion tracking in 1 ml Danieau's solution for 10 min, 500 μl Danieau's solution was replaced by 0.024 mM muscimol working solution (treated, 0.012 mM final concentration) or pure Danieau's solution (untreated) in which larvae were incubated for 1 h. After incubation, locomotor activity of treated and untreated larvae was recorded as described before. Only data derived from post-treatment tracking was considered for analysis.

Table 9: **List of pharmacological substances applied during behavioral validation and corresponding information on tested and/or applied treatment procedures.** Bold labeled information highlights treatment procedure finally applied for actual data collection. (MO) splice-morphants.

Substance	Target	Effect	Company	Applied on	Stock concentration	Diluted in	Concentrations tested	Treatment
L-allylglycine	Gad	antagonist	Santa Cruz Biotechnology	**AB/AB**	1000 mM	ddH2O	25, 50, 75, **100 mM**	**1-8 h**
SR-95531/ gabazine hydrobromide	GABA-A-R	antagonist	Thermo Fisher Scientific	**AB/AB**		nuclease-free water	0.1, **10 mM**	1-8 h, **injection**
muscimol hydrobromide	GABA-A-R	agonist	Merck KGaA	*foxp2* **CRISPR**	70 mM	ddH2O	**0.05**, 0.075, 0.1 mM	**48 h**
CGP-55845 hydrochloride	GABA-B-R	antagonist	Hello Bio	**AB/AB**		Danieau's+ 0.1% DMSO	**0.1 mM**	1-8 h, **48 h**
R-baclofen	GABA-B-R	agonist	Hello Bio	**AB/AB**, *foxp2* CRISPR	20 mM	nuclease-free water	**0.025, 0.05, 0.1 mM**	**48 h**
methylphenidate hydrochloride	dopamine/ noradrenaline	reuptake inhibitor	Merck KGaA	*foxp2* **CRISPR**, *gad1b* **MO**	8 mM	ddH2O	0.005, 0.01, **0.012**, 0.015, 0.02, 0.025 mM	**1 h**, 48 h

Immunohistochemistry (IHC) on cryosections and whole-mounts

Unless stated differently, the yolk and the eyes of immunostained whole-mounts (< 5 dpf) were removed after the staining procedure was completed. For 5 dpf old larvae, the brain of the previously fixed larvae was dissected first (by removing the eyes, the jaw, the yolk, and the skin overlying the brain), before the staining procedure was started. In general, immunostained morphants and mutants were genotyped prior to image acquisition using a small fraction of

tail tissue for gDNA extraction and subsequent genotyping PCR. For detailed information on antibodies and dilutions applied for IHC, see Table 10.

Anti-Gad1b: 30 hpf old mutant and wildtype embryos were rehydrated from 100 % MeOH into PBST.

Anti-GABA: 30 hpf old, PFA-fixed morphant, mutant, and wildtype embryos were directly processed for immunolabeling without prior dehydration and storage in 100 % MeOH.

Anti-Gad1b/anti-GABA: The specimens were equilibrated in tris-HCl (pH 9.0) for 5 min at RT and for 15 min at 70 °C. After 3 min at RT and several washes in PBST, the specimens were rinsed with ddH$_2$O on ice and permeabilized with pre-chilled (-20 °C) acetone at 4 °C for 20 min. Subsequently, the acetone was removed, and the specimens were rinsed with ddH$_2$O and washed with 0.8 % PBT (1x PBS + 0.8 % triton X-100). Then, the specimens were blocked in 10 % blocking buffer (for recipe see appendix) for 1 h at RT before they were labeled with primary antibody (Table 10) diluted in 2 % blocking buffer (for recipe see appendix) overnight (anti-Gad1b) or three days (anti-GABA) at 4 °C. After the primary antibody was washed off with 0.8 % PBT, the specimens were incubated for 3 hours at RT (anti-Gad1b) or two days at 4 °C (anti-GABA) in secondary goat anti-rabbit IgG (H+L) conjugated to Alexa Fluor 488 (Table 10) diluted in 2 % blocking buffer. Finally, immunolabeled embryos were washed in PBST, dissected, and stored in 80 % glycerol (in PBST) at 4 °C in the dark for image acquisition.

Anti-GFP: Following storage at -20 °C, cryosections of RNA ISH labeled embryos were circled with a Dako pen (Agilent Technologies, Santa Clara, CA, USA) and incubated for 2 hours at RT. Then, the sections were washed in PBST and expressed GFP/EGFP was labeled by incubation in polyclonal rabbit anti-GFP primary antibody (Table 10, diluted in 2 % blocking buffer) for 3 hours at RT. Afterward, the sections were extensively washed in PBST before they were incubated in diluted (2 % blocking buffer) secondary goat anti-rabbit IgG (H+L) conjugated to Alexa Fluor 488 (Table 10) for 2 hours at RT. Subsequently, the sections were washed three times 10 min in PBST, with 100 μg/ml DAPI applied to the first washing solution. Afterward, the PBST was drained, and the sections were mounted with 1 % Mowiol 4-88 (Carl Roth GmbH & Co. KG, Karlsruhe, BW, Germany) and a coverslip for final storage at 4 °C in the dark.

Anti-cleaved caspase 3 (cCasp3): Fixation of 24 hpf old morphant, mutant, and wildtype embryos were performed in 4 % PFA for 3 hours at RT before the embryos were dehydrated through a MeOH series (in 0.8 % PBT) with final storage in 100 % MeOH. For the staining procedure, the specimens were directly transferred to pre-chilled (-20 °C) 100 % acetone and penetrated for 7 min at -20 °C. After the specimens were rehydrated in 50 % MeOH for 1 h at -20 °C and washed in ddH$_2$O and 0.8 % PBT at RT, they were incubated in DMSO-containing blocking buffer (for recipe see appendix) for 1 h at RT. Next, blocked specimens were labeled with a polyclonal rabbit anti-cleaved caspase 3 (Asp175) primary antibody (Table 10, diluted in DMSO-containing blocking buffer) for three days at 4 °C. After the primary antibody was washed off by 0.8 % PBT, the specimens were incubated in secondary goat anti-rabbit IgG (H+L) conjugated to Alexa Fluor 488 (Table 10, diluted in DMSO-containing blocking buffer) for two days at 4 °C. Finally, after several washes in 0.8 % PBT, the specimens were stored in 80 % glycerol in PBST at 4 °C in the dark.

Anti-acetylated tubulin (AcTub): Unlike other immunostainings described above, anti-AcTub labeling was performed on fixed and already dissected 24 hpf old embryos and 5 dpf old larvae. Fixation was performed in 4 % PFA at RT for 1 h per 24 hours of development. After fixation and dissection, the specimens were washed in PBS and dehydrated through a MeOH series into 100 % MeOH. After at least one night of incubation in 100 % MeOH at -20 °C, the specimens were rehydrated into 0.5 % PBT and permeabilized with Proteinase K (20-28 hpf: 10 μg/ml 8-12 min, 5 dpf: 40 μg/ml 20 min) at RT. Next, the specimens were washed in 0.5 % PBT once before they were post-fixed in 4 % PFA for 20 min at RT. After several washes in 0.5 % PBT, the specimens were incubated in DMSO-containing blocking buffer for 1 h at RT. Afterward, the specimens were labeled with monoclonal mouse anti-acetylated tubulin primary antibody (Table 10, diluted in DMSO-containing blocking buffer) overnight at 4 °C. Following several washes in 0.5 % PBT, the specimens were incubated in secondary goat-anti-mouse IgG (H+L) conjugated to Alexa Fluor 488 (Table 10, diluted in DMSO-containing blocking buffer) overnight at 4 °C. Finally, the specimens were washed in 0.5 % PBT before they were stored in 80 % glycerol in PBST at 4 °C in the dark.

Table 10: **Primary and secondary antibodies applied for immunohistochemistry.** (MO) splice-morphants.

Antibody	Antigen	Species	Clonality	Company	Cat#	RRID:	Dilution	Applied on
anti-Gad1b	glutamate decarboxylase 1b (Gad1b)	rabbit	polyclonal	Abcam	ab209717		1:100	*foxp2* CRISPR
anti-GABA	gamma-aminobutyric acid (GABA)	rabbit	polyclonal	Merck KGaA	A2052	AB_477652	1:100	*gad1b* MO, *grm8a* CRISPR+MO
anti-GFP	GFP	rabbit	polyclonal	antibodies-online	TP401	AB_10013661	1:500	Tg(Etvmat:GFP)
anti-cCasp3	cleaved caspase 3 (cCasp3)	rabbit	polyclonal	Cell Signaling Technology	9661	AB_2341188	1:500	*foxp2* CRISPR, *grm8a* + *grm8b* MO + CRISPR, *gad1b* MO
anti-AcTub	acetylated tubulin (AcTub)	mouse	monoclonal	Merck KGaA	T7451	AB_609894	1:500	*foxp2* CRISPR
anti-rabbit IgG Alexa Fluor 488	rabbit IgG	goat	polyclonal	Thermo Fisher Scientific	A-11034	AB_2576217	1:1000	
anti-mouse IgG Alexa Fluor 488	mouse IgG	goat	polyclonal	Thermo Fisher Scientific	A-11029	AB_138404	1:1000	

Microscopy and image processing

Light microscopy: Images of RNA ISH on whole-mounts, adult slices, and cryosections were taken on a Zeiss Axiophot light microscope through three Plan-Neofluar objectives (2.5x/0.075, Ph2 20x/0.50, and 40x/0.75) by a Zeiss AxioCam MRc digital camera and the AxioVision Rel.4.8 Ink. software (Carl Zeiss AG, Oberkochen, BW, Germany). Single images of adult brain slices were merged into a final composite by the grid/collection stitching plugin of ImageJ (Preibisch et al. 2009).

Live images of 5 dpf old larvae were taken at a Nikon SMZ1000 stereomicroscope equipped with a Nikon Plan Apo 1x objective (Nikon, Minato, TKY, Japan) and a Canon EOS 550D SLR digital camera (Canon, Ōta, TKY, Japan).

Fluorescence microscopy: Image acquisition of IHC - RNA ISH double labelings was performed at a Leica DMI 6000B fully automated inverted fluorescence microscope by a monochrome Leica DFC350 FX digital camera through an HCX PL APO 63x/1.40 0.60 DIL oil-objective (Leica Camera AG, Wetzlar, HE, Germany). The digital camera was connected to the Leica Application Suite software (LAS 2.7.0.9329), which automatically generated a merged composite of single images after the acquisition was completed.

Images for size measurements were taken at a Leica M205 FA fluorescence microscope through a Leica Planapo 1.0x objective with a Leica DFC 420C digital camera. The camera was connected to the Leica Application Suite V3.8 Ink. software (Leica Camera AG, Wetzlar, HE, Germany).

Confocal laser-scanning microscopy: Image acquisition on anti-AcTub and anti-cCasp3 immunostained specimens was performed at a Zeiss LSM 780 confocal microscope through a Plan APO

20x/0.8 objective. The confocal microscope was equipped with a Lasos Argon 488 nm laser (Lasos Lasertechnik GmbH, Jena, TH, Germany) and connected to the ZEN 2012 SP1 software (Carl Zeiss AG, Oberkochen, BW, Germany). Following acquisition, images were processed by brightness adjustment and background subtraction in Fiji 2.0.0 (Schindelin et al. 2012) for better visibility. For background subtraction, the sliding paraboloid algorithm of ImageJ (Sternberg 1983) was applied first before the images were processed by a convoluted background subtraction with a Gaussian convolution filter of the ImageJ toolbox BioVoxxel (Brocher 2015, Jan 5).

Anti-Gad1b and anti-GABA immunolabeled specimens were imaged with a Nikon Eclipse Ti confocal microscope through a Plan APO VC 20x/0.75 objective. The confocal microscope was equipped with a Coherent Sapphire 488 nm laser (Coherent, Santa Clara, CA, USA) and connected to the NIS Elements AR 3.22.15 software (Nikon, Minato, TKY, Japan). After image acquisition, brightness was adjusted using Fiji 2.0.0. (Schindelin et al. 2012).

Final figures were arranged in the vector graphics software Inkscape 1.0.1. (www.inkscape.org).

Quantifications and size measurements

Size measurements: Different size parameters of fixed 24 hpf old embryos were assessed using Fiji 2.0.0. (Schindelin et al. 2012). Size differences were determined based on head area, yolk diameter, and total length. The head area comprised the region between the most anterior part of the head and the midbrain-hindbrain boundary. The yolk diameter was measured between the edge of circular and elongated yolk sac and the center of the most ventral part of the eye. To assess the total length, the distance between the posterior end of the tail (ignoring the fin) and the dorsal part of the midbrain-hindbrain boundary was measured. Size parameters were all determined in squared pixels (pixel^2).

Quantification of commissure and tract formation: Based on a qualitative rating scale ranging from zero to four, five fully blinded raters assessed the commissure and tract formation in 24 hpf old *foxp2* mutants and wildtype siblings. For the assessment, confocal images on anti-AcTub stainings processed by brightness adjustment and background subtraction were used.

The applied rating scale was established on images of anti-AcTub stained wildtype individuals and comprised the following levels: (0) commissures/tracts are entirely absent, (1) single commissure/tract fibers are visible but diffusely stained, (2) several commissure fibers are visible, but the overall fiber bundle appears smaller, (3) commissures/tracts are entirely present, but less distributed (4) wildtype-like commissure and tract formation.

Cell number quantification: The total number of Gad1b- or GABA-positive cells in 30 hpf old mutants, morphants, and wildtypes was assessed either by manual cell counting or by an automatic approach based on a recently published machine learning interface (Segebarth et al. 2020) kindly provided and applied by Dennis Segebarth and Robert Blum. For manual counting itself, but also to provide training material to the algorithm, the ImageJ plugin "Cell Counter" by Kurt De Vos (2001) was applied on brightness-adjusted confocal images. Cell number quantification was performed separately on the hindbrain and forebrain/midbrain.

Data processing and statistical analysis

The open-source interface R-Studio (RStudio Team 2020) was used for data processing, data plotting, and statistical analysis. For each behavioral experiment, one test trial was performed to determine the corresponding effect sizes (based on Cliff's delta in the *effsize* package (Vargha and Delaney 2000)) and calculate appropriate sample sizes (by the software G^*Power3.1.9.4 (Faul et al. 2007, 2009), α and β set to 0.05) accordingly. Most datasets were standardized by z-score transformation to pool or compare behavioral data extracted by different versions of the tracking software. The distribution of individual datasets was determined by Shapiro-Wilk's test, and statistical tests were selected accordingly. Group differences between two samples were calculated by the unpaired Wilcoxon sign rank test (non-parametric) or the unpaired t-test (parametric) and between multiple samples by the Kruskal-Wallis rank sum test (non-parametric) or by one-way ANOVA (parametric). To control for alpha inflation due to multiple group comparisons, the Tukey's HSD post hoc test or Dunn's post hoc test was applied for parametric or non-parametric data, respectively. In addition, the Benjamini-Hochberg stepwise adjustment was applied to control the false discovery rate. The overall significance level was set to 0.05.

4 Results

4.1   Metabotropic glutamate receptor 8 (Grm8a/Grm8b)

4.1.1   Characterization and comparison of *grm8a* and *grm8b* spatio-temporal expression pattern in the developing and mature zebrafish brain

ADHD represents a disorder of the brain with reported structural and functional changes for the patient's developing and mature CNS. Consequently, promising risk candidates combine expression in the developing and mature CNS with functional relevance for developmental and/or neurobiological processes. RNA *in situ* hybridization (ISH) is a crucial technique to verify the former and speculate about the latter. Through transcript labeling on whole-mount or sectioned specimens, individual gene expression is localized and, if performed across developmental stages, provides information on how expression progresses over time. To characterize the gene expression pattern of the *GRM8* zebrafish paralogs *grm8a* and *grm8b* and extract both spatial and temporal information, RNA ISH was performed on embryonic (24 hpf, 30 hpf, 36 hpf, 48 hpf), early larval (72 hpf), and adult zebrafish tissue. Expression of *grm8a* and *grm8b* in the zebrafish CNS was already confirmed for early larval stages (Haug et al. 2013) however has not yet been investigated with regard to its developmental trajectory.

Embryonic and early larval development:

The expression patterns of both paralogs display common and distinct expression domains during development (summarized in Table 11). Both paralogs show restricted expression at early and broad expression at later developmental stages, although the temporal effect is more pronounced for *grm8a*. Transcripts are revealed first at 24 hpf with presence in the telencephalon and ventral tegmentum for both, and in the hypothalamus and the medulla oblongata for *grm8b* only (Fig. 8). For both paralogs, the expression pattern observed at 24 hpf maintained with progressing development and expanded and/or were accompanied by expression in divergent brain regions (Fig. 8, Fig. 31, Fig. 32).

Brain regions with a similar expression for *grm8a* and *grm8b* (Fig. 8, Fig. 31, Fig. 32) comprise the subpallium (30-72 hpf), the ventral tegmentum (24-72 hpf), the optic tectum (72 hpf), and the ganglion and inner nuclear layer of the retina (72 hpf). Regions with comparable expression but with temporal discrepancies (most likely attributable to staining quality) are the preoptic region (8a: 36-72 hpf; 8b: 30-72 hpf) and the hypothalamus (8a: 30-72 hpf; 8b: 24-72 hpf).

In the medulla oblongata, both expression patterns differ in temporal and spatial distribution. While *grm8a* expression appears in bilateral stripes at 30 hpf (Fig. 31C-D, K-N), *grm8b* transcripts are detected in scattered cell clusters first (24 hpf) before expression adapts a similar stripe-like pattern by 48 hpf (Fig. 8B). Besides, at 72 hpf *grm8a* is expressed in the medial anterior medulla oblongata (MO, Fig. 31R (arrows)), a subregion that is assumed to integrate sensory and modulatory input and provide regulatory output onto (pre-)motor areas (Naumann et al. 2016).

Divergent temporal distribution of *grm8a* and *grm8b* transcripts is observed for the thalamus and the olfactory bulb. In the thalamus, *grm8a* transcripts are detected first (36 hpf, Fig. 8A) before *grm8b* expression is revealed at 72 hpf (Fig. 32O). Further, the most anterior telencephalon, which gives rise to the olfactory bulbs, displays distinct *grm8b* transcript labeling until 72 hpf (Fig. 8B, 32O) when *grm8a* expression is detected as well (Fig. 31O).

Besides brain regions with similar expression patterns or minor temporal or spatial variations in transcript localization, distinct expression of *grm8a* or *grm8b* is observed in some areas. Areas exclusively labeled for *grm8a* transcripts are the posterior tuberculum with expression starting at 30 hpf (Fig. 31K), the cerebellum with first transcripts labeled at 48 hpf (Fig. 8A), and the pretectum labeled at 72 hpf (Fig. 31O, Q). Interestingly, like the medial anterior MO, these regions were shown to be involved in sensorimotor integration and/or motor control (Ahrens et al. 2012, Naumann et al. 2016, Jha and Thirumalai 2020).

Distinct *grm8b* expression was observed for the pallium (Fig. 8B, Fig. 32K), a brain area assumed to comprise equivalents to the mammalian isocortex (central pallium), the amygdala (medial pallium), and the hippocampus (dorsolateral pallium) (Ganz et al. 2015, Mueller et al. 2011).
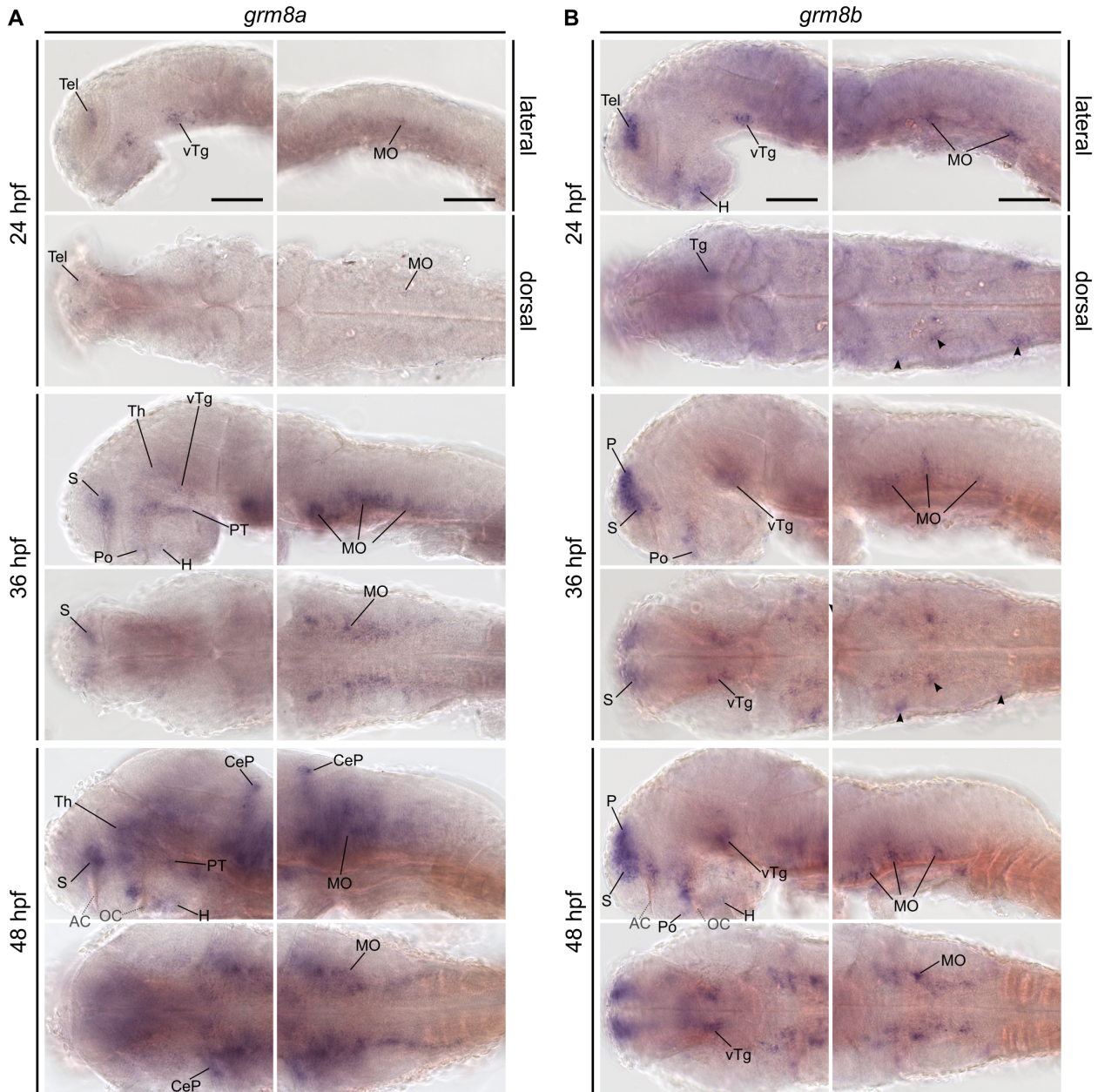
Figure 8: **Comparison of *grm8a* and *grm8b* transcript labeling in the developing CNS of zebrafish.** *grm8a* (A) and *grm8b* (B) whole-mount RNA *in situ* hybridization in the developing CNS of 24 hpf, 36 hpf, and 48 hpf old wildtype zebrafish embryos. Developmental stage increases from top to bottom, presented from lateral and dorsal views with anterior displayed to the left. Details on both expression patterns are described in the main text. A summary of both expression patterns is given in Table 11. For anatomical abbreviations, see Table 13. Scale bars represent 100 μm. Adjusted from Lueffe et al. 2021b.

To summarize, the present data confirm *grm8a* and *grm8b* expression in the developing CNS of zebrafish. Further, temporal and spatial discrepancies suggest that both paralogs take over common and distinct functions during (neuro-)development. Distinct functions may comprise sensorimotor integration and/or motor control for Grm8a and functional properties related to the mammalian limbic system, such as fear or associative learning for Grm8b. However, paralog-specific functional investigations are required to examine these hypotheses further.

Adult brain:

Brain regions with previously distinct expression for *grm8a* or *grm8b* become more similar with time. This process is exemplified by the pallium, the thalamus, and the posterior tuberculum. The distinct expression during embryonic development (Fig. 8, Fig. 31C, E, G, K, Fig. 32C, E, G, K) aligns until 72 hpf (Fig. 31I, O, Fig. 32I, O) and diminishes when adulthood is reached (Fig. 9, Fig. 10). In adulthood, both *grm8a* and *grm8b* are expressed in the lateral, medial, and posterior pallium (P, Fig. 9A-E, Fig. 10A-D), in the ventral (VT, Fig. 9E, Fig. 10D-E) and dorsal thalamus (DT, Fig. 9F-G, Fig. 10F-G) and the periventricular nucleus of the posterior tuberculum (TPp, Fig. 9F-G, Fig. 10F-G) and the area encompassing the posterior tubercular nucleus or the paraventricular organ (PTN/PVO, Fig. 9F-H, Fig. 10F-H).

Brain regions with similar patterns for both paralogs during development remain similar in the adult brain. This comprises expression in the subpallium (S, revealed in the central, ventral, and dorsal subpallium, and the entopeduncular nuclei (EN, Fig. 9C-E, Fig. 10B-D)), the preoptic region (Po, Fig. 9D-E, Fig. 10D), the hypothalamus (with expression in the diffuse nucleus of the inferior lobe (DIL, Fig. 9G, Fig. 10G), the lateral hypothalamic nucleus (LH, Fig. 9H, Fig. 10G-H) and the ventral, dorsal and caudal zone of the periventricular hypothalamus (Hv, Hd, Hc, Fig. 9F-I, Fig. 10E-J)), the tegmentum (with expression in the area encompassing the lateral valvular nucleus and dorsal tegmental nucleus (NLV/DTN, Fig. 9I, Fig. 10I)) and the optic tectum (with expression in the periventricular gray zone (PGZ, Fig. 9F-I, Fig. 10F-J)).

Diencephalic nuclei in the caudal tuberculum that were not explicitly described in the developing brain comprise the torus lateralis (TLa, Fig. 9G, Fig. 10G) and the preglomerular nuclei (PG, Fig. 9H-I, Fig. 10G), both with comparably weaker labeling for *grm8b* transcript.

Notably, less pronounced *grm8b* expression in the developing cerebellum maintains into adulthood (with expression in the corpus cerebelli (CCe, Fig. 9I-K, Fig. 10H-K), the valvular cerebelli (Va, Fig. 9H-I, Fig. 10G-I), the medial octavolateralis nucleus (MON, Fig. 9J, Fig. 10K) and the eminentia granularis (EG, Fig. 9J, Fig. 10K)). Similarly, *grm8b* expression remains comparably weak in the pretectum (periventricular pretectal nucleus (PP, Fig. 9F-G, Fig. 10F-G)). Interestingly, pretectum and/or cerebellum are connected with the reticular formation

(RF), the vagal lobe (LX), and the torus semicularis (TS) (Kaslin and Brand 2016,Kramer et al. 2019), three brain regions exclusively labeled for *grm8a* transcript in the adult brain (Fig. 9I-M).

The comparably restricted pattern of *grm8b* expression observed in the developing MO is observed in the adult brain too. While *grm8a* transcript is detected in the reticular formation (RF, Fig. 9J-M), the vagal motor nucleus (NXm, Fig. 9L-M) and the vagal (LX, Fig. 9L-M) and facial lobe (LVII, Fig. 9L), *grm8b* transcript is restricted to the facial (LVII, Fig. 10L) and the glossopharyngeal lobe (LIX, Fig. 10L).

The only structures with consistently stronger *grm8b* transcript labeling are the olfactory bulbs (OB, Fig. 10A). Despite a generally higher staining intensity for *grm8a* at 72 hpf (Fig. 31I-J, O-S) and in the adult brain (Fig. 9), *grm8a* expression is less pronounced in the olfactory bulbs at both developmental time points.

In summary, reported *grm8a* and *grm8b* expression in the embryonic, larval, and adult brain confirms and complements expression studies in zebrafish (Haug et al. 2013) and other vertebrate species (Duvoisin et al. 1995, Saugstad et al. 1997, Shigemoto et al. 1997, Messenger et al. 2002). With verified expression in brain tissue throughout and after completion of brain development, the present data supports a functional role for both paralogs in the development and maintenance of the CNS in zebrafish. Thus, *grm8a* and *grm8b* are valuable candidates for further investigations on functional circuits that may be implicated in ADHD pathology. Of particular interest for these investigations is the mutual expression in developing and adult brain regions involved in motor functions such as the subpallium (with the entopeduncular nucleus, the proposed equivalent to the internal segment of the globus pallidus (GPi)), the posterior tuberculum, the thalamus, the cerebellum, and the medulla oblongata (with reticular formation, vagal and facial lobe).
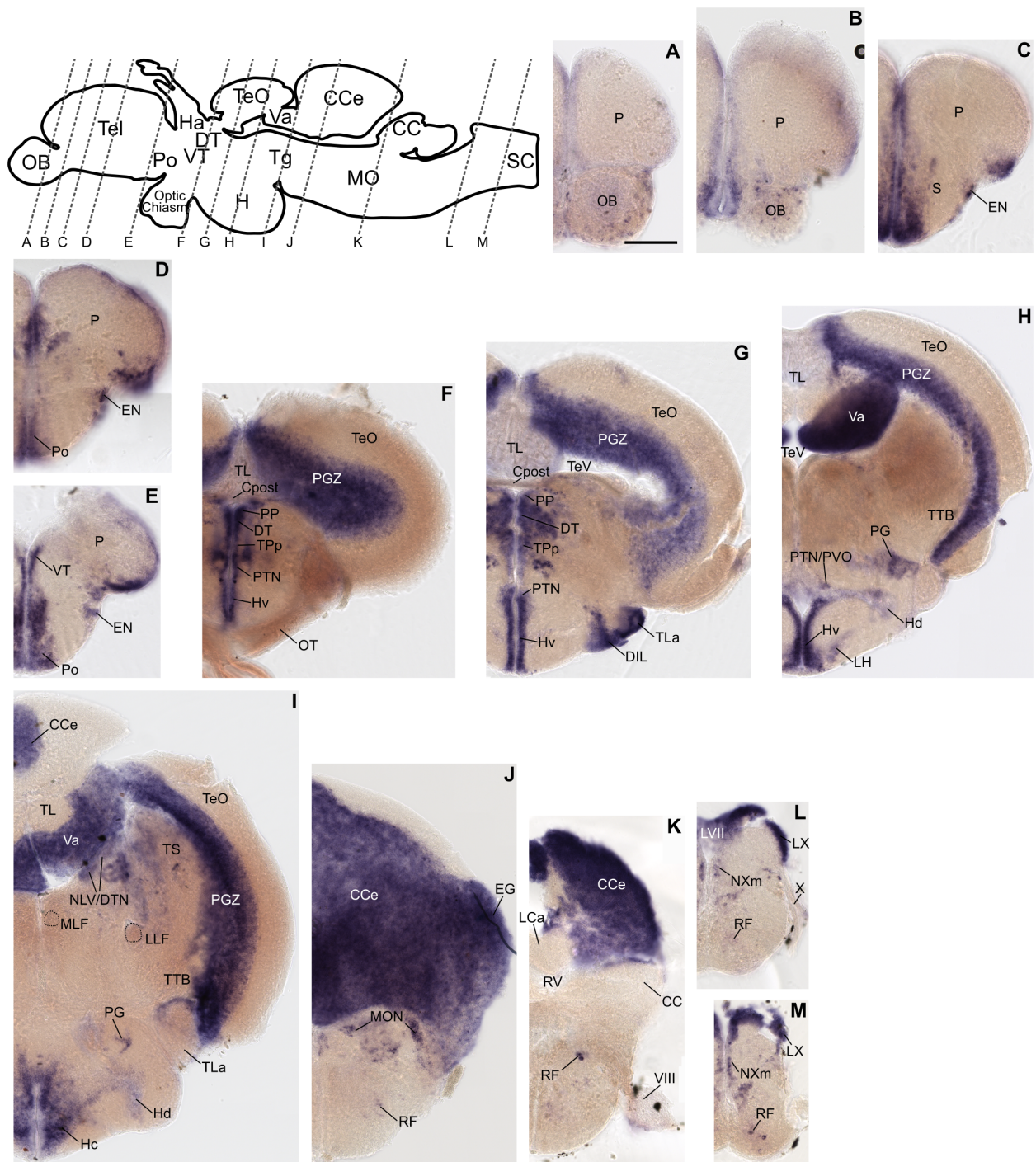
Figure 9: **grm8a expression pattern in the adult brain of zebrafish.** Cross-sections of adult zebrafish brains labeled for *grm8a* transcripts by RNA *in situ* hybridization. Sections are sequentially displayed from anterior to posterior as indicated by the scheme. Corresponding cutting sites are illustrated by dashed lines in the scheme. A detailed description of *grm8a* expression is part of the main text. For anatomical abbreviations, see Table 13. Scale bar, 200 μm. Adjusted from Lueffe et al. 2021b.
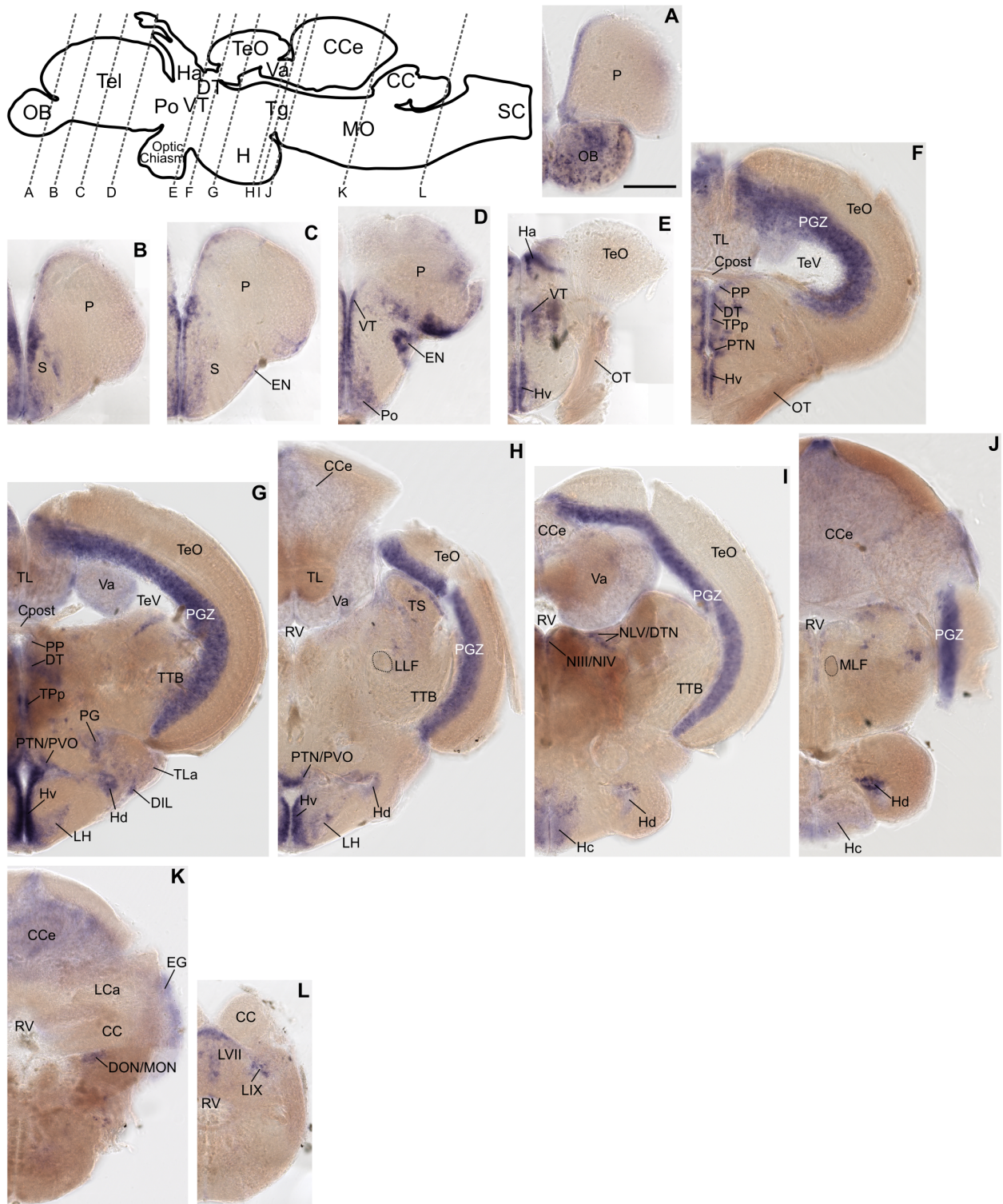
Figure 10: **grm8b expression pattern in the adult brain of zebrafish.** Cross-sections of adult zebrafish brains labeled for *grm8b* transcripts by RNA *in situ* hybridization. Sections are sequentially displayed from anterior to posterior as indicated by the scheme. Corresponding cutting sites are illustrated by dashed lines in the scheme. A detailed description of *grm8b* expression is part of the main text. For anatomical abbreviations, see Table 13. Scale bar, 200 μm. Adjusted from Lueffe et al. 2021b.

4.1.2   *grm8a* is expressed by a subset of GABAergic and monoaminergic cells in the developing CNS of zebrafish

Type III metabotropic glutamate receptors (mGluRs III), including GRM8, are located at the presynapse and function as release regulator for various neurotransmitter (Shigemoto et al. 1997, Cartmell and Schoepp 2000, Schoepp 2001, Corti et al. 2002, Ferraguti et al. 2005, Marabese et al. 2005, Swanson et al. 2005). Accordingly, mGluRs III are expected to be critical for balanced facilitation and inhibition of excitatory and inhibitory synaptic transmission in the nervous system (Piet et al. 2003, Panatier et al. 2004, Bragina et al. 2015). Several psychiatric disorders, including ADHD, are linked to neurochemical alterations that are assumed to disrupt the equilibrium of excitation and inhibition in the nervous system of patients, known as E/I imbalance (Bollmann et al. 2015, Gao and Penzes 2015, Nelson and Valakh 2015, Canitano and Pallagrosi 2017, Foss-Feig et al. 2017). Hence, determining the transmitter identity of *grm8* expressing cells in different brain regions is vital to understand which transmitter system(s) might be affected by Grm8 loss of function.

Two-color RNA ISH (Fig. 11, Fig. 34, Fig. 35) or (one-color) RNA ISH combined with IHC (Fig. 12) were carried out on wildtype (36, 48 and 72 hpf) or Etvmat2:GFP transgenic zebrafish (72 hpf), respectively, to reveal *grm8a* expression in GABAergic (*gad1a*-positive) or monoaminergic (*vmat2*-positive) cells during development. The GABAergic and monoaminergic transmitter systems were investigated due to several associated ADHD risk candidates such as *GAD1*, *SERT*, *DAT1*, *DRD2-5*, *TPH1-2*, and *NET1* and/or reported neurochemical alterations in ADHD affected individuals (Forssberg et al. 2006, Volkow et al. 2007b), Ludolph et al. 2008, Gizer et al. 2009, Oades 2008, Edden et al. 2012, Bollmann et al. 2015, Ulke et al. 2019, Puts et al. 2020). Moreover, the *grm8a* expression pattern in the medulla oblongata closely resembles characteristic hallmarks of *gad1a* and *gad1b* expression in embryos of the same stage (Fig. 11A-D, Fig. 33).

Technical advantages and a broader expression pattern of *grm8a* compared to *grm8b* RNA ISH (Fig. 8, Fig. 31, Fig. 32), together with a largely similar expression of *gad1a* and *gad1b* (Fig. 33), were major arguments for the selection of *grm8a* and *gad1a* for the following colocalization analysis.
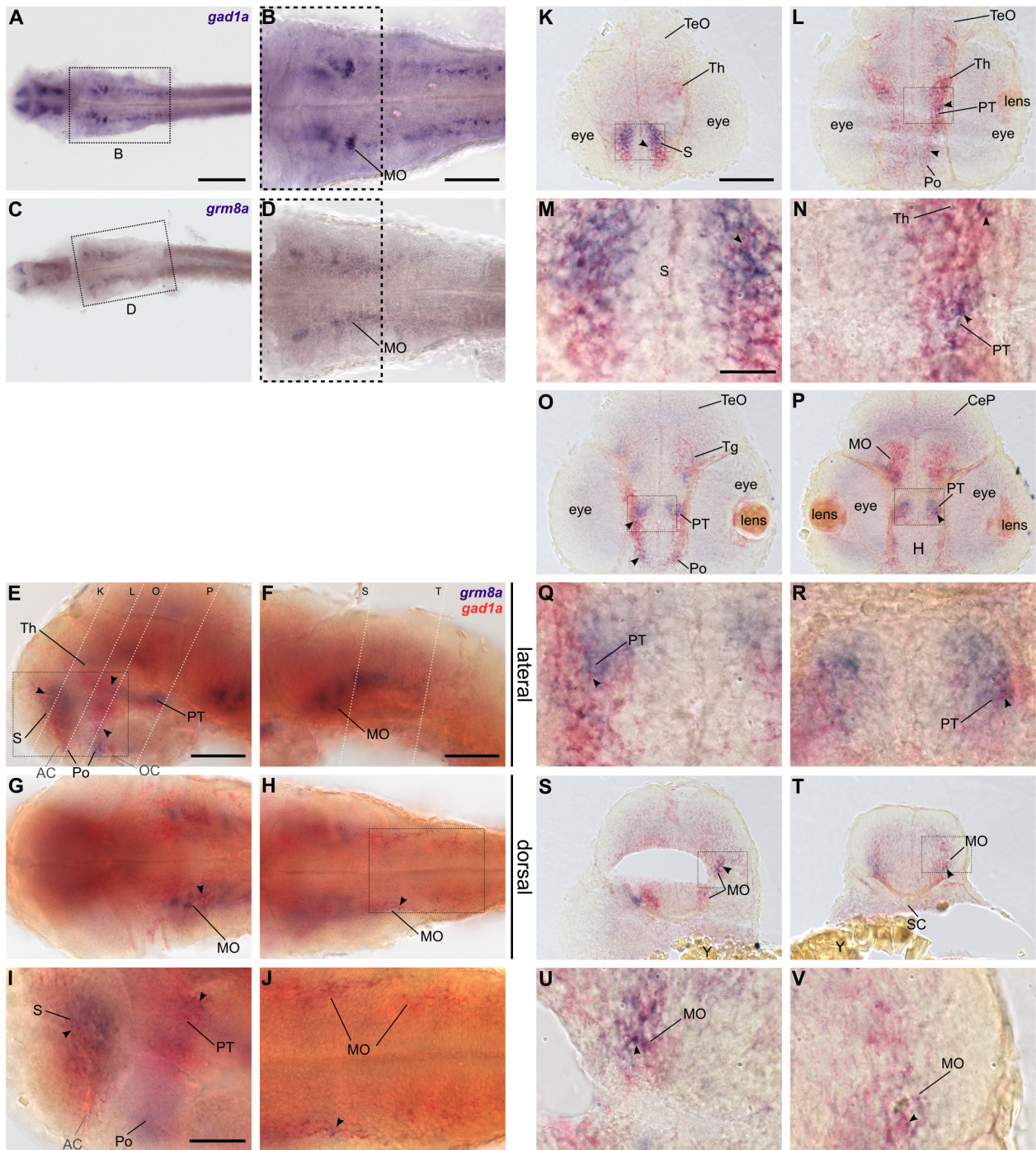
Figure 11: ***grm8a* is expressed by a subset of *gad1a*-positive cells in the developing CNS of zebrafish.** (A-D) Whole-mount preparations of 36 hpf old wildtype embryos labeled for *gad1a* (A-B) or *grm8a* (C-D) transcripts by RNA *in situ* hybridization (ISH) display striking similarities in the hindbrain expression pattern (boxed area). Magnifications of boxed areas in A, C are displayed in B, D respectively. Images are all displayed from dorsal view with anterior displayed to the left. Scale bars represent 200 μm in overview and 100 μm in magnified images (E-J) Whole-mount two-color RNA ISH for *grm8a* (blue) and *gad1a* (red) on 36 hpf old wildtype embryos. Preparations are displayed from lateral (E, F, and I) and dorsal views (G, H, and J) with anterior to the left. Boxed areas in E, H are magnified in I, J, respectively. Dashed white lines in E and F illustrate cutting sites for cross-sections displayed in K-V. Magnifications of boxed areas in K, L, O, P, S, and T are displayed in M, N, Q, R, U, and V, respectively. Arrows indicate brain regions with apparent colocalization that are described in detail in the main text and are listed in Table 11. For anatomical abbreviations, see Table 13. Scale bars represent 100 μm in overview and 50 μm in magnified images. Adjusted from Lueffe et al. 2021b.

grm8a expression in gad1a-positive cells:

For all developmental stages examined, co-localization of *grm8a* and *gad1a* expression was confirmed on whole-mounts and cryosections. Throughout development, co-localization was revealed for the subpallium (S, Fig. 11E, I, K, M, Fig. 34A, E, G, I, Fig. 35A, E, G-J), the thalamus (Th, Fig. 11E, K, L, N, Fig. 34A, Fig. 35A) and the medulla oblongata (MO, Fig. 11F-H, J, P, S-V, Fig. 34B, D, F, K-R, Fig. 35B, D, F, L, O-R). Further, at 36 hpf and 48 hpf, both expression patterns overlap in the posterior tuberculum (PT, Fig. 11E, I, L, N, O-R, Fig. 34A, H, J) and the preoptic region (Po, Fig. 11E, I, L, O, Fig. 34A, E, H). At later stages, *grm8a* and *gad1a* expression colocalize in the optic tectum (TeO, Fig. 34A, H, Fig. 35A, K) and the cerebellum (CeP, Fig. 34B, C, K-L, Fig. 35B, C, L, N, O) at 48 hpf and 72 hpf and in the pretectum at 72 hpf only (Fig. 35A, C, K, M). *grm8a* expression in GABAergic cells beyond described CNS pattern was detected in the inner nuclear layer of the retina (INL, Fig. 35H, K) at 72 hpf. Notably, co-localization was observed with high incidence in previously mentioned brain regions associated with motor functions, including the subpallium, the posterior tuberculum, the thalamus, the cerebellum, and the medulla oblongata.

grm8a expression in vmat2-positive cells:

In contrast to the extensive colocalization of *grm8a* and *gad1a*, the overlap between *grm8a*-positive punctae and *vmat2*-expressing (monoaminergic) cells appears to be restricted to single cells of a a limited number of brain regions. The most frequent overlap was observed for the different cell cluster and tracts of the rostral/intermediate (H, Fig. 12D, H) and caudal hypothalamus (H, Fig. 12I, J, N) as well as for individual cells of the raphe nuclei (Fig. 12K-L, O-P). Additionally, colocalization was revealed for single cells in the optic recess region (ORR, Fig. 12C, G) and the telencephalon (Tel, Fig. 12A, E), whereas an overlap of *grm8a* and *vmat2* expression in the posterior tuberculum (PT, Fig. 12B, F) and the dorsolateral medulla oblongata (MO, Fig. 12I, M) can neither be confirmed nor denied.

To summarize, with the confirmed expression of *grm8a* in a subset of GABAergic and monoaminergic cells across different regions of the developing zebrafish brain, the present data indicates for the first time that Grm8a might be involved in the release regulation of non-glutamatergic

excitation and GABAergic inhibition in zebrafish. Further, the data suggest that besides glutamate, GABAergic neurotransmission might play a pivotal role in behavioral phenotypes induced by Grm8a loss of function.
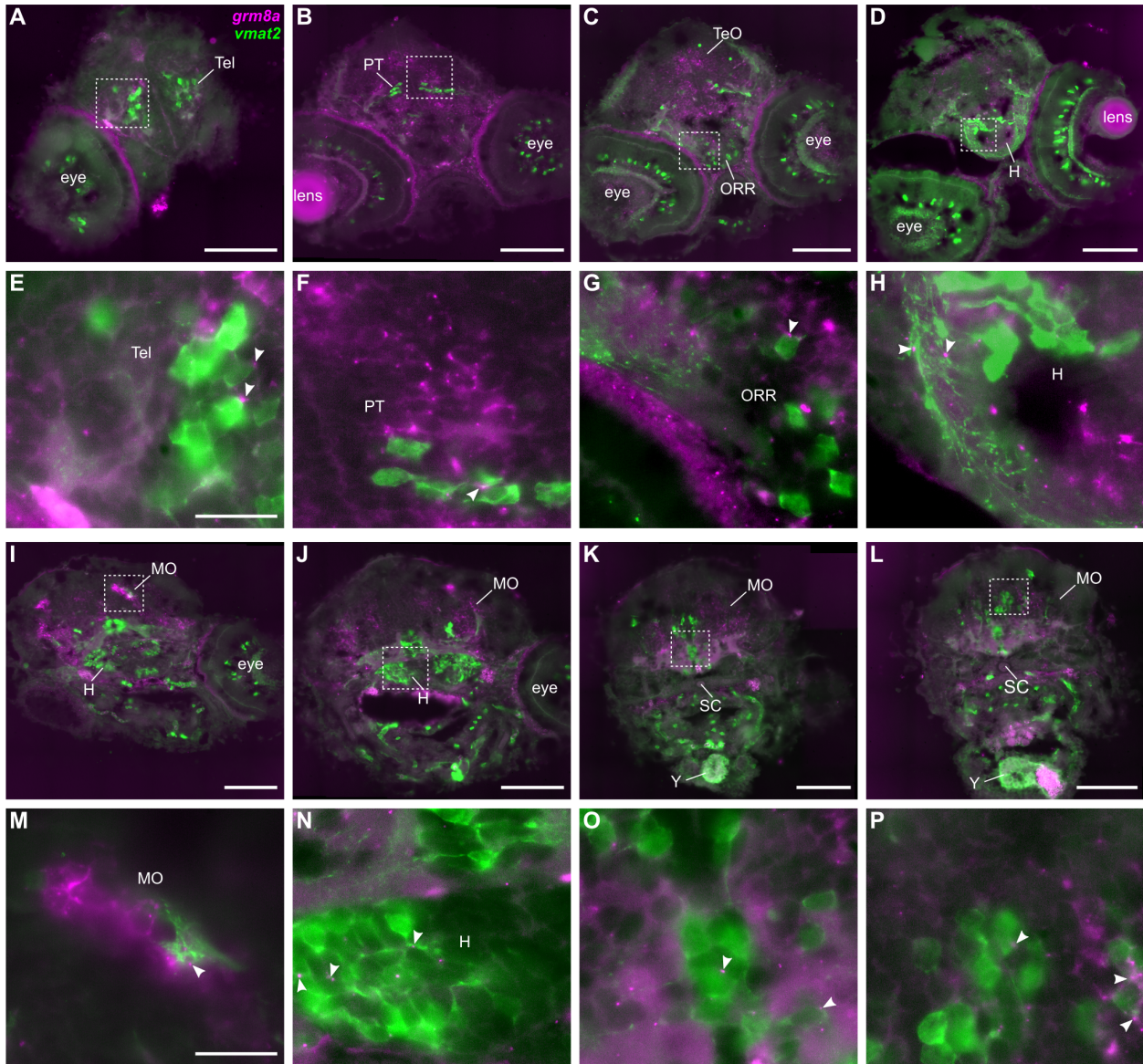
Figure 12: Colocalization of *grm8a* transcript labeling with *vmat2*-expressing cells in the CNS of 72 hpf old transgenic zebrafish larvae. Cross-sections of Tg(Etvmat2:GFP) larvae (72 hpf) labeled for *grm8a* transcripts by RNA *in situ* hybridization (magenta) and for expressed GFP (green) by immunohistochemistry. Magnifications of boxed areas in A-D and I-L are displayed in E-H and M-P, respectively. Arrows indicate colocalization or close proximity of *grm8a*-positive punctae and anti-*vmat2*:GFP immunolabeling. Brain regions with apparent colocalization are described in the main text and summarized in Table 11. Anatomical abbreviations are listed in Table 13. Scale bars represent 100 μm in overview and 20 μm in magnified images.

Table 11: **Summary of the spatio-temporal expression pattern for *grm8a* and *grm8b* and regional overlap with *gad1a* transcript or *vmat2*:GFP labeling.** Developmental stage is given in "hours post fertilization (hpf)". Anatomical abbreviations are listed in Table 13. "Grey" indicates temporal differences of (possibly) low relevance due to differences in staining quality. "Blue" points out temporal differences between both expression patterns. "Red" highlights distinct expression domains and "orange" or "yellow" label expression domains that display colocalization with *gad1a* transcript (at 36 hpf, 48 hpf, and/or 72 hpf) or *vmat2*:GFP labeling (at 72 hpf), respectively.

	OB	Tel	S	P	Po	Th	Pr	H	PT	vTg	TeO	CeP	MO	GCL	INL
grm8a															
24 hpf		x								x					
30 hpf			x					x	x	x		x			
36 hpf			x		x	x		x	x	x		x			
48 hpf			x		x	x		x	x	x		x			
72 hpf	x		x		x	x	x	x	x	x	x	x	x	x	x
overlap with *gad1a*		x		x	x	x	x	x				x			x
overlap with *vmat2*:GFP		x						x	x			x			
grm8b															
24 hpf		x						x		x			x		
30 hpf			x	x	x			x		x			x		
36 hpf	x		x	x	x			x		x			x		
48 hpf	x		x	x	x			x		x			x		
72 hpf	x		x		x	x		x		x	x		x	x	x

4.1.3   Generation and genetic and morphological validation of *grm8a* and *grm8b* splice-morphants

The successful verification of *grm8a* and *grm8b* expression in the developing and mature brain suggests a functional role for both paralogs in the CNS of zebrafish that needs further investigation. Experimental data on GRM8/Grm8a/Grm8b function is limited in mammals (Linden et al. 2002, Duvoisin et al. 2005, Schmid and Fendt 2006) and absent in zebrafish. Hence two complementary strategies, namely a splice-morpholino-derived knockdown and a gene-editing-induced knockout by CRISPR/Cas9, were applied to generate paralog-specific loss of function zebrafish models for *grm8a* and *grm8b*.

The splice-morpholino-derived knockdown approach has significant advantages for the functional characterization of GRM8 paralogs. First, the knockdown strategy is expected to mimic copy number deletions (observed for *GRM8* in ADHD patients (Elia et al. 2012)) more realistically than a complete functional knockout. Secondly, the transient effect, but also the knockdown strategy in general, bears lower risks for compensatory mechanisms like upregulation of paralogous genes (Rossi et al. 2015, El-Brolosy et al. 2019).

The splice-morpholinos are expected to target the splice-donor of *grm8a* exon 4 (Fig. 13A) or *grm8b* exon 3 (Fig. 13D). In both cases, the splice-morpholino causes exon exclusion of *grm8a* exon 4 (Fig. 14A) or *grm8b* exon 3 (Fig. 14E). The corresponding misspliced transcripts were detected at 24 hours post fertilization (hpf) for *grm8a* (Fig. 13B) and at both 24 hpf and 5 dpf

for *grm8b* (Fig. 13E). In addition, morphants show a reduction of wildtype transcript besides comparable cDNA levels (*β-actin*, Fig. 13B, E). Missplicing, in either case, causes a frameshift and suggests a premature disruption of translation by the induced stop codon in *grm8a* exon 5 (Fig. 13B) or *grm8b* exon 4 (Fig. 13E) that both encode parts of the ligand-binding domain (for full-length amino acid sequence see Fig. 16B, D). Accordingly, functional domains located downstream of the induced stop codon, like transmembrane domains, are expected to be lost in the truncated gene product.

Previous studies on *Grm8* knockout mice revealed no morphological abnormalities except occasional reports on differences in weight gain (Gerlai et al. 2002, Linden et al. 2002, Duvoisin et al. 2005). Similarly, the overall morphology of *grm8a* and *grm8b* morphants is normal (Fig. 13C, F). However, size measurements revealed a differential effect on total body length with decreased (Fig. 14B) or increased body length (Fig. 14F) upon *grm8a* or *grm8b* knockdown, respectively. Additional parameters like head size or yolk diameter are not affected (Fig. 14B, F). Likewise, there is no apparent effect on cell apoptosis (Fig. 14D, G). The previously reported expression colocalization of *grm8a* and *gad1a* suggests a functional role for Grm8a in GABAergic neurons of the developing zebrafish brain. Interestingly, manual quantifications of GABA-positive cells in immunohistochemically labeled 30 hpf old *grm8a* morphant and uninjected control embryos revealed a differential effect, namely a significantly decreased number (about 50 % less) in forebrain/midbrain and a significantly increased number (about 20 % more) in the respective hindbrain of *grm8a* morphant individuals (Fig. 14C).

In summary, the paralog-specific splice-morpholinos for *grm8a* or *grm8b* effectively induce missplicing, leading to truncated and presumably non-functional gene products. Further, morphological investigations demonstrated that none of the adverse splice-morpholino effects, like induction of anatomical malformations, increased cell death, or delayed development, apply to the presented *grm8a* and *grm8b* morphants. However, a significant effect on body length is noticed in both cases. Of particular interest is the differential effect on GABAergic cell quantity in different brain regions of *grm8a* morphants, despite no apparent effects on cell apoptosis. With preceding observations on *grm8a* and *gad1a* expression colocalization, these quantifications further support a Grm8a function in the GABAergic system of developing zebrafish.
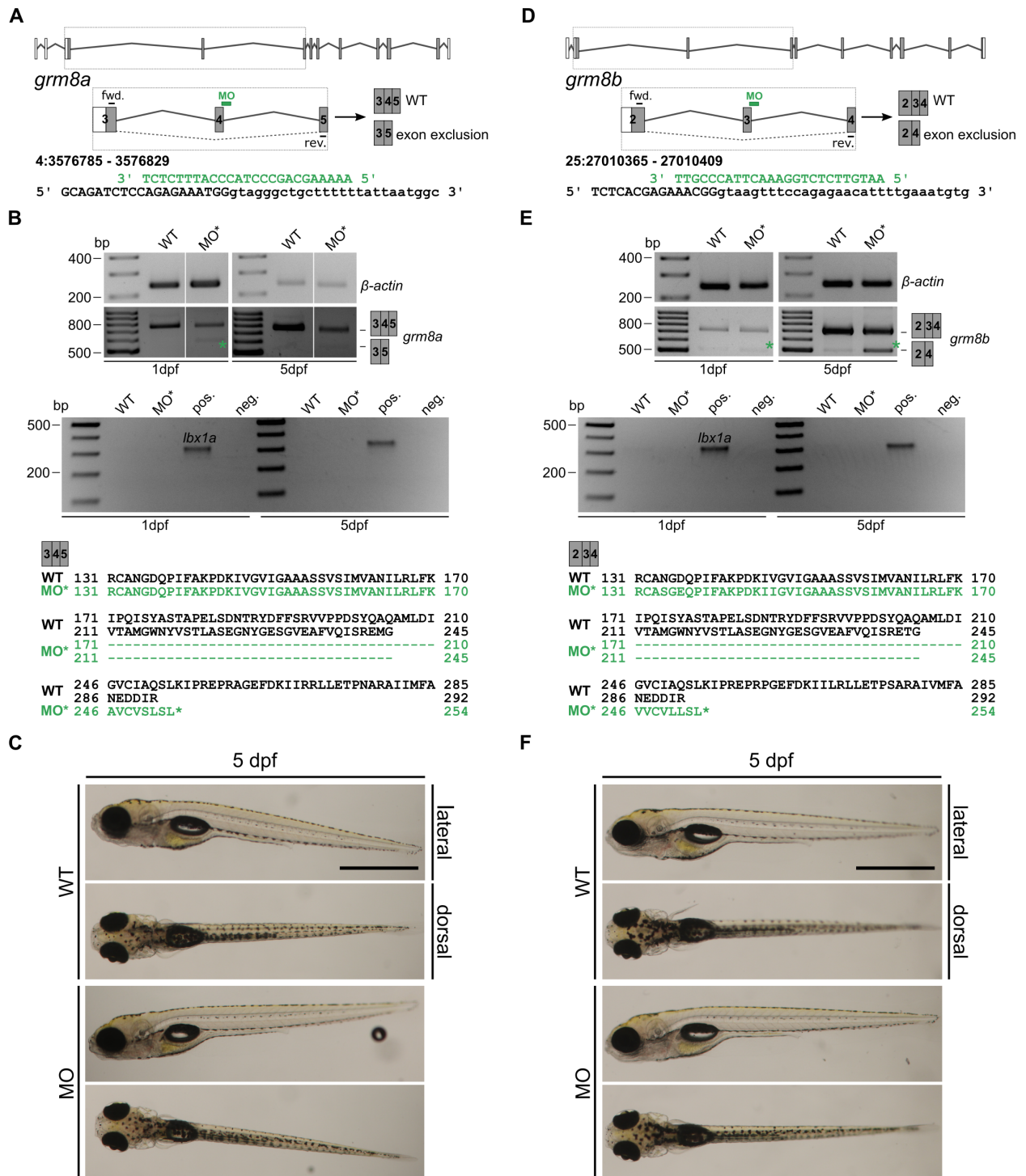
Figure 13: **Validation of paralog-specific splice-morphants for *grm8a* and *grm8b*.** (A, D) Exon-intron structure of *grm8a* (A) and *grm8b* (D) with coding and non-coding exons displayed in grey and white, respectively. Genomic regions containing splice-morpholino (MO, green) and primer binding sites are boxed and magnified below. MO-binding induces missplicing (dashed line) with exon 4 or exon 3 exclusion in *grm8a* (A) or *grm8b* (D), respectively. (B, E) RT-PCR-based verification of exon exclusion detected misspliced transcripts at 1 dpf for *grm8a* (B, green asterisk, 554 bp) and at 1 dpf and 5 dpf for *grm8b* (E, green asterisk, 500 bp) morphants (MO), plus a reduction of wildtype transcript at 5 dpf for *grm8b* (717 bp) and at 1 dpf and 5 dpf for *grm8a* MO (771 bp). MO and uninjected control (WT) probes show comparable levels of cDNA (*β-actin*, 239 bp, top) and no genomic DNA contamination (*lbx1a*, 353 bp, center). Predicted amino acid sequence (bottom) for exon 3-5 (B, *grm8a*) or 2-4 (E, *grm8b*) of wildtype (WT, black) and misspliced transcript (MO, green) suggest a premature disruption of translation by the induced stop-codon (asterisk). (C, F) Live images of 5 dpf old *grm8a* (C) or *grm8b* MO (F) and corresponding uninjected controls (WT) show no gross morphological alterations. Images are all displayed with anterior to the left and from lateral and dorsal views. Scale bar, 1 mm.
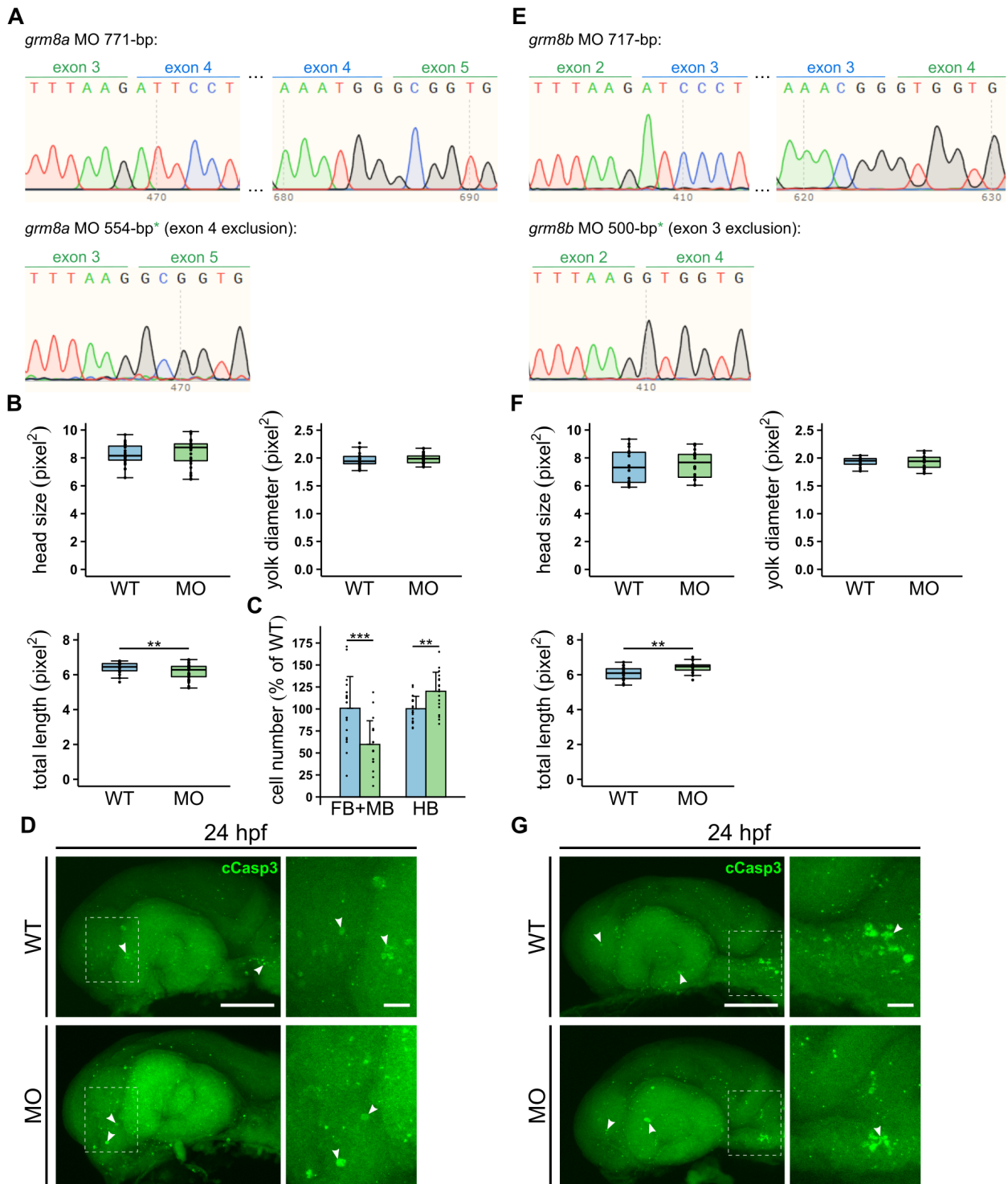
Figure 14: **Genetic and anatomical description of *grm8a* and *grm8b* splice-morphants.** (A, E) cDNA sequencing traces of differentially sized PCR products derived from *grm8a* (A) or *grm8b* (E) morphants (MO). Exon exclusion in the misspliced transcript (bottom and described in Fig. 13) is confirmed by absent *grm8a* exon 4 (A, blue) or *grm8b* exon 3 (E, blue). (B, F) Comparison of head size (top left), yolk diameter (top right) and total length (bottom left) between *grm8a* MO (C green, n=30) or *grm8b* MO (F green, n=20) and corresponding uninjected controls (WT blue, n=23 (*grm8a*), n=15 (*grm8b*)). Size measurements are all given in squared pixel (pixel^2). **P<0.01. (C) Manual quantification of the relative number of GABA-positive cells in the forebrain/midbrain (FB/MB) or hindbrain (HB) of 30 hpf old *grm8a* MO (green, n=10) compared to uninjected controls (WT, blue, n=12). **P<0.01, ***P<0.001. (D, G) Anti-cleaved caspase 3 (cCasp3) immunohistochemistry reveals no apparent effect on cell apoptosis in the CNS of 24 hpf old *grm8a* (D) or *grm8b* MO (G) and uninjected controls (WT). Boxed regions of overview images (left panel) are magnified to the right. Arrows point out individual apoptotic (cCasp3-positive, green) cells. Images are all displayed with anterior to the left. Scale bars represent 100 μm in overview (left) and 20 μm in magnified images (right). C. Drepper contributed to manual cell countings.

4.1.4   Behavioral validation of *grm8a* and *grm8b* splice-morphants revealed alterations in locomotor activity and thigmotaxis behavior

Considerable expression of *grm8a* and *grm8b* in motor regions emphasizes a possible involvement in motor-related functions. Accordingly, a former behavioral study described (novelty-induced) hyperactivity in GRM8-deficient mice, suggesting that GRM8 might be crucial for the regulation of (locomotor) activity (Gerlai et al. 2002). Increased (locomotor) activity is a characteristic hallmark of ADHD symptomatology. Hence investigating the role of Grm8a and Grm8b in activity modulation might be crucial for unraveling pathophysiological mechanisms that underly ADHD endophenotypes such as hyperactivity.

To test for activity changes upon Grm8a and Grm8b loss of function, locomotion of 5 dpf old *grm8a* and *grm8b* morphants was tracked over 10 min, separated into a 5 min habituation and a 5 min test phase (Fig. 15A), and compared to uninjected control larvae of the same developmental stage. Locomotor activity was assessed based on swimming velocity, distance, duration, and number of events for three different activity levels, namely inactivity (< 0.2 cm/s), low activity (0.2 cm/s $<$ and < 1 cm/s) and high activity (> 1 cm/s).

For both *grm8a* and *grm8b* morphants, a significant increase in locomotor activity was observed (Fig. 15B). The detected increase in swimming velocity (total and during low activity) and swimming distance was accompanied by an increased duration of high activity and an elevated number of low and high swimming events. Additionally, the duration of inactivity in both morphant groups was significantly reduced (Fig. 15B). Hence similar to mice (Gerlai et al. 2002), Grm8a and Grm8b seem to be involved in the regulation of (locomotor) activity in zebrafish larvae.

Besides hyperactivity, altered fear response is a frequent observation in *Grm8* knockout mice (Linden et al. 2002, Duvoisin et al. 2005, Robbins et al. 2007) and attributed to GRM8 deficiency in the amygdala (Schmid and Fendt 2006, Fendt et al. 2013). Interestingly, *grm8a* and predominantly *grm8b* expression was detected in the zebrafish pallium, an assumed equivalent to the mammalian amygdala (hippocampus and isocortex) (Ganz et al. 2015, Mueller et al. 2011), suggesting a possible role for Grm8a and/or Grm8b in the regulation of fear-

related behavior in zebrafish larvae. A cross-species involvement of GRM8 in fear regulation is of particular interest due to the substantial comorbidity rate (∼25 %) between ADHD and anxiety disorders with yet unknown biological background (D'Agati et al. 2019).

To test for an altered fear response, the thigmotaxis behavior of *grm8a* and *grm8b* morphants was monitored and compared to uninjected controls. Therefore, each well was virtually subdivided into an inner and outer zone (Fig. 15A), and the duration spent in the outer zone was measured.

Interestingly, *grm8a* morphants showed a significant increase in thigmotaxis behavior, whereas thigmotaxis of *grm8b* morphants was unchanged (Fig. 15C). Although these findings are surprising due to the prominent presence of *grm8b* transcripts in the zebrafish pallium, they confirm the significance of GRM8 (in zebrafish Grm8a) for the regulation of fear response.
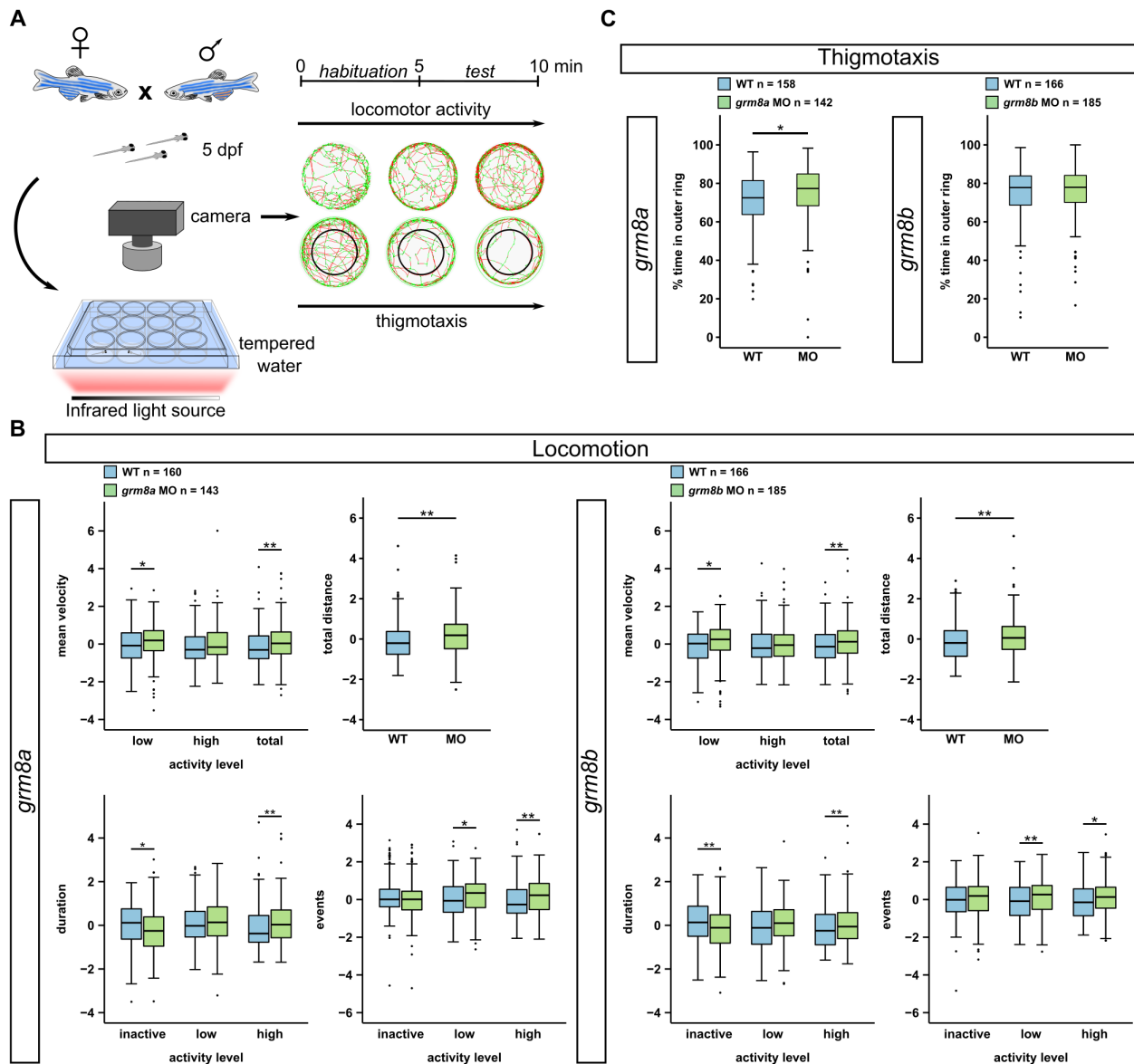
Figure 15: **Investigation of locomotor activity and thigmotaxis behavior of *grm8a* and *grm8b* splice-morphants.** (A) Schematic illustrating animal crossing, behavioral setup, and test procedure for locomotor tracking and thigmotaxis measurements in 5 dpf old larvae. Circles display representative swimming tracks for low (left), intermediate (center), and high (right) locomotor activity/thigmotaxis behavior. Different activity levels are displayed in black (inactivity; < 0.2 cm/s), green (low activity; 0.2 cm/s < and < 1 cm/s) and red (high activity; > 1 cm/s). Adjusted from Lueffe et al. 2021a. (B) Locomotor activity of 5 dpf old *grm8a* (left panel) or *grm8b* (right panel) morphants (MO, green) compared to corresponding uninjected controls (WT, blue). Locomotor activity is determined by mean velocity (during low or high activity or combined (total), top left), total distance swum (top right) and the duration of (bottom left) and number of events (bottom right) for inactivity, low and high activity. Raw datasets were standardized by z-score transformation. (C) Comparative analysis of thigmotaxis behavior for *grm8a* (left, green) or *grm8b* MO (right, green) and corresponding uninjected controls (WT, blue). Thigmotaxis is characterized as the percentage of time spent in the outer ring (A). Sample sizes are given by n at the top. *P<0.05, **<0.01.

4.1.5   Generation and genetic and morphological validation of paralog-specific *grm8* CRISPR/Cas9 mutant lines

Besides previously mentioned benefits of the splice-morpholino approach for functional investigations on Grm8a and Grm8b, detrimental effects like off-target effects or limited reproducibility of the injection volume require independent confirmation of observed phenotypes. CRISPR/Cas9-induced gene editing is successfully applied in zebrafish to induce loss of function mutations (Chang et al. 2013, Hwang et al. 2013, Jao et al. 2013) with a comparatively low off-target mutation rate of 1-2.5 % (Hruscha et al. 2013). Hence, due to its ease, efficacy, specificity, and the possibility to segregate off-target mutation by several outcrosses, CRISPR/Cas9 is a valuable technique to verify observations based on splice-morpholino-derived knockdowns.

For each paralog, several CRISPR/Cas9 mutant lines were generated and genetically identified before two lines with functional mutations were maintained, and one was studied for morphological and behavioral phenotypes. The designed sgRNAs target exon 4 and exon 2 of *grm8a* (Fig. 16A) and *grm8b* (Fig. 16C), respectively. For *grm8a*, sgRNA binding induced a 17 bp deletion in the first (Fig. 16A, Fig. 17A) and a multiple base substitution over 19 bp (Fig. 40A) in exon 4 of the second line. For *grm8b*, a 13 bp (Fig. 16C, Fig. 17E) and a 5 bp deletion in exon 2 (Fig. 40C) were identified. Although not verified, all four mutations are expected to be functional. But morphological and behavioral investigations were restricted to the *grm8a* 17 bp and the *grm8b* 13 bp deletion mutations.

The CRISPR/Cas9-induced 17 bp deletion mutation in *grm8a* exon 4 induces a frameshift and premature stop codon, suggesting a premature termination of translation N-terminal of the ligand-binding domain (Fig. 16B). Similarly, the deletion-induced frameshift in *grm8b* interrupts the amino acid sequence by a stop codon located N-terminal to the ligand-binding domain (Fig. 16D). For both deletion mutations, functional domains located downstream of the induced stop codon, like the seven transmembrane domains, are expected to be lost in the truncated gene product (Fig. 16B, D).
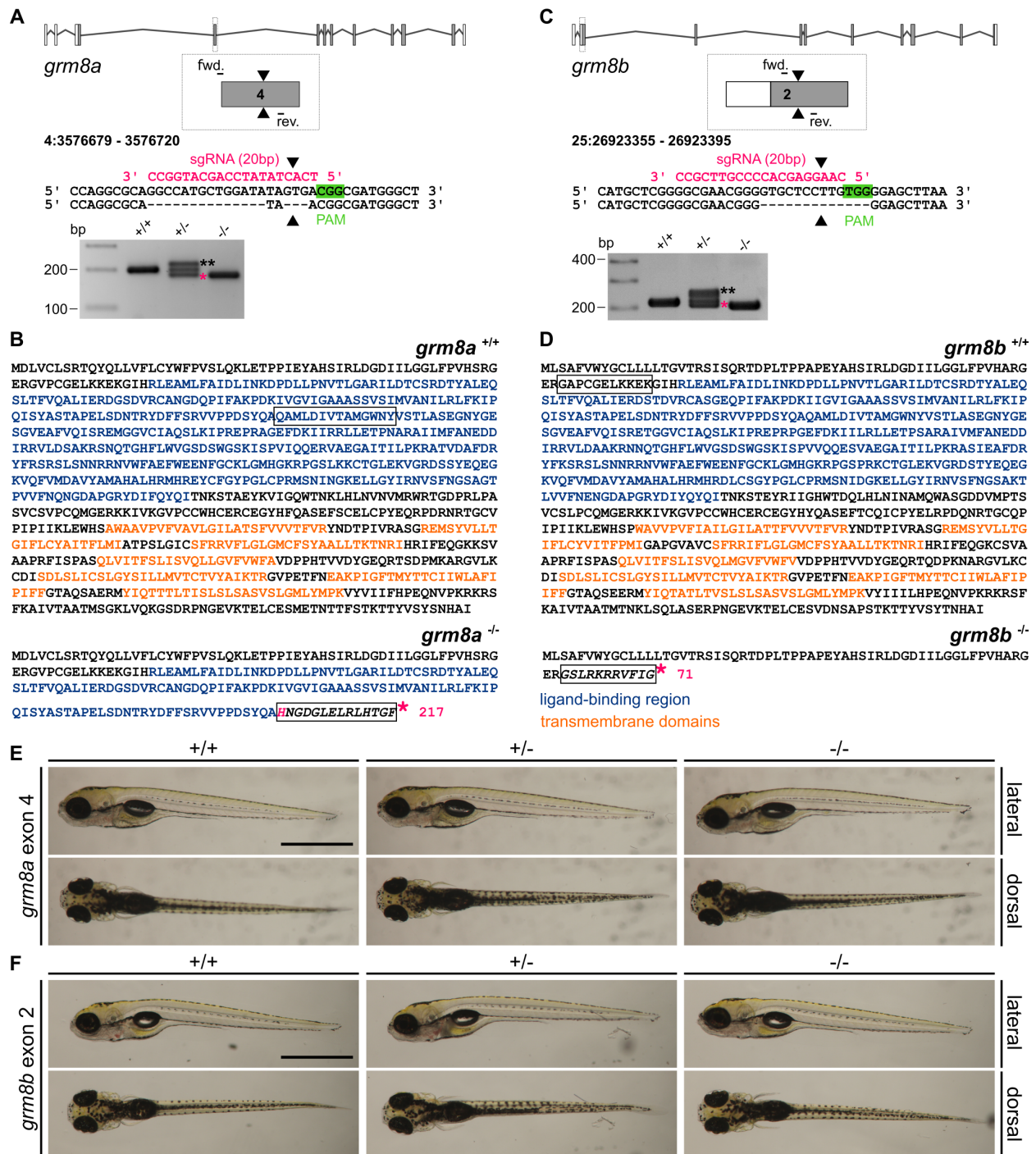
Figure 16: **Generation and verification of paralog-specific CRISPR/Cas9 mutant lines for *grm8a* and *grm8b*.** (A, C) Exon-intron structure of *grm8a* (A) or *grm8b* (C), including coding (grey) and non-coding exons (white). Magnification of exon 4 (*grm8a*) and exon 2 (*grm8b*) illustrating sgRNA (pink) binding and Cas9-induced double-strand break (black triangle) together with primer bindings sites for subsequent genotyping PCR (bottom). The double-strand break induced a 17 bp deletion in *grm8a* (A, center) and a 13 bp deletion in *grm8b* (C, center). The deletion mutations are displayed by a PCR product of 177 bp for *grm8a*^{+/-} and *grm8a*^{-/-} (A, pink asterisk) and of 204 bp for *grm8b*^{+/-} and *grm8b*^{-/-} (C, pink asterisk). Besides, genotyping PCR displays a heterodimer of wildtype and mutated allele for *grm8a*^{+/-} and *grm8b*^{+/-} (black asterisks). (B, D) Predicted amino acid sequence for wildtype (top) and mutated allele (bottom) indicate a frame shift (black box) and subsequently, a premature disruption of translation by the induced stop-codon (pink asterisk) in (B, *grm8a*) or upstream to (D, *grm8b*) the ligand-binding region (blue). Transmembrane domains (orange) located downstream of the induced stop-codon are expected to be lost in the truncated gene product. (E, F) Live images (with anterior to the left) of hetero-([+/-]) and homoallelic ([-/-]) *grm8a* (E) or *grm8b* mutants (F) and corresponding wildtype siblings ([+/+]) revealed no gross morphological alterations. Scale bar, 1 mm. The generation and injection of the sgRNAs were performed by M. Bauer. Adjusted from Lueffe et al. 2021b.

The above described *grm8a* and *grm8b* morphants displayed no morphological alterations (Fig. 13C, F). Similarly, the morphology of *grm8a* (Fig. 16E) and *grm8b* CRISPR/Cas9 mutants (Fig. 16F) is normal. However, unlike morphants, size measurements of mutant embryos detected no significant alterations in body length (Fig. 17C, F) except for a weak but not statistically significant reduction of *grm8b* mutant length (Fig. 17F). Observations on cell apoptosis revealed no difference between mutants and wildtype siblings for both paralogs (Fig. 17D, G). Likewise, investigations on later developmental stages found no indications for early lethality of both mutant lines.

Interestingly, like in *grm8a* morphants (Fig. 14C), the hindbrain of heterozygous *grm8a* mutants contains a larger number of GABAergic cells (Fig. 17B), confirming that the effect is directly related to Grm8a loss of function and not due to any morpholino off-target effect. In contrast, the reduction of GABA-positive cells in forebrain/midbrain regions is not reproduced in *grm8a* mutants (Fig. 17B).

In conclusion, the wildtype-like appearance of *grm8a* and *grm8b* CRISPR/Cas9 mutants confirms previous observations on morphants and indicates that Grm8a and Grm8b are not relevant for anatomical development and survival in general. However, the significant effect on GABAergic cell quantity in the hindbrain of *grm8a* mutants and morphants suggests a region-specific involvement in GABAergic cell proliferation and/or survival .
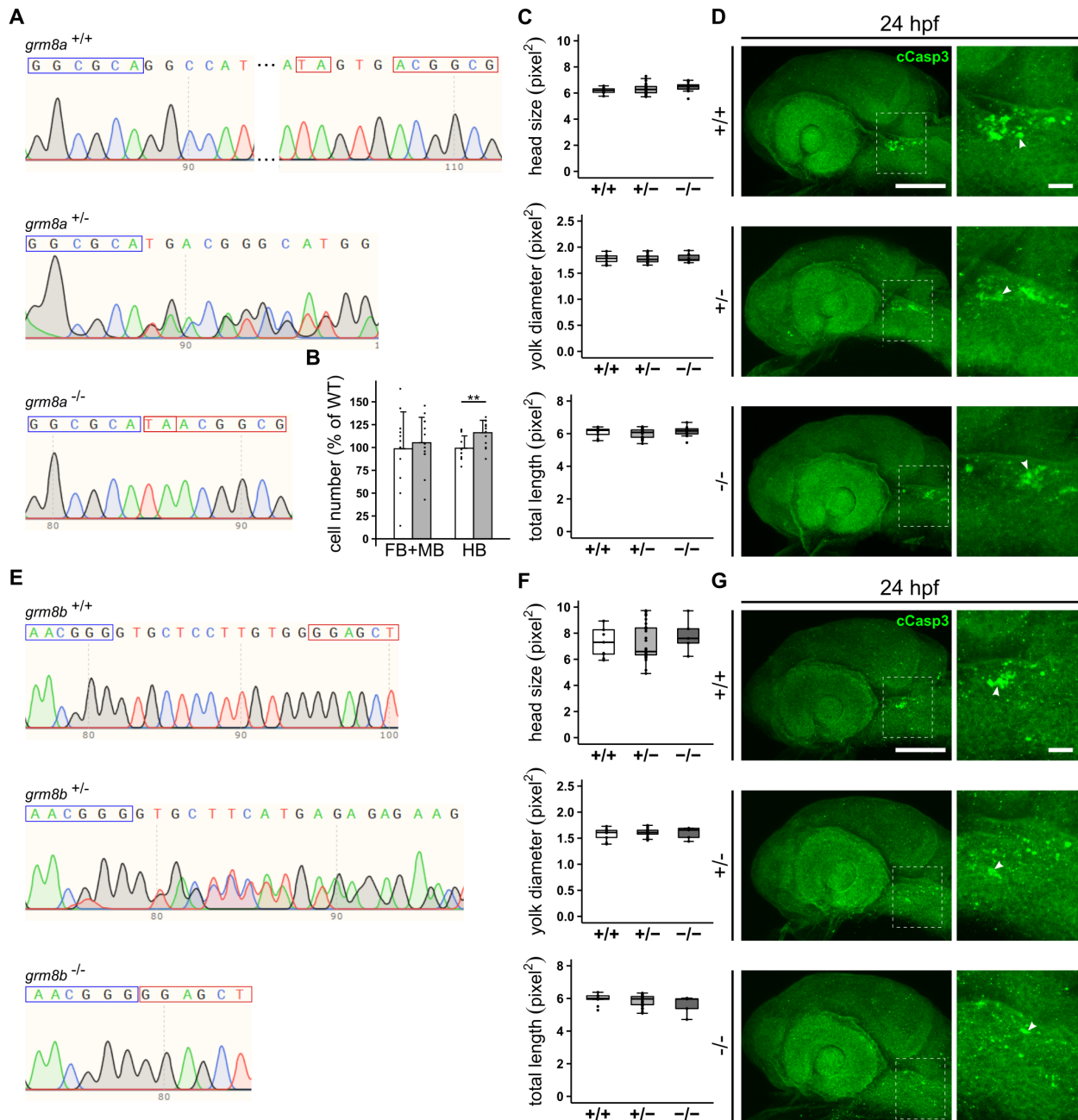
Figure 17: **Genetic and anatomical description of *grm8a* and *grm8b* CRISPR/Cas9 mutants.** (A, E) DNA sequencing traces for *grm8a* (A) or *grm8b* (E) genotyping PCR product derived from hetero- ($^{+/-}$) and homoallelic ($^{-/-}$) *grm8a* (A) or *grm8b* mutants (E) and corresponding wildtype siblings ($^{+/+}$). The deletion mutations (see Fig. 16) in *grm8a* (A) or *grm8b* mutants (E) is confirmed by the loss (between blue and red box) of 17 nt for *grm8a*$^{-/-}$ (A, bottom) or 13 nt for *grm8b*$^{-/-}$ (E, bottom). Heteroallelic *grm8a* (A, center) or *grm8b* mutants (E, center) display multiple traces, starting from the deletion mutation (blue box) onwards and representing a mixture of wildtype (top) and mutated allele (bottom). (B) Relative number of GABA-positive cells in the forebrain/midbrain (FB/MB) and hindbrain (HB) of 30 hpf old *grm8a*$^{+/-}$ (grey, n=7) compared to *grm8a*$^{+/+}$ (white, n=6). **P<0.01. (C, F) Comparison of head size (top), yolk diameter (center), and total length (bottom) of 24 hpf old hetero- (light grey) and homoallelic (dark grey) *grm8a* (C) or *grm8b* mutants (F) and corresponding wildtype siblings (white). Size measurements are all given in squared pixel (pixel^2). (D, G) Anti-cleaved caspase 3 (cCasp3, green) immunohistochemistry revealed no apparent effect on cell apoptosis in the CNS of 24 hpf old hetero- ($^{+/-}$) and homoallelic ($^{-/-}$) *grm8a* (D) or *grm8b* mutants (G) compared to wildtype siblings ($^{+/+}$). Magnifications of boxed areas in the overview images (left panel) are displayed to the right with arrows pointing out individual cCasp3-positive (apoptotic) cells. Images are oriented with anterior to the left. Scale bars represent 100 μm for overview and 20 μm for magnification images. C. Drepper contributed to manual cell countings. Adjusted from Lueffe et al. 2021b.

4.1.6   *grm8* CRISPR/Cas9 mutants and corresponding splice-morphants display differential locomotor and thigmotaxis phenotypes

Behavioral investigations on *grm8a* and *grm8b* morphants revealed a hyperlocomotive phenotype for both and increased thigmotaxis behavior for *grm8a* morphants only. To verify a correlation between Grm8a and Grm8b loss of function and altered locomotor and thigmotaxis behavior, *grm8a* and *grm8b* CRISPR/Cas9 mutants were monitored using identical experimental conditions.

Surprisingly, *grm8a* and *grm8b* mutants behave differently compared to their corresponding morphants. While *grm8a* and *grm8b* morphants are hyperactive during motion tracking (Fig. 15B), *grm8a* mutants exhibit a hypoactive phenotype with reduced "high" velocity and a general reduction in total mean velocity (Fig. 18A). Additional parameters like total distance swum and the duration and number of "high active" swimming events show a similar trend but fail to reach statistical significance (Fig. 18A). For *grm8b* mutants, no effect on locomotor activity was observed (Fig. 18A).

Also, the thigmotaxis behavior is differentially altered in mutants compared to morphants. While *grm8a* morphants showed increased thigmotaxis behavior (Fig. 15C), *grm8a* mutants merely display a similar trend (Fig. 18B). In contrast, the thigmotaxis behavior was unaffected in *grm8b* morphants (Fig. 15C) but is significantly increased in the corresponding mutants (Fig. 18B).

The discrepancy between morphant and mutant phenotype is puzzling, however a frequently reported issue across studies (Kok et al. 2015, Joris et al. 2017). In contrast to many studies which predominantly fail to recapitulate the morphant phenotype in general (Law and Sargent 2014, Novodvorsky et al. 2015), the present data confirms altered locomotor and thigmotaxis behavior in mutants, however in opposing directions (locomotion activity) or with differential effects (thigmotaxis). Interestingly, investigations using a higher *grm8b* splice-morpholino concentration recapitulate the mutant-like hypoactivity (Fig. 36), suggesting that altered locomotor activity upon Grm8a and Grm8b loss of function might be dose-dependent.

Dose-dependent discrepancies between mutants and morphants are often associated with a well-known phenomenon known as genetic compensation. In particular zebrafish, which, due to whole-genome duplication, possess two copies for many genes, are known to be affected by genetic compensation under full knockout conditions (Rossi et al. 2015, El-Brolosy et al. 2019, Ma et al. 2019).
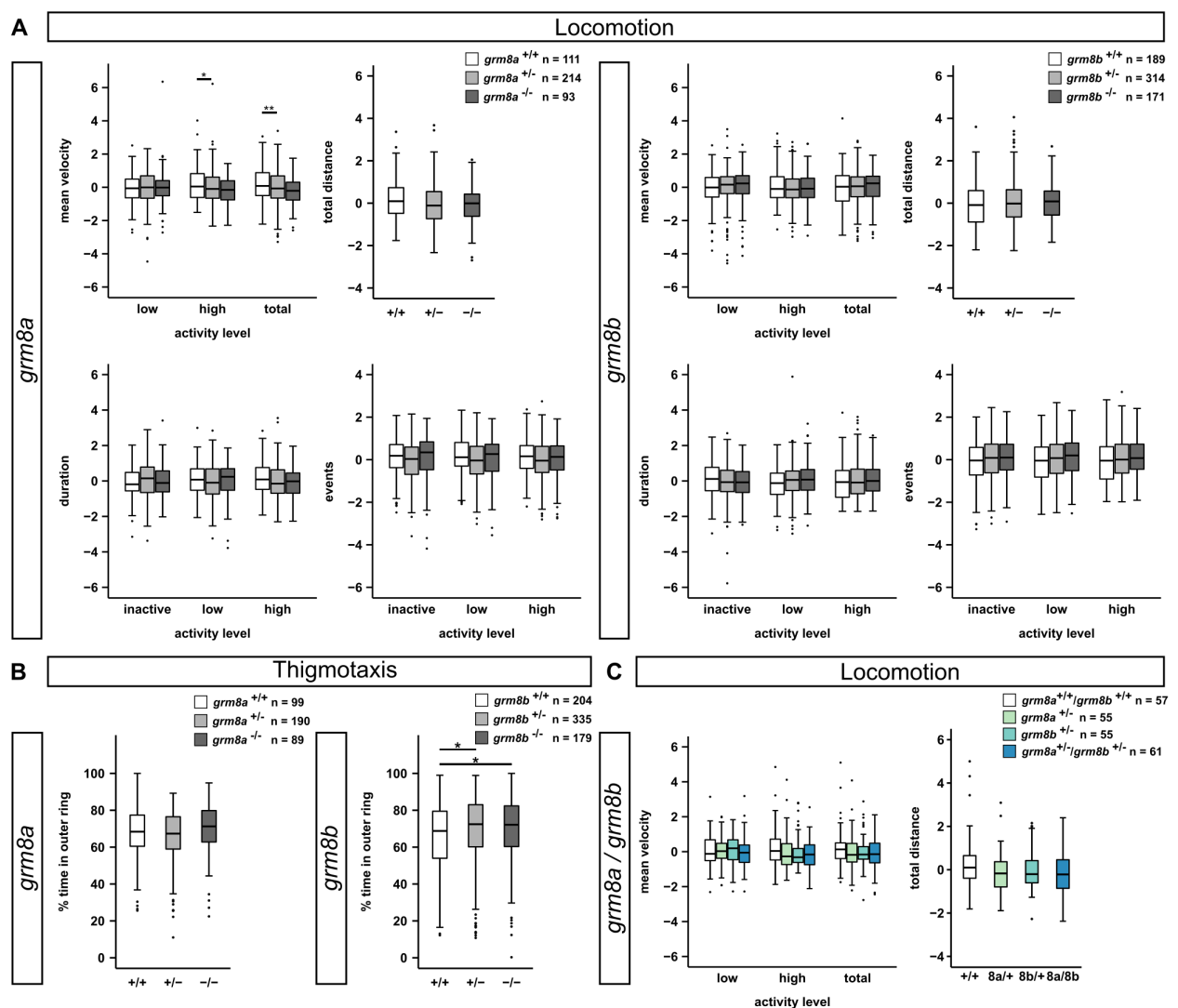
Figure 18: **Investigation of locomotor activity and thigmotaxis behavior revealed differential phenotypes for *grm8a* and *grm8b* CRISPR/Cas9 mutants.** (A) Locomotor activity of *grm8a* (left panel) or *grm8b* (right panel) hetero- (light grey, $^{+/-}$) and homoallelic mutants (dark grey, $^{-/-}$) and wildtype siblings (white, $^{+/+}$). Locomotor activity is determined by mean velocity (during low or high activity or combined (total), top left), total distance swum (top right) and the duration of (bottom left) and number of events (bottom right) for inactivity, low and high activity. Raw datasets were standardized by z-score transformation. (B) Thigmotaxis analysis in hetero- (light grey) and homoallelic (dark grey) *grm8a* (left) or *grm8b* mutants (right) compared to corresponding wildtype siblings (white). Thigmotaxis is characterized as the percentage of time spent in the outer ring (see Fig. 15 for illustration). (C) Locomotor activity displayed as mean velocity (during low or high activity or combined (total), left) and total distance swum (right) of single (light green (*grm8a*$^{+/-}$), light blue(*grm8b*$^{+/-}$)) and double (dark blue) heterozygous *grm8a* and/or *grm8b* mutants compared to wildtype siblings (white, *grm8a*$^{+/+}$/*grm8b*$^{+/+}$). Sample sizes are given by n at the top. *P<0.05, **<0.01. Adjusted from Lueffe et al. 2021b.

In order to test whether genetic compensation contributes to the hypoactive phenotype observed for *grm8a* mutants, heterozygous double mutants with a genetic disruption of *grm8a* and *grm8b* were generated and behaviorally monitored. Even though all groups failed to reach statistical significance (probably due to low statistical power), individuals across single and double mutants tend to be less active, displayed by a reduced mean velocity (total and during high activity) and total distance swum (Fig. 13C). Admitting that a gene expression analysis by qPCR and the generation of homozygous double mutants are required for final confirmation, there is evidence that the discrepancy between morphants and mutants does not result from genetic compensation of the respective paralog.

To conclude, Grm8a and Grm8b are crucial for the regulation of locomotor activity and fear-related response in zebrafish larvae. Both paralogs exert an anxiogenic effect upon loss of function, whereas the functional implication in activity regulation needs further investigation. With the generation, validation, and preliminary behavioral characterization of two paralog-specific mutant lines and splice-inhibiting oligonucleotides, the present study provides a valuable framework for further investigations on the underlying mechanism(s) of observed mutant and morphant phenotypes. Notably, the revealed *gad1a* colocalization and altered GABAergic cell quantity in motor-related brain regions highlight the GABAergic system for future research approaches on the molecular link between the genetic disruption of *grm8a* or *grm8b* and ADHD associated phenotypes.

4.2 Forkhead-box transcription factor P2 (Foxp2)

4.2.1 Spatio-temporal expression of *foxp2* shows a high incidence for motor-related brain regions

With *foxp2a* and *foxp2b*, conservation analysis identified two *FOXP2* paralogs in the teleost genome, which presumably emerged by the teleost-specific whole-genome duplication event (Song et al. 2013). In zebrafish, only *foxp2a* (known as *foxp2*) still exists, whereas *foxp2b* is hypothesized to be lost due to pseudogenization (Song et al. 2013). The expression dynamics of *foxp2* were described by others before (Shah et al. 2004, Bonkowsky and Chien 2005). To confirm previous findings, both on a temporal and spatial level, and complement them by a detailed description of *foxp2* expression in the adult brain, RNA ISH was performed on embryonic (10 and 18 somites, 24 hpf, 30 hpf, 36 hpf, and 48 hpf) and early larval (72 hpf) whole-mounts and adult brain sections of wildtype zebrafish.

Embryonic and early larval development:

Surprisingly, expression analyses at 10 and 18 somites (14-16 hpf) did not confirm a previously reported presence of *foxp2* transcript at 10 hpf (Bonkowsky and Chien 2005). Instead, *foxp2* transcript is revealed first at 24 hpf in the telencephalon (Tel, Fig. 19A, B, Fig. 23A), where it is persistently detected throughout development (Fig. 19A-J, K, M, O, Q, Fig. 23A) with expression in the subpallium (S) and the pallium (P) at 36 and 48 hpf (Fig. 19E, G, Fig. 23A). Besides telencephalon, *foxp2* transcripts are labeled in the ventral tegmentum (vTg) and the hypothalamus (H) starting at 30 hpf (Fig. 19C, K) and in the preoptic region (Po), the posterior tuberculum (PT), the thalamus (Th), the optic tectum (TeO), and the medulla oblongata (MO) starting at 36 hpf (Fig. 19E-F, Fig. 23A). Both patterns maintain with progressing development and are further accompanied by expression in the cerebellum (CeP) and the lower rhombic lip (LRL) at 48 hpf (Fig. 19G-H, Fig. 23A) and outside the CNS in the ganglion cell (GCL) and inner nuclear layer (INL) of the retina (Fig. 19S) and dorsally along the spinal cord (SC) at 72 hpf (Fig. 19T). Although *foxp2* expression in the MO is consistently detected throughout development, the pattern is initially confined (36 hpf, Fig. 19E-F, Fig. 23A) before it becomes

comparably broad at 48 hpf (Fig. 19G-H, Fig. 23A) and 72 hpf (Fig. 19I, J, P, R). First, *foxp2* transcripts are revealed in three bilateral, longitudinal cell cluster (Fig. 23A) before the rostro-medial and caudal cluster extend to form two bilateral stripes along the rostro-caudal axis, and the most lateral cluster expands to become part of the lateral rhombic lip (LRL) at 48 hpf (Fig. 23A). Further, according to transverse sections, the rostro-caudal stripes also expand along the dorso-ventral axis (Fig. 39O-P).
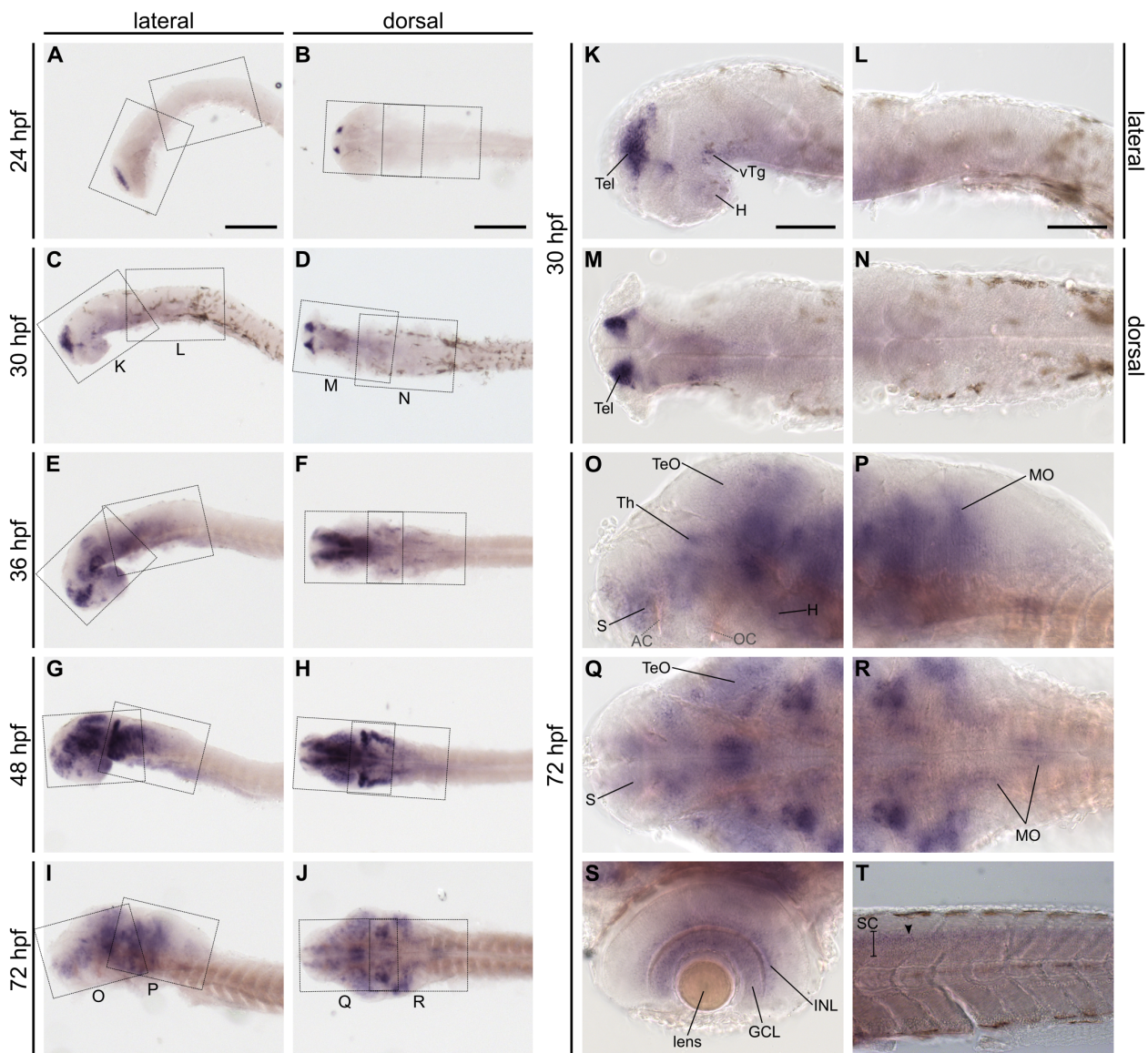
Figure 19: *foxp2* **spatio-temporal gene expression pattern in the developing zebrafish revealed by whole-mount RNA** *in situ* **hybridization (ISH).** (Left panel) Lateral (A, C, E, G, I) and dorsal (B, D, F, H, J) overview of developing zebrafish (24 hpf, 30 hpf, 36 hpf, 48 hpf, 72 hpf) labeled for *foxp2* transcripts by RNA ISH. Boxed areas in C, D, and I, J are magnified in K-N and O-R, respectively. Remaining magnifications for boxed areas in A, B, E, F, G, and H are displayed in Fig. 23A. Transcript labeling outside the CNS is shown in the eye from dorsal (S) and in the spinal cord (arrow) from lateral view (T). All images are shown with anterior to the left. For anatomical abbreviations, see Table 13. A detailed description of *foxp2* expression is part of the main text. Scale bar represents 200 μm in overview and 100 μm in magnification images. Adjusted from Lueffe et al. 2021a.

Adult brain:

FOXP2 expression in the postnatal and adult brain of mammals and other species (Ferland et al. 2003, Takahashi et al. 2003, Teramitsu et al. 2004, Campbell et al. 2009) suggests a functional role for *FOXP2* beyond developmental processes. In adult zebrafish, knowledge about the spatial distribution of *foxp2* transcript is limited (Shah et al. 2004). To verify previous observations and provide a detailed description of *foxp2*-positive brain regions to conclude how *foxp2* expression continues after completion of brain development in zebrafish, RNA ISH was applied on cross-sections of adult zebrafish brains.

In line with previous observations in the developing brain, *foxp2* expression is revealed in all major compartments of the mature CNS. *foxp2* transcripts are labeled in scattered cells throughout the olfactory bulbs (Fig. 20A) and in all major areas of the telencephalon, including the medial, lateral, and posterior pallium (P, Fig. 20A-E) and the subpallium (S, Fig. 20B-E) with ventral, dorsal, central and lateral zone and entopeduncular nuclei (EN, Fig. 20D-E). In general, transcript labeling is particularly intense along the ventricular side of the ventral and dorsal telencephalon and comparatively faint in the central pallium, which might be attributable to disparities in cell density. Further, intense labeling is observed for the preoptic region (Po, Fig. 20D-F), the habenula (Ha, Fig. 20F), the ventral (VT, Fig. 20F) and dorsal thalamic nuclei (DT, Fig. 20G-H), and the pretectal complex (Pc, Fig. 20F) including the periventricular pretectal nucleus (PP, Fig. 20G-H). Similar to the telencephalon, *foxp2* in the posterior tuberculum and the hypothalamus is predominantly expressed close to the ventricular system comprising the periventricular nucleus of the posterior tuberculum (TPp, Fig. 20G-H), the posterior tuberal nucleus and/or the paraventricular organ (PTN/PVO, Fig. 20G-I), the anterior tuberal nucleus (ATN, Fig. 20H), the lateral hypothalamic nucleus (LH, Fig. 20I) and the caudal (Hc, Fig. 20J), dorsal (Hd, Fig. 20I-J) and ventral zone (Hv, Fig. 20G-H) of the periventricular hypothalamus. *foxp2* expression not facing the ventricular system is detected in the central and/or diffuse nucleus of the inferior lobe (CIL/DIL, Fig. 20G, H, J, K) and the torus lateralis (TLa, Fig. 20G, H, I, J). In line with previous observations in the mesencephalon (Shah et al. 2004), intense labeling of the periventricular gray zone (PGZ, Fig. 20G-J) of the optic tectum and scattered cells throughout the torus semicularis (TS, Fig. 20I-J) was observed. Further, single

foxp2-expressing cells are found close to the tectal ventricle (TeV) in an area harboring the nucleus lateralis valvulae (NLV) and/or the dorsal tegmental nucleus (DTN, Fig. 20I) and around the medial (MLF) and lateral longitudinal fascicle (LLF, Fig. 20J). In addition, a prominently labeled cell population is revealed close to the tectal ventricle (TeV), where the oculomotor and trochlear nucleus is situated (NIII/NIV, Fig. 20I). In the cerebellum, *foxp2* expression is particularly strong in the granular cell layer of the corpus cerebelli (CCe, Fig. 20K, L) and the eminentia granularis (EG, Fig. 20K) and faint in scattered cells of the caudal cerebellar lobe (LCa, Fig. 20K, L). The medulla oblongata is intensely labeled for *foxp2* transcript in the inferior olive (IO, Fig. 20M, N), the medial funicular nucleus (MFN, Fig. 15O) as well as on the dorsal surface of the lobus fascialis (LVII, Fig. 20M), and the lobus vagus (LX, Fig. 20M-O). Additionally, *foxp2*-positive cell populations are detected in the medial octavolateralis nucleus (MON, Fig. 20K, L) and throughout the reticular formation (RF, Fig. 20K, L, N, O). The *foxp2* labeling in the vagal motor nucleus (NXm, Fig. 20M) is detectable but appears comparatively faint.

To summarize, the spatio-temporal characterization of *foxp2* expression partially confirms earlier observations in the developing and adult zebrafish brain. However, in contrast to a former report (Bonkowsky and Chien 2005), expression was first detected at 24 hpf and develops into a broader pattern than previously reported (Shah et al. 2004). Nonetheless, the presented expression data support a central role for Foxp2 both in the developing and mature CNS of zebrafish. Again, of particular interest is the high incidence of *foxp2* expression in brain regions essential for motor functions. Similar to *grm8a* and *grm8b* expression, these regions comprise the subpallium with prominent expression in the mature entopeduncular nucleus, the posterior tuberculum, the thalamus, the cerebellum and the medulla oblongata with expression in the reticular formation, the vagal and facial lobe and, specifically to *foxp2*, with expression in the inferior olive and the vagal motor nucleus. Interestingly, for some regions, the human equivalent was shown to be affected by structural, functional and/or neurochemical alterations in ADHD (Mackie et al. 2007, Ellison-Wright et al. 2008, Ivanov et al. 2010, Nakao et al. 2011, Hart et al. 2013, Ivanov et al. 2014, Elvsåshagen et al. 2020, Puts et al. 2020), thus emphasizing the translational importance of further investigations on Foxp2 function and Foxp2-regulated circuitries in zebrafish.
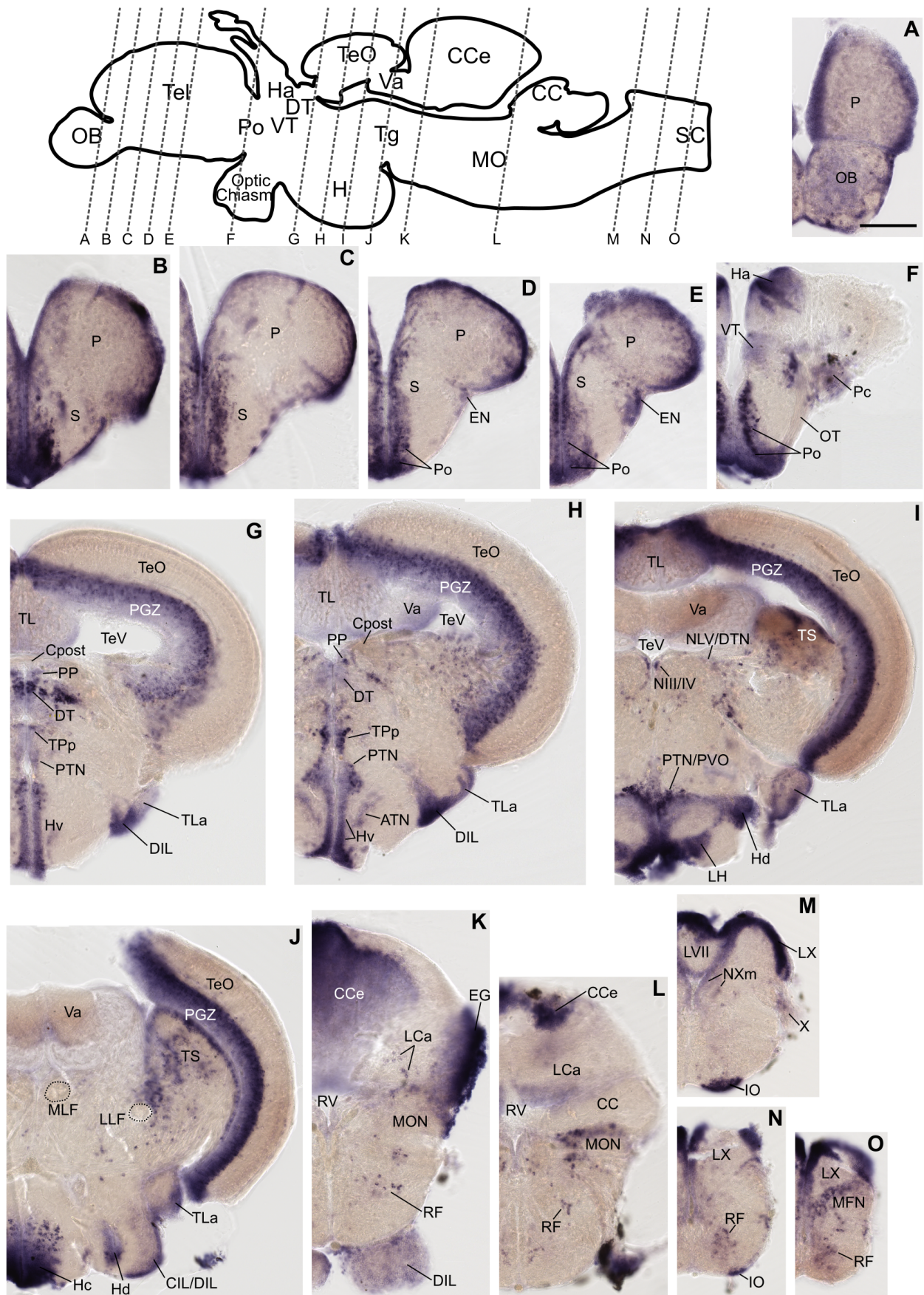
Figure 20: *foxp2* **expression pattern in the adult zebrafish brain revealed by RNA** *in situ* **hybridization (ISH).**
(A-O) Cross-sections of an adult zebrafish brain labeled for *foxp2* transcripts by RNA ISH. Images are shown from anterior to posterior as indicated by the scheme displayed at the top. Details on *foxp2* expression pattern are described in the main text. For anatomical abbreviations, see Table 13. Scale bar represents 200 µm.

4.2.2 *foxp2* expression co-localizes with expression of the ADHD risk candidate and GABAergic marker gene *gad1(a)* in brain regions essential for motor functions

Motivated by altered dopamine levels in FOXP2 mutants (Enard et al. 2009) and transcriptional targets like the dopamine D1 receptor (D1R) and its downstream signaling molecule DARPP-32 (Hisaoka et al. 2010, Vernes et al. 2011, Murugan et al. 2013), previous studies suggest modulation of dopaminergic signaling as a major function of FOXP2. In fact, FOXP2 and D1R colocalize in the mammalian brain, however, in GABA-releasing medium spiny neurons (van Rhijn et al. 2018). To determine whether *foxp2* is expressed by GABAergic and/or monoaminergic neurons in the developing zebrafish brain, a two-color RNA ISH for *foxp2* and *gad1a* on wildtype and a combination of RNA ISH and IHC on enhancer-trap *vmat2*:GFP transgenic zebrafish were performed at different developmental stages (36 hpf, 48 hpf, and 72 hpf). Due to the aforementioned similarity between *gad1a* and *gad1b* expression and technical benefits of *gad1a* over *gad1b* RNA ISH, colocalization was determined for *foxp2* and *gad1a* expression.

foxp2 expression in gad1a-positive cells:

Like *grm8a*, *foxp2* expression colocalizes with *gad1a* transcript labeling in numerous embryonic and early larval brain regions. This comprises the subpallium (S, Fig. 38A, C, E, G, I, Fig. 21A, C, E, G, I, Fig. 39A, C, E, G-I), the thalamus (Th, Fig. 38A, C, H, J, K, Fig. 21A, C, E, G, H, J, Fig. 39A, C, E, G, H, J, K, M) and the lateral and dorsal medulla oblongata (MO, Fig. 38B, C, D, F, L, N-R, Fig. 21B, D, F, L, N-R, Fig. 39B, D, F, L, N-R). Further, colocalization was observed for the posterior tuberculum (PT, Fig. 38A, K, M, Fig. 21A, H, J) at 36 hpf and 48 hpf and in the optic tectum (TeO, Fig. 39A, C, G, H, K, L) and, outside the CNS, in the inner nuclear layer (INL, Fig. 39G, H, K) of the retina at 72 hpf. In the cerebellum (CeP, Fig. 38C, L, O, Fig. 21B, L, Fig. 39O) and the ganglion cell layer (GCL, Fig. 39G, H), a colocalization with *gad1a* expression cannot be confirmed due to diffuse staining quality. Notably, as reported for *grm8a*, also *foxp2* expression substantially overlap with *gad1a* transcript labeling in brain regions essential for motor functions.
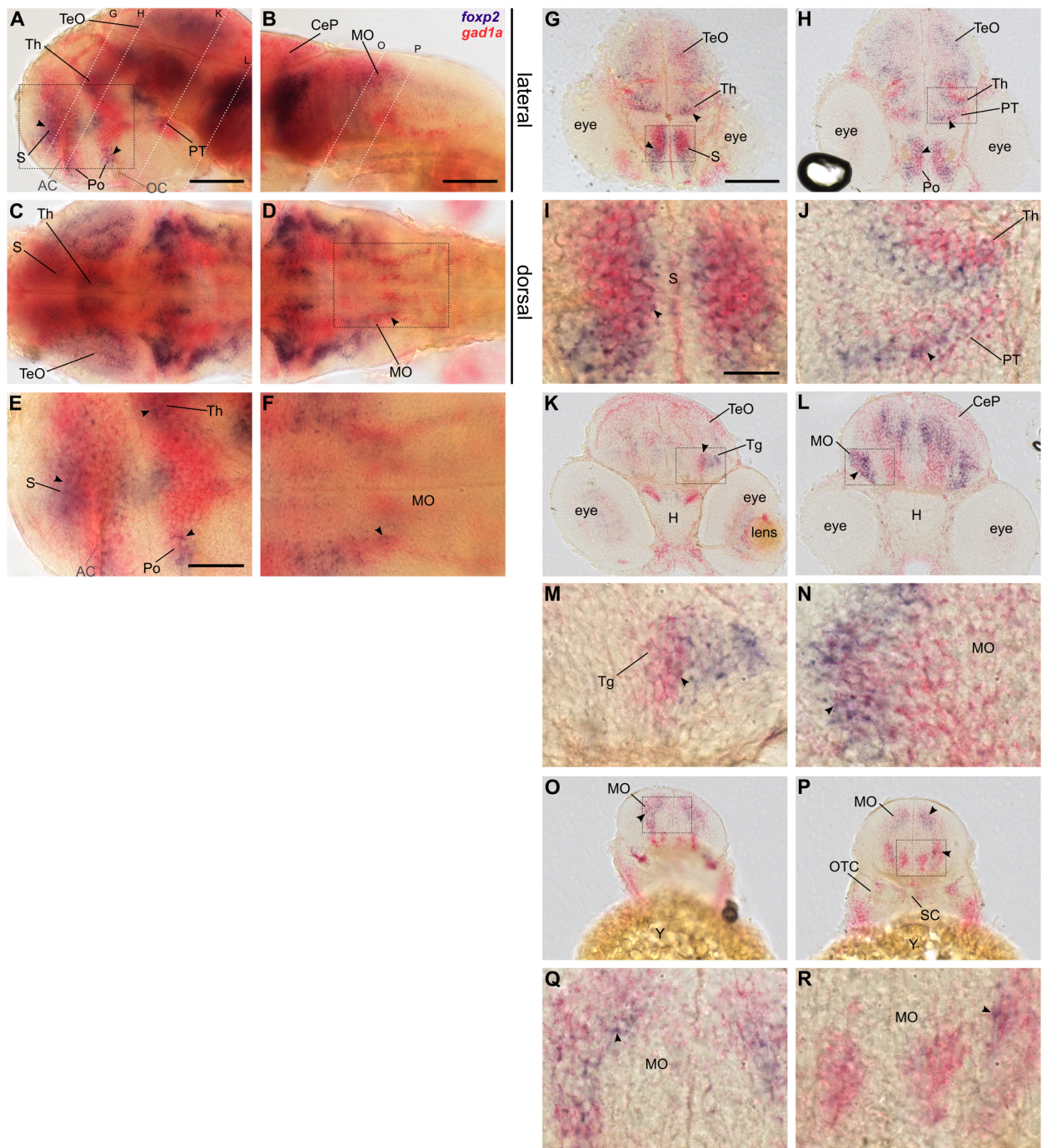
Figure 21: **Two-color RNA *in situ* hybridization reveals colocalization of *foxp2* and *gad1a* expression in the CNS of 48 hpf old zebrafish.** Transcript labeling for *foxp2* (blue) and *gad1a* (red) in 48 hpf old wildtype embryos, displayed for the CNS from lateral (A, B, E) and dorsal (C, D, F) views with anterior to the left. Boxed areas in A and D are magnified in E and F. Dashed white lines illustrate cutting sites for cross-sections shown in G-R. (I, J, M, N, Q, R) Magnifications of boxed regions in G, H, K, L, O, P, respectively. Arrows point out colocalization in overview and magnified images. For anatomical abbreviations, see Table 13. Scale bars represent 100 μm in overview and 50 μm in magnified images. Adjusted from Lueffe et al. 2021a.

foxp2 expression in vmat2-positive cells:

While *foxp2* and *gad1a* expression pattern colocalize extensively across brain regions, the overlap between *foxp2* transcript labeling and *vmat2* expression is restricted to single cells of the

ventral telencephalon (Tel, Fig. 22A, B, E, F), the raphe nuclei (Fig. 22L, P) and the rostral/intermediate (Fig. 22I, M) and caudal hypothalamus (Fig. 22J, N). Especially in the ventral telencephalon, where both patterns are in proximity, the overlap is restricted to single cells close to the midline (Fig. 22A, E). In other brain regions like the pretectum (Pc, Fig. 22D, H), the optic tectum (TeO, Fig. 22I), the cerebellum (CeP, Fig. 22J), and the dorsal medulla oblongata (MO, Fig. 22J-L) *vmat2* and *foxp2* expression are spatially distinct.
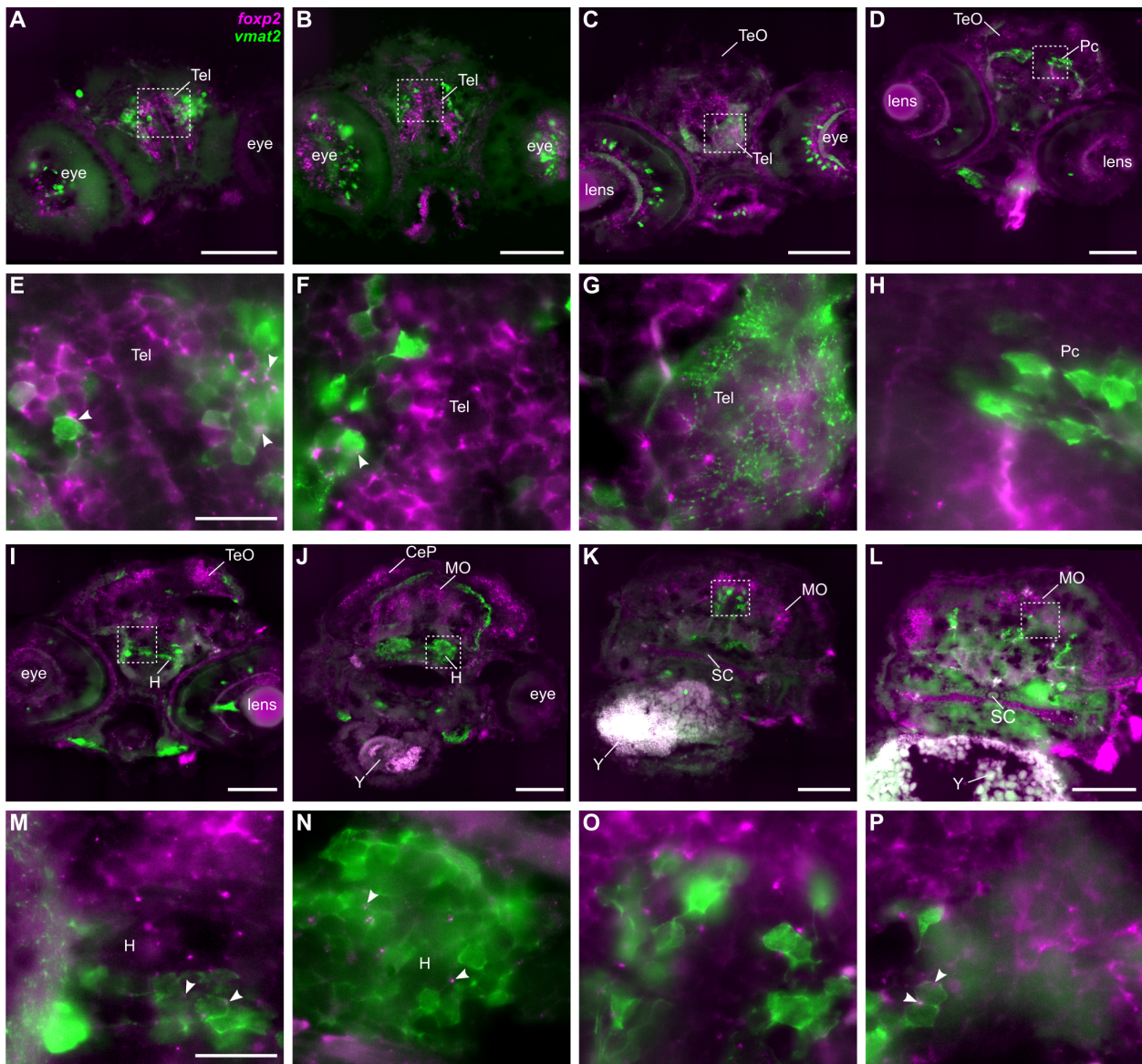
Figure 22: ***foxp2* expression in *vmat2*-positive cells of 72 hpf old zebrafish larvae.** CNS cross-sections of Tg(Etvmat2:GFP) larvae (72 hpf) immunostained for expressed GFP (green) and labeled for *foxp2* transcripts by RNA *in situ* hybridization (magenta). Magnifications of boxed areas in A-D and I-L are displayed in E-H and M-P, respectively. Arrows indicate colocalization or close proximity of *foxp2*-positive punctae and anti-*vmat2*:GFP immunolabeling. Brain regions with apparent colocalization are described in the main text. Anatomical abbreviations are listed in Table 13. Scale bars represent 100 μm in overview and 20 μm in magnified images.

In summary, the observed co-localization between *foxp2* and *gad1a* in several brain regions, including tel-, di-, mes- and rhombencephalon, demonstrates that GABAergic neurons express *foxp2* throughout the developing CNS of zebrafish. Together with the aforementioned verification of FOXP2 in GABAergic MSNs and altered MSN signaling upon FOXP2 loss of function in mice (van Rhijn et al. 2018), these findings indicate that Foxp2 might be crucial for functional properties of GABAergic neurons in zebrafish larvae as well.

In contrast, colocalization between *foxp2* and *vmat2* expression suggests that except for a possible function in the ventral forebrain and hypothalamus, Foxp2 plays a minor role in the monoaminergic system of 72 hpf old zebrafish larvae.

4.2.3   Generation and genetic and morphological validation of a *foxp2* CRISPR/Cas9 mutant line

Since former studies failed to interfere with Foxp2 function using splice-morpholinos (Bonkowsky and Chien 2005), the gene-editing tool CRISPR/Cas9 was applied to create a functional knockout of *foxp2*. Therefore, a sgRNA was designed to target exon 10 (coding exon 6) of the zebrafish *foxp2* gene (Fig. 23B, Fig. 24A). The induced double-strand break and activated repair mechanisms caused a 40 bp (Fig. 23B, Fig. 24A) or 7 bp deletion mutation (Fig. 40E), of which the former was functionally investigated. The mutation-induced frameshift generates a continuous change in the amino acid sequence and premature disruption of the zinc-finger domain by the induced stop codon (Fig. 23C). Since functional domains like nuclear localization signals, leucine-zipper, forkhead, and CtBP1-binding domain are located downstream of the induced stop codon (Fig. 23C), a complete loss of the domains and associated functions is expected for the truncated protein. According to previous investigations on the human R328X coding variant, located within the CRISPR/Cas9 affected sequence (Fig. 23C), a disruption upstream of the aforementioned domains interferes with stability, nuclear localization, DNA-binding, and transactivation capabilities of the FOXP2 protein (Vernes et al. 2006). Therefore, similar deficiencies are expected for the gene product of the described deletion mutation.

According to qPCR-based expression analysis in *foxp2* mutants and wildtype siblings, the 40 bp deletion results in a dose-dependent reduction of *foxp2* transcripts (Fig. 23D) likely caused by nonsense-mediated decay. Although the increased level of *foxp1a* (and perhaps *foxp1b*) transcript (Fig. 23D) suggests a genetic compensation by Foxp1 (a Foxp2 interaction partner with shared transcriptional targets (Araujo et al. 2015)), the significant upregulation of *cntnap2b* expression (usually suppressed by Foxp2 (Vernes et al. 2008)), still confirms Foxp2 loss of function.

Former investigations on homo- and heteroallelic *Foxp2* knockout mice reported postnatal lethality for the former and a mild to moderate developmental delay for the latter as major morphological phenotypes (French and Fisher 2014). Homozygous mutants for the here described deletion mutation ($foxp2^{-/-}$) show a deficit in the development or inflation of the swim bladder (Fig. 23E) in about 20 % of the cases and suffer premature death between 5 days and 3 months post fertilization. In contrast, the gross morphology (Fig. 23E) and survival rate of heterozygous mutants ($foxp2^{+/-}$) are normal. Additionally, size measurements revealed no significant effect on head size, yolk diameter, or total body length for $foxp2^{+/-}$ and $foxp2^{-/-}$ (Fig. 24B). Hence unlike mice, zebrafish show no indications for a developmental delay upon Foxp2 loss of function.

Motivated by the observed *foxp2* expression in GABAergic cells, Gad1b-positive cells in $foxp2^{+/-}$ were labeled by anti-Gad1b IHC and manually quantified relative to wildtype siblings. Although fewer Gad1b-positive cells were detected in the hindbrain of some $foxp2^{+/-}$ individuals, the relative quantity in the forebrain/midbrain and hindbrain failed to reach statistical significance (Fig. 24D). Accordingly, the apoptosis level, identified by anti-cCasp3 IHC, in 24 hpf old $foxp2^{+/-}$ and $foxp2^{-/-}$ appears normal when compared to wildtype siblings (Fig. 24C).
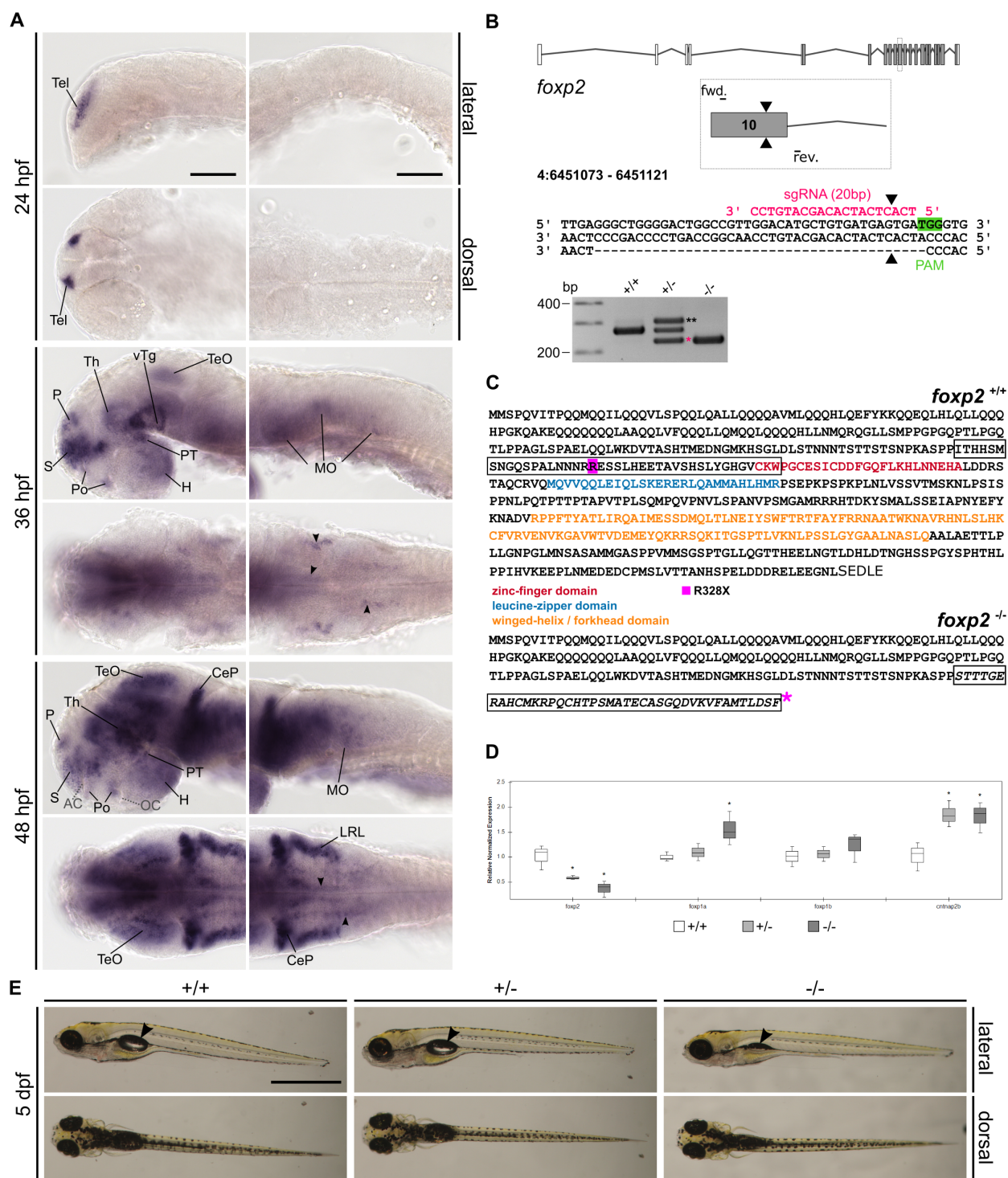
Figure 23: *foxp2* **transcript labeling in the developing CNS of zebrafish and generation and verification of a** *foxp2* **CRISPR/Cas9 mutant line.** (A) *foxp2* expression in the developing zebrafish brain (24 hpf, 36 hpf, 48 hpf) revealed by whole-mount RNA *in situ* hybridization (ISH). Developmental stage increases from top to bottom and is displayed from lateral and dorsal views with anterior to the left. For anatomical abbreviations, see Table 13. Scale bars: 100 μm. (B) Schematic of *foxp2* exon-intron structure with coding and non-coding exons displayed in grey and white, respectively. sgRNA binding (pink), Cas9-induced double-strand break (black triangle), and genotyping primer binding sites are indicated in *foxp2* exon 10. The induced 40 bp deletion mutation is displayed as 228 bp large PCR product (pink asterisk) in heterozygous (*foxp2*$^{+/-}$) and homozygous (*foxp2*$^{-/-}$) mutants together with a ∼320 bp large heterodimer of wildtype and mutated product (black asterisks) in *foxp2*$^{+/-}$ only. (C) Amino acid sequence of wildtype (top) and predicted mutant allele (bottom). The deletion mutation induces a frame shift (boxed sequence) and a premature stop codon (pink asterisk) in the zinc-finger domain (red). The human gene variant R328X (pink box) lies within the induced frame shift. (D) qPCR-based expression analysis

of *foxp2*, *foxp1a*, *foxp1b* and *cntnap2b* in *foxp2$^{+/+}$* (white), *foxp2$^{+/-}$* (light grey), *foxp2$^{-/-}$* (dark grey), displayed as relative normalized expression. *P<0.05. (E) Live images of *foxp2$^{+/+}$*, *foxp2$^{+/-}$* and *foxp2$^{-/-}$* at 5 dpf with anterior displayed to the left. A deficit in the development or inflation of the swim bladder (black arrow) is observed for *foxp2$^{-/-}$*. Scale bar, 1 mm. The generation and injection of the sgRNA were performed by M. Bauer. qPCR was performed by Z. Gioga. Adjusted from Lueffe et al. 2021a.

4.2.4   Commissures and tracts of *foxp2* mutants appear transiently disorganized during development

Gene ontology of FOXP2-regulated gene networks and morphological alterations affecting neurite length and arborization in *Foxp2*-mutant animal and cell culture models indicate regulation of neurite development, growth, and guidance as major functions of FOXP2 (Enard et al. 2009, Schulz et al. 2010, Vernes et al. 2011, Chen et al. 2016, Castells-Nobau et al. 2019). In zebrafish, the role of Foxp2 and Foxp2-regulated networks in neuritogenesis is unclear. While a recently described *foxp2* zinc-finger mutant failed to recapitulate axon pathfinding errors (Xing et al. 2012), a zinc-finger-based genetic interference with *cntnap2* was demonstrated to induce delayed commissure formation in zebrafish larvae (Hoffman et al. 2016). Since the present deletion mutation significantly interferes with *cntnap2b* expression, the corresponding mutant and wildtype siblings were investigated for significant deficits in commissure and tract formation during development. Therefore, brain commissures and tracts were visualized by an anti-AcTub immunostaining on 20 hpf, 24 hpf, 28 hpf, and 5 dpf old *foxp2* mutant and wildtype siblings.

At 20hpf and 24 hpf, the anterior (AC) and post-optic commissure (POC), as well as the supra-optic tract (SOT), appear structurally disorganized in *foxp2$^{-/-}$* and unchanged in *foxp2$^{+/-}$* (Fig. 24F). An observation-based estimate of five fully blinded confirmed the effect stating a significant impact on the average commissure/tract formation for all areas examined at 24 hpf (Fig. 24E). Interestingly, at 28 hpf and 5 dpf, neither *foxp2$^{+/-}$* nor *foxp2$^{-/-}$* show any morphological differences for the AC, POC, and SOT compared to wildtype siblings (Fig. 24F). Hence, these findings indicate a delay in the early commissure and tract formation in *foxp2$^{-/-}$*, which recovers until 28 hpf. Further, due to the great similarity to *cntnap2* mutants, it is assumed that the transient effect on commissure and tract formation in *foxp2$^{-/-}$* (Fig. 24F) is caused by the upregulation of *cntnap2b* expression described above (Fig. 23D).
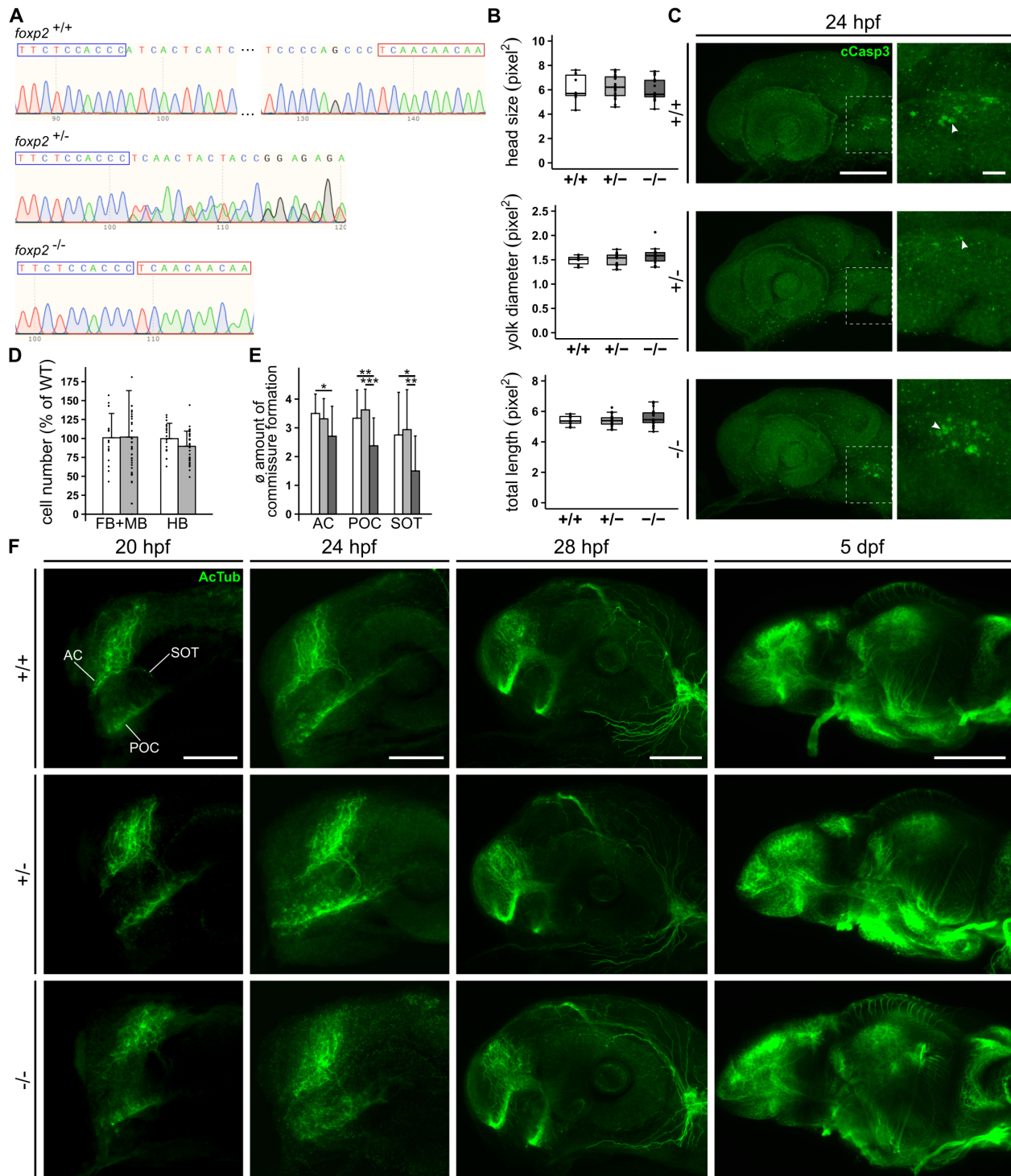
Figure 24: **Genetic and anatomical characterization of *foxp2* CRISPR/Cas9 mutants.** (A) DNA sequencing traces for *foxp2*$^{+/+}$, *foxp2*$^{+/-}$ and *foxp2*$^{-/-}$ genotyping PCR products confirm the loss of 40 nt for *foxp2*$^{-/-}$ (between blue and red box) described as 40 bp deletion mutation in Fig. 23. *foxp2*$^{+/-}$ contain a mixture of wildtype (top) and mutated allele (bottom) displayed by multiple traces from the deletion mutation onwards (end of blue box). (B) Comparison of head size (top), yolk diameter (center) and total length (bottom) for 24 hpf old *foxp2*$^{+/+}$ (white, n=10), *foxp2*$^{+/-}$ (light grey, n=24) and *foxp2*$^{-/-}$ (dark grey, n=19). Size measurements are all given in squared pixel (pixel^2). (C) Cell apoptosis in the CNS of 24 hpf old *foxp2*$^{+/+}$, *foxp2*$^{+/-}$ and *foxp2*$^{-/-}$ revealed by anti-cleaved caspase 3 (cCasp3) immunohistochemistry. Magnifications of boxed areas in the left column are displayed to the right with arrows indicating individual cCasp3-positive (apoptotic) cells. Scale bars represent 100 μm in overview (left) and 20 μm in magnified images (right). (D) Relative number of Gad1b-positive cells in the forebrain/midbrain (FB/MB) and hindbrain (HB) of 30 hpf old *foxp2*$^{+/-}$ (light grey, n=14) compared to *foxp2*$^{+/+}$ (white, n=6). (E) Qualitative evaluation of the average commissure and tract formation for the anterior (AC) and post-optic commissure (POC) and supra-optic tract (SOT) based on anti-acetylated tubulin (AcTub) staining

in 24 hpf old *foxp2$^{+/+}$* (white, n=3), *foxp2$^{+/-}$* (light grey, n=4) and *foxp2$^{-/-}$* (dark grey, n=6) embryos. *P<0.05, **P<0.01, ***P<0.001. (F) Representative anti-AcTub immunostaining (green) in the CNS of 20 hpf, 24 hpf, 28 hpf, and 5 dpf old *foxp2* mutants (*foxp2$^{+/-}$*, *foxp2$^{-/-}$*) and wildtype siblings (*foxp2$^{+/+}$*). 20 hpf and 24 hpf *foxp2* mutants display a disorganized appearance of AC, POC, and SOT, which recovers until 28 hpf. Images are oriented with anterior to the left. Scale bars, 50 μm (20 hpf, 24 hpf) and 100 μm (28 hpf, 5 dpf). C. Drepper and A. D'Orazio contributed to manual cell quantifications. Adjusted from Lueffe et al. 2021a.

4.2.5   Foxp2 loss of function causes increased locomotor activity in zebrafish larvae

The detection of *foxp2* transcripts in motor-related brain regions indicates a possible role for Foxp2 in motor functions of zebrafish. Accordingly, functional studies in FOXP2/FoxP-deficient mammals, birds, and flies revealed a disruption of motor functions ranging from the complex generation of sequenced orofacial movements during speech in humans (Lai et al. 2001, Vargha-Khadem et al. 2005), vocalization, vocal imitation, and motor learning in rodents and birds (Shu et al. 2005, Haesler et al. 2007, Fujita et al. 2008, Groszer et al. 2008, French et al. 2012, Kurt et al. 2012, Castellucci et al. 2016, Usui et al. 2017) to the execution and/or regulation of basic motor patterns such as flight and locomotion in flies (Lawton et al. 2014, Mendoza et al. 2014, Castells-Nobau et al. 2019). To test whether Foxp2 is implicated in the regulation of locomotor activity in zebrafish larvae, locomotion behavior of 5 dpf old *foxp2* mutants and wildtype siblings was monitored as described for *grm8a* and *grm8b* mutants and morphants before.

During motion tracking, *foxp2* mutants show a gene-dose-dependent increase in locomotor activity characterized by a significant increase in swimming velocity and total distance swum (Fig. 25A). In addition, both *foxp2$^{+/-}$* and *foxp2$^{-/-}$* display a significantly increased duration and velocity of "high active" swimming (Fig. 25A), whereas an increased number of "high active" swimming events was exclusively observed for *foxp2$^{+/-}$* (Fig. 25A). To summarize, Foxp2-deficiency in zebrafish larvae causes hyperlocomotion, thus supporting a potential role for Foxp2 in (locomotor-) activity regulation of zebrafish larvae.

To test whether Foxp2-deficiency induces NDD (neurodevelopmental disorder)-relevant be-havioral phenotypes beyond hyperlocomotion, the thigmotaxis behavior of *foxp2* mutants was examined as well. In line with normal anxiety levels of *Foxp2* knockout mice (Co et al. 2020), the thigmotaxis assay revealed no significant phenotype for *foxp2*$^{+/-}$ and *foxp2*$^{-/-}$ larvae (Fig. 25B).
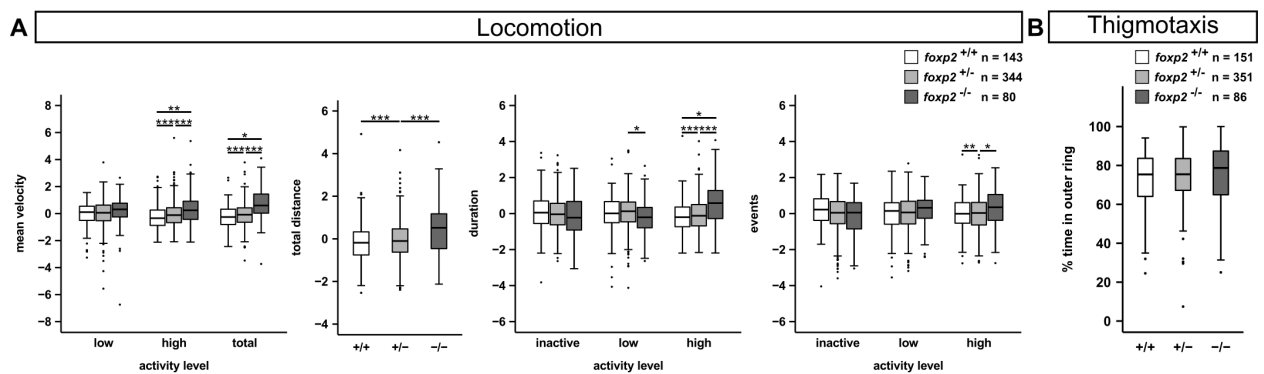
Figure 25: **Behavioral assessment of locomotor activity and thigmotaxis behavior revealed a hyperlocomotive phenotype for *foxp2* mutants.** (A) Locomotor activity of *foxp2*$^{+/+}$ (white), *foxp2*$^{+/-}$ (light grey) and *foxp2*$^{-/-}$ (dark grey) determined by mean velocity during low, high or both (total) activity (levels), total distance swum, and duration or events of inactivity, low and high activity. Z-score transformation was applied to standardize raw datasets. (B) Thigmotaxis behavior of *foxp2*$^{+/+}$ (white), *foxp2*$^{+/-}$ (light grey), and *foxp2*$^{-/-}$ (dark grey) measured as "percentage of time spent in the outer ring" (see Fig. 15 for illustration). The sample sizes are given by n. *P<0.05, **P<0.01, ***P<0.001. Adjusted from Lueffe et al. 2021a.

In summary, behavioral investigations on Foxp2 function confirm an implication in activity regulation but reject a significant role in the regulation of thigmotaxis behavior of zebrafish larvae.

4.3   Relevance of glutamate decarboxylase 1 (Gad1) and GABAergic signaling for the regulation of locomotor activity in zebrafish larvae

The detection of *foxp2, grm8a,* and *grm8b* transcript in *gad1(a)*-positive neurons in brain regions involved in motor functions together with observed activity phenotypes upon *foxp2, grm8a,* and *grm8b* loss of function, suggest that Gad1-regulated GABAergic inhibition is crucial for the regulation of locomotor activity in zebrafish larvae. To test this hypothesis, two complementary strategies were applied to interfere with Gad function. First, the *gad1b* transcript was targeted using a *gad1b* splice-morpholino before the morphant behavior was independently verified by applying the Gad antagonist L-allylglycine on wildtype larvae. *gad1b* was selected as splice-morpholino target due to a higher amino acid similarity to the human GAD1 (Gad1a: 81 %, Gad1b: 84 %, ensemble.org (GRCz11)).

The *gad1b* splice-morpholino is designed to bind to the splice-donor of *gad1b* exon 8 (Fig. 26A). In consequence, the *gad1b* intron 8 is skipped during splicing (Fig. 26A) and remains part of a misspliced transcript (Fig. 27A) which was detected as 500 bp large PCR product in 1 dpf and 5 dpf old *gad1b* morphants (MO, Fig. 26B). Besides, the splice-morpholino leads to a reduction of wildtype transcript which partly recovers until 5 dpf (Fig. 26B). The missplicing-induced frameshift causes a premature stop codon (Fig. 26B) that disrupts translation within the erroneously retained intron 8. Although qualitative observations revealed no gross morphological alterations for *gad1b* morphants at 5 dpf (Fig. 26C), corresponding size measurements at 24 hpf determined a slight but significant reduction in body length on the back of unchanged head size and yolk diameter (Fig. 27B). Further, anti-cCasp3 immunolabeling detected an increase in cell apoptosis in the CNS of *gad1b* morphants compared to uninjected controls (WT, Fig. 27C). In contrast, L-allylglycine-treated wildtypes neither displayed apparent differences in size nor cell apoptosis when examined after 8 hours of treatment and behavioral monitoring. These discrepancies might be attributable to the acute treatment strategy later in development. In order to confirm the functionality of the applied *gad1b* splice-morpholino beyond transcript level, the number of GABA-positive cells in the hindbrain of *gad1b* MO was manually and, for comparative purposes, automatically quantified (Segebarth et al. 2020). The transient knock-

down of *gad1b* (and thus presumably Gad1b) is expected to result in reduced GABA synthesis and thus in a lower number of anti-GABA labeled cells in the CNS of *gad1b* morphants. Accordingly, preliminary findings of both quantification methods confirmed fewer GABA-positive cells in the hindbrain of *gad1b* morphants (Fig. 27D), thus supporting the functionality of the applied *gad1b* splice-morpholino.

4.3.1   *gad1b*/Gad-deficiency induces hyperlocomotion and increased thigmotaxis behavior in zebrafish larvae

The locomotor activity of *gad1b* morphants was assessed as described before with uninjected, stage-matched individuals serving as corresponding controls. Like *foxp2* mutants and, *grm8a* and *grm8b* morphants, *gad1b* morphants showed a hyperlocomotive phenotype during tracking. The significantly increased swimming velocity (total, low and high), swimming distance, and duration and number of "high active" swimming events observed for *gad1b* morphants (Fig. 26D) resemble various characteristics of hyperlocomotion seen in *foxp2* mutants (Fig. 25A), and *grm8a* and *grm8b* morphants (Fig. 15B). In contrast, attributes like the significantly reduced duration and quantity of inactive phases seem specific to the phenotype of *gad1b*, *grm8a*, and *grm8b* morphants (Fig. 26D, Fig. 15B).

Besides hyperlocomotion, *gad1b* morphants display significantly increased thigmotaxis behavior (Fig. 26E). Thus, the *gad1b* morphant phenotype also resembles altered fear response observed for *grm8a* morphants (Fig. 15C) and *grm8b* mutants (Fig. 18B).

Since *gad1b* morphants display significant size differences (Fig. 27B) and increased cell apoptosis (Fig. 27C), it cannot be excluded that developmental and/or anatomical alterations contribute to the observed hyperlocomotion. To pharmacologically reproduce the activity phenotype independent of any morphological defects, the locomotor activity of L-allylglycine treated wildtype larvae was monitored and compared to that of untreated controls. Although hyperlocomotion is more pronounced in response to L-allylglycine treatment (Fig. 26F), it still resembles the increased locomotor activity of *gad1b* morphants (Fig. 26D). Taken together, these findings show that interfering with *gad1b* or Gad activity induces hyperlocomotion in ze-

brafish larvae and thus provides further evidence for the significant role of Gad1 and GABAergic signaling in the activity regulation of zebrafish larvae.

4.3.2   Interference with GABA-A-R and GABA-B-R function differentially alters locomotor activity in zebrafish larvae

GABAergic signaling occurs via two distinct receptor classes, the ionotropic GABA-A- and the metabotropic GABA-B-receptors (GABA-A-R, GABA-B-R). To investigate the functional relevance of both in activity regulation of zebrafish, wildtype larvae were treated with the selective antagonists SR-95531 (GABA-A-R) and CGP-55845 (GABA-B-R) and monitored as described above. Interestingly, 5 dpf old wildtype larvae respond differentially to both substances with hyperlocomotion upon SR-95531 (Fig. 26G) and hypolocomotion upon CGP-55845 exposure (Fig. 26H). Surprisingly, the GABA-B-R agonist R-baclofen (Fig. 37), similarly, induced hypolocomotion in wildtype zebrafish larvae. To summarize, interfering with GABAergic signaling on the transcript, enzyme, and receptor level results in altered locomotor activity, which corroborates the hypothesis that GABAergic signaling is crucial for locomotor activity regulation in zebrafish larvae.
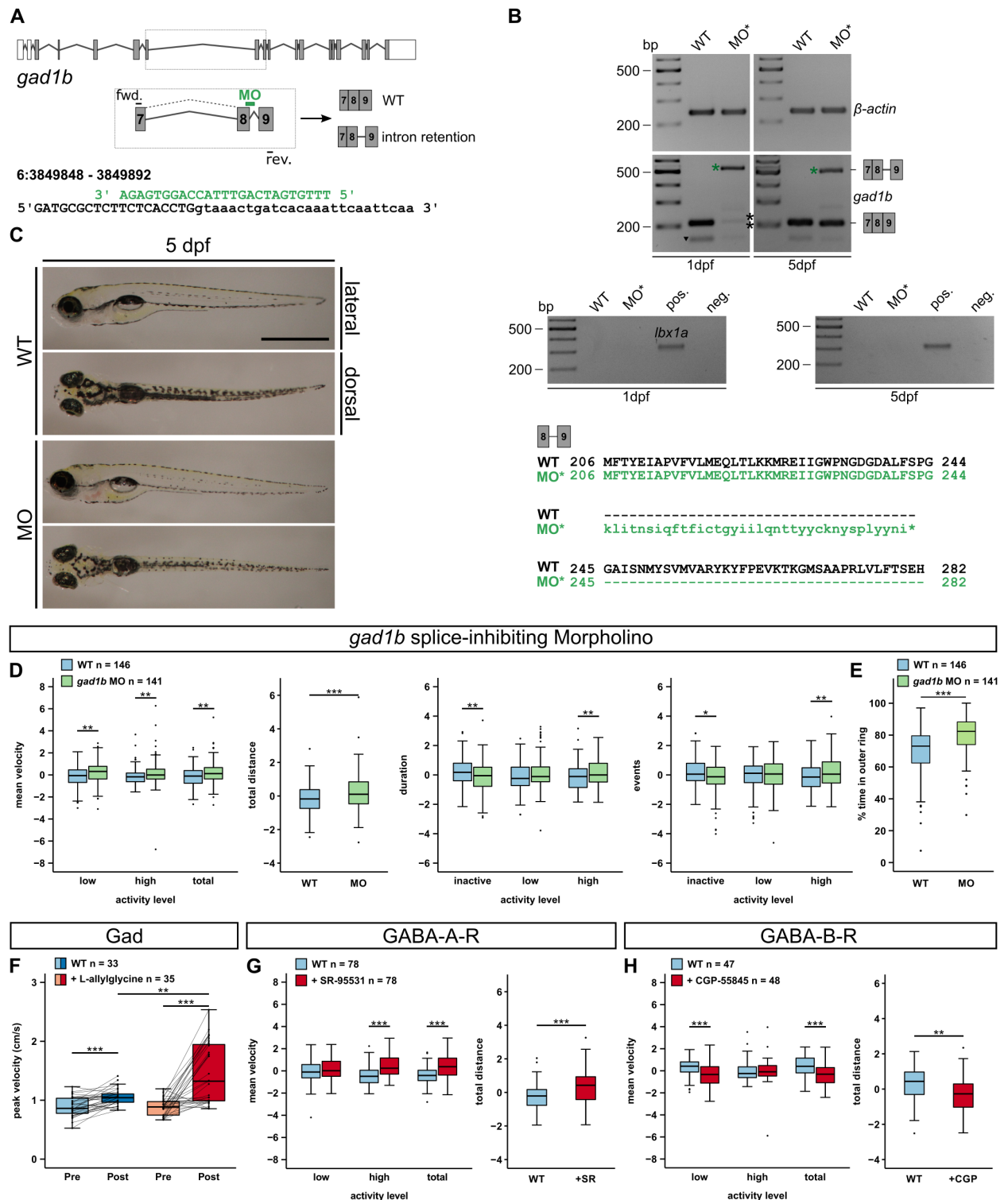
Figure 26: ***gad1b* splice-inhibiting morpholino and implication of GABAergic signaling in the regulation of locomotor activity and thigmotaxis behavior of 5 dpf old zebrafish larvae.** (A) Schematic of *gad1b* exon-intron structure with coding and non-coding exons displayed in grey and white, respectively. Boxed area displays magnification of exon-intron structure of exon 7 to exon 9 with illustrated morpholino- (MO, green) and primer binding sites. (B) RT-PCR displays *gad1b*-MO-induced retention of intron 8 as 500 bp large PCR product at 1 dpf and 5 dpf (green asterisk) and a reduction of wildtype transcript at 1 dpf (black asterisks). Control PCRs confirm comparable cDNA levels (*β-actin*, 239 bp) and absent genomic DNA contamination (*lbx1a*, 353 bp). Black triangle points out primer off-target PCR product. (B, bottom) According to the predicted amino acid sequence (displayed for exon 8, intron 8 and exon 9), intron 8 retention induces a premature stop codon (asterisk) in *gad1b* intron 8. (C) Live image of a *gad1b* morphant (MO) and uninjected control larva (WT) at 5 dpf. Scale bar represents 1 mm. (D) Comparison of locomotor activity parameters measured for 5 dpf old *gad1b* morphants (MO, light green) and

uninjected control larvae (WT, light blue). Significant differences were revealed for all parameters examined, including mean velocity (in low/high activity or combined (total)), total distance swum, and duration of and number of events for all three activity levels (inactivity, low and high activity). (E) Comparison of thigmotaxis behavior for 5 dpf old *gad1b* MO and uninjected control larvae (WT). (F) Maximum mean velocity (of 5 min) reached by 5 dpf old wildtype larvae before (Pre) treated with Danieau's solution (light blue) or 100 mM Gad-inhibitor L-allylglycine (light red) or within 8 hours after treatment (dark blue and dark red, respectively). Activity changes of individual larvae are illustrated by the incorporated line plot. (G, H) Effect of 10 mM GABA-A-R antagonist (SR-95531) injection at one-cell stage (red) or 48 hours incubation in GABA-B-R antagonist (CGP-55845, red) on locomotor activity compared to uninjected or Danieau's solution-incubated controls, respectively (light blue). (D, G, H) Z-score transformation was applied to standardize raw datasets. $^*P<0.05$, $^{**}P<0.01$, $^{***}P<0.001$. The behavioral assessment of the GABA-A-R antagonist was performed by A. D'Orazio and analyzed by T. Lüffe. Further, A. D'Orazio contributed to the behavioral assessment of the *gad1b* MO. Adjusted from Lueffe et al. 2021a.
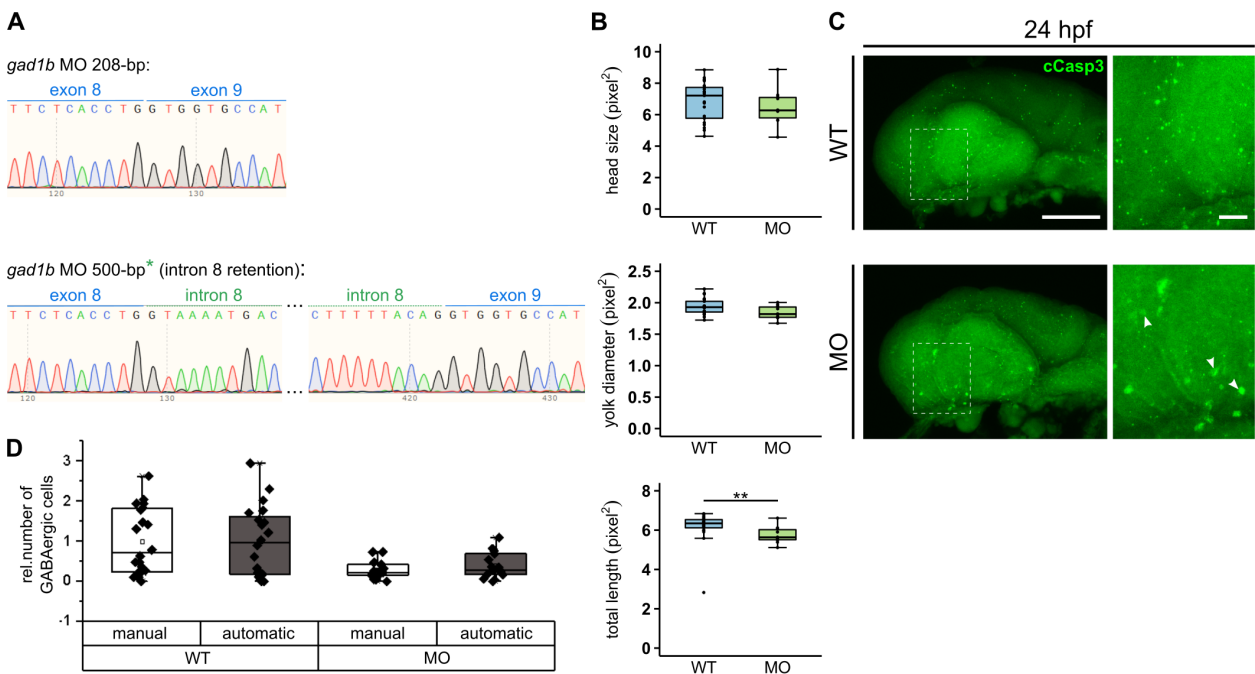
Figure 27: **Genetic and anatomical characterization of *gad1b* splice-morphants.** (A) cDNA sequencing traces of differentially sized PCR products derived from *gad1b* morphants (MO) (see Figure 21). Traces display splice-morpholino-induced *gad1b* intron 8 retention (green) in the misspliced transcript (500 bp, bottom) and the correctly spliced wildtype transcript comprising exon 8 and exon 9 (208 bp, top). (B) Comparison of head size (top), yolk diameter (center), and total length (bottom) between *gad1* MO (MO, grey, n=10) and uninjected control embryos (WT, white, n=21) at 24 hpf. Size measurements are all given in squared pixel (pixel^2). $^{**}P<0.01$. (C) Increased cell apoptosis in the CNS of 24 hpf old *gad1b* MO compared to wildtype controls, revealed by anti-cleaved caspase 3 (cCasp3, green) immunohistochemistry. Magnifications of boxed regions are displayed to the right with arrows pointing out individual cCasp3-positive (apoptotic) cells in the CNS of a *gad1b* MO. Images are presented with anterior to the left. Scale bars represent 100 μm in overview (left) and 20 μm in magnified images (right). (D) Preliminary analysis for the automatic (algorithm (Segebarth et al. 2020)) and manual quantification (by V. Schöffler, C. Lillesaar and T. Lüffe) of the relative number of GABA-positive cells in the hindbrain of 30 hpf old *gad1b* MO and wildtype controls. Adjusted from Lueffe et al. 2021a.

4.4   Significance of GABAergic signaling for Foxp2 function in activity regulation

So far, it was shown that the expression of *foxp2* and *gad1a* colocalizes in brain regions essential for motor functions (Fig. 21, Fig. 38, Fig. 39) and, that interfering with *gad1b*, Gad or GABA-A-R (Fig. 26D, F, G) function elicits hyperlocomotion that closely resembles characteristics of *foxp2* mutant behavior (Fig. 25A). Consequently, it is asked whether GABAergic signaling components involved in activity regulation are altered upon Foxp2 loss of function. In fact, expression analysis by qPCR revealed a significant reduction of *gad1b* transcript (and putatively increased levels for *gad1a* and *gad2*) in *foxp2* mutants (Fig. 28A). To verify whether reduced (Gad-mediated) GABA synthesis and thus reduced GABAergic signaling underly hyperlocomotion in *foxp2* mutants, *foxp2*$^{+/-}$ were treated with the GABA-A-R agonist muscimol to compensate for an alleged deficit in GABAergic signaling.

In line with previous observations, untreated *foxp2*$^{+/-}$ display significantly increased locomotor activity compared to wildtype siblings (Fig. 28B). However, upon muscimol treatment, hyperlocomotion of *foxp2*$^{+/-}$ is reduced to wildtype-like activity, whereas the locomotor activity of wildtype siblings themselves is not significantly altered (Fig. 28B). These findings show that increasing GABA-A-R-mediated inhibition rescues hyperlocomotion of *foxp2* mutants and thus support the notion that reduced GABAergic signaling underlies hyperlocomotion of *foxp2* mutants.

4.5   Foxp2 as a (central) regulator of genetic and functional networks implicated in psychiatric disorders

4.5.1   *foxp2* mutants and *gad1b* splice-morphants differentially respond to MPH treatment compared to corresponding controls

Like other core symptoms described for ADHD patients, hyperactivity is primarily treated by the well-established psychostimulant methylphenidate (MPH, for more details, see 1.1.5). Since both *FOXP2* and *GAD1* represent putative ADHD risk genes (Bruxel et al. 2016, Demontis et al.

2019), hyperlocomotion of *foxp2* mutants and *gad1b* morphants was targeted for a functional rescue by an acute application of MPH.

Interestingly, neither *foxp2* mutants (Fig. 23C) nor *gad1b* morphants (Fig. 23D) respond to MPH, whereas in line with its stimulating properties, MPH evokes mutant-like hyperlocomotion in the corresponding controls (Fig. 23C, D). The differential response to MPH of wildtypes versus mutants and morphants suggests that *foxp2* and *gad1b* loss of function directly or indirectly affects MPH targets or MPH-relevant signaling networks. Hence, *foxp2-* and *gad1b*-dependent networks, involved in activity regulation, represent exciting targets for future investigations on the neuromechanistic action of MPH in ADHD therapy.
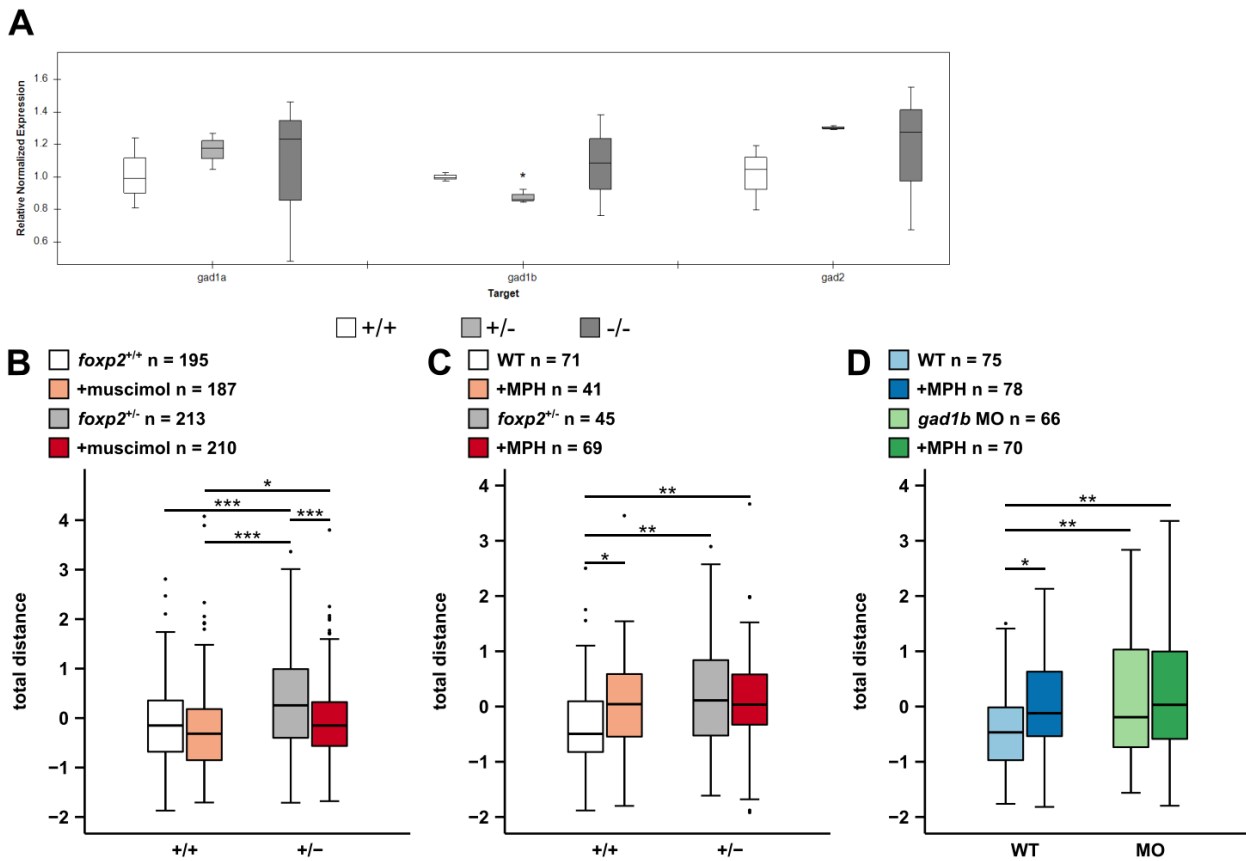
Figure 28: **Implication of GABAergic signaling in *foxp2*$^{+/-}$ hyperlocomotion and a methylphenidate (MPH) rescue approach in *foxp2* mutants and *gad1b* morphants.** (A) Relative normalized expression of *gad1a*, *gad1b* and *gad2* in *foxp2*$^{+/+}$ (white), *foxp2*$^{+/-}$ (light grey) and *foxp2*$^{-/-}$ (dark grey) siblings based on qPCR. *$P<0.05$. (B) Total distance swum by *foxp2*$^{+/+}$ and *foxp2*$^{+/-}$ in response to 48 hours incubation in 0.05 mM GABA-A-R agonist muscimol (light red and dark red, respectively) or Danieau's solution (white and grey, respectively). (C, D) Total distance swum by *foxp2*$^{+/+}$ and *foxp2*$^{+/-}$ (C) or *gad1b* MO and uninjected controls (D) after acute treatment (1 h) with 0.012 mM MPH (light red, dark red and dark blue and dark green, respectively) or pure Danieau's solution (white, grey and light blue, light green, respectively). Sample sizes are given by n. Z-score transformation was applied for standardization of raw datasets. *$P<0.05$, **$P<0.01$, ***$P<0.001$. The MPH-rescue experiment on *foxp2* mutants was performed by V. Schöffler. Adjusted from Lueffe et al. 2021a.

4.5.2   Foxp2 regulates numerous risk genes implicated in various psychiatric disorders

Numerous alleged FOXP2 target genes were revealed by genome-wide ChIP-chip screens (Spiteri et al. 2007, Vernes et al. 2007, 2008, 2011). Interestingly, many of these genes were described in the context of risk loci for NDDs and other psychiatric disorders, suggesting that FOXP2 might be a central regulator of genetic and functional networks affected in psychiatric conditions. To test this hypothesis on a small scale, transcript levels for risk loci-associated and alleged FOXP2 target genes were determined in *foxp2* mutants (for target gene list, see Table 8). Besides the aforementioned increase in *cntnap2b* expression (Fig. 23D), a risk candidate for autism, epilepsy, Tourette syndrome, OCD, schizophrenia, intellectual disability, language impairment, ADHD and associated with hyperactivity in corresponding knockout mice (Verkerk et al. 2003, Strauss et al. 2006, Belloso et al. 2007, Alarcón et al. 2008, Arking et al. 2008, Bakkaloglu et al. 2008, Friedman et al. 2008, Rossi et al. 2008, Jackman et al. 2009, Poot et al. 2010, Zweier et al. 2009, Elia et al. 2010, Mefford et al. 2010, Petrin et al. 2010, Sehested et al. 2010, O'Dushlaine et al. 2011, Peñagarikano et al. 2011, Rodenas-Cuadrado et al. 2014), significantly elevated transcript levels were also observed for *adgrl3* (associated with ADHD and SUD (Arcos-Burgos et al. 2010, Ribasés et al. 2011, Acosta et al. 2016, Martinez et al. 2016, Arcos-Burgos et al. 2019)) (Fig. 29A) and *mef2cb* (associated with ADHD and intellectual disability susceptibility as well as altered anxiety-like behavior in mice (Li et al. 2008, Zweier et al. 2010, Zhao et al. 2018, Demontis et al. 2019, Yauy et al. 2019)) (Fig. 29C) . Although most targets failed to reach statistical significance in *foxp2* mutants, the transcript levels still tend to be increased for many of them. This applies to the paralog *mef2ca* (Fig. 29C), additional ADHD risk candidates like *dusp6*, *pcdh7a*, *sema6d* (Fig. 29B, C, D (Demontis et al. 2019)) and risk candidates for other psychiatric disorders like schizophrenia (*slitrk2*, Fig. 29A (Piton et al. 2011)), bipolar disorder (*dusp6*, Fig. 29B (Lee et al. 2006, Kim et al. 2012)), anxiety disorders (*ntrk2b*, Fig. 29C (Purves et al. 2020)) and autism (*ppp1r1b*, Fig. 29D (Hettinger et al. 2012)). Taken together, although the majority of genes were not significantly altered, the observed trend for many of them still indicates that Foxp2-regulated gene networks are exciting targets for future studies on shared genetic liability and/or etiopathogenesis of different psychiatric disorders.
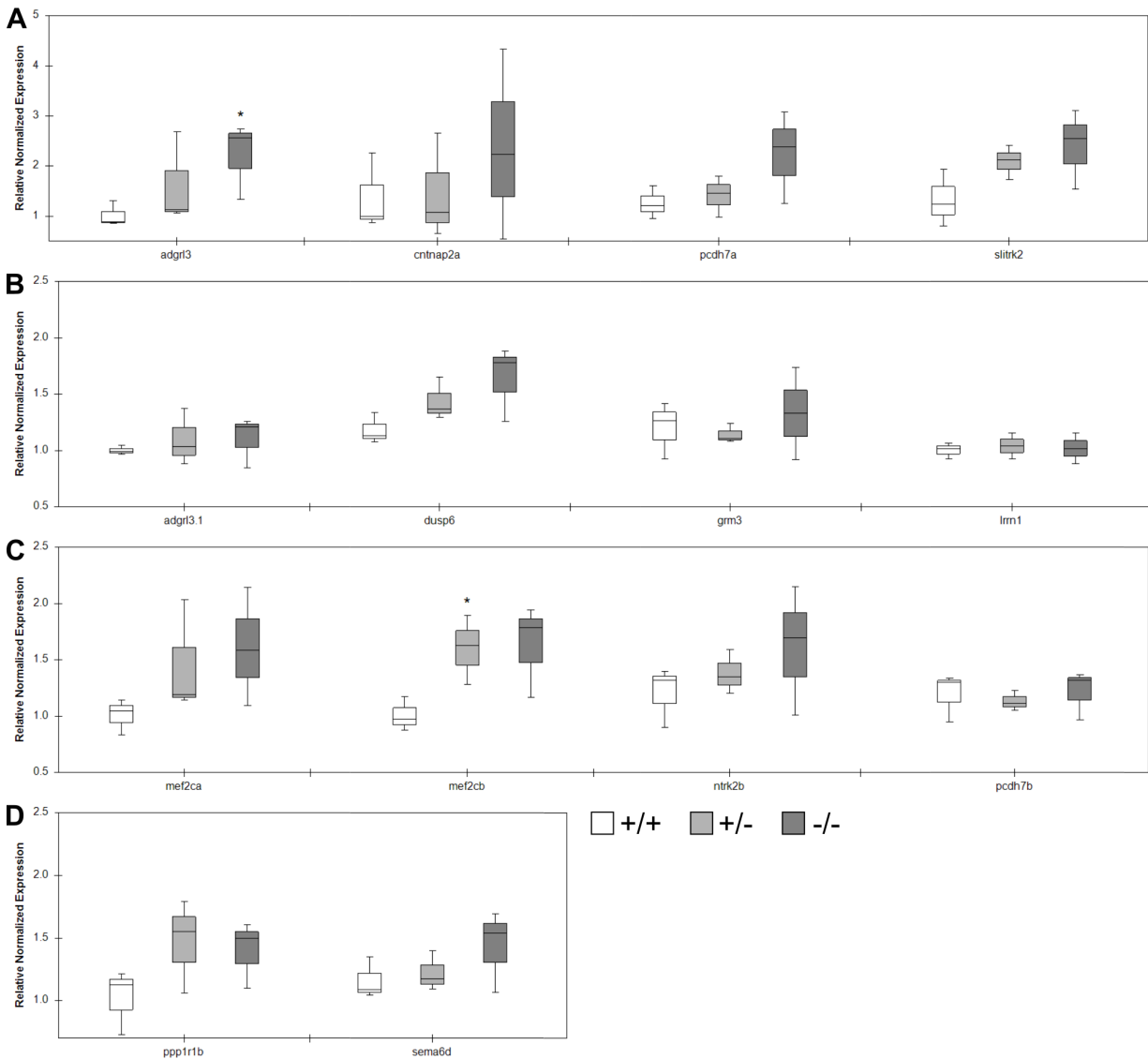
Figure 29: **Relative normalized expression of putative Foxp2 target genes in *foxp2* CRISPR/Cas9 mutants.** For expression normalization, the housekeeping genes actin, beta 1 (*actb1*), and glyceraldehyde-3-phosphate dehydrogenase (*gapdh*) were used. Relative normalized expression of putative Foxp2 target genes was determined in *foxp2*$^{+/+}$ (white), *foxp2*$^{+/-}$ (light grey), and *foxp2*$^{-/-}$ (dark grey), of which *foxp2*$^{+/+}$ served as controls. Examined target genes are listed in Table 8. Statistically relevant values are listed in Table 15. *P<0.05. qPCR was performed by Z. Gioga. Adjusted from Lueffe et al. 2021a.

5 Discussion

Despite the continuously growing number of potential risk genes in neurodevelopmental disorders like ADHD, the mechanistic link to neurological and functional alterations of ADHD patients remains elusive for most of them. The present work started to fill this gap by providing information on expression domains, corresponding neurochemical identity and anatomical, genetic, and functional alterations upon loss of function for the ADHD risk gene paralogs *grm8a*, *grm8b*, *foxp2*, and *gad1b*. In addition, with the generation and validation of CRISPR/Cas9 mutant lines and splice-morphants, it paves the way for further investigations on mechanistic alterations underlying ADHD symptomatology.

Besides the general verification of *grm8a*, *grm8b*, and *foxp2* transcripts in the CNS of developing and adult zebrafish, RNA ISH-based analysis revealed expression in brain regions implicated in motor functions like subpallium, thalamus, cerebellum and medulla oblongata. Accordingly, behavioral investigations in the established CRISPR/Cas9 mutants and splice-morphants confirmed a role for Grm8a, Grm8b, Foxp2, and Gad1b in locomotor activity regulation of zebrafish larvae. In addition, Grm8a, Grm8b, and Gad1b were identified to be involved in the regulation of fear-related response. Motivated by a similar activity phenotype in *gad1b* morphants, an implication of deficient GABAergic signaling in altered activity regulation was suggested and behaviorally and pharmacologically confirmed. Observed colocalization between *foxp2*, *grm8a*, and *gad1a* expression and altered GABAergic cell quantity upon Grm8a loss of function further indicate that altered GABAergic signaling underly impaired activity regulation in *foxp2* mutants and *grm8a* (and *grm8b*) morphants and mutants. The functional rescue of *foxp2* mutant hyperactivity by GABA-A-R activation (using the GABA-A-R agonist muscimol) supports the hypothesis, thus demonstrating for the first time that altered GABAergic signaling is implicated in impaired activity regulation upon Foxp2 loss of function. Finally, qPCR-based expression analysis tested the hypothesis that Foxp2 acts as a regulator in biological pathways that may, at least partly, explain the polygenic architecture of ADHD and genetically and functionally link multiple psychiatric disorders.

5.1   Expression, but not behavioral analysis, suggests subfunctionalization of Grm8a and Grm8b in locomotor activity regulation and fear response.

Although repeatedly associated with various mental disorders (Serajee et al. 2003, Takaki et al. 2004, Elia et al. 2012, Li et al. 2016, Sangu et al. 2017), GRM8 still represents one of the least explored metabotropic glutamate receptors. Accordingly, neuronal mechanisms involved in Grm8 function are unknown in zebrafish. Due to whole-genome duplication, functional investigations of GRM8 in zebrafish comprise two paralogs, namely Grm8a and Grm8b. Although slightly (2 amino acids) higher for Grm8a, both paralogs show substantial amino acid similarity (93 %) to the human GRM8, indicating that both could implement the ancestral function.

In order to evaluate to which extent both paralogs resemble *Grm8* expression patterns of other vertebrate species, take over common or distinct functions, and are affected by a possible neo- or subfunctionalization that requires consideration during functional investigations, the expression pattern of both paralogs was examined. The similarity of *Grm8* expressing brain regions in rodents and suggested anatomical equivalents with *grm8a* and/or *grm8b* expression in zebrafish argues against a neofunctionalization of Grm8a and Grm8b (Messenger et al. 2002, Haug et al. 2013). However, expression domains specific to Grm8a or Grm8b, especially during early development like in the posterior tuberculum (*grm8a*), the cerebellum (*grm8a*) and the pallium (*grm8b*), indicate that both paralogs underwent a partial subfunctionalization. Several brain regions implicated in sensory-motor integration or motor control in the di- and rhombencephalon show distinct or comparably stronger expression for *grm8a* indicating that associated functions might be specific to Grm8a. One example is the posterior tuberculum, which comprises a number of dopamine-synthesizing neuronal populations in the zebrafish diencephalon that, like dopaminergic neurons of the substantia nigra/ventral tegmental area in mammals, provide input to the (teleostean) striatum (Rink and Wullimann 2001, 2004, Tay et al. 2011, Wullimann and Umeasalugo 2020). *Grm8* expression in the substantia nigra (SN) was also detected in mice with stronger labeling in the BG-innervating SN pars compacta (Messenger et al. 2002). Together with the thalamus, which equally displays distinct *grm8a*

expression during early zebrafish development and highest *Grm8* transcript labeling in mice (Messenger et al. 2002), the SN plays a significant role in the BG motor circuit. Alterations of the BG motor circuit induce severe deficits in motor execution and motor control implicated in various movement disorders like Parkinson's and Huntington's disease (Reiner et al. 1988, Thompson et al. 1988, Filion and Tremblay 1991, Carter et al. 1999, Kravitz et al. 2010, André et al. 2011, Deng et al. 2014). Structural and functional alterations in ADHD also affect brain regions involved in the BG motor loop (Ivanov et al. 2010, Norman et al. 2016, Hoogman et al. 2017), and hyperactivity is one of the core phenotypes of ADHD. Hence on account of *grm8a/grm8b/Grm8* expression in brain regions involved in the BG motor circuit (or functional equivalents) it is assumed that the deficiency of either Grm8a specifically or Grm8a and Grm8b interferes with motor control in the di- or telencephalon (Saugstad et al. 1997). Accordingly, the here established *grm8a* and *grm8b* morphants show altered locomotor activity, however, in contrast to distinct *grm8a* expression in the thalamus and posterior tuberculum, with a similar hyperlocomotive phenotype upon Grm8a and Grm8b loss of function. Therefore, it is questionable whether distinct expression domains of either *grm8a* or *grm8b* account for the observed activity phenotype of *grm8a* and *grm8b* morphants. Instead, overlapping expression in regions like the teleostean striatum (subpallium) with GPi (entopeduncular nucleus (EN)) may play a significant role.

The discrepancy between the increased locomotor activity of *grm8a* and *grm8b* morphants and the decreased (*grm8a*) and unchanged (*grm8b*) locomotor activity of *grm8* mutants raises questions about the true impact of Grm8a and Grm8b loss of function on activity regulation. Several publications suggest that discrepancies between morphant and mutant behavior arise from genetic compensation under full knockout conditions (Rossi et al. 2015, El-Brolosy et al. 2019). Since Grm8a and Grm8b show a substantial similarity in their amino acid sequence (∼93 %) and partially gene expression pattern they were assumed to compensate each other mutually upon loss of function. However, altered locomotor activity of *grm8a-* and unchanged locomotor activity of *grm8b* mutants indicate that Grm8b fails to compensate Grm8a loss of function entirely. This could be explained by the broader expression pattern of *grm8a* compared to *grm8b* (Haug et al. 2013).

If Grm8b partially fails to compensate Grm8a loss of function due to differential expression, this is expected to shift the mutant effect from several to individual brain regions. For instance, the posterior tuberculum, specific to the *grm8a* expression pattern, is unlikely to be affected by Grm8b compensation, whereas in the subpallium (with expression of both paralogs) a compensation could be possible. Neurons of both regions are assumed to be implicated in a functional equivalent of the mammalian BG motor circuit and, therefore, are expected to be involved in the observed locomotor phenotype of *grm8a* and *grm8b* morphants and mutants. Functional investigations in mice have demonstrated that mGluR III impairment on disparate levels of the BG motor circuit induces opposing alterations of motor regulation (Lopez et al. 2007). Thus, the difference between several affected brain regions in morphants and just a fraction of it affected in mutants (due to partial compensation by Grm8b) provides a possible explanation for the opposed locomotor phenotypes of *grm8a* morphants and *grm8a* mutants.

Behavioral investigations for a potential compensation effect failed to demonstrate significant differences between single (*grm8a* or *grm8b* disrupted) and double mutants (both disrupted). Likewise, preliminary results from qPCR-based expression analysis (not shown) revealed no significant upregulation of *grm8b* or *grm8a* expression in *grm8a* or *grm8b* mutants, respectively. However, since other mGluRs III, like Grm4 and Grm7, likewise show a substantial amino acid similarity (Grm4: 85 %, Grm7: 86 %) and considerable overlap in expressing brain regions to Grm8a and Grm8b (Haug et al. 2013), they also represent likely candidates for a potential compensation effect in *grm8a* and *grm8b* mutants. Therefore, future attempts to unravel possible compensation effects in *grm8a* and *grm8b* mutants should consider *grm4* and *grm7* for prospective expression analyses.

Besides genetic compensation, GRM8 implication in fear response (Linden et al. 2002, Duvoisin et al. 2005, Robbins et al. 2007, Fendt et al. 2010) is expected to influence the locomotor activity phenotype. Investigations in mice demonstrated that altered locomotor activity upon GRM8 loss of function is triggered by novelty and enclosed environment (Gerlai et al. 2002, Duvoisin et al. 2005). Innate fear response in mammals and fish is regulated by the amygdala and the medial pallium, respectively (Zangrossi et al. 1999, Portavella et al. 2004, Lal et al.

2018). However, despite specific expression of *grm8b* in the developing (medial) pallium, *grm8a* morphants and *grm8b* mutants equally display increased thigmotaxis behavior. Accordingly, no correlation between thigmotaxis and locomotor activity phenotype in Grm8a- and Grm8b-deficient larvae was observed. Thus, altered fear response upon Grm8a and Grm8b loss of function is expected to interfere with the locomotor activity of Grm8a- and Grm8b-deficient individuals to the same extent.

Like mice (Malherbe et al. 1999), *grm8a* and *grm8b* expression in zebrafish indicates similar abundance in the developing and adult zebrafish brain but with temporal differences in the dimension of transcript distribution. Further, paralog-specific expression patterns like in the pallium, the thalamus and the posterior tuberculum become more similar with time, suggesting that paralog-specific functional alterations alleviate but do not disappear with age. Especially brain regions implicated in sensory-motor integration like cerebellum and pretectum maintain *grm8a*-specific expression and thus are expected to cause persistent alterations in sensory-motor integration in Grm8a-deficient individuals.

Taken together, disparate effects on thigmotaxis and locomotor activity in *grm8a* or *grm8b* mutants and *grm8a* or *grm8b* morphants indicate that paralog-specific expression domains do not primarily account for the observed behavioral phenotypes but shape the individual responsiveness to putative compensation mechanisms. However, distinct expression of *grm8a* in brain regions implicated in sensory-motor integration suggests that additional behavioral assays are required to determine paralog-specific phenotypes. Further, missing indications for a neofunctionalization of Grm8a or Grm8b and observed similarity in the activity phenotype of *grm8a* and *grm8b* morphants suggest that further investigations of Grm8 function in activity regulation should consider the simultaneous disruption of both GRM8 paralogs.

5.2   Deficient GABAergic signaling is implicated in genetically induced alteration of activity regulation and possibly fear response upon Foxp2, Grm8a, (and Grm8b) loss of function

Neurochemical alterations are a repeatedly described condition in ADHD neuropathology (Forssberg et al. 2006, Carrey et al. 2007, Edden et al. 2012, Puts et al. 2020) and predominantly studied with respect to dopaminergic transmission for two reasons. Firstly, the successful therapy of ADHD symptoms using psychostimulants (Faraone et al. 2006b, Castells et al. 2011) and secondly, observations on genetic abnormalities of dopamine signaling components in ADHD patients (Li et al. 2006, Gizer et al. 2009). In fact, the dopaminergic system is involved in the regulation and/or generation of several behavioral outputs reported to be affected in ADHD, like locomotor activity (Draper et al. 2007, Yates et al. 2016). However, besides the dopamine transporter or receptors (Li et al. 2006, Gizer et al. 2009), only minor experimental support exists for a function of putative ADHD risk candidates in dopaminergic signaling. Accordingly, no direct involvement of GRM8 in dopaminergic transmission is described so far, whereas experimental evidence indicates that the dopamine-synthesizing enzyme tyrosine hydroxylase (TH), the dopamine D1 receptor (D1R) as well as its downstream signaling molecule DARPP-32 are transcriptional targets of FOXP2 (Murugan et al. 2013, Co et al. 2019, Day et al. 2019).

In the present work, *grm8a* and *foxp2* expression domains were screened for a possible colocalization with the expression pattern of the monoaminergic marker gene *vmat2*. Intriguingly, *grm8a* and *foxp2* overlap with *vmat2* expression in several brain regions, including the ventral telencephalon which encompasses the teleostean striatum. Notably, colocalization in the ventral telencephalon is restricted to single cells, whereas the majority of *foxp2-* and *grm8a-*expressing cells are merely located in proximity to *vmat2*-positive cells. Therefore, it is assumed that most *foxp2-* and *grm8a* expressing neurons in the ventral telencephalon receive monoaminergic input, presumably from posterior tuberculum (Rink and Wullimann 2001), instead of releasing it themselves. Intriguingly, the situation is similar in mammals. Both *Foxp2* and *Grm8* are expressed by GABAergic (D1R/Grm8)-medium-spiny neurons (MSNs) in the mammalian striatum (van Rhijn et al. 2018, Savell et al. 2020) that receive dopaminergic in-

put (D1R-MSN) from the SN and play a significant role in the BG motor circuit. *foxp2* and *grm8a* expression in GABAergic neurons of the zebrafish CNS was investigated by a two-color RNA ISH with the GABAergic marker and ADHD risk gene paralog *gad1a*. Both *foxp2* and *grm8a* substantially overlap with *gad1a* expression across several brain regions comprising the ventral telencephalon (subpallium), thus indicating two things. Firstly, Foxp2 and Grm8a are probably implicated in a functional equivalent of the mammalian BG motor circuit in zebrafish. Secondly, GABAergic transmission plays a significant role in Foxp2 and Grm8a function and thus presumably, in the genetic etiopathogenesis of ADHD.

Intriguingly, there is growing evidence from genetics, functional imaging, and animal models (Yang et al. 2013a) suggesting that altered GABAergic signaling plays a yet underrated role in ADHD pathology. Functional imaging studies consistently reported altered GABA levels in multiple brain regions of ADHD patients (Edden et al. 2012, Bollmann et al. 2015, Puts et al. 2020). In addition, several genetic variants of GABAergic signaling components like the GABA-transporter GAT1 and multiple GABA-A-R subunits correlate with the risk and/or severity of ADHD (Polan et al. 2014, Naaijen et al. 2017, Yuan et al. 2017). Accordingly, *GAD1* polymorphisms were associated with the hyperactive/impulsive presentation of ADHD (Bruxel et al. 2016). Interestingly, colocalization of *foxp2, grm8a,* and *gad1a* expression was primarily observed in brain regions implicated in motor functions like the subpallium, the posterior tuberculum and the medulla oblongata. Further, *foxp2* mutants and *grm8a* and *grm8b* morphants were demonstrated to be hyperlocomotive similar to *Gad1* knockout mice (Yang et al. 2013a, Smith 2018), the here presented *gad1b* morphants as well as GABA-A-R antagonist (L-allylglycine) treated wildtype larvae. Together with the functional rescue of *foxp2* mutant hyperactivity by increasing GABA-A-R mediated inhibition with the GABA-A-R agonist muscimol, the present work demonstrates that altered GABAergic signaling underly deficient activity regulation upon Foxp2 and potentially Grm8a loss of function. Thus, with Grm8a, Grm8b, Gad1b, and Foxp2 this work presents risk candidate paralogs that link genetic predisposition, neuropathological alteration, and an ADHD-associated phenotype. Further, the collected data emphasizes the particular importance of uncovering Foxp2, Grm8a and Grm8b function in GABAergic transmission of functional circuits involved in activity regulation to understand how genetic risk

variants like those described for *FOXP2* and *GRM8* (Elia et al. 2012, Demontis et al. 2019) contribute to ADHD symptoms like hyperactivity.

So far, the biological mechanism(s) through which Foxp2, Grm8a, and Grm8b interfere with GABAergic signaling is unclear. Previous investigations identified FOXP2 as a transcriptional regulator of *Gad1* (Vernes et al. 2011, van Rhijn et al. 2018) and revealed altered GABA-mediated inhibitory currents in striatal MSNs of *Foxp2* knockout mice (van Rhijn et al. 2018). The present work likewise shows altered *gad1b* expression in *foxp2* mutants. Thus, Foxp2 deficiency is expected to interfere with GABAergic signaling on the level of Gad1(b)-mediated GABA synthesis. Moreover, FOXP2 promotes GABAergic synapse formation through inhibition of *Mef2c* (Chen et al. 2016, Harrington et al. 2016). According to the applied qPCR-based analysis, expression of *mef2c* is upregulated in *foxp2* mutants suggesting that the GABAergic synapse formation could be significantly impaired as well. In addition, FOXP2 acts as a transcriptional regulator of *Shhrs* (Vernes et al. 2011). *Shhrs* gives rise to a long non-coding RNA that controls the expression of the transcription factors DLX5 and DLX6 (Feng et al. 2006), which play a significant role in the development and correct functioning of GABAergic neurons (Levi et al. 2003, Long et al. 2003, Cho et al. 2015, Wang et al. 2010). Thus, Foxp2 loss of function might already interfere with the GABAergic system during neurodevelopmental processes such as neuronal migration and/or differentiation (Perera et al. 2004). The previously reported reduction of GABA positive cells upon *cntnap2* loss of function (Hoffman et al. 2016), a FOXP2/Foxp2 target gene confirmed by the present and by previous data (Vernes et al. 2008, 2011, Adam et al. 2017), was not observed in *foxp2* mutants, thus unlikely plays a significant role for the hyperlocomotive phenotype.

In *grm8a* morphants and mutants, however, the number of GABA-positive cells is significantly altered. Recent findings from cancer research suggest that GRM8 regulates cell proliferation through inhibition of cAMP- and activation of MAPK pathway (Zhang et al. 2019). Thus, alterations in GABAergic cell quantity upon Grm8a loss of function may indicate that disturbed proliferation underly impaired GABA-regulated processes. In addition, the neuroprotective properties of GRM8, including the regulation of ER Ca^{2+} release (Woo et al. 2021) and trans-

mitter release regulation (Marabese et al. 2005, Erdmann et al. 2012), suggest that the reduction of GABA-positive cells in the forebrain of *grm8a* morphants could also be an indicator for increased excitotoxicity. Interestingly, excitotoxicity following depletion of presynaptic glutamate is repeatedly described as a major consequence of ischemic hypoxia (Choi and Rothman 1990), an environmental risk factor in ADHD etiology (Getahun et al. 2013). Since GRM8 was shown to modulate the resilience to excitotoxicity (Woo et al. 2021), the genetic interference with GRM8 function may facilitate neuronal damage in response to ischemic hypoxia during neonatal, pregnancy, labor, or delivery complications.

Like FOXP2, experimental data demonstrates that GRM8 is involved in synapse development. GRM8 as well as other mGluRs III, are implicated in the generation of transsynaptic complexes (Dunn et al. 2019) similar to the ADHD risk candidate LPHN3 (Jackson et al. 2016). Transsynaptic complexes ensure targeted synaptic connectivity and modulate synaptic function (Dunn et al. 2019, Sando et al. 2019). Accordingly, disruption results in impaired transmitter signaling and neuropsychiatric manifestations like hyperactivity and increased fear response (Dunn et al. 2019). Therefore, the disturbed function of Grm8a or Grm8b on GABA-releasing terminals may interfere with GABAergic synapse formation and/or targeted signal transmission, causing observed alterations in locomotor activity regulation and thigmotaxis behavior. Besides indirect effects via GABAergic cell quantity or synapse development, the reported function in the presynaptic release regulation of GABA (Marabese et al. 2005) implies that Grm8a and Grm8b deficiency may interfere with GABAergic signaling directly.

Pronounced thigmotaxis behavior upon Grm8a, Grm8b and Gad1b loss of function is in line with the enhanced fear response of *Grm8* and *Gad1* knockout mice (Linden et al. 2002, Miyata et al. 2021). Further, the behavioral similarity to the here presented *gad1b* morphants and GAD1-deficient mice supports the assumption (Fendt et al. 2010) that altered GABAergic signaling underly impaired fear response upon Grm8a and Grm8b loss of function. In addition, it provides translational support for the suggested link between *GAD1* polymorphisms and anxiety susceptibility in humans (Hettema et al. 2006, Donner et al. 2012) and points out *GRM8* and *GAD1* disruption as possible genetic rationales for comorbid anxiety in ADHD (D'Agati

et al. 2019). Importantly, the unchanged thigmotaxis behavior of *foxp2* mutants suggests that in line with previous assumptions, alteration of activity regulation and fear response involves different types of GABAergic interneurons (Miyata et al. 2021) and thus different GABAergic mechanisms that require separate investigations in future research approaches.

5.3 Morphological and functional observations suggest that GABAergic alterations upon Foxp2, Grm8a, and Grm8b loss of function are rooted in the ventral forebrain

Gene expression analysis and behavioral investigations upon genetic and/or pharmacological disruption of Grm8a, Grm8b, Gad1b, and Foxp2 function provide strong evidence that Foxp2, Grm8a, and Grm8b loss of function interfere with GABAergic signaling inducing deficient activity regulation in zebrafish larvae. Accordingly, literature (as discussed previously) indicates that FOXP2 and GRM8 are implicated in multiple developmental and functional processes that ensure the correct functioning of GABAergic systems. However, while the implication of Foxp2, Grm8a, and Grm8b in GABAergic signaling is experimentally supported, it can only be speculated about the identity of affected brain regions or functional circuits.

Recent investigations of cortical and subcortical transmitter levels in ADHD affected individuals found GABA to be solely reduced in the patient's striatum (Puts et al. 2020). Intriguingly, *Foxp2* expression in GABAergic neurons is most frequently described for striatal dopamine D1 receptor (D1R)-expressing medium spiny neurons (MSNs) (Vernes et al. 2011, van Rhijn et al. 2018, Savell et al. 2020). Similarly, *Grm8* expression in the striatum was demonstrated in the past (Malherbe et al. 1999, Messenger et al. 2002) and has recently been localized to a probably novel class of GABAergic medium spiny neurons (Grm8-MSNs) with also strong expression of *Foxp2* (Savell et al. 2020). Likewise, the present work reveals overlapping expression of *foxp2*, *grm8a* and *gad1a* in the ventral telencephalon (subpallium), which comprises the teleostean striatum. In addition, former investigations demonstrated colocalized *foxp2* and *dlx5/dlx6* (marker for GABAergic forebrain neurons) expression in the zebrafish telencephalon (Bonkowsky and Chien 2005). Together with the reduced number of GABA-positive neurons in the telencephalon of *cntnap2* (Foxp2 target) mutants (Hoffman et al. 2016) and presented *grm8a* morphants, present and previous findings indicate that altered GABAergic signaling upon Foxp2, Grm8a, and Grm8b loss of function could be rooted in the ventral telencephalon (subpallium).

Predominant expression of *Foxp2* in direct pathway (D1R-positive) MSNs (Vernes et al. 2011, van Rhijn et al. 2018) and altered inhibitory currents in D1R- and not D2R MSNs of *Foxp2* mutants (van Rhijn et al. 2018) imply that FOXP2 loss of function primarily disrupts GABAergic signaling in D1R-expressing MSNs of the striatum. Accordingly, the ratio of D1R to D2R in striatal MSNs of *Foxp2* mutants was demonstrated to be significantly reduced (Xiao et al. 2021). In zebrafish, the existence of a direct and indirect-like pathway in the telencephalon remains unclear (Wullimann 2014). Studying the BG and its functional circuits in the lamprey, the phylogenetically oldest living vertebrate species, revealed that the BG organization, including the existence of direct and indirect pathway (Stephenson-Jones et al. 2011, 2012) and their segregated expression of and differential modulation via D1R and D2R (Ericsson et al. 2013) is conserved throughout vertebrate (including non-mammalian) evolution. Accordingly, investigations in zebrafish identified subpallial inhibitory cell cluster with a molecular profile similar to mammalian D1R-MSNs and D2R-MSNs (Aguda 2019). Further, they revealed SNc-striatum-like dopaminergic projections from the posterior tuberculum to the subpallium (Rink and Wullimann 2001), and measured opposing effects on movement initiation upon D1R or D2R activation (Souza et al. 2011). Thus, experimental evidence argues for the existence of anatomical and functional equivalents of direct and indirect pathway in zebrafish.

Like the predominant function of FOXP2 in direct pathway MSNs, experimental evidence indicates that the psychostimulant MPH reduces molecular and functional alterations specifically in the direct pathway of the striatal BG (Brandon and Steiner 2003, Yano and Steiner 2005, Frank et al. 2007). Intriguingly, the present work showed that in contrast to the induction of hyperlocomotion in wildtype controls, neither *foxp2* mutants nor *gad1b* morphants respond to MPH treatment. This indicates that Foxp2 and Gad1b loss of function disrupts biological mechanisms involved in MPH function and locomotor activity regulation. Admitting that zebrafish possess a functional equivalent of direct pathway MSNs, it is expected that altered expression of D1R (upon Foxp2 loss of function) and downstream Gad1b (upon genetic interference with *gad1b* and Foxp2 function) disrupt GABAergic signaling evoked by the increased extracellular dopamine level upon striatal reuptake inhibition by MPH (Hurd and Ungerstedt 1989, Butcher et al. 1991, Volkow et al. 2001).

Thus, the present work provides experimental evidence that alterations of the dopaminergic system act upstream of disturbed GABAergic signaling upon Foxp2 and Gad1b loss of function. This supports the hypothesis in ADHD neurochemistry (1.1.4.3) that besides alterations of dopamine and dopaminergic signaling components, dopamine fails to modulate other transmitter systems (Sagvolden et al. 2005) like the here suggested downstream release of GABA in striatal MSNs. However, further research is required to confirm the hypothesis and explore whether altered GABAergic signaling upon Foxp2, Grm8a, and Grm8b loss of function is rooted in the ventral telencephalon and more explicitly in D1R-MSN-like neurons of zebrafish larvae.

5.4   Is FOXP2 a master regulator in ADHD polygenicity and comorbidity?

Observed contribution of different ADHD risk candidate paralogs like Foxp2, Grm8a, Grm8b, and Gad1b to the expression of a similar (ADHD-associated) behavioral phenotype like hyper-locomotion supports the polygenic architecture of ADHD. To date, multiple ADHD risk candidates were identified (Gizer et al. 2009, Williams et al. 2010, Elia et al. 2012, Demontis et al. 2019). However, while their functional role in ADHD pathology is now being addressed, it remains largely unclear how the disruption of this complex genetic network is implemented. Facing the same situation in other psychiatric disorders, researchers explored the hypothesis that the functional disruption of individual transcription factors and, consequently, the differential expression of the corresponding regulons contribute to the manifold genetic (and functional) alterations observed in various psychiatric disorders (Pfaffenseller et al. 2016, Doostparast Torshizi et al. 2019, Bristot et al. 2020). In fact, they identified 40 of the so-called master regulator (MR) candidates for bipolar disorder, schizophrenia, and MDD and demonstrate that MRs contribute to overlapping and disorder-specific attributes as well as the general susceptibility to psychiatric disorders (Bristot et al. 2020).

So far, no MR candidate was identified in ADHD etiology. However, throughout the present study, it was noticed that several ADHD risk genes (including *GAD1* and *GRM8*) coincide with target genes of the ADHD risk candidate and transcription factor FOXP2 (Spiteri et al. 2007, Konopka et al. 2009, Vernes et al. 2011, Elia et al. 2012, Chen et al. 2016, Bruxel et al. 2016, Zhao et al. 2018). Accordingly, a literature-based comparison reveals that 13 out of 27 ADHD risk genes (suggested by GWAS) (Demontis et al. 2019) are listed as transcriptional targets of FOXP2 by ChIP datasets (Vernes et al. 2011, Rouillard et al. 2016). Together, these findings suggest FOXP2 as a possible MR in the genetic etiology of ADHD.

The present work tested this hypothesis on a small scale, determining expression alterations of multiple ADHD-associated genes (Lasky-Su et al. 2008, Ribasés et al. 2008, Arcos-Burgos et al. 2010, Elia et al. 2010, Williams et al. 2010, Ribasés et al. 2011, Lange et al. 2012, Jain et al. 2012, Bruxel et al. 2016, Shinwari et al. 2017, Lange et al. 2018, Zhao et al. 2018, Demontis et al. 2019, Klein et al. 2020) in the *foxp2* mutant line. Five out of seventeen paralogous genes

of ADHD candidates examined by the present study showed significantly altered transcript levels and additional five a similar trend. Hence Foxp2 appears to be an important regulator of ADHD-associated gene sets. Since only three out of twelve aforementioned FOXP2 targets and ADHD risk candidates were included in the analysis, it is expected that the regulatory network, affected upon FOXP2/Foxp2 loss of function and with functional relevance in ADHD, is even larger as indicated by the present data. Therefore, the functional disruption of FOXP2 represents one possible explanation for the complex genetic alterations and polygenic contribution in ADHD etiology.

In line with the frequent occurrence of comorbid disorders in ADHD patients (Gnanavel et al. 2019), ADHD risk candidates overlap to a substantial degree with putative risk genes of other psychiatric disorders (Lotan et al. 2014) suggesting that comorbidity is based on shared genetic liability. Interestingly, gene networks of individual MRs show similar activation patterns across different psychiatric disorders (Bristot et al. 2020), indicating that the functional disruption of individual MRs possibly underly genetic, functional, and/or behavioral similarity across different psychiatric disorders. The incidence with which risk variants of other disorders cluster to the genetic network controlled by FOXP2 is striking. Accordingly, several FOXP2 target genes investigated by the present work are related to multiple disorders (Lee et al. 2006, Alarcón et al. 2008, Friedman et al. 2008, Hettinger et al. 2012, Kim et al. 2012, Arcos-Burgos et al. 2019) and, as mentioned before, show altered transcript levels upon Foxp2 loss of function. Therefore, altered FOXP2 function is speculated to contribute to genetic and functional underpinnings of comorbid psychiatric disorders in ADHD patients.

In a joint effort, researcher of the Cross-Disorders Group of the Psychiatric Genomics Consortium investigated the genetic underpinnings of overarching genetic influence in eight psychiatric disorders (Cross-Disorder Group of the Psychiatric Genomics Consortium 2019). One hundred nine pleiotropic loci with significant relevance in two or more genetically related disorders were identified and assigned to single or multiple genes (Cross-Disorder Group of the Psychiatric Genomics Consortium 2019). Intriguingly, ten (*NEGR1, SLC30A9, KCNQ5, MRPS33, APOPT1, KCNB1, L3MBTL3, CTNND1, SOX5, RBFOX1*) out of eighteen genes, mapped to the top

pleiotropic loci, are published transcriptional targets of FOXP2 (Vernes et al. 2011, Rouillard et al. 2016). This supports the notion that FOXP2 regulated networks are part of the shared genetic basis between different psychiatric disorders. Notably, the second most pleiotropic locus (with implication in ADHD, autism spectrum disorder, schizophrenia, bipolar disorder, MDD, Tourette syndrome, and OCD) was assigned to the intronic region of the FOXP2 target gene *RBFOX1* (Cross-Disorder Group of the Psychiatric Genomics Consortium 2019). Like FOXP2, knockout mice indicate a role for RBFOX1 in early brain development (Hamada et al. 2015, 2016), suggesting that impaired FOXP2 function possibly confer neurodevelopmental alterations to multiple psychiatric disorders.

To summarize, based on expression analysis in *foxp2* mutants and evidence from the literature, this work suggests FOXP2 regulated networks to be involved in the polygenic architecture of ADHD and the shared genetic basis of different psychiatric disorders.

FOXP2/Foxp2

ADHD polygenicity?   comorbidity?

**genes linked to top
pleiotropic loci in
psychiatry**

ADHD GWAS

ST3GAL3
KDM4A
KDM4A-AS1
PTPRF
SLC6A9
ARTN
DPH2
ATP6V0B
B4GALT2
CCDC24
IPO13
Intergenic x2
SPAG16
PCDH7
LINC02497
LINC00461
MIR9-2
LINC02060
TMEM161B-AS1
MIR3666
LINC01288
SORCS3
DUSP6
POC1B
SEMA6D
LINC01572

ADHD

adgrl3
adgrl3.1
mef2ca/*mef2cb*
dusp6
pcdh7a/*pcdh7b*
sema6d
gad1a/*gad1b*
cntnap2a/*cntnap2b*
grm3
foxp1a/*foxp1b*
lrrn1
ntrk2b

BP

dusp6
gad1a/*gad1b*
grm3
foxp1a/*foxp1b*

SUD

adgrl3
grm3

Tourette

cntnap2a/*cntnap2b*

MDD

mef2ca/*mef2cb*
dusp6

epilepsy

mef2ca/*mef2cb*
pcdh7a/*pcdh7b*
gad1a/*gad1b*
cntnap2a/*cntnap2b*
ntrk2b

ID

mef2ca/*mef2cb*
gad1a/*gad1b*
cntnap2a/*cntnap2b*
foxp1a/*foxp1b*

anxiety disorders

foxp1a/*foxp1b*
ntrk2b

OCD

cntnap2a/*cntnap2b*
foxp1a/*foxp1b*

ASD

cntnap2a/*cntnap2b*
foxp1a/*foxp1b*
lrrn1
ppp1r1b

SCZ

mef2ca/*mef2cb*
dusp6
sema6d
gad1a/*gad1b*
cntnap2a/*cntnap2b*
grm3
foxp1a/*foxp1b*
slitrk2

NEGR1
LINC01122
PLCL1
SLC30A9
NAA11
KCNQ5
DFNA5
MRPS33
SORCS3
CTNND1
NOX4
SOX5
RGS6
APOPT1
RBFOX1
DCC
KCNB1
L3MBTL3

Figure 30: **Is FOXP2 a master regulator of ADHD associated and psychiatric disorder overarching gene sets with implication in ADHD polygenicity and comorbidity?** (ADHD GWAS) Genes linked to ADHD risk loci, identified by a genome-wide-association study (Demontis et al. 2019). (Grey box, right) Genes associated with the top most pleiotropic loci across eight different psychiatric disorders (Cross-Disorder Group of the Psychiatric Genomics Consortium 2019). Genes labeled bold are published FOXP2 target genes (Spiteri et al. 2007, Vernes et al. 2007, 2008, Konopka et al. 2009, Vernes et al. 2011, Chen et al. 2016). (White boxes) Paralogous genes of published risk candidates for attention-deficit/hyperactivity disorder (ADHD), bipolar disorder (BP), intellectual disability (ID), substance use disorder (SUD), anxiety disorders, Tourette syndrome (Tourette), obsessive-compulsive disorder (OCD), major depressive disorder (MDD), autism spectrum disorder (ASD), epilepsy, and schizophrenia (SCZ) (see 4.5.2 as well as Straub et al. 2007, Davis et al. 2009, Peñagarikano et al. 2011, Kandaswamy et al. 2013, Le Fevre et al. 2013, Paciorkowski et al. 2013, International League Against Epilepsy Consortium on Complex Epilepsies 2014, Nurnberger et al. 2014, O'Brien et al. 2014, Malki et al. 2015, Hyde et al. 2016, Autism Spectrum Disorders Working Group of The Psychiatric Genomics Consortium 2017, Machado Torres et al. 2017, Siper et al. 2017, Sundararajan et al. 2018, Wang et al. 2018, Arrúe et al. 2019, Chatron et al. 2020) and tested by the present study for gene expression alterations upon Foxp2 loss of function. Genes labeled in red or blue showed a significant increase or decrease in expression upon Foxp2 loss of function, respectively. Genes marked in light red displayed a trend towards increased expression when Foxp2 was functionally disrupted.

6   Conclusion and future perspectives

In conclusion, the present thesis substantiates a role for Grm8a, Grm8b, Foxp2, and Gad1b in neurobiological processes of the developing CNS and thus the assumed implication in pathological processes of neurodevelopmental disorders like ADHD. Most interestingly, it demonstrates that these processes are crucial for locomotor activity regulation and involve GABAergic signaling. This suggests altered GABAergic signaling in activity regulating circuits as a common mechanistic underpinning of ADHD-associated phenotypes like hyperactivity upon genetic disruption of the distinct ADHD risk candidate paralogs Grm8a, Grm8b, Foxp2, and Gad1b. In addition, it highlights these circuits and their GABAergic components as exciting targets for future investigations on neuromechanistic alterations underlying hyperactivity in ADHD patients. Notably, in the context of the current literature, the present work provides preliminary evidence that Grm8a, Grm8b and/or Foxp2 interfere with GABAergic signaling on the level of Gad1(b)-mediated GABA synthesis, GABAergic cell proliferation and/or survival, transmitter release regulation, and/or GABAergic synapse formation. Further, insensitivity to MPH upon Gad1b and Foxp2 loss of function indicates that the altered GABAergic signaling components in activity regulating circuits are modulated by dopaminergic neurotransmission.

The identity of these circuits requires further investigation. However, previous publications report an expression and/or functional implication of *Grm8*/GRM8 and *Foxp2*/FOXP2 in GABAergic neurons of the mammalian striatum (Vernes et al. 2011, van Rhijn et al. 2018, Savell et al. 2020). Accordingly, the present work revealed expression colocalization between *foxp2*, *grm8a* and *gad1a* in the ventral telencephalon and altered GABAergic cell quantity in the telencephalon of *grm8a* morphants. Thus, present and previous findings concordantly indicate that Grm8a, Foxp2, and Gad1b loss of function possibly disrupt GABA-dependent activity circuits in the striatal BG.

In summary, this thesis provides experimental evidence that the ADHD risk candidate paralogs Grm8a, (Grm8b), Foxp2, and Gad1b interfere with activity regulation via GABAergic signaling supporting GRM8, FOXP2, and GAD1 as likely players in ADHD etiopathogenesis. Further, it stresses the importance of the GABAergic system in ADHD pathology. Finally, the thesis provi-

des preliminary evidence that FOXP2-regulated networks are involved in the polygenic architecture of ADHD and the genetic and functional comorbidity between ADHD and other psychiatric disorders.

With the generation and validation of *foxp2, grm8a,* and *grm8b* CRISPR/Cas9 mutant lines, the present work established a biological framework to study Grm8a-, Grm8b-, and Foxp2-dependent networks, processes, and functions in more detail in future research projects. This comprises, for instance, the investigation of biological processes by which Grm8a, (Grm8b), and Foxp2 interfere with GABAergic signaling. On account of the suggested regulatory function of Foxp2 in Gad1b-mediated GABA synthesis, of Grm8a and/or Grm8b in cell proliferation and/or cell survival and Grm8a, Grm8b, and Foxp2 in GABAergic synapse formation, future projects should consider GABA quantification, immunohistochemical labeling of proliferation and/or apoptosis markers, and the investigation of the synaptic ultrastructure in *grm8a, grm8b,* and/or *foxp2* CRISPR/Cas9 mutants. Besides, brain-wide activity mapping in *foxp2* and/or *grm8a* mutants, based on p-ERK immunolabeling or whole-brain calcium-imaging with simultaneous tail bend monitoring, provide the opportunity to localize the effect on GABA-dependent activity circuits to specific brain regions or individual neuronal populations in the larval brain. In addition, established protocols and profound experience with the generation of CRISPR/Cas9 knockout lines facilitate the future implementation of more sophisticated CRISPR/Cas9 knockout strategies like region- or cell type-specific mutant lines. This complements aforementioned localization strategies and allows to characterize the contribution of Grm8a, Grm8b or Foxp2 in individual brain regions or specific cell types to observed activity phenotypes. Besides the investigation of mechanistic underpinnings of altered locomotor activity, future projects should perform a more detailed evaluation of locomotion characteristics like tail bend amplitude or frequency for the established mutant lines. Further, these projects should aim for a more comprehensive analysis of *foxp2, grm8a,* and *grm8b* mutant behavior, like the assessment of impulsivity, fear response, and sociability, to determine whether Foxp2, Grm8a, and Grm8b are involved in NDD associated phenotypes beyond hyperactivity. In addition, ongoing characterization of adult mutant behavior will allow conclusions about

the developmental trajectory of NDD relevant phenotypes upon Foxp2, Grm8a, and Grm8b loss of function.

Finally, speculations about the implication of FOXP2-regulated networks in ADHD polygenicity and comorbidity require profound experimental support and, therefore, should be addressed in future research agendas by applying a transcriptome analysis of *foxp2* mutants and mapping the results onto existing datasets of pleiotropic loci and loci associated with ADHD risk.

References

Acosta, M.T., et al. (2016). *ADGRL3 (LPHN3)* variants are associated with a refined phenotype of ADHD in the MTA study. *Molecular Genetics & Genomic Medicine*, 4(5):540–547.

Adam, I., Mendoza, E., Kobalz, U., Wohlgemuth, S., and Scharff, C. (2017). *CNTNAP2* is a direct FoxP2 target *in vitro* and *in vivo* in zebra finches: Complex regulation by age and activity. *Genes, Brain, and Behavior*, 16(6):635–642.

Addington, A.M., et al. (2005). *GAD1* (2q31.1), which encodes glutamic acid decarboxylase (GAD$_{67}$), is associated with childhood-onset schizophrenia and cortical gray matter volume loss. *Molecular Psychiatry*, 10(6):581–588.

Aguda, V.L. (2019). *Identification of Subpallial Neuronal Populations across Zebrafish Larval Stages That Express Molecular Markers for the Striatum*. Thesis, University of Toronto.

Ahrens, M.B., et al. (2012). Brain-wide neuronal dynamics during motor adaptation in zebrafish. *Nature*, 485(7399):471–477.

Alarcón, M., et al. (2008). Linkage, association, and gene-expression analyses identify *CNTNAP2* as an autism-susceptibility gene. *American Journal of Human Genetics*, 82(1):150–159.

Alberts-Corush, J., Firestone, P., and Goodman, J.T. (1986). Attention and impulsivity characteristics of the biological and adoptive parents of hyperactive and normal control children. *The American Journal of Orthopsychiatry*, 56(3):413–423.

Ali, S., Champagne, D.L., and Richardson, M.K. (2012). Behavioral profiling of zebrafish embryos exposed to a panel of 60 water-soluble compounds. *Behavioural Brain Research*, 228(2):272–283.

Almeida, L.G., et al. (2010). Reduced right frontal cortical thickness in children, adolescents and adults with ADHD and its correlation to clinical variables: A cross-sectional study. *Journal of Psychiatric Research*, 44(16):1214–1223.

Ambrosino, S., de Zeeuw, P., Wierenga, L.M., van Dijk, S., and Durston, S. (2017). What can cortical development in attention-deficit/hyperactivity disorder teach us about the early developmental mechanisms involved? *Cerebral Cortex*, 27(9):4624–4634.

American Psychiatric Association (APA) (1968). *Diagnostic and Statistical Manual of Mental Disorders (2nd Ed.)*. American Psychiatric Association, Washington, D.C.

Amsterdam, A., et al. (1999). A large-scale insertional mutagenesis screen in zebrafish. *Genes & Development*, 13(20):2713–2724.

Anastopoulos, A.D., et al. (2011). Self-regulation of emotion, functional impairment, and comorbidity among children with AD/HD. *Journal of Attention Disorders*, 15(7):583–592.

Andersen, S.L., Laurberg, P., Wu, C.S., and Olsen, J. (2014). Attention-deficit hyperactivity disorder and autism spectrum disorder in children born to mothers with thyroid dysfunction: A Danish nationwide cohort study. *BJOG: An International Journal of Obstetrics and Gynaecology*, 121(11):1365–1374.

André, V.M., Fisher, Y.E., and Levine, M.S. (2011). Altered balance of activity in the striatal

direct and indirect pathways in mouse models of Huntington's disease. *Frontiers in Systems Neuroscience*, 5:46.

Antinucci, P., et al. (2020). A calibrated optogenetic toolbox of stable zebrafish opsin lines. *eLife*, 9:e54937.

APA (1980). *Diagnostic and Statistical Manual of Mental Disorders (3rd Ed.)*. American Psychiatric Association, Washington, D.C.

APA (1987). *Diagnostic and Statistical Manual of Mental Disorders (3rd Ed., Revised)*. American Psychiatric Association, Washington, D.C.

APA (1994). *Diagnostic and Statistical Manual of Mental Disorders (4th Ed.)*. American Psychiatric Association, Washington, D.C.

APA (2000). *Diagnostic and Statistical Manual of Mental Disorders (4th Ed. Text Rev.)*. American Psychiatric Association, Washington, D.C.

APA (2013). *Diagnostic and Statistical Manual of Mental Disorders (5th Ed.)*. American Psychiatric Association, Washington, D.C.

Araujo, D.J., et al. (2015). FoxP1 orchestration of ASD-relevant signaling pathways in the striatum. *Genes & Development*, 29(20):2081–2096.

Archer, T., Palomo, T., and Fredriksson, A. (2002). Functional deficits following neonatal dopamine depletion and isolation housing: Circular water maze acquisition under pre-exposure conditions and motor activity. *Neurotoxicity Research*, 4(5):503.

Arcos-Burgos, M., et al. (2010). A common variant of the latrophilin 3 gene, *LPHN3*, confers susceptibility to ADHD and predicts effectiveness of stimulant medication. *Molecular Psychiatry*, 15(11):1053–1066.

Arcos-Burgos, M., et al. (2019). *ADGRL3 (LPHN3)* variants predict substance use disorder. *Translational Psychiatry*, 9(1):1–15.

Arking, D.E., et al. (2008). A common genetic variant in the neurexin superfamily member *CNTNAP2* increases familial risk of autism. *American Journal of Human Genetics*, 82(1):160–164.

Arnold, L.E., et al. (2014). Three-year latent class trajectories of attention-deficit/hyperactivity disorder (ADHD) symptoms in a clinical sample not selected for ADHD. *Journal of the American Academy of Child & Adolescent Psychiatry*, 53(7):745–760.

Arnsten, A.F.T. (2009). The emerging neurobiology of attention-deficit hyperactivity disorder: The key role of the prefrontal association cortex. *The Journal of Pediatrics*, 154(5):I–S43.

Arrúe, A., et al. (2019). *GAD1* gene polymorphisms are associated with bipolar I disorder and with blood homovanillic acid levels but not with plasma GABA levels. *Neurochemistry International*, 124:152–161.

Asada, H., et al. (1997). Cleft palate and decreased brain gamma-Aminobutyric acid in mice lacking the 67-kDa isoform of glutamic acid decarboxylase. *Proceedings of the National Academy of Sciences of the United States of America*, 94(12):6496–6499.

Autism Spectrum Disorders Working Group of The Psychiatric Genomics Consortium (2017). Meta-analysis of GWAS of over 16,000 individuals with autism spectrum disorder highlights a novel locus at 10q24.32 and a significant overlap with schizophrenia. *Molecular Autism*, 8:21.

Awapara, J., Landua, A.J., Fuerst, R., and Seale, B. (1950). Free gamma-Aminobutyric acid in brain. *The Journal of Biological Chemistry*, 187(1):35–39.

Bagwell, C.L., Molina, B.S., Pelham, W.E., and Hoza, B. (2001). Attention-deficit hyperactivity disorder and problems in peer relations: Predictions from childhood to adolescence. *Journal of the American Academy of Child and Adolescent Psychiatry*, 40(11):1285–1292.

Bakkaloglu, B., et al. (2008). Molecular cytogenetic analysis and resequencing of contactin associated protein-like 2 in autism spectrum disorders. *American Journal of Human Genetics*, 82(1):165–173.

Barbaresi, W.J., et al. (2013). Mortality, ADHD, and psychosocial adversity in adults with childhood ADHD: A prospective study. *Pediatrics*, 131(4):637–644.

Barkley, R.A. (1997). Behavioral inhibition, sustained attention, and executive functions: Constructing a unifying theory of ADHD. *Psychological Bulletin*, 121(1):65–94.

Barkley, R.A. (2014). *Attention-Deficit Hyperactivity Disorder, Fourth Edition: A Handbook for Diagnosis and Treatment*. Guilford Publications.

Barkley, R.A. and Fischer, M. (2018). Hyperactive child syndrome and estimated life expectancy at young adult follow-up: The role of ADHD persistence and other potential predictors:. *Journal of Attention Disorders*, 23(9):907–923.

Barkley, R.A. and Peters, H. (2012). The earliest reference to ADHD in the medical literature? Melchior Adam Weikard's description in 1775 of "attention deficit" (Mangel der Aufmerksamkeit, Attentio Volubilis). *Journal of Attention Disorders*, 16(8):623–630.

Barrett, E., et al. (2013). The individual-specific and diverse nature of the preterm infant microbiota. *Archives of Disease in Childhood. Fetal and Neonatal Edition*, 98(4):F334–340.

Battaglioli, G., Liu, H., and Martin, D.L. (2003). Kinetic differences between the isoforms of glutamate decarboxylase: Implications for the regulation of GABA synthesis. *Journal of Neurochemistry*, 86(4):879–887.

Behar, T.N., Schaffner, A.E., Scott, C.A., Greene, C.L., and Barker, J.L. (2000). GABA receptor antagonists modulate postmitotic cell migration in slice cultures of embryonic rat cortex. *Cerebral Cortex (New York, N.Y.: 1991)*, 10(9):899–909.

Belloso, J.M., et al. (2007). Disruption of the *CNTNAP2* gene in a t(7;15) translocation family without symptoms of Gilles de la Tourette syndrome. *European Journal of Human Genetics*, 15(6):711–713.

Berridge, C.W., et al. (2006). Methylphenidate preferentially increases catecholamine neurotransmission within the prefrontal cortex at low doses that enhance cognitive function. *Biological Psychiatry*, 60(10):1111–1120.

Biederman, J., Faraone, S.V., Keenan, K., Knee, D., and Tsuang, M.T. (1990). Family-genetic

and psychosocial risk factors in DSM-III attention-deficit disorder. *Journal of the American Academy of Child and Adolescent Psychiatry*, 29(4):526–533.

Biederman, J., Mick, E., and Faraone, S.V. (2000). Age-dependent decline of symptoms of attention-deficit hyperactivity disorder: Impact of remission definition and symptom type. *The American Journal of Psychiatry*, 157(5):816–818.

Biederman, J., et al. (1992). Further evidence for family-genetic risk factors in attention-deficit hyperactivity disorder. Patterns of comorbidity in probands and relatives psychiatrically and pediatrically referred samples. *Archives of General Psychiatry*, 49(9):728–738.

Biederman, J., et al. (1995a). Family-environment risk factors for attention-deficit hyperactivity disorder. A test of Rutter's indicators of adversity. *Archives of General Psychiatry*, 52(6):464–470.

Biederman, J., et al. (1995b). Impact of adversity on functioning and comorbidity in children with attention-deficit hyperactivity disorder. *Journal of the American Academy of Child and Adolescent Psychiatry*, 34(11):1495–1503.

Biederman, J., et al. (2008). Towards further understanding of the comorbidity between attention-deficit hyperactivity disorder and bipolar disorder: A MRI study of brain volumes. *Psychological Medicine*, 38(7):1045–1056.

Biederman, J., et al. (2019). Vortioxetine for attention-deficit hyperactivity disorder in adults: A randomized, double-blind, placebo-controlled, proof-of-concept study. *Journal of Psychopharmacology*, 33(4):511–521.

Bledsoe, J., Semrud-Clikeman, M., and Pliszka, S.R. (2009). A magnetic resonance imaging study of the cerebellar vermis in chronically treated and treatment-naïve children with attention-deficit/hyperactivity disorder combined type. *Biological Psychiatry*, 65(7):620–624.

Bollmann, S., et al. (2015). Developmental changes in gamma-Aminobutyric acid levels in attention-deficit/hyperactivity disorder. *Translational Psychiatry*, 5:e589.

Bonkowsky, J.L. and Chien, C.B. (2005). Molecular cloning and developmental expression of *foxP2* in zebrafish. *Developmental Dynamics*, 234(3):740–746.

Bonvicini, C., Faraone, S.V., and Scassellati, C. (2016). Attention-deficit hyperactivity disorder in adults: A systematic review and meta-analysis of genetic, pharmacogenetic and biochemical studies. *Molecular Psychiatry*, 21(7):872–884.

Bouchatta, O., et al. (2018). Neonatal 6-OHDA lesion model in mouse induces attention-deficit/hyperactivity disorder (ADHD)-like behaviour. *Scientific Reports*, 8(1):15349.

Bowers, J.M. and Konopka, G. (2012). The role of the FOXP family of transcription factors in ASD. *Disease Markers*, 33(5):251–260.

Bowers, J.M., Perez-Pouchoulen, M., Edwards, N.S., and McCarthy, M.M. (2013). *Foxp2* mediates sex differences in ultrasonic vocalization by rat pups and directs order of maternal retrieval. *Journal of Neuroscience*, 33(8):3276–3283.

Boy, F., et al. (2010). Individual differences in subconscious motor control predicted by GABA concentration in SMA. *Current Biology*, 20(19):1779–1785.

Boy, F., et al. (2011). Dorsolateral prefrontal gamma-Aminobutyric acid in men predicts individual differences in rash impulsivity. *Biological Psychiatry*, 70(9):866–872.

Bragina, L., et al. (2015). Differential expression of metabotropic glutamate and GABA receptors at neocortical glutamatergic and GABAergic axon terminals. *Frontiers in Cellular Neuroscience*, 9:345.

Brainstorm Consortium, et al. (2018). Analysis of shared heritability in common disorders of the brain. *Science*, 360(6395).

Brandon, C.L. and Steiner, H. (2003). Repeated methylphenidate treatment in adolescent rats alters gene regulation in the striatum. *European Journal of Neuroscience*, 18(6):1584–1592.

Bristot, G., De Bastiani, M.A., Pfaffenseller, B., Kapczinski, F., and Kauer-Sant'Anna, M. (2020). Gene regulatory network of dorsolateral prefrontal cortex: A master regulator analysis of major psychiatric disorders. *Molecular Neurobiology*, 57(3):1305–1316.

Brocher, J. (2015, Jan 5). The BioVoxxel image processing and analysis toolbox.

Brookes, K., et al. (2006a). The analysis of 51 genes in DSM-IV combined type attention-deficit hyperactivity disorder: Association signals in *DRD4, DAT1* and 16 other genes. *Molecular Psychiatry*, 11(10):934–953.

Brookes, K.J., et al. (2006b). A common haplotype of the dopamine transporter gene associated with attention-deficit/hyperactivity disorder and interacting with maternal use of alcohol during pregnancy. *Archives of General Psychiatry*, 63(1):74–81.

Brophy, K., Hawi, Z., Kirley, A., Fitzgerald, M., and Gill, M. (2002). Synaptosomal-associated protein 25 (*SNAP-25*) and attention deficit hyperactivity disorder (ADHD): Evidence of linkage and association in the Irish population. *Molecular Psychiatry*, 7(8):913–917.

Brown, J.A., et al. (2015). Inhibition of parvalbumin-expressing interneurons results in complex behavioral changes. *Molecular Psychiatry*, 20(12):1499–1507.

Brunkow, M.E., et al. (2001). Disruption of a new forkhead/winged-helix protein, scurfin, results in the fatal lymphoproliferative disorder of the scurfy mouse. *Nature Genetics*, 27(1):68–73.

Bruxel, E.M., et al. (2016). *GAD1* gene polymorphisms are associated with hyperactivity in attention-deficit/hyperactivity disorder. *American Journal of Medical Genetics. Part B, Neuropsychiatric Genetics*, 171(8):1099–1104.

Bu, D.F. and Tobin, A.J. (1994). The exon-intron organization of the genes (*GAD1* and *GAD2*) encoding two human glutamate decarboxylases (GAD67 and GAD65) suggests that they derive from a common ancestral GAD. *Genomics*, 21(1):222–228.

Bu, D.F., et al. (1992). Two human glutamate decarboxylases, 65-kDa GAD and 67-kDa GAD, are each encoded by a single gene. *Proceedings of the National Academy of Sciences of the United States of America*, 89(6):2115–2119.

Bunte, T.L., Schoemaker, K., Hessen, D.J., van der Heijden, P.G.M., and Matthys, W. (2014). Stability and change of ODD, CD and ADHD diagnosis in referred preschool children. *Journal of Abnormal Child Psychology*, 42(7):1213–1224.

Burt, S.A. (2009). Rethinking environmental contributions to child and adolescent psychopathology: A meta-analysis of shared environmental influences. *Psychological Bulletin*, 135(4):608–637.

Butcher, S.P., Liptrot, J., and Aburthnott, G.W. (1991). Characterisation of methylphenidate and nomifensine induced dopamine release in rat striatum using in vivo brain microdialysis. *Neuroscience Letters*, 122(2):245–248.

Bymaster, F.P., et al. (2002). Atomoxetine increases extracellular levels of norepinephrine and dopamine in prefrontal cortex of rat: A potential mechanism for efficacy in attention-deficit/hyperactivity disorder. *Neuropsychopharmacology*, 27(5):699–711.

Campbell, P., Reep, R.L., Stoll, M.L., Ophir, A.G., and Phelps, S.M. (2009). Conservation and diversity of *Foxp2* expression in muroid rodents: Functional implications. *The Journal of Comparative Neurology*, 512(1):84–100.

Canitano, R. and Pallagrosi, M. (2017). Autism spectrum disorders and schizophrenia spectrum sisorders: Excitation/inhibition imbalance and developmental trajectories. *Frontiers in Psychiatry*, 8:69.

Cantwell, D.P. (1975). Genetics of hyperactivity. *Journal of Child Psychology and Psychiatry*, 16(3):261–264.

Cargill, M., et al. (1999). Characterization of single-nucleotide polymorphisms in coding regions of human genes. *Nature Genetics*, 22(3):231–238.

Carlsson, M.L. (2001). On the role of prefrontal cortex glutamate for the antithetical phenomenology of obsessive compulsive disorder and attention-deficit hyperactivity disorder. *Progress in Neuro-Psychopharmacology & Biological Psychiatry*, 25(1):5–26.

Carlsson, A., Waters, N., and Carlsson, M.L. (1999). Neurotransmitter interactions in schizophrenia-therapeutic implications. *Biological Psychiatry*, 46(10):1388–1395.

Carrey, N.J., MacMaster, F.P., Gaudet, L., and Schmidt, M.H. (2007). Striatal creatine and glutamate/glutamine in attention-deficit/hyperactivity disorder. *Journal of Child and Adolescent Psychopharmacology*, 17(1):11–17.

Carrey, N., et al. (2003). Metabolite changes resulting from treatment in children with ADHD: A 1H-MRS Study. *Clinical Neuropharmacology*, 26(4):218–221.

Carter, R.J., et al. (1999). Characterization of progressive motor deficits in mice transgenic for the human Huntington's disease mutation. *Journal of Neuroscience*, 19(8):3248–3257.

Cartmell, J. and Schoepp, D.D. (2000). Regulation of neurotransmitter release by metabotropic glutamate receptors. *Journal of Neurochemistry*, 75(3):889–907.

Casey, B.J., et al. (2007). Frontostriatal connectivity and its role in cognitive control in parent-child dyads with ADHD. *The American Journal of Psychiatry*, 164(11):1729–1736.

Casey, J.P., et al. (2012). A novel approach of homozygous haplotype sharing identifies candidate genes in autism spectrum disorder. *Human Genetics*, 131(4):565–579.

Castellanos, F.X., et al. (2002). Developmental trajectories of brain volume abnormal-

ities in children and adolescents with attention-deficit/hyperactivity disorder. *JAMA*, 288(14):1740–1748.

Castellanos, F.X., et al. (2008). Cingulate-precuneus interactions: A new locus of dysfunction in adult attention-deficit/hyperactivity disorder. *Biological Psychiatry*, 63(3):332–337.

Castells, X., et al. (2011). Efficacy of methylphenidate for adults with attention-deficit hyperactivity disorder: A meta-regression analysis. *CNS Drugs*, 25(2):157–169.

Castells-Nobau, A., et al. (2019). Conserved regulation of neurodevelopmental processes and behavior by FoxP in *Drosophila*. *PLoS ONE*, 14(2).

Castellucci, G.A., McGinley, M.J., and McCormick, D.A. (2016). Knockout of *Foxp2* disrupts vocal development in mice. *Scientific Reports*, 6:23305.

Catalá-López, F., et al. (2017). The pharmacological and non-pharmacological treatment of attention-deficit hyperactivity disorder in children and adolescents: A systematic review with network meta-analyses of randomised trials. *PLOS ONE*, 12(7):e0180355.

Caye, A., Swanson, J.M., Coghill, D., and Rohde, L.A. (2019). Treatment strategies for ADHD: An evidence-based guide to select optimal treatment. *Molecular Psychiatry*, 24(3):390–408.

Caye, A., et al. (2016). Predictors of persistence of ADHD into adulthood: A systematic review of the literature and meta-analysis. *European Child & Adolescent Psychiatry*, 25(11):1151–1159.

Chabout, J., et al. (2016). A *Foxp2* mutation implicated in human speech deficits alters sequencing of ultrasonic vocalizations in adult male mice. *Frontiers in Behavioral Neuroscience*, 10:197.

Chang, N., et al. (2013). Genome editing with RNA-guided Cas9 nuclease in zebrafish embryos. *Cell Research*, 23(4):465–472.

Chang, Z., et al. (2014). Maternal age at childbirth and risk for ADHD in offspring: A population-based cohort study. *International Journal of Epidemiology*, 43(6):1815–1824.

Chao, L.L. and Knight, R.T. (1995). Human prefrontal lesions increase distractibility to irrelevant sensory inputs. *Neuroreport*, 6(12):1605–1610.

Chatron, N., et al. (2020). Bi-allelic *GAD1* variants cause a neonatal onset syndromic developmental and epileptic encephalopathy. *Brain*, 143(5):1447–1461.

Chen, Q., Heston, J.B., Burkett, Z.D., and White, S.A. (2013). Expression analysis of the speech-related genes *FoxP1* and *FoxP2* and their relation to singing behavior in two songbird species. *Journal of Experimental Biology*, 216(19):3682–3692.

Chen, W., et al. (2008). DSM-IV combined type ADHD shows familial association with sibling trait scores: A sampling strategy for QTL linkage. *American Journal of Medical Genetics. Part B, Neuropsychiatric Genetics*, 147B(8):1450–1460.

Chen, Q., et al. (2014). Maternal pre-pregnancy body mass index and offspring attention-deficit hyperactivity disorder: A population-based cohort study using a sibling-comparison design. *International Journal of Epidemiology*, 43(1):83–90.

Chen, Y.C., et al. (2016). *Foxp2* controls synaptic wiring of corticostriatal circuits and vocal communication by opposing *Mef2c*. *Nature Neuroscience*, 19(11):1513–1522.

Chen, Q., et al. (2017). Familial aggregation of attention-deficit/hyperactivity disorder. *Journal of Child Psychology and Psychiatry, and Allied Disciplines*, 58(3):231–239.

Cheon, K.A., et al. (2003). Dopamine transporter density in the basal ganglia assessed with [^{123}I]IPT SPET in children with attention-deficit hyperactivity disorder. *European Journal of Nuclear Medicine and Molecular Imaging*, 30(2):306–311.

Chess, S. (1960). Diagnosis and treatment of the hyperactive child. *New York State Journal of Medicine*, 60:2379–2385.

Chien, I.C., Lin, C.H., Chou, Y.J., and Chou, P. (2012). Prevalence, incidence, and stimulant use of attention-deficit hyperactivity disorder in Taiwan, 1996-2005: A national population-based study. *Social Psychiatry and Psychiatric Epidemiology*, 47(12):1885–1890.

Childress, A.C., et al. (2020). A randomized, double-blind, placebo-controlled study of HLD200, a delayed-release and extended-release methylphenidate, in children with attention-deficit/hyperactivity disorder: An evaluation of safety and efficacy throughout the day and across settings. *Journal of Child and Adolescent Psychopharmacology*, 30(1):2–14.

Chiu, Y.C., et al. (2014). Foxp2 regulates neuronal differentiation and neuronal subtype specification. *Developmental Neurobiology*, 74(7):723–738.

Cho, S.C., et al. (2010). Effect of environmental exposure to lead and tobacco smoke on inattentive and hyperactive symptoms and neurocognitive performance in children. *Journal of Child Psychology and Psychiatry, and Allied Disciplines*, 51(9):1050–1057.

Cho, K.K.A., et al. (2015). Gamma rhythms link prefrontal interneuron dysfunction with cognitive inflexibility in *Dlx5/6*$^{(+/-)}$ mice. *Neuron*, 85(6):1332–1343.

Choi, D.W. and Rothman, S.M. (1990). The role of glutamate neurotoxicity in hypoxic-ischemic neuronal death. *Annual Review of Neuroscience*, 13:171–182.

Chu, C.L., et al. (2018). Availability of dopamine transporters and auditory P300 abnormalities in adults with attention-deficit hyperactivity disorder: Preliminary results. *CNS Spectrums*, 23(4):264–270.

Chun, L., Zhang, W.h., and Liu, J.f. (2012). Structure and ligand recognition of class C GPCRs. *Acta Pharmacologica Sinica*, 33(3):312–323.

Class, Q.A., Rickert, M.E., Larsson, H., Lichtenstein, P., and D'Onofrio, B.M. (2014). Fetal growth and psychiatric and socioeconomic problems: Population-based sibling comparison. *The British Journal of Psychiatry*, 205(5):355–361.

Clements, S.D. (1966). Minimal brain dysfunction in children; Terminology and identification. Phase I of a three-phase project. *US Department of Health, Education and Welfare*.

Clements, S.D. and Peters, J.E. (1962). Minimal brain dysfunctions in the school-age child. Diagnosis and treatment. *Archives of General Psychiatry*, 6:185–197.

Clements, C.C., et al. (2015). Prenatal antidepressant exposure is associated with risk for

attention-deficit hyperactivity disorder but not autism spectrum disorder in a large health system. *Molecular Psychiatry*, 20(6):727–734.

Co, M., Anderson, A.G., and Konopka, G. (2020). FOXP transcription factors in vertebrate brain development, function, and disorders. *Developmental Biology*, page e375.

Co, M., Hickey, S.L., Kulkarni, A., Harper, M., and Konopka, G. (2019). Cortical Foxp2 supports behavioral flexibility and developmental dopamine D1 receptor expression. *Cerebral Cortex*.

Comings, D.E., et al. (1991). The dopamine D2 receptor locus as a modifying gene in neuropsychiatric disorders. *JAMA*, 266(13):1793–1800.

Condie, B.G., Bain, G., Gottlieb, D.I., and Capecchi, M.R. (1997). Cleft palate in mice with a targeted mutation in the gamma-Aminobutyric acid-producing enzyme glutamic acid decarboxylase 67. *Proceedings of the National Academy of Sciences of the United States of America*, 94(21):11451–11455.

Conn, P.J. and Pin, J.P. (1997). Pharmacology and functions of metabotropic glutamate receptors. *Annual Review of Pharmacology and Toxicology*, 37:205–237.

Connor, D.F., Fletcher, K.E., and Swanson, J.M. (1999). A meta-analysis of clonidine for symptoms of attention-deficit hyperactivity disorder. *Journal of the American Academy of Child & Adolescent Psychiatry*, 38(12):1551–1559.

Cook, E.H., et al. (1995). Association of attention-deficit disorder and the dopamine transporter gene. *American Journal of Human Genetics*, 56(4):993–998.

Cortese, S. (2012). The neurobiology and genetics of attention-deficit/hyperactivity disorder (ADHD): What every clinician should know. *European Journal of Paediatric Neurology*, 16(5):422–433.

Cortese, S., Faraone, S.V., Bernardi, S., Wang, S., and Blanco, C. (2016). Gender differences in adult attention-deficit/hyperactivity disorder: Results from the national epidemiologic survey on alcohol and related conditions (NESARC). *The Journal of Clinical Psychiatry*, 77(4):0–0.

Corti, C., Aldegheri, L., Somogyi, P., and Ferraguti, F. (2002). Distribution and synaptic localisation of the metabotropic glutamate receptor 4 (mGluR4) in the rodent CNS. *Neuroscience*, 110(3):403–420.

Corti, C., et al. (1998). Cloning and characterization of alternative mRNA forms for the rat metabotropic glutamate receptors mGluR7 and mGluR8. *European Journal of Neuroscience*, 10(12):3629–3641.

Costa Dias, T.G., et al. (2013). Reward circuit connectivity relates to delay discounting in children with attention-deficit/hyperactivity disorder. *European Neuropsychopharmacology*, 23(1):33–45.

Courvoisie, H., Hooper, S.R., Fine, C., Kwock, L., and Castillo, M. (2004). Neurometabolic functioning and neuropsychological correlates in children with ADHD-H: Preliminary findings. *The Journal of Neuropsychiatry and Clinical Neurosciences*, 16(1):63–69.

Cross-Disorder Group of the Psychiatric Genomics Consortium (2019). Genomic relationships,

novel loci, and pleiotropic mechanisms across eight psychiatric disorders. *Cell*, 179(7):1469–1482.e11.

Cross-Disorder Group of the Psychiatric Genomics Consortium, et al. (2013). Genetic relationship between five psychiatric disorders estimated from genome-wide SNPs. *Nature Genetics*, 45(9):984–994.

Cuthbert, B.N. and Insel, T.R. (2013). Toward the future of psychiatric diagnosis: The seven pillars of RDoC. *BMC Medicine*, 11:126.

D'Agati, E., Curatolo, P., and Mazzone, L. (2019). Comorbidity between ADHD and anxiety disorders across the lifespan. *International Journal of Psychiatry in Clinical Practice*, 23(4):238–244.

Dalsgaard, S., Østergaard, S.D., Leckman, J.F., Mortensen, P.B., and Pedersen, M.G. (2015). Mortality in children, adolescents, and adults with attention-deficit hyperactivity disorder: A nationwide cohort study. *Lancet*, 385(9983):2190–2196.

Daly, G., Hawi, Z., Fitzgerald, M., and Gill, M. (1999). Mapping susceptibility loci in attention-deficit hyperactivity disorder: Preferential transmission of parental alleles at *DAT1, DBH* and *DRD5* to affected children. *Molecular Psychiatry*, 4(2):192–196.

Davis, L.K., et al. (2009). Novel copy number variants in children with autism and additional developmental anomalies. *Journal of Neurodevelopmental Disorders*, 1(4):292–301.

Day, N.F., Hobbs, T.G., Heston, J.B., and White, S.A. (2019). Beyond critical period learning: Striatal FoxP2 affects the active maintenance of learned vocalizations in adulthood. *eNeuro*, 6(2).

de Silva, M.G., et al. (2003). Disruption of a novel member of a sodium/hydrogen exchanger family and *DOCK3* is associated with an attention-deficit hyperactivity disorder-like phenotype. *Journal of Medical Genetics*, 40(10):733–740.

del Campo, N., et al. (2013). A positron emission tomography study of nigro-striatal dopaminergic mechanisms underlying attention: Implications for ADHD and its treatment. *Brain*, 136(11):3252–3270.

Demontis, D., et al. (2016). Whole-exome sequencing reveals increased burden of rare functional and disruptive variants in candidate risk genes in individuals with persistent attention-deficit/hyperactivity disorder. *Journal of the American Academy of Child and Adolescent Psychiatry*, 55(6):521–523.

Demontis, D., et al. (2019). Discovery of the first genome-wide significant risk loci for attention-deficit/hyperactivity disorder. *Nature Genetics*, 51(1):63–75.

Deng, Y.P., Wong, T., Wan, J.Y., and Reiner, A. (2014). Differential loss of thalamostriatal and corticostriatal input to striatal projection neuron types prior to overt motor symptoms in the Q140 knock-in mouse model of Huntington's disease. *Frontiers in Systems Neuroscience*, 8:198.

Deriziotis, P., et al. (2014). De novo *TBR1* mutations in sporadic autism disrupt protein functions. *Nature Communications*, 5:4954.

Diaz Heijtz, R. and Castellanos, F.X. (2006). Differential effects of a selective dopamine D1-like receptor agonist on motor activity and *c-fos* expression in the frontal-striatal circuitry of SHR and Wistar-Kyoto rats. *Behavioral and Brain Functions*, 2(1):18.

Dibbets, P., Evers, E.A.T., Hurks, P.P.M., Bakker, K., and Jolles, J. (2010). Differential brain activation patterns in adult attention-deficit hyperactivity disorder (ADHD) associated with task switching. *Neuropsychology*, 24(4):413–423.

Dickstein, S.G., Bannon, K., Castellanos, F.X., and Milham, M.P. (2006). The neural correlates of attention-deficit hyperactivity disorder: An ALE meta-analysis. *Journal of Child Psychology and Psychiatry, and Allied Disciplines*, 47(10):1051–1062.

Dirkx, R., et al. (1995). Targeting of the 67-kDa isoform of glutamic acid decarboxylase to intracellular organelles is mediated by its interaction with the NH_2-terminal region of the 65-kDa isoform of glutamic acid decarboxylase. *The Journal of Biological Chemistry*, 270(5):2241–2246.

Donner, J., et al. (2012). Support for involvement of glutamate decarboxylase 1 and neuropeptide Y in anxiety susceptibility. *American Journal of Medical Genetics. Part B, Neuropsychiatric Genetics*, 159B(3):316–327.

Doostparast Torshizi, A., et al. (2019). Deconvolution of transcriptional networks identifies TCF4 as a master regulator in schizophrenia. *Science Advances*, 5(9):eaau4139.

Doshi, J.A., et al. (2012). Economic impact of childhood and adult attention-deficit/hyperactivity disorder in the United States. *Journal of the American Academy of Child & Adolescent Psychiatry*, 51(10):990–1002.e2.

Dougherty, D.D., et al. (1999). Dopamine transporter density in patients with attention-deficit hyperactivity disorder. *Lancet*, 354(9196):2132–2133.

Douglas, V.I. (1972). Stop, look and listen: The problem of sustained attention and impulse control in hyperactive and normal children. *Canadian Journal of Behavioural Science*, 4(4):259–282.

Douw, L., Wakeman, D.G., Tanaka, N., Liu, H., and Stufflebeam, S.M. (2016). State-dependent variability of dynamic functional connectivity between frontoparietal and default networks relates to cognitive flexibility. *Neuroscience*, 339:12–21.

Dramsdahl, M., et al. (2011). Adults with attention-deficit/hyperactivity disorder - A brain magnetic resonance spectroscopy study. *Frontiers in Psychiatry*, 2:65.

Draper, I., Kurshan, P.T., McBride, E., Jackson, F.R., and Kopin, A.S. (2007). Locomotor activity is regulated by D2-like receptors in *Drosophila*: An anatomic and functional analysis. *Developmental Neurobiology*, 67(3):378–393.

Dresel, S., et al. (2000). Attention-deficit hyperactivity disorder: Binding of [^{99m}Tc]TRODAT-1 to the dopamine transporter before and after methylphenidate treatment. *European Journal of Nuclear Medicine*, 27(10):1518–1524.

Druart, M., Groszer, M., and Le Magueresse, C. (2020). An etiological *Foxp2* mutation impairs neuronal gain in layer VI cortico-thalamic cells through increased $GABA_B$/GIRK signaling. *Journal of Neuroscience*, 40(44):8543–8555.

Du, J., et al. (2008). Comprehensive analysis of polymorphisms throughout *GAD1* gene: A family-based association study in schizophrenia. *Journal of Neural Transmission*, 115(3):513–519.

Duncan, L.E., Ostacher, M., and Ballon, J. (2019). How genome-wide association studies (GWAS) made traditional candidate gene studies obsolete. *Neuropsychopharmacology*, 44(9):1518–1523.

Dunn, H.A., Zucca, S., Dao, M., Orlandi, C., and Martemyanov, K.A. (2019). ELFN2 is a post-synaptic cell adhesion molecule with essential roles in controlling group III mGluRs in the brain and neuropsychiatric behavior. *Molecular Psychiatry*, 24(12):1902–1919.

Durston, S., et al. (2007). Neural and behavioral correlates of expectancy violations in attention-deficit hyperactivity disorder. *Journal of Child Psychology and Psychiatry, and Allied Disciplines*, 48(9):881–889.

Duvoisin, R.M., Villasana, L., Davis, M.J., Winder, D.G., and Raber, J. (2011). Opposing roles of mGluR8 in measures of anxiety involving non-social and social challenges. *Behavioural Brain Research*, 221(1):50–54.

Duvoisin, R.M., Villasana, L., Pfankuch, T., and Raber, J. (2010). Sex-dependent cognitive phenotype of mice lacking mGluR8. *Behavioural Brain Research*, 209(1):21–26.

Duvoisin, R.M., Zhang, C., and Ramonell, K. (1995). A novel metabotropic glutamate receptor expressed in the retina and olfactory bulb. *Journal of Neuroscience*, 15(4):3075–3083.

Duvoisin, R.M., et al. (2005). Increased measures of anxiety and weight gain in mice lacking the group III metabotropic glutamate receptor mGluR8. *The European Journal of Neuroscience*, 22(2):425–436.

Ebisu, H., Iwai-Takekoshi, L., Fujita-Jimbo, E., Momoi, T., and Kawasaki, H. (2017). Foxp2 regulates identities and projection patterns of thalamic nuclei during development. *Cerebral Cortex*, 27(7):3648–3659.

Edden, R.A.E., Crocetti, D., Zhu, H., Gilbert, D.L., and Mostofsky, S.H. (2012). Reduced GABA concentration in attention-deficit/hyperactivity disorder. *Archives of General Psychiatry*, 69(7):750.

Eisenberg, L. (1957). Psychiatric implications of brain damage in children. *The Psychiatric Quarterly*, 31(1):72–92.

El-Brolosy, M.A., et al. (2019). Genetic compensation triggered by mutant mRNA degradation. *Nature*, 568(7751):193–197.

Elia, J., Ambrosini, P., and Berrettini, W. (2008). ADHD characteristics: I. Concurrent co-morbidity patterns in children & adolescents. *Child and Adolescent Psychiatry and Mental Health*, 2(1):15.

Elia, J., Borcherding, B.G., Rapoport, J.L., and Keysor, C.S. (1991). Methylphenidate and dextroamphetamine treatments of hyperactivity: Are there true nonresponders? *Psychiatry Research*, 36(2):141–155.

Elia, J., et al. (2010). Rare structural variants found in attention-deficit hyperactivity dis-

order are preferentially associated with neurodevelopmental genes. *Molecular Psychiatry*, 15(6):637–646.

Elia, J., et al. (2012). Genome-wide copy number variation study associates metabotropic glutamate receptor gene networks with attention-deficit hyperactivity disorder. *Nature Genetics*, 44(1):78–84.

Ellis, L.D., Seibert, J., and Soanes, K.H. (2012). Distinct models of induced hyperactivity in zebrafish larvae. *Brain Research*, 1449:46–59.

Ellison-Wright, I., Ellison-Wright, Z., and Bullmore, E. (2008). Structural brain change in attention-deficit hyperactivity disorder identified by meta-analysis. *BMC Psychiatry*, 8:51.

Elvsåshagen, T., et al. (2020). The genetic architecture of human brainstem structures and their involvement in common brain disorders. *Nature Communications*, 11(1):4016.

Enard, W., et al. (2002). Molecular evolution of *FOXP2*, a gene involved in speech and language. *Nature*, 418(6900):869–872.

Enard, W., et al. (2009). A humanized version of *Foxp2* affects cortico-basal ganglia circuits in mice. *Cell*, 137(5):961–971.

Ende, G., et al. (2016). Impulsivity and aggression in female BPD and ADHD patients: Association with ACC glutamate and GABA concentrations. *Neuropsychopharmacology*, 41(2):410–418.

Epstein, J.N., et al. (2000). Familial aggregation of ADHD characteristics. *Journal of Abnormal Child Psychology*, 28(6):585–594.

Erdmann, E., et al. (2012). Depression of release by mGluR8 alters Ca^{2+} dependence of release machinery. *Cerebral Cortex*, 22(7):1498–1509.

Ericsson, J., et al. (2013). Dopamine differentially modulates the excitability of striatal neurons of the direct and indirect pathways in lamprey. *Journal of Neuroscience*, 33(18):8045–8054.

Erlander, M.G., Tillakaratne, N.J., Feldblum, S., Patel, N., and Tobin, A.J. (1991). Two genes encode distinct glutamate decarboxylases. *Neuron*, 7(1):91–100.

Ernst, M., Zametkin, A.J., Matochik, J.A., Jons, P.H., and Cohen, R.M. (1998). DOPA decarboxylase activity in attention-deficit hyperactivity disorder adults. A [fluorine-18]fluorodopa positron emission tomographic study. *Journal of Neuroscience*, 18(15):5901–5907.

Ernst, M., et al. (2003). Neural substrates of decision making in adults with attention-deficit hyperactivity disorder. *The American Journal of Psychiatry*, 160(6):1061–1070.

Erskine, H.E., et al. (2016). Long-term outcomes of attention-deficit/hyperactivity disorder and conduct disorder: A systematic review and meta-analysis. *Journal of the American Academy of Child & Adolescent Psychiatry*, 55(10):841–850.

Esclapez, M., Tillakaratne, N.J., Kaufman, D.L., Tobin, A.J., and Houser, C.R. (1994). Comparative localization of two forms of glutamic acid decarboxylase and their mRNAs in rat brain supports the concept of functional differences between the forms. *Journal of Neuroscience*, 14(3.2):1834–1855.

Estruch, S.B., et al. (2018). Proteomic analysis of FOXP proteins reveals interactions between cortical transcription factors associated with neurodevelopmental disorders. *Human Molecular Genetics*, 27(7):1212–1227.

Evans, D.I., Jones, R.S.G., and Woodhall, G. (2000). Activation of presynaptic group III metabotropic receptors enhances glutamate release in rat entorhinal cortex. *Journal of Neurophysiology*, 83(5):2519–2525.

Faraone, S.V. (2018). The pharmacology of amphetamine and methylphenidate: Relevance to the neurobiology of attention-deficit/hyperactivity disorder and other psychiatric comorbidities. *Neuroscience and Biobehavioral Reviews*, 87:255–270.

Faraone, S.V., Biederman, J., and Mick, E. (2006a). The age-dependent decline of attention-deficit hyperactivity disorder: A meta-analysis of follow-up studies. *Psychological Medicine*, 36(2):159–165.

Faraone, S.V., Biederman, J., and Monuteaux, M.C. (2000). Toward guidelines for pedigree selection in genetic studies of attention-deficit hyperactivity disorder. *Genetic Epidemiology*, 18(1):1–16.

Faraone, S.V., Biederman, J., Spencer, T.J., and Aleardi, M. (2006b). Comparing the efficacy of medications for ADHD using meta-analysis. *Medscape General Medicine*, 8(4):4.

Faraone, S.V., Spencer, T., Aleardi, M., Pagano, C., and Biederman, J. (2004). Meta-analysis of the efficacy of methylphenidate for treating adult attention-deficit/hyperactivity disorder. *Journal of Clinical Psychopharmacology*, 24(1):24–29.

Faraone, S.V., et al. (2005). Molecular genetics of attention-deficit/hyperactivity disorder. *Biological Psychiatry*, 57(11):1313–1323.

Faraone, S.V., et al. (2015). Attention-deficit/hyperactivity disorder. *Nature Reviews Disease Primers*, 1(1):1–23.

Fatemi, S.H., et al. (2005). GABAergic dysfunction in schizophrenia and mood disorders as reflected by decreased levels of glutamic acid decarboxylase 65 and 67 kDa and Reelin proteins in cerebellum. *Schizophrenia Research*, 72(2-3):109–122.

Faul, F., Erdfelder, E., Buchner, A., and Lang, A.G. (2009). Statistical power analyses using G*Power 3.1: Tests for correlation and regression analyses. *Behavior Research Methods*, 41(4):1149–1160.

Faul, F., Erdfelder, E., Lang, A.G., and Buchner, A. (2007). G*Power 3: A flexible statistical power analysis program for the social, behavioral, and biomedical sciences. *Behavior Research Methods*, 39(2):175–191.

Fenalti, G., et al. (2007). GABA production by glutamic acid decarboxylase is regulated by a dynamic catalytic loop. *Nature Structural & Molecular Biology*, 14(4):280–286.

Fendt, M., et al. (2010). The effect of mGlu8 deficiency in animal models of psychiatric diseases. *Genes, Brain, and Behavior*, 9(1):33–44.

Fendt, M., et al. (2013). Differential roles of mGlu(7) and mGlu(8) in amygdala-dependent behavior and physiology. *Neuropharmacology*, 72:215–223.

Feng, J., et al. (2006). The *Evf-2* noncoding RNA is transcribed from the Dlx-5/6 ultracon-served region and functions as a Dlx-2 transcriptional coactivator. *Genes & Development*, 20(11):1470–1484.

Ferland, R.J., Cherry, T.J., Preware, P.O., Morrisey, E.E., and Walsh, C.A. (2003). Characterization of *Foxp2* and *Foxp1* mRNA and protein in the developing and mature brain. *The Journal of Comparative Neurology*, 460(2):266–279.

Ferraguti, F., et al. (2005). Metabotropic glutamate receptor 8-expressing nerve terminals target subsets of GABAergic neurons in the hippocampus. *Journal of Neuroscience*, 25(45):10520–10536.

Ferreira, P.E.M.S., et al. (2009). Differentiating attention-deficit/hyperactivity disorder inat-tentive and combined types: A 1H-magnetic resonance spectroscopy study of fronto-striato-thalamic regions. *Journal of Neural Transmission*, 116(5):623–629.

Ferrucci, M., et al. (2019). The effects of amphetamine and methamphetamine on the release of norepinephrine, dopamine and acetylcholine from the brainstem reticular formation. *Frontiers in Neuroanatomy*, 13:48.

Filion, M. and Tremblay, L. (1991). Abnormal spontaneous activity of globus pallidus neurons in monkeys with MPTP-induced parkinsonism. *Brain Research*, 547(1):140–144.

Findling, R.L., et al. (2019). Dasotraline in children with attention-deficit/hyperactivity dis-order: A six-week, placebo-controlled, fixed-dose trial. *Journal of Child and Adolescent Psychopharmacology*, 29(2):80–89.

Fisher, S.E., Vargha-Khadem, F., Watkins, K.E., Monaco, A.P., and Pembrey, M.E. (1998). Lo-calisation of a gene implicated in a severe speech and language disorder. *Nature Genetics*, 18(2):168–170.

Foley, J.E., et al. (2009). Targeted mutagenesis in zebrafish using customized zinc finger nu-cleases. *Nature Protocols*, 4(12):1855.

Forde, N.J., et al. (2017). No association between cortical gyrification or intrinsic curvature and attention-deficit/hyperactivity disorder in adolescents and young adults. *Frontiers in Neuroscience*, 11:218.

Forssberg, H., Fernell, E., Waters, S., Waters, N., and Tedroff, J. (2006). Altered pattern of brain dopamine synthesis in male adolescents with attention-deficit hyperactivity disorder. *Behavioral and Brain Functions*, 2:40.

Foss-Feig, J.H., et al. (2017). Searching for cross-diagnostic convergence: Neural mechanisms governing excitation and inhibition balance in schizophrenia and autism spectrum disorders. *Biological Psychiatry*, 81(10):848–861.

Frank, M.J., Santamaria, A., O'Reilly, R.C., and Willcutt, E. (2007). Testing computational mod-els of dopamine and noradrenaline dysfunction in attention-deficit/hyperactivity disorder. *Neuropsychopharmacology*, 32(7):1583–1599.

Franke, B., et al. (2018). Live fast, die young? A review on the developmental trajectories of ADHD across the lifespan. *European Neuropsychopharmacology*, 28(10):1059–1088.

Freese, L., et al. (2012). GABA system changes in methylphenidate sensitized female rats. *Behavioural Brain Research*, 231(1):181–186.

French, G.M. (1959). Locomotor effects of regional ablations of frontal cortex in rhesus monkeys. *Journal of Comparative and Physiological Psychology*, 52(1):18.

French, C.A. and Fisher, S.E. (2014). What can mice tell us about Foxp2 function? *Current Opinion in Neurobiology*, 28:72–79.

French, C.A., et al. (2012). An aetiological *Foxp2* mutation causes aberrant striatal activity and alters plasticity during skill learning. *Molecular Psychiatry*, 17(11):1077–1085.

French, C.A., et al. (2019). Differential effects of *Foxp2* disruption in distinct motor circuits. *Molecular Psychiatry*, 24(3):447–462.

Friedman, J.I., et al. (2008). *CNTNAP2* gene dosage variation is associated with schizophrenia and epilepsy. *Molecular Psychiatry*, 13(3):261–266.

Frodl, T. and Skokauskas, N. (2012). Meta-analysis of structural MRI studies in children and adults with attention-deficit hyperactivity disorder indicates treatment effects. *Acta Psychiatrica Scandinavica*, 125(2):114–126.

Frye, R.E., et al. (2010). Surface area accounts for the relation of gray matter volume to reading-related skills and history of dyslexia. *Cerebral Cortex*, 20(11):2625–2635.

Fujihara, K., et al. (2015). Glutamate decarboxylase 67 deficiency in a subset of GABAergic neurons induces schizophrenia-related phenotypes. *Neuropsychopharmacology*, 40(10):2475–2486.

Fujita, E., et al. (2008). Ultrasonic vocalization impairment of *Foxp2* (R552H) knockin mice related to speech-language disorder and abnormality of Purkinje cells. *Proceedings of the National Academy of Sciences*, 105(8):3117–3122.

Fusar-Poli, P., Rubia, K., Rossi, G., Sartori, G., and Balottin, U. (2012). Striatal dopamine transporter alterations in ADHD: Pathophysiology or adaptation to psychostimulants? A meta-analysis. *The American Journal of Psychiatry*, 169(3):264–272.

Gainetdinov, R.R., et al. (1999). Role of serotonin in the paradoxical calming effect of psychostimulants on hyperactivity. *Science*, 283(5400):397–401.

Ganz, J., et al. (2015). Subdivisions of the adult zebrafish pallium based on molecular marker analysis. *F1000Research*, 3:308.

Gao, R. and Penzes, P. (2015). Common mechanisms of excitatory and inhibitory imbalance in schizophrenia and autism spectrum disorders. *Current Molecular Medicine*, 15(2):146–167.

Gao, Y., et al. (2019). Impairments of large-scale functional networks in attention-deficit/hyperactivity disorder: A meta-analysis of resting-state functional connectivity. *Psychological Medicine*, 49(15):2475–2485.

Gaub, M. and Carlson, C.L. (1997). Gender differences in ADHD: A meta-analysis and critical review. *Journal of the American Academy of Child and Adolescent Psychiatry*, 36(8):1036–1045.

Gerlai, R., Adams, B., Fitch, T., Chaney, S., and Baez, M. (2002). Performance deficits of mGluR8 knockout mice in learning tasks: The effects of null mutation and the background genotype. *Neuropharmacology*, 43(2):235–249.

Gesell, A. and Amatruda, C.S. (1941). *Developmental Diagnosis; Normal and Abnormal Child Development*. Hoeber, Oxford, England.

Getahun, D., et al. (2013). *In utero* exposure to ischemic-hypoxic conditions and attention-deficit/hyperactivity disorder. *Pediatrics*, 131(1):e53–61.

Ghanizadeh, A. (2009). Psychiatric comorbidity differences in clinic-referred children and adolescents with ADHD according to the subtypes and gender:. *Journal of Child Neurology*, 24(6):679–84.

Giacopuzzi, E., et al. (2017). Exome sequencing in schizophrenic patients with high levels of homozygosity identifies novel and extremely rare mutations in the GABA/glutamatergic pathways. *PLOS ONE*, 12(8):e0182778.

Giros, B., Jaber, M., Jones, S.R., Wightman, R.M., and Caron, M.G. (1996). Hyperlocomotion and indifference to cocaine and amphetamine in mice lacking the dopamine transporter. *Nature*, 379(6566):606–612.

Gizer, I.R., Ficks, C., and Waldman, I.D. (2009). Candidate gene studies of ADHD: A meta-analytic review. *Human Genetics*, 126(1):51–90.

Gnanavel, S., Sharma, P., Kaushal, P., and Hussain, S. (2019). Attention-deficit hyperactivity disorder and comorbidity: A review of literature. *World Journal of Clinical Cases*, 7(17):2420–2426.

Godefroy, O. and Rousseaux, M. (1996). Divided and focused attention in patients with lesion of the prefrontal cortex. *Brain and Cognition*, 30(2):155–174.

Goitia, B., et al. (2013). Differential effects of methylphenidate and cocaine on GABA transmission in sensory thalamic nuclei. *Journal of Neurochemistry*, 124(5):602–612.

Gokcen, C., Kocak, N., and Pekgor, A. (2011). Methylenetetrahydrofolate reductase gene polymorphisms in children with attention-deficit hyperactivity disorder. *International Journal of Medical Sciences*, 8(7):523–528.

Goldstein, K. (1942). *Aftereffects of Brain Injuries in War: Their Evaluation and Treatment. The Application of Psychologic Methods in the Clinic*. Grune & Stratton, Oxford, England.

Gong, X., et al. (2004). Association between the *FOXP2* gene and autistic disorder in Chinese population. *American Journal of Medical Genetics. Part B, Neuropsychiatric Genetics*, 127B(1):113–116.

Graetz, B.W., Sawyer, M.G., and Baghurst, P. (2005). Gender differences among children with DSM-IV ADHD in Australia. *Journal of the American Academy of Child and Adolescent Psychiatry*, 44(2):159–168.

Greven, C.U., et al. (2015). Developmentally stable whole-brain volume reductions and developmentally sensitive caudate and putamen volume alterations in those with attention-deficit/hyperactivity disorder and their unaffected siblings. *JAMA Psychiatry*, 72(5):490–499.

Grizenko, N., et al. (2012). Maternal stress during pregnancy, ADHD symptomatology in children and genotype: Gene-environment interaction. *Journal of the Canadian Academy of Child and Adolescent Psychiatry*, 21(1):9–15.

Gross, C.G. (1963). Locomotor activity following lateral frontal lesions in rhesus monkeys. *Journal of Comparative and Physiological Psychology*, 56:232–236.

Groszer, M., et al. (2008). Impaired synaptic plasticity and motor learning in mice with a point mutation implicated in human speech deficits. *Current Biology*, 18(5):354–362.

Guidotti, A., et al. (2000). Decrease in reelin and glutamic acid decarboxylase$_{67}$ (GAD$_{67}$) expression in schizophrenia and bipolar disorder: A postmortem brain study. *Archives of General Psychiatry*, 57(11):1061–1069.

Haesler, S., et al. (2004). *FoxP2* expression in avian vocal learners and non-learners. *Journal of Neuroscience*, 24(13):3164–3175.

Haesler, S., et al. (2007). Incomplete and inaccurate vocal imitation after knockdown of *FoxP2* in songbird basal ganglia nucleus Area X. *PLOS Biology*, 5(12):e321.

Halmøy, A., Klungsøyr, K., Skjærven, R., and Haavik, J. (2012). Pre- and perinatal risk factors in adults with attention-deficit/hyperactivity disorder. *Biological Psychiatry*, 71(5):474–481.

Hamada, N., et al. (2015). Role of the cytoplasmic isoform of *RBFOX1/A2BP1* in establishing the architecture of the developing cerebral cortex. *Molecular Autism*, 6(1):56.

Hamada, N., et al. (2016). Essential role of the nuclear isoform of *RBFOX1*, a candidate gene for autism spectrum disorders, in the brain development. *Scientific Reports*, 6:30805.

Hammerness, P., Biederman, J., Petty, C., Henin, A., and Moore, C.M. (2010). Brain biochemical effects of methylphenidate treatment using proton magnetic spectroscopy in youth with attention-deficit hyperactivity disorder: A controlled pilot study. *CNS Neuroscience & Therapeutics*, 18(1):34–40.

Harrington, A.J., et al. (2016). MEF2C regulates cortical inhibitory and excitatory synapses and behaviors relevant to neurodevelopmental disorders. *eLife*, 5:e20059.

Hart, E.L., Lahey, B.B., Loeber, R., Applegate, B., and Frick, P.J. (1995). Developmental change in attention-deficit hyperactivity disorder in boys: A four-year longitudinal study. *Journal of Abnormal Child Psychology*, 23(6):729–749.

Hart, H., Radua, J., Mataix-Cols, D., and Rubia, K. (2012). Meta-analysis of fMRI studies of timing in attention-deficit hyperactivity disorder (ADHD). *Neuroscience & Biobehavioral Reviews*, 36(10):2248–2256.

Hart, H., Radua, J., Nakao, T., Mataix-Cols, D., and Rubia, K. (2013). Meta-analysis of functional magnetic resonance imaging studies of inhibition and attention in attention-deficit/hyperactivity disorder: Exploring task-specific, stimulant medication, and age effects. *JAMA Psychiatry*, 70(2):185–198.

Harvey-Girard, E., Giassi, A.C.C., Ellis, W., and Maler, L. (2012). Organization of the gymnotiform fish pallium in relation to learning and memory: IV. Expression of conserved transcription factors and implications for the evolution of dorsal telencephalon. *The Journal of Comparative Neurology*, 520(15):3395–3413.

Hashimoto, T., et al. (2003). Gene expression deficits in a subclass of GABA neurons in the prefrontal cortex of subjects with schizophrenia. *Journal of Neuroscience*, 23(15):6315–6326.

Haug, M.F., Gesemann, M., Mueller, T., and Neuhauss, S.C. (2013). Phylogeny and expression divergence of metabotropic glutamate receptor genes in the brain of zebrafish (*Danio rerio*). *Journal of Comparative Neurology*, 521(7):1533–1560.

Hawi, Z., et al. (2002). Serotonergic system and attention-deficit hyperactivity disorder (ADHD): A potential susceptibility locus at the 5-HT$_{1B}$ receptor gene in 273 nuclear families from a multi-centre sample. *Molecular Psychiatry*, 7(7):718–725.

Haydar, T.F., Wang, F., Schwartz, M.L., and Rakic, P. (2000). Differential modulation of proliferation in the neocortical ventricular and subventricular zones. *Journal of Neuroscience*, 20(15):5764–5774.

Heckers, S., et al. (2002). Differential hippocampal expression of glutamic acid decarboxylase 65 and 67 messenger RNA in bipolar disorder and schizophrenia. *Archives of General Psychiatry*, 59(6):521–529.

Helms, C.M., Gubner, N.R., Wilhelm, C.J., Mitchell, S.H., and Grandy, D.K. (2008). D4 receptor deficiency in mice has limited effects on impulsivity and novelty seeking. *Pharmacology, Biochemistry, and Behavior*, 90(3):387–393.

Henriksen, L., Wu, C.S., Secher, N.J., Obel, C., and Juhl, M. (2015). Medical augmentation of labor and the risk of ADHD in offspring: A population-based study. *Pediatrics*, 135(3):e672–677.

Herskovits, E.H., et al. (1999). Is the spatial distribution of brain lesions associated with closed-head injury predictive of subsequent development of attention-deficit/hyperactivity disorder? Analysis with brain-image database. *Radiology*, 213(2):389–394.

Hesslinger, B., et al. (2002). Frontoorbital volume reductions in adult patients with attention-deficit hyperactivity disorder. *Neuroscience Letters*, 328(3):319–321.

Hettema, J.M., et al. (2006). Association between glutamic acid decarboxylase genes and anxiety disorders, major depression, and neuroticism. *Molecular Psychiatry*, 11(8):752–762.

Hettinger, J.A., et al. (2012). *DRD2* and *PPP1R1B (DARPP-32)* polymorphisms independently confer increased risk for autism spectrum disorders and additively predict affected status in male-only affected sib-pair families. *Behavioral and Brain Functions*, 8:19.

Hickey, S.L., Berto, S., and Konopka, G. (2019). Chromatin decondensation by FOXP2 promotes human neuron maturation and expression of neurodevelopmental disease genes. *Cell Reports*, 27(6):1699–1711.e9.

Higashijima, S.I., Mandel, G., and Fetcho, J.R. (2004). Distribution of prospective glutamatergic, glycinergic, and GABAergic neurons in embryonic and larval zebrafish. *The Journal of Comparative Neurology*, 480(1):1–18.

Hinshaw, S.P., Owens, E.B., Sami, N., and Fargeon, S. (2006). Prospective follow-up of girls with attention-deficit/hyperactivity disorder into adolescence: Evidence for continuing cross-domain impairment. *Journal of Consulting and Clinical Psychology*, 74(3):489–499.

Hire, A.J., Ashcroft, D.M., Springate, D.A., and Steinke, D.T. (2018). ADHD in the United Kingdom: Regional and socioeconomic variations in incidence rates amongst children and adolescents (2004-2013). *Journal of Attention Disorders*, 22(2):134–142.

Hirota, T., Schwartz, S., and Correll, C.U. (2014). Alpha-2 agonists for attention-deficit/hyperactivity disorder in youth: A systematic review and meta-analysis of monotherapy and add-on trials to stimulant therapy. *Journal of the American Academy of Child & Adolescent Psychiatry*, 53(2):153–173.

Hisaoka, T., Nakamura, Y., Senba, E., and Morikawa, Y. (2010). The forkhead transcription factors, Foxp1 and Foxp2, identify different subpopulations of projection neurons in the mouse cerebral cortex. *Neuroscience*, 166(2):551–563.

Hjern, A., Weitoft, G.R., and Lindblad, F. (2010). Social adversity predicts ADHD-medication in school children – a national cohort study. *Acta Paediatrica*, 99(6):920–924.

Ho, T.P., et al. (1996). Situational versus pervasive hyperactivity in a community sample. *Psychological Medicine*, 26(2):309–321.

Hoekzema, E., et al. (2011). Training-induced neuroanatomical plasticity in ADHD: A tensor-based morphometric study. *Human Brain Mapping*, 32(10):1741–1749.

Hoffman, E.J., et al. (2016). Estrogens suppress a behavioral phenotype in zebrafish mutants of the autism risk Gene, *CNTNAP2*. *Neuron*, 89(4):725–733.

Hong, S.B., et al. (2014). Connectomic disturbances in attention-deficit/hyperactivity disorder: A whole-brain tractography analysis. *Biological Psychiatry*, 76(8):656–663.

Hoogman, M., et al. (2017). Subcortical brain volume differences in participants with attention-deficit hyperactivity disorder in children and adults: A cross-sectional mega-analysis. *The Lancet Psychiatry*, 4(4):310–319.

Howe, K., et al. (2013). The zebrafish reference genome sequence and its relationship to the human genome. *Nature*, 496(7446):498–503.

Howe, K.L., et al. (2021). Ensembl 2021. *Nucleic Acids Research*, 49(D1):D884–D891.

Hoza, B., et al. (2005). What aspects of peer relationships are impaired in children with attention-deficit/hyperactivity disorder? *Journal of Consulting and Clinical Psychology*, 73(3):411–423.

Hruscha, A. and Schmid, B. (2015). Generation of zebrafish models by CRISPR /Cas9 genome editing. *Methods in Molecular Biology (Clifton, N.J.)*, 1254:341–350.

Hruscha, A., et al. (2013). Efficient CRISPR/Cas9 genome editing with low off-target effects in zebrafish. *Development*, 140(24):4982–4987.

Huang, P., et al. (2011). Heritable gene targeting in zebrafish using customized TALENs. *Nature Biotechnology*, 29(8):699–700.

Hurd, Y.L. and Ungerstedt, U. (1989). *In vivo* neurochemical profile of dopamine uptake inhibitors and releasers in rat caudate-putamen. *European Journal of Pharmacology*, 166(2):251–260.

Hwang, W.Y., et al. (2013). Efficient genome editing in zebrafish using a CRISPR-Cas system. *Nature Biotechnology*, 31(3):227–229.

Hyde, C.L., et al. (2016). Identification of 15 genetic loci associated with risk of major depression in individuals of European descent. *Nature Genetics*, 48(9):1031–1036.

Hynd, G.W., Semrud-Clikeman, M., Lorys, A.R., Novey, E.S., and Eliopulos, D. (1990). Brain morphology in developmental dyslexia and attention-deficit disorder/hyperactivity. *Archives of Neurology*, 47(8):919–926.

Inoue, Y., Ikeda, M., and Shimizu, T. (2004). Proteome-wide classification and identification of mammalian-type GPCRs by binary topology pattern. *Computational Biology and Chemistry*, 28(1):39–49.

Insel, T., et al. (2010). Research domain criteria (RDoC): Toward a new classification framework for research on mental disorders. *The American Journal of Psychiatry*, 167(7):748–751.

International League Against Epilepsy Consortium on Complex Epilepsies (2014). Genetic determinants of common epilepsies: A meta-analysis of genome-wide association studies. *The Lancet. Neurology*, 13(9):893–903.

Ioannidis, J.P.A., Ntzani, E.E., Trikalinos, T.A., and Contopoulos-Ioannidis, D.G. (2001). Replication validity of genetic association studies. *Nature Genetics*, 29(3):306–309.

Isaacson, J.S. (2000). Synaptic transmission: Spillover in the spotlight. *Current Biology*, 10(13):R475–R477.

Itakura, T., et al. (2008). The medaka *FoxP2*, a homologue of human language gene *FOXP2*, has a diverged structure and function. *Journal of Biochemistry*, 143(3):407–416.

Ivanov, I., Murrough, J.W., Bansal, R., Hao, X., and Peterson, B.S. (2014). Cerebellar morphology and the effects of stimulant medications in youths with attention-deficit-hyperactivity disorder. *Neuropsychopharmacology*, 39(3):718–726.

Ivanov, I., et al. (2010). Morphological abnormalities of the thalamus in youths with attention-deficit hyperactivity disorder. *The American Journal of Psychiatry*, 167(4):397–408.

Jackman, C., Horn, N.D., Molleston, J.P., and Sokol, D.K. (2009). Gene associated with seizures, autism, and hepatomegaly in an Amish girl. *Pediatric Neurology*, 40(4):310–313.

Jackson, B.C., Carpenter, C., Nebert, D.W., and Vasiliou, V. (2010). Update of human and mouse forkhead box (*FOX*) gene families. *Human Genomics*, 4(5):345–352.

Jackson, V.A., et al. (2016). Super-complexes of adhesion GPCRs and neural guidance receptors. *Nature Communications*, 7(1):11184.

Jain, M., et al. (2012). A cooperative interaction between *LPHN3* and 11q doubles the risk for ADHD. *Molecular Psychiatry*, 17(7):741–747.

Jao, L.E., Wente, S.R., and Chen, W. (2013). Efficient multiplex biallelic zebrafish genome editing using a CRISPR nuclease system. *Proceedings of the National Academy of Sciences*, 110(34):13904–13909.

Jarick, I., et al. (2014). Genome-wide analysis of rare copy number variations reveals *PARK2* as a candidate gene for attention-deficit/hyperactivity disorder. *Molecular Psychiatry*, 19(1):115–121.

Jašarević, E., Howerton, C.L., Howard, C.D., and Bale, T.L. (2015). Alterations in the vaginal microbiome by maternal stress are associated with metabolic reprogramming of the offspring gut and brain. *Endocrinology*, 156(9):3265–3276.

Jensen, C.M. and Steinhausen, H.C. (2015). Comorbid mental disorders in children and adolescents with attention-deficit/hyperactivity disorder in a large nationwide study. *Attention Deficit and Hyperactivity Disorders*, 7(1):27–38.

Jha, U. and Thirumalai, V. (2020). Neuromodulatory selection of motor neuron recruitment patterns in a visuomotor behavior increases speed. *Current Biology*, 30(5):788–801.e3.

Joris, M., et al. (2017). Number of inadvertent RNA targets for morpholino knockdown in *Danio rerio* is largely underestimated: Evidence from the study of Ser/Arg-rich splicing factors. *Nucleic Acids Research*, 45(16):9547–9557.

Kahn, R.S., Khoury, J., Nichols, W.C., and Lanphear, B.P. (2003). Role of dopamine transporter genotype and maternal prenatal smoking in childhood hyperactive-impulsive, inattentive, and oppositional behaviors. *The Journal of Pediatrics*, 143(1):104–110.

Kalueff, A.V., et al. (2013). Towards a comprehensive catalog of zebrafish behavior 1.0 and beyond. *Zebrafish*, 10(1):70–86.

Kanaani, J., Lissin, D., Kash, S.F., and Baekkeskov, S. (1999). The hydrophilic isoform of glutamate decarboxylase, GAD67, is targeted to membranes and nerve terminals independent of dimerization with the hydrophobic membrane-anchored isoform, GAD65. *Journal of Biological Chemistry*, 274(52):37200–37209.

Kandaswamy, R., et al. (2013). Genetic association, mutation screening, and functional analysis of a Kozak sequence variant in the metabotropic glutamate receptor 3 gene in bipolar disorder. *JAMA Psychiatry*, 70(6):591–598.

Kandemir, H., et al. (2014). Evaluation of several micro RNA (miRNA) levels in children and adolescents with attention-deficit hyperactivity disorder. *Neuroscience Letters*, 580:158–162.

Kang, E., et al. (2019). Interplay between a mental disorder risk gene and developmental polarity switch of GABA action leads to excitation-inhibition imbalance. *Cell Reports*, 28(6):1419–1428.e3.

Karam, R.G., et al. (2015). Persistence and remission of ADHD during adulthood: A 7-year clinical follow-up study. *Psychological Medicine*, 45(10):2045–2056.

Kaslin, J. and Brand, M. (2016). *Essentials of Cerebellum and Cerebellar Disorders: A Primer for Graduate Students (The Zebrafish Cerebellum)*. Springer.

Kates, W.R., et al. (2002). MRI parcellation of the frontal lobe in boys with attention-deficit hyperactivity disorder or Tourette syndrome. *Psychiatry Research*, 116(1-2):63–81.

Kato, M., et al. (2014). Human speech- and reading-related genes display partially overlapping expression patterns in the marmoset brain. *Brain and Language*, 133:26–38.

Kaufman, D.L., Houser, C.R., and Tobin, A.J. (1991). Two forms of the gamma-Aminobutyric acid synthetic enzyme glutamate decarboxylase have distinct intraneuronal distributions and cofactor interactions. *Journal of Neurochemistry*, 56(2):720–723.

Kennard, M.A., Spencer, S., and Fountain Jr, G. (1941). Hyperactivity in monkeys following lesions of the frontal lobes. *Journal of Neurophysiology*.

Kessler, R.C., et al. (2006). The prevalence and correlates of adult ADHD in the United States: Results from the National Comorbidity Survey Replication. *The American Journal of Psychiatry*, 163(4):716–723.

Kim, S.H., et al. (2012). The genetic association of *DUSP6* with bipolar disorder and its effect on ERK activity. *Progress in Neuro-Psychopharmacology & Biological Psychiatry*, 37(1):41–49.

Kim, J.H., et al. (2019). Molecular networks of FOXP family: Dual biologic functions, interplay with other molecules and clinical implications in cancer progression. *Molecular Cancer*, 18(1):180.

Kimmel, C.B., Ballard, W.W., Kimmel, S.R., Ullmann, B., and Schilling, T.F. (1995). Stages of embryonic development of the zebrafish. *Developmental Dynamics*, 203(3):253–310.

Kinoshita, A., et al. (1996). Presynaptic localization of a metabotropic glutamate receptor, mGluR8, in the rhinencephalic areas: A light and electron microscope study in the rat. *Neuroscience Letters*, 207(1):61–64.

Klein, M., et al. (2020). Contribution of intellectual disability–related genes to ADHD risk and to locomotor activity in *Drosophila*. *American Journal of Psychiatry*, 177(6):526–536.

Knobel, M., Wolman, M.B., and Mason, E. (1959). Hyperkinesis and organicity in children. *A.M.A. Archives of General Psychiatry*, 1:310–321.

Koblan, K.S., et al. (2015). Dasotraline for the treatment of attention-deficit/hyperactivity disorder: A randomized, double-blind, placebo-controlled, proof-of-concept trial in adults. *Neuropsychopharmacology*, 40(12):2745–2752.

Koerner, J.F. and Cotman, C.W. (1981). Micromolar L-2-amino-4-phosphonobutyric acid selectively inhibits perforant path synapses from lateral entorhinal cortex. *Brain Research*, 216(1):192–198.

Kok, F.O., et al. (2015). Reverse genetic screening reveals poor correlation between morpholino-induced and mutant phenotypes in zebrafish. *Developmental Cell*, 32(1):97–108.

Kokel, D. and Peterson, R.T. (2008). Chemobehavioural phenomics and behaviour-based psychiatric drug discovery in the zebrafish. *Briefings in Functional Genomics & Proteomics*, 7(6):483–490.

Kolata, S.M., et al. (2018). Neuropsychiatric phenotypes produced by GABA reduction in mouse cortex and hippocampus. *Neuropsychopharmacology*, 43(6):1445–1456.

Konofal, E., et al. (2014). Pilot phase II study of mazindol in children with attention-deficit/hyperactivity disorder. *Drug Design, Development and Therapy*, 8:2321–2332.

Konopka, G., et al. (2009). Human-specific transcriptional regulation of CNS development genes by FOXP2. *Nature*, 462(7270):213–217.

Koulen, P., Kuhn, R., Wässle, H., and Brandstätter, J.H. (1999). Modulation of the intracellular calcium concentration in photoreceptor terminals by a presynaptic metabotropic glutamate receptor. *Proceedings of the National Academy of Sciences*, 96(17):9909–9914.

Koulen, P., Liu, J., Nixon, E., and Madry, C. (2005). Interaction between mGluR8 and calcium channels in photoreceptors is sensitive to pertussis toxin and occurs via G protein beta/gamma subunit signaling. *Investigative Ophthalmology & Visual Science*, 46(1):287–291.

Kowalczyk, O.S., et al. (2019). Methylphenidate and atomoxetine normalise fronto-parietal underactivation during sustained attention in ADHD adolescents. *European Neuropsychopharmacology*, 29(10):1102–1116.

Kozol, R.A., et al. (2016). Function over form: Modeling groups of inherited neurological conditions in zebrafish. *Frontiers in Molecular Neuroscience*, 9:55.

Kramer, A., Wu, Y., Baier, H., and Kubo, F. (2019). Neuronal architecture of a visual center that processes optic flow. *Neuron*, 103(1):118–132.e7.

Kraut, A.A., et al. (2013). Comorbidities in ADHD children treated with methylphenidate: A database study. *BMC Psychiatry*, 13:11.

Kravitz, A.V., et al. (2010). Regulation of parkinsonian motor behaviours by optogenetic control of basal ganglia circuitry. *Nature*, 466(7306):622–626.

Kuczenski, R. and Segal, D.S. (2002). Exposure of adolescent rats to oral methylphenidate: Preferential effects on extracellular norepinephrine and absence of sensitization and cross-sensitization to methamphetamine. *Journal of Neuroscience*, 22(16):7264–7271.

Kunishima, N., et al. (2000). Structural basis of glutamate recognition by a dimeric metabotropic glutamate receptor. *Nature*, 407(6807):971–977.

Kurt, S., Fisher, S.E., and Ehret, G. (2012). Foxp2 mutations impair auditory-motor association learning. *PloS One*, 7(3):e33130.

la Fougère, C., et al. (2006). Value of ^{99m}Tc-TRODAT-1 SPECT to predict clinical response to methylphenidate treatment in adults with attention-deficit hyperactivity disorder. *Nuclear Medicine Communications*, 27(9):733–737.

Labun, K., et al. (2019). CHOPCHOP v3: Expanding the CRISPR web toolbox beyond genome editing. *Nucleic Acids Research*, 47(W1):W171–W174.

LaHoste, G.J., et al. (1996). Dopamine D4 receptor gene polymorphism is associated with attention-deficit hyperactivity disorder. *Molecular Psychiatry*, 1(2):121–124.

Lai, C.S., Fisher, S.E., Hurst, J.A., Vargha-Khadem, F., and Monaco, A.P. (2001). A forkhead-domain gene is mutated in a severe speech and language disorder. *Nature*, 413(6855):519–523.

Lai, C.S.L., Gerrelli, D., Monaco, A.P., Fisher, S.E., and Copp, A.J. (2003). *FOXP2* expression

during brain development coincides with adult sites of pathology in a severe speech and language disorder. *Brain*, 126(11):2455–2462.

Lai, C.S., et al. (2000). The *SPCH1* region on human 7q31: Genomic characterization of the critical interval and localization of translocations associated with speech and language disorder. *American Journal of Human Genetics*, 67(2):357–368.

Lal, P., et al. (2018). Identification of a neuronal population in the telencephalon essential for fear conditioning in zebrafish. *BMC Biology*, 16(1):45.

Lange, M., Froc, C., Grunwald, H., Norton, W.H., and Bally-Cuif, L. (2018). Pharmacological analysis of zebrafish *lphn3.1* morphant larvae suggests that saturated dopaminergic signaling could underlie the ADHD-like locomotor hyperactivity. *Progress in Neuro-Psychopharmacology & Biological Psychiatry*, 84(Pt A):181–189.

Lange, K.W., Reichl, S., Lange, K.M., Tucha, L., and Tucha, O. (2010). The history of attention-deficit hyperactivity disorder. *Attention Deficit and Hyperactivity Disorders*, 2(4):241–255.

Lange, M., et al. (2012). The ADHD-susceptibility gene *lphn3.1* modulates dopaminergic neuron formation and locomotor activity during zebrafish development. *Molecular Psychiatry*, 17(9):946–954.

Langley, K., Heron, J., Smith, G.D., and Thapar, A. (2012). Maternal and paternal smoking during pregnancy and risk of ADHD symptoms in offspring: Testing for intrauterine effects. *American Journal of Epidemiology*, 176(3):261–268.

Langley, K., et al. (2011). Clinical and cognitive characteristics of children with attention-deficit hyperactivity disorder, with and without copy number variants. *The British Journal of Psychiatry*, 199(5):398–403.

Laroche, F., et al. (2008). Polymorphisms of coding trinucleotide repeats of homeogenes in neurodevelopmental psychiatric disorders. *Psychiatric Genetics*, 18(6):295–301.

Larsson, H., Chang, Z., D'Onofrio, B.M., and Lichtenstein, P. (2014). The heritability of clinically diagnosed attention-deficit hyperactivity disorder across the lifespan. *Psychological Medicine*, 44(10):2223–2229.

Larsson, J.O., Larsson, H., and Lichtenstein, P. (2004). Genetic and environmental contributions to stability and change of ADHD symptoms between 8 and 13 years of age: A longitudinal twin study. *Journal of the American Academy of Child and Adolescent Psychiatry*, 43(10):1267–1275.

Lasky-Su, J., et al. (2007). A study of how socioeconomic status moderates the relationship between SNPs encompassing *BDNF* and ADHD symptom counts in ADHD families. *Behavior Genetics*, 37(3):487–497.

Lasky-Su, J., et al. (2008). Genome-wide association scan of quantitative traits for attention-deficit hyperactivity disorder identifies novel associations and confirms candidate gene associations. *American Journal of Medical Genetics. Part B, Neuropsychiatric Genetics*, 147B(8):1345–1354.

Lau, C.G. and Murthy, V.N. (2012). Activity-dependent regulation of inhibition via GAD67. *Journal of Neuroscience*, 32(25):8521–8531.

Laucht, M., et al. (2007). Interacting effects of the dopamine transporter gene and psychosocial adversity on attention-deficit/hyperactivity disorder symptoms among 15-year-olds from a high-risk community sample. *Archives of General Psychiatry*, 64(5):585–590.

Laufer, M.W., Denhoff, E., and Solomons, G. (1957). Hyperkinetic impulse disorder in children's behavior problems. *Psychosomatic Medicine*, 19(1):38–49.

Laugesen, K., Olsen, M.S., Telén Andersen, A.B., Frøslev, T., and Sørensen, H.T. (2013). *In utero* exposure to antidepressant drugs and risk of attention-deficit hyperactivity disorder: A nationwide Danish cohort study. *BMJ open*, 3(9):e003507.

Law, S.H.W. and Sargent, T.D. (2014). The serine-threonine protein kinase PAK4 is dispensable in zebrafish: Identification of a morpholino-generated pseudophenotype. *PloS One*, 9(6):e100268.

Lawton, K.J., Wassmer, T.L., and Deitcher, D.L. (2014). Conserved role of *Drosophila melanogaster* FoxP in motor coordination and courtship song. *Behavioural Brain Research*, 268:213–221.

Lazarus, M.S., Krishnan, K., and Huang, Z.J. (2015). GAD67 deficiency in parvalbumin interneurons produces deficits in inhibitory transmission and network disinhibition in mouse prefrontal cortex. *Cerebral Cortex*, 25(5):1290–1296.

Le Fevre, A.K., et al. (2013). *FOXP1* mutations cause intellectual disability and a recognizable phenotype. *American Journal of Medical Genetics. Part A*, 161A(12):3166–3175.

Lee, K.Y., Ahn, Y.M., Joo, E.J., Chang, J.S., and Kim, Y.S. (2006). The association of *DUSP6* gene with schizophrenia and bipolar disorder: Its possible role in the development of bipolar disorder. *Molecular Psychiatry*, 11(5):425–426.

Lee, S.S., Humphreys, K.L., Flory, K., Liu, R., and Glass, K. (2011). Prospective association of childhood attention-deficit/hyperactivity disorder (ADHD) and substance use and abuse/dependence: A meta-analytic review. *Clinical Psychology Review*, 31(3):328–341.

Lee, J., et al. (2020). Defining the homo- and heterodimerization propensities of metabotropic glutamate receptors. *Cell Reports*, 31(5):107605.

Lei, D., et al. (2015). Functional MRI reveals different response inhibition between adults and children with ADHD. *Neuropsychology*, 29(6):874–881.

Lesch, K.P., et al. (2011). Genome-wide copy number variation analysis in attention-deficit/hyperactivity disorder: Association with neuropeptide Y gene dosage in an extended pedigree. *Molecular Psychiatry*, 16(5):491–503.

Leucht, S., Hierl, S., Kissling, W., Dold, M., and Davis, J.M. (2012). Putting the efficacy of psychiatric and general medicine medication into perspective: Review of meta-analyses. *The British Journal of Psychiatry*, 200(2):97–106.

Levi, G., et al. (2003). The *Dlx5* homeodomain gene is essential for olfactory development and connectivity in the mouse. *Molecular and Cellular Neurosciences*, 22(4):530–543.

Levin, P.M. (1938). Restlessness in children. *Archives of Neurology & Psychiatry*, 39(4):764–770.

Levy, F., Hay, D.A., McStephen, M., Wood, C., and Waldman, I. (1997). Attention-deficit hyperactivity disorder: A category or a continuum? Genetic analysis of a large-scale twin study. *Journal of the American Academy of Child and Adolescent Psychiatry*, 36(6):737–744.

Li, B.M. and Mei, Z.T. (1994). Delayed-response deficit induced by local injection of the *A*2-adrenergic antagonist yohimbine into the dorsolateral prefrontal cortex in young adult monkeys. *Behavioral and Neural Biology*, 62(2):134–139.

Li, D., Sham, P.C., Owen, M.J., and He, L. (2006). Meta-analysis shows significant association between dopamine system genes and attention-deficit hyperactivity disorder (ADHD). *Human Molecular Genetics*, 15(14):2276–2284.

Li, S., Weidenfeld, J., and Morrisey, E.E. (2004). Transcriptional and DNA binding activity of the Foxp1/2/4 family is modulated by heterotypic and homotypic protein interactions. *Molecular and Cellular Biology*, 24(2):809–822.

Li, H., Yamagata, T., Mori, M., and Momoi, M.Y. (2005). Absence of causative mutations and presence of autism-related allele in *FOXP2* in Japanese autistic patients. *Brain and Development*, 27(3):207–210.

Li, H., et al. (2008). Transcription factor MEF2C influences neural stem/progenitor cell differentiation and maturation *in vivo*. *Proceedings of the National Academy of Sciences*, 105(27):9397–9402.

Li, W., et al. (2016). Significant association of *GRM7* and *GRM8* genes with schizophrenia and major depressive disorder in the Han Chinese population. *European Neuropsychopharmacology*, 26(1):136–146.

Lichtenstein, P., Carlström, E., Råstam, M., Gillberg, C., and Anckarsäter, H. (2010). The genetics of autism spectrum disorders and related neuropsychiatric disorders in childhood. *The American Journal of Psychiatry*, 167(11):1357–1363.

Liew, Z., Ritz, B., Rebordosa, C., Lee, P.C., and Olsen, J. (2014). Acetaminophen use during pregnancy, behavioral problems, and hyperkinetic disorders. *JAMA Pediatrics*, 168(4):313–320.

Liew, Z., et al. (2015). Attention-deficit/hyperactivity disorder and childhood autism in association with prenatal exposure to perfluoroalkyl substances: A nested case–control study in the Danish national birth cohort. *Environmental Health Perspectives*, 123(4):367–373.

Lin, H.Y. and Gau, S.S.F. (2015). Atomoxetine treatment strengthens an anti-correlated relationship between functional brain networks in medication-naïve adults with attention-deficit hyperactivity disorder: A randomized double-blind placebo-controlled clinical trial. *International Journal of Neuropsychopharmacology*, 19(3):pyv094.

Linden, A.M., Baez, M., Bergeron, M., and Schoepp, D.D. (2003). Increased *c-Fos* expression in the centromedial nucleus of the thalamus in metabotropic glutamate 8 receptor knockout mice following the elevated plus maze test. *Neuroscience*, 121(1):167–178.

Linden, A.M., et al. (2002). Increased anxiety-related behavior in mice deficient for metabotropic glutamate 8 (mGlu8) receptor. *Neuropharmacology*, 43(2):251–259.

Lionel, A.C., et al. (2011). Rare copy number variation discovery and cross-disorder comparisons identify risk genes for ADHD. *Science Translational Medicine*, 3(95):95ra75.

Long, J.E., Garel, S., Depew, M.J., Tobet, S., and Rubenstein, J.L.R. (2003). DLX5 regulates development of peripheral and central components of the olfactory system. *Journal of Neuroscience*, 23(2):568–578.

Long, J., et al. (2016). Distinct interactions between fronto-parietal and default mode networks in impaired consciousness. *Scientific Reports*, 6:38866.

Lopez, S., et al. (2007). Targeting group III metabotropic glutamate receptors produces complex behavioral effects in rodent models of Parkinson's disease. *Journal of Neuroscience*, 27(25):6701–6711.

Lopez-Larson, M.P., King, J.B., Terry, J., McGlade, E.C., and Yurgelun-Todd, D. (2012). Reduced insular volume in attention-deficit hyperactivity disorder. *Psychiatry Research*, 204(1):32–39.

Lotan, A., et al. (2014). Neuroinformatic analyses of common and distinct genetic components associated with major neuropsychiatric disorders. *Frontiers in Neuroscience*, 8:331.

Lowe, N., et al. (2004). Joint analysis of the *DRD5* marker concludes association with attention-deficit/hyperactivity disorder confined to the predominantly inattentive and combined subtypes. *The American Journal of Human Genetics*, 74(2):348–356.

Lu, M.M., Li, S., Yang, H., and Morrisey, E.E. (2002). *Foxp4*: A novel member of the *Foxp* subfamily of winged-helix genes co-expressed with *Foxp1* and *Foxp2* in pulmonary and gut tissues. *Mechanisms of Development*, 119:197–202.

Ludolph, A.G., et al. (2008). Dopaminergic dysfunction in attention-deficit hyperactivity disorder (ADHD), differences between pharmacologically treated and never treated young adults: A 3,4-dihdroxy-6-[^{18}F]fluorophenyl-l-alanine PET study. *NeuroImage*, 41(3):718–727.

Lueffe, T.M., et al. (2021a). Increased locomotor activity via regulation of GABAergic signalling in *foxp2* mutant zebrafish – implications for neurodevelopmental disorders. *Translational Psychiatry*, (accepted).

Lueffe, T.M., et al. (2021b). (in preparation).

Lundorf, M.D., et al. (2005). Mutational screening and association study of glutamate decarboxylase 1 as a candidate susceptibility gene for bipolar affective disorder and schizophrenia. *American Journal of Medical Genetics. Part B, Neuropsychiatric Genetics*, 135B(1):94–101.

Lupien, S.J., et al. (2017). The DSM5/RDoC debate on the future of mental health research: Implication for studies on human stress and presentation of the signature bank. *Stress*, 20(1):2–18.

Luthman, J., Fredriksson, A., Lewander, T., Jonsson, G., and Archer, T. (1989). Effects of d-amphetamine and methylphenidate on hyperactivity produced by neonatal 6-hydroxydopamine treatment. *Psychopharmacology*, 99(4):550–557.

Ma, C.L., Arnsten, A.F.T., and Li, B.M. (2005). Locomotor hyperactivity induced by blockade of prefrontal cortical *A*2-adrenoceptors in monkeys. *Biological Psychiatry*, 57(2):192–195.

Ma, Z., et al. (2019). PTC-bearing mRNA elicits a genetic compensation response via Upf3a and COMPASS components. *Nature*, 568(7751):259–263.

Machado Torres, C., et al. (2017). NTRK2 (*TrkB* gene) variants and temporal lobe epilepsy: A genetic association study. *Epilepsy Research*, 137:1–8.

Mackie, S., et al. (2007). Cerebellar development and clinical outcome in attention-deficit hyperactivity disorder. *The American Journal of Psychiatry*, 164(4):647–655.

MacMaster, F.P., Carrey, N., Sparkes, S., and Kusumakar, V. (2003). Proton spectroscopy in medication-free pediatric attention-deficit/hyperactivity disorder. *Biological Psychiatry*, 53(2):184–187.

Makris, N., et al. (2007). Cortical thinning of the attention and executive function networks in adults with attention-deficit/hyperactivity disorder. *Cerebral Cortex (New York, N.Y.: 1991)*, 17(6):1364–1375.

Malherbe, P., et al. (1999). Cloning and functional expression of alternative spliced variants of the human metabotropic glutamate receptor 8. *Molecular Brain Research*, 67(2):201–210.

Malin, A.J. and Till, C. (2015). Exposure to fluoridated water and attention-deficit hyperactivity disorder prevalence among children and adolescents in the United States: An ecological association. *Environmental Health*, 14(1):17.

Malki, K., et al. (2015). Identification of genes and gene pathways associated with major depressive disorder by integrative brain analysis of rat and human prefrontal cortex transcriptomes. *Translational Psychiatry*, 5(3):e519–e519.

Maltezos, S., et al. (2014). Glutamate/glutamine and neuronal integrity in adults with ADHD: A proton MRS study. *Translational Psychiatry*, 4:e373.

Manes, F., et al. (2002). Decision-making processes following damage to the prefrontal cortex. *Brain*, 125(Pt 3):624–639.

Manor, I., et al. (2001). Family-based association study of the serotonin transporter promoter region polymorphism (5-HTTLPR) in attention-deficit hyperactivity disorder. *American Journal of Medical Genetics*, 105(1):91–95.

Manor, I., et al. (2012). A randomized, double-blind, placebo-controlled, multicenter study evaluating the efficacy, safety, and tolerability of extended-release metadoxine in adults with attention-deficit/hyperactivity disorder. *The Journal of Clinical Psychiatry*, 73(12):1517–1523.

Marabese, I., et al. (2005). Differential roles of mGlu8 receptors in the regulation of glutamate and gamma-Aminobutyric acid release at periaqueductal grey level. *Neuropharmacology*, 49:157–166.

Maric, D., et al. (2001). GABA expression dominates neuronal lineage progression in the embryonic rat neocortex and facilitates neurite outgrowth via $GABA_A$ autoreceptor/Cl^- channels. *Journal of Neuroscience*, 21(7):2343–2360.

Martin, D.L., Martin, S.B., Wu, S.J., and Espina, N. (1991). Regulatory properties of brain glutamate decarboxylase (GAD): The apoenzyme of GAD is present principally as the smaller of two molecular forms of GAD in brain. *Journal of Neuroscience*, 11(9):2725–2731.

Martinez, A.F., et al. (2016). An ultraconserved brain-specific enhancer within *ADGRL3 (LPHN3)* underpins attention-deficit/hyperactivity disorder susceptibility. *Biological Psychiatry*, 80(12):943–954.

Mataró, M., Garcia-Sánchez, C., Junqué, C., Estévez-González, A., and Pujol, J. (1997). Magnetic resonance imaging measurement of the caudate nucleus in adolescents with attention-deficit hyperactivity disorder and its relationship with neuropsychological and behavioral measures. *Archives of Neurology*, 54(8):963–968.

Max, J.E., et al. (2002). Putamen lesions and the development of attention-deficit/hyperactivity symptomatology. *Journal of the American Academy of Child & Adolescent Psychiatry*, 41(5):563–571.

McCann, D., et al. (2007). Food additives and hyperactive behaviour in 3-year-old and 8/9-year-old children in the community: A randomised, double-blinded, placebo-controlled trial. *The Lancet*, 370(9598):1560–1567.

Mefford, H.C., et al. (2010). Genome-wide copy number variation in epilepsy: Novel susceptibility loci in idiopathic generalized and focal epilepsies. *PLOS Genetics*, 6(5):e1000962.

Mendelson, W., Johnson, N., and Stewart, M.A. (1971). Hyperactive children as teenagers: A follow-up study. *The Journal of Nervous and Mental Disease*, 153(4):273–279.

Mendoza, E. and Scharff, C. (2017). Protein-protein interaction among the FoxP family members and their regulation of two target genes, *VLDLR* and *CNTNAP2* in the zebra finch song system. *Frontiers in Molecular Neuroscience*, 10:112.

Mendoza, E., et al. (2014). *Drosophila FoxP* mutants are deficient in operant self-learning. *PLOS ONE*, 9(6):e100648.

Mendoza, E., et al. (2015). Differential coexpression of *FoxP1, FoxP2*, and *FoxP4* in the zebra finch (*Taeniopygia guttata*) song system. *The Journal of Comparative Neurology*, 523(9):1318–1340.

Meng, X., Noyes, M.B., Zhu, L.J., Lawson, N.D., and Wolfe, S.A. (2008). Targeted gene inactivation in zebrafish using engineered zinc-finger nucleases. *Nature Biotechnology*, 26(6):695–701.

Menkes, M.M., Rowe, J.S., and Menkes, J.H. (1967). A twenty-five year follow-up study on the hyperkinetic child with minimal brain dysfunction. *Pediatrics*, 39(3):393–399.

Menon, V. (2011). Large-scale brain networks and psychopathology: A unifying triple network model. *Trends in Cognitive Sciences*, 15(10):483–506.

Messenger, M.J., Dawson, L.G., and Duty, S. (2002). Changes in metabotropic glutamate receptor 1-8 gene expression in the rodent basal ganglia motor loop following lesion of the nigrostriatal tract. *Neuropharmacology*, 43(2):261–271.

Mészáros, A., et al. (2009). Pharmacotherapy of adult attention-deficit hyperactivity disorder (ADHD): A meta-analysis. *The International Journal of Neuropsychopharmacology*, 12(8):1137–1147.

Meyer, V. (1957). Critique of psychological approaches to brain damage. *Journal of Mental Science*, 103(430):80–109.

Meyer, A. and Schartl, M. (1999). Gene and genome duplications in vertebrates: The one-to-four (-to-eight in fish) rule and the evolution of novel gene functions. *Current Opinion in Cell Biology*, 11(6):699–704.

Mezzich, J.E. (2002). International surveys on the use of ICD-10 and related diagnostic systems. *Psychopathology*, 35(2-3):72–75.

Mick, E., et al. (2010). Family-based genome-wide association scan of attention-deficit/hyperactivity disorder. *Journal of the American Academy of Child and Adolescent Psychiatry*, 49(9):898–905.e3.

Millichap, J. (2002). Putamen stroke lesions and ADHD or ADHD/traits. *Pediatric Neurology Briefs*, 16(5):40–40.

Mittal, V.A. and Wakschlag, L.S. (2017). Research Domain Criteria (RDoC) grows up: Strengthening neurodevelopmental investigation within the RDoC framework. *Journal of Affective Disorders*, 216:30–35.

Miyata, S., et al. (2019). Loss of glutamate decarboxylase 67 in somatostatin-expressing neurons leads to anxiety-like behavior and alteration in the Akt/GSK3β signaling pathway. *Frontiers in Behavioral Neuroscience*, 13:131.

Miyata, S., et al. (2021). Global knockdown of glutamate decarboxylase 67 elicits emotional abnormality in mice. *Molecular Brain*, 14(1):5.

Moore, C.M., et al. (2006). Differences in brain chemistry in children and adolescents with attention-deficit hyperactivity disorder with and without comorbid bipolar disorder: A proton magnetic resonance spectroscopy study. *The American Journal of Psychiatry*, 163(2):316–318.

Morrison, J.R. and Stewart, M.A. (1973). The psychiatric status of the legal families of adopted hyperactive children. *Archives of General Psychiatry*, 28(6):888–891.

Mostofsky, S.H., Cooper, K.L., Kates, W.R., Denckla, M.B., and Kaufmann, W.E. (2002). Smaller prefrontal and premotor volumes in boys with attention-deficit/hyperactivity disorder. *Biological Psychiatry*, 52(8):785–794.

Mous, S.E., et al. (2014). Gyrification differences in children and adolescents with velocardiofacial syndrome and attention-deficit/hyperactivity disorder: A pilot study. *Psychiatry Research: Neuroimaging*, 221(2):169–171.

Mowlem, F.D., et al. (2019). Sex differences in predicting ADHD clinical diagnosis and pharmacological treatment. *European Child & Adolescent Psychiatry*, 28(4):481–489.

Mrug, S., et al. (2012). Peer rejection and friendships in children with attention-deficit/hyperactivity disorder: Contributions to long-term outcomes. *Journal of Abnormal Child Psychology*, 40(6):1013–1026.

Mueller, T., Dong, Z., Berberoglu, M.A., and Guo, S. (2011). The dorsal pallium in zebrafish, *Danio rerio* (Cyprinidae, Teleostei). *Brain Research*, 1381:95–105.

Mueller, T. and Wullimann, M.F. (2009). An evolutionary interpretation of teleostean forebrain anatomy. *Brain, Behavior and Evolution*, 74(1):30–42.

Mueller, D.T. and Wullimann, M. (2015). *Atlas of Early Zebrafish Brain Development: A Tool for Molecular Neurogenetics*. Academic Press.

Mukamel, Z., et al. (2011). Regulation of *MET* by FOXP2, genes implicated in higher cognitive dysfunction and autism risk. *Journal of Neuroscience*, 31(32):11437–11442.

Mulligan, R.C., et al. (2011). Neural correlates of inhibitory control in adult ADHD: Evidence from the Milwaukee longitudinal sample. *Psychiatry Research*, 194(2):119–129.

Murugan, M., Harward, S., Scharff, C., and Mooney, R. (2013). Diminished FoxP2 levels affect dopaminergic modulation of corticostriatal signaling important to song variability. *Neuron*, 80(6):1464–1476.

Muto, T., Tsuchiya, D., Morikawa, K., and Jingami, H. (2007). Structures of the extracellular regions of the group II/III metabotropic glutamate receptors. *Proceedings of the National Academy of Sciences of the United States of America*, 104(10):3759–3764.

Naaijen, J., et al. (2017). Glutamatergic and GABAergic gene sets in attention-deficit/hyperactivity disorder: Association to overlapping traits in ADHD and autism. *Translational Psychiatry*, 7(1):e999.

Nagarajan, R.P., Hogart, A.R., Gwye, Y., Martin, M.R., and LaSalle, J.M. (2006 Oct-Dec). Reduced *MeCP2* expression is frequent in autism frontal cortex and correlates with aberrant *MECP2* promoter methylation. *Epigenetics*, 1(4):e1–11.

Nageye, F. and Cortese, S. (2019). Beyond stimulants: A systematic review of randomised controlled trials assessing novel compounds for ADHD. *Expert Review of Neurotherapeutics*, 19(7):707–717.

Nakanishi, S. (1992). Molecular diversity of glutamate receptors and implications for brain function. *Science*, 258(5082):597–603.

Nakanishi, S., et al. (1994). Molecular diversity of glutamate receptors and their physiological functions. *EXS*, 71:71–80.

Nakao, T., Radua, J., Rubia, K., and Mataix-Cols, D. (2011). Gray matter volume abnormalities in ADHD: Voxel-based meta-analysis exploring the effects of age and stimulant medication. *The American Journal of Psychiatry*, 168(11):1154–1163.

Narr, K.L., et al. (2009). Widespread cortical thinning is a robust anatomical marker for attention-deficit / hyperactivity disorder (ADHD). *Journal of the American Academy of Child and Adolescent Psychiatry*, 48(10):1014–1022.

Nasevicius, A. and Ekker, S.C. (2000). Effective targeted gene 'knockdown' in zebrafish. *Nature Genetics*, 26(2):216–220.

Nasser, A., et al. (2020a). Evaluation of the effect of SPN-812 (viloxazine extended-release) on QTc interval in healthy adults. *The Journal of Clinical Psychiatry*, 81(6).

Nasser, A., et al. (2020b). A phase III, randomized, placebo-controlled trial to assess the efficacy and safety of once-daily SPN-812 (viloxazine extended-release) in the treatment of attention-deficit/hyperactivity disorder in school-age children. *Clinical Therapeutics*, 42(8):1452–1466.

Naumann, E.A., et al. (2016). From whole-brain data to functional circuit models: The zebrafish optomotor response. *Cell*, 167(4):947–960.e20.

Nelson, S.B. and Valakh, V. (2015). Excitatory/inhibitory balance and circuit homeostasis in autism spectrum disorders. *Neuron*, 87(4):684–698.

Neuman, R.J., et al. (2007). Prenatal smoking exposure and dopaminergic genotypes interact to cause a severe ADHD subtype. *Biological Psychiatry*, 61(12):1320–1328.

Neuray, C., et al. (2020). Early-infantile onset epilepsy and developmental delay caused by bi-allelic *GAD1* variants. *Brain*, 143(8):2388–2397.

Newcorn, J.H., et al. (2001). Symptom profiles in children with ADHD: Effects of comorbidity and gender. *Journal of the American Academy of Child and Adolescent Psychiatry*, 40(2):137–146.

Nicolescu, R., et al. (2010). Environmental exposure to lead, but not other neurotoxic metals, relates to core elements of ADHD in Romanian children: Performance and questionnaire data. *Environmental Research*, 110(5):476–483.

Nigg, J.T., Nikolas, M., Mark Knottnerus, G., Cavanagh, K., and Friderici, K. (2010). Confirmation and extension of association of blood lead with attention-deficit/hyperactivity disorder (ADHD) and ADHD symptom domains at population-typical exposure levels. *Journal of Child Psychology and Psychiatry, and Allied Disciplines*, 51(1):58–65.

Nigg, J.T., et al. (2008). Low blood lead levels associated with clinically diagnosed attention-deficit/hyperactivity disorder and mediated by weak cognitive control. *Biological Psychiatry*, 63(3):325.

Niklasson, L., Rasmussen, P, Oskarsdóttir, S., and Gillberg, C. (2009 Jul-Aug). Autism, ADHD, mental retardation and behavior problems in 100 individuals with 22q11 deletion syndrome. *Research in Developmental Disabilities*, 30(4):763–773.

Nikolas, M.A. and Burt, S.A. (2010). Genetic and environmental influences on ADHD symptom dimensions of inattention and hyperactivity: A meta-analysis. *Journal of Abnormal Psychology*, 119(1):1–17.

Norman, L.J., et al. (2016). Structural and functional brain abnormalities in attention-deficit/hyperactivity disorder and obsessive-compulsive disorder: A comparative meta-analysis. *JAMA Psychiatry*, 73(8):815–825.

Nøvik, T.S., et al. (2006). Influence of gender on attention-deficit/hyperactivity disorder in Europe-ADORE. *European Child & Adolescent Psychiatry*, 15 Suppl 1:I15–24.

Novodvorsky, P, et al. (2015). *Klf2a*[sh317] mutant zebrafish do not recapitulate morpholino-induced vascular and haematopoietic phenotypes. *PloS One*, 10(10):e0141611.

Nurnberger, J.I., et al. (2014). Identification of pathways for bipolar disorder: A meta-analysis. *JAMA Psychiatry*, 71(6):657–664.

Oades, R.D. (2008). Dopamine-serotonin interactions in attention-deficit hyperactivity disorder (ADHD). *Progress in Brain Research*, 172:543–565.

O'Brien, N.L., et al. (2014). The functional *GRM3* Kozak sequence variant rs148754219 affects the risk of schizophrenia and alcohol dependence as well as bipolar disorder. *Psychiatric Genetics*, 24(6):277–278.

Ode, A., et al. (2014). Fetal exposure to perfluorinated compounds and attention-deficit hyperactivity disorder in childhood. *PLOS ONE*, 9(4):e95891.

Ode, A., et al. (2015). Manganese and selenium concentrations in umbilical cord serum and attention-deficit hyperactivity disorder in childhood. *Environmental Research*, 137:373–381.

O'Dushlaine, C., et al. (2011). Molecular pathways involved in neuronal cell adhesion and membrane scaffolding contribute to schizophrenia and bipolar disorder susceptibility. *Molecular Psychiatry*, 16(3):286–292.

Okamoto, K. and Aoki, K. (1963). Development of a strain of spontaneously hypertensive rats. *Japanese Circulation Journal*, 27:282–293.

Onnink, A.M.H., et al. (2014). Brain alterations in adult ADHD: Effects of gender, treatment and comorbid depression. *European Neuropsychopharmacology*, 24(3):397–409.

Otasowie, J., Castells, X., Ehimare, U.P., and Smith, C.H. (2014). Tricyclic antidepressants for attention-deficit hyperactivity disorder (ADHD) in children and adolescents. *The Cochrane Database of Systematic Reviews*, 9:CD006997.

Paciorkowski, A.R., et al. (2013). *MEF2C* haploinsufficiency features consistent hyperkinesis, variable epilepsy, and has a role in dorsal and ventral neuronal developmental pathways. *Neurogenetics*, 14(2):99–111.

Palmer, E.D. and Finger, S. (2003). An early description of ADHD (inattentive subtype): Dr. Alexander Crichton and 'mental restlessness' (1798). *Child Psychology and Psychiatry Review*, 6(2):66–73.

Panatier, A., Poulain, D.A., and Oliet, S.H.R. (2004). Regulation of transmitter release by high-affinity group III mGluRs in the supraoptic nucleus of the rat hypothalamus. *Neuropharmacology*, 47(3):333–341.

Panula, P., et al. (2010). The comparative neuroanatomy and neurochemistry of zebrafish CNS systems of relevance to human neuropsychiatric diseases. *Neurobiology of Disease*, 40(1):46–57.

Papaleo, F., Erickson, L., Liu, G., Chen, J., and Weinberger, D.R. (2012). Effects of sex and COMT genotype on environmentally modulated cognitive control in mice. *Proceedings of the National Academy of Sciences of the United States of America*, 109(49):20160–20165.

Papaleo, F., et al. (2008). Genetic dissection of the role of catechol-O-methyltransferase in cognition and stress reactivity in mice. *Journal of Neuroscience*, 28(35):8709–8723.

Park, S., et al. (2014). Differential perinatal risk factors in children with attention-deficit/hyperactivity disorder by subtype. *Psychiatry Research*, 219(3):609–616.

Park, S., et al. (2015). Associations between serotonin transporter gene (*SLC6A4*) methylation and clinical characteristics and cortical thickness in children with ADHD. *Psychological Medicine*, 45(14):3009–3017.

Parker, M.O., et al. (2013). Development and automation of a test of impulse control in zebrafish. *Frontiers in Systems Neuroscience*, 7:65.

Pärtty, A., Kalliomäki, M., Wacklin, P., Salminen, S., and Isolauri, E. (2015). A possible link between early probiotic intervention and the risk of neuropsychiatric disorders later in childhood: A randomized trial. *Pediatric Research*, 77(6):823–828.

Pedersen, S.L., et al. (2020). Real-world changes in adolescents' ADHD symptoms within the day and across school and non-school days. *Journal of Abnormal Child Psychology*.

Pelham, W.E., et al. (2001). Once-a-day concerta methylphenidate versus three-times-daily methylphenidate in laboratory and natural settings. *Pediatrics*, 107(6):e105–e105.

Peñagarikano, O., et al. (2011). Absence of CNTNAP2 leads to epilepsy, neuronal migration abnormalities, and core autism-related deficits. *Cell*, 147(1):235–246.

Peng, J. (2019). Gene redundancy and gene compensation: An updated view. *Journal of Genetics and Genomics*, 46(7):329–333.

Pengra, I.G.G., Marchaterre, M.A., and Bass, A.H. (2018). *FoxP2* expression in a highly vocal teleost fish with comparisons to tetrapods. *Brain, Behavior and Evolution*, 91(2):82–96.

Perera, M., et al. (2004). Defective neuronogenesis in the absence of Dlx5. *Molecular and Cellular Neurosciences*, 25(1):153–161.

Pérez-Crespo, L., Canals-Sans, J., Suades-González, E., and Guxens, M. (2020). Temporal trends and geographical variability of the prevalence and incidence of attention-deficit/hyperactivity disorder diagnoses among children in Catalonia, Spain. *Scientific Reports*, 10(1):6397.

Perlov, E., et al. (2007). Reduced cingulate glutamate/glutamine-to-creatine ratios in adult patients with attention-deficit/hyperactivity disorder - a magnet resonance spectroscopy study. *Journal of Psychiatric Research*, 41(11):934–941.

Perlov, E., et al. (2010). H^1-MR-spectroscopy of cerebellum in adult attention-deficit/hyperactivity disorder. *Journal of Psychiatric Research*, 44(14):938–943.

Petrides, M. (1986). The effect of periarcuate lesions in the monkey on the performance of symmetrically and asymmetrically reinforced visual and auditory go, no- go tasks. *Journal of Neuroscience*, 6(7):2054–2063.

Petrin, A.L., et al. (2010). Identification of a microdeletion at the 7q33-q35 disrupting the *CNTNAP2* gene in a Brazilian stuttering case. *American Journal of Medical Genetics*, 152A(12):3164–3172.

Pfaffenseller, B., et al. (2016). Differential expression of transcriptional regulatory units in the prefrontal cortex of patients with bipolar disorder: Potential role of early growth response gene 3. *Translational Psychiatry*, 6(5):e805.

Piet, R., Bonhomme, R., Theodosis, D.T., Poulain, D.A., and Oliet, S.H.R. (2003). Modulation of GABAergic transmission by endogenous glutamate in the rat supraoptic nucleus. *European Journal of Neuroscience*, 17(9):1777–1785.

Pin, J.P. and Duvoisin, R. (1995). The metabotropic glutamate receptors: Structure and functions. *Neuropharmacology*, 34(1):1–26.

Piton, A., et al. (2011). Systematic resequencing of X-chromosome synaptic genes in autism spectrum disorder and schizophrenia. *Molecular Psychiatry*, 16(8):867–880.

Plessen, K.J., et al. (2006). Hippocampus and amygdala morphology in attention-deficit/hyperactivity disorder. *Archives of General Psychiatry*, 63(7):795–807.

Plichta, M.M. and Scheres, A. (2014). Ventral-striatal responsiveness during reward anticipation in ADHD and its relation to trait impulsivity in the healthy population: A meta-analytic review of the fMRI literature. *Neuroscience and Biobehavioral Reviews*, 38:125–134.

Pliszka, S. and AACAP Work Group on Quality Issues (2007). Practice parameter for the assessment and treatment of children and adolescents with attention-deficit/hyperactivity disorder. *Journal of the American Academy of Child and Adolescent Psychiatry*, 46(7):894–921.

Polan, M.B., et al. (2014). Neurodevelopmental disorders among individuals with duplication of 4p13 to 4p12 containing a GABA$_A$ receptor subunit gene cluster. *European Journal of Human Genetics*, 22(1):105–109.

Poot, M., et al. (2010). Disruption of *CNTNAP2* and additional structural genome changes in a boy with speech delay and autism spectrum disorder. *Neurogenetics*, 11(1):81–89.

Portavella, M., Torres, B., Salas, C., and Papini, M.R. (2004). Lesions of the medial pallium, but not of the lateral pallium, disrupt spaced-trial avoidance learning in goldfish (*Carassius auratus*). *Neuroscience Letters*, 362(2):75–78.

Posner, J., Polanczyk, G.V., and Sonuga-Barke, E. (2020). Attention-deficit hyperactivity disorder. *The Lancet*, 395(10222):450–462.

Prasad, A., et al. (2012). A discovery resource of rare copy number variations in individuals with autism spectrum disorder. *G3: Genes, Genomes, Genetics*, 2(12):1665–1685.

Preibisch, S., Saalfeld, S., and Tomancak, P. (2009). Globally optimal stitching of tiled 3D microscopic image acquisitions. *Bioinformatics*, 25(11):1463–1465.

Purves, K.L., et al. (2020). A major role for common genetic variation in anxiety disorders. *Molecular Psychiatry*, 25(12):3292–3303.

Puts, N.A., et al. (2020). Reduced striatal GABA in unmedicated children with ADHD at 7T. *Psychiatry Research. Neuroimaging*, 301:111082.

Qiu, A., et al. (2009). Basal ganglia volume and shape in children with attention-deficit hyperactivity disorder. *The American Journal of Psychiatry*, 166(1):74–82.

Ralph, R.J., Paulus, M.P., Fumagalli, F., Caron, M.G., and Geyer, M.A. (2001). Prepulse inhibition deficits and perseverative motor patterns in dopamine transporter knock-out mice: Differential effects of D1 and D2 receptor antagonists. *Journal of Neuroscience*, 21(1):305–313.

Ramos-Quiroga, J.A., et al. (2014). Genome-wide copy number variation analysis in adult attention-deficit and hyperactivity disorder. *Journal of Psychiatric Research*, 49:60–67.

Ramtekkar, U.P, Reiersen, A.M., Todorov, A.A., and Todd, R.D. (2010). Sex and age differences in attention-deficit/hyperactivity disorder symptoms and diagnoses: Implications for DSM-V and ICD-11. *Journal of the American Academy of Child and Adolescent Psychiatry*, 49(3):217–28.e1–3.

Raznahan, A., et al. (2010). Cortical anatomy in autism spectrum disorder: An *in vivo* MRI study on the effect of age. *Cerebral Cortex*, 20(6):1332–1340.

Reed, G.M., Mendonça Correia, J., Esparza, P., Saxena, S., and Maj, M. (2011). The WPA-WHO global survey of psychiatrists' attitudes towards mental disorders classification. *World Psychiatry*, 10(2):118–131.

Reif, A., et al. (2009). Influence of functional variant of neuronal nitric oxide synthase on impulsive behaviors in humans. *Archives of General Psychiatry*, 66(1):41–50.

Reiner, A., et al. (1988). Differential loss of striatal projection neurons in Huntington disease. *Proceedings of the National Academy of Sciences*, 85(15):5733–5737.

Ribasés, M., et al. (2008). Association study of 10 genes encoding neurotrophic factors and their receptors in adult and child attention-deficit/hyperactivity disorder. *Biological Psychiatry*, 63(10):935–945.

Ribasés, M., et al. (2011). Contribution of *LPHN3* to the genetic susceptibility to ADHD in adulthood: A replication study. *Genes, Brain, and Behavior*, 10(2):149–157.

Ribasés, M., et al. (2012). An association study of sequence variants in the forkhead box P2 (*FOXP2*) gene and adulthood attention-deficit/hyperactivity disorder in two European samples. *Psychiatric Genetics*, 22(4):155–160.

Rice, F., et al. (2019). Characterizing developmental trajectories and the role of neuropsychiatric genetic risk variants in early-onset depression. *JAMA Psychiatry*, 76(3):306–313.

Rink, E. and Wullimann, M.F. (2001). The teleostean (zebrafish) dopaminergic system ascending to the subpallium (striatum) is located in the basal diencephalon (posterior tuberculum). *Brain Research*, 889(1):316–330.

Rink, E. and Wullimann, M.F. (2004). Connections of the ventral telencephalon (subpallium) in the zebrafish (*Danio rerio*). *Brain Research*, 1011(2):206–220.

Rivero, O., et al. (2015). Cadherin-13, a risk gene for ADHD and comorbid disorders, impacts GABAergic function in hippocampus and cognition. *Translational Psychiatry*, 5(10):e655–e655.

Robbins, T.W. (2002). The 5-choice serial reaction time task: Behavioural pharmacology and functional neurochemistry. *Psychopharmacology*, 163(3-4):362–380.

Robbins, T.W. (2005). Chemistry of the mind: Neurochemical modulation of prefrontal cortical function. *Journal of Comparative Neurology*, 493(1):140–146.

Robbins, M.J., Ciruela, F., Rhodes, A., and McIlhinney, R.A. (1999). Characterization of the dimerization of metabotropic glutamate receptors using an N-terminal truncation of mGluR1$_{alpha}$. *Journal of Neurochemistry*, 72(6):2539–2547.

Robbins, M.J., et al. (2007). Evaluation of the mGlu8 receptor as a putative therapeutic target in schizophrenia. *Brain Research*, 1152:215–227.

Roberts, E. and Frankel, S. (1950). Gamma-Aminobutyric acid in brain: Its formation from glutamic acid. *The Journal of Biological Chemistry*, 187(1):55–63.

Roberts, E. and Frankel, S. (1951). Further studies of glutamic acid decarboxylase in brain. *The Journal of Biological Chemistry*, 190(2):505–512.

Rodenas-Cuadrado, P., Ho, J., and Vernes, S.C. (2014). Shining a light on *CNTNAP2*: Complex functions to complex disorders. *European Journal of Human Genetics*, 22(2):171–178.

Rodenas-Cuadrado, P.M., et al. (2018). Mapping the distribution of language related genes *FoxP1, FoxP2*, and *CntnaP2* in the brains of vocal learning bat species. *The Journal of Comparative Neurology*, 526(8):1235–1266.

Romano, C., Yang, W.L., and O'Malley, K.L. (1996). Metabotropic glutamate receptor 5 is a disulfide-linked dimer. *The Journal of Biological Chemistry*, 271(45):28612–28616.

Rommelse, N.N.J., Franke, B., Geurts, H.M., Hartman, C.A., and Buitelaar, J.K. (2010). Shared heritability of attention-deficit/hyperactivity disorder and autism spectrum disorder. *European Child & Adolescent Psychiatry*, 19(3):281–295.

Ronald, A., Simonoff, E., Kuntsi, J., Asherson, P., and Plomin, R. (2008). Evidence for overlapping genetic influences on autistic and ADHD behaviours in a community twin sample. *Journal of Child Psychology and Psychiatry, and Allied Disciplines*, 49(5):535–542.

Rossi, E., et al. (2008). A 12Mb deletion at 7q33-q35 associated with autism spectrum disorders and primary amenorrhea. *European Journal of Medical Genetics*, 51(6):631–638.

Rossi, A., et al. (2015). Genetic compensation induced by deleterious mutations but not gene knockdowns. *Nature*, 524(7564):230–233.

Rouillard, A.D., et al. (2016). The harmonizome: A collection of processed datasets gathered to serve and mine knowledge about genes and proteins. *Database*, 2016:baw100.

RStudio Team (2020). RStudio: Integrated development environment for R. RStudio, PBC.

Rubenstein, J.L.R. and Merzenich, M.M. (2003). Model of autism: Increased ratio of excitation/inhibition in key neural systems. *Genes, Brain, and Behavior*, 2(5):255–267.

Rubia, K., et al. (2009). Methylphenidate normalises activation and functional connectivity deficits in attention and motivation networks in medication-naïve children with ADHD during a rewarded continuous performance task. *Neuropharmacology*, 57(7-8):640–652.

Rubinstein, M., et al. (1997). Mice lacking dopamine D4 receptors are supersensitive to ethanol, cocaine, and methamphetamine. *Cell*, 90(6):991–1001.

Rucklidge, J.J. and Tannock, R. (2001). Psychiatric, psychosocial, and cognitive functioning of female adolescents with ADHD. *Journal of the American Academy of Child and Adolescent Psychiatry*, 40(5):530–540.

Russell, V.A. (2003). Dopamine hypofunction possibly results from a defect in glutamate-stimulated release of dopamine in the nucleus accumbens shell of a rat model for attention-

deficit hyperactivity disorder-the spontaneously hypertensive rat. *Neuroscience and Biobehavioral Reviews*, 27(7):671–682.

Russell, A.E., Ford, T., and Russell, G. (2015). Socioeconomic associations with ADHD: Findings from a mediation analysis. *PloS One*, 10(6):e0128248.

Sagvolden, T. (2000). Behavioral validation of the spontaneously hypertensive rat (SHR) as an animal model of attention-deficit/hyperactivity disorder (AD/HD). *Neuroscience and Biobehavioral Reviews*, 24(1):31–39.

Sagvolden, T., Johansen, E.B., Aase, H., and Russell, V.A. (2005). A dynamic developmental theory of attention-deficit/hyperactivity disorder (ADHD) predominantly hyperactive/impulsive and combined subtypes. *The Behavioral and Brain Sciences*, 28(3):397–468.

Sandhu, K.V., et al. (2014). Glutamic acid decarboxylase 67 haplodeficiency impairs social behavior in mice. *Genes, Brain, and Behavior*, 13(4):439–450.

Sando, R., Jiang, X., and Südhof, T.C. (2019). Latrophilin GPCRs direct synapse specificity by coincident binding of FLRTs and teneurins. *Science*, 363(6429).

Sangu, N., et al. (2017). A 7q31.33q32.1 microdeletion including *LRRC4* and *GRM8* is associated with severe intellectual disability and characteristics of autism. *Human Genome Variation*, 4:17001.

Satterstrom, F.K., et al. (2020). Large-scale exome sequencing study implicates both developmental and functional changes in the neurobiology of autism. *Cell*, 180(3):568–584.e23.

Saugstad, J.A., Kinzie, J.M., Shinohara, M.M., Segerson, T.P., and Westbrook, G.L. (1997). Cloning and expression of rat metabotropic glutamate receptor 8 reveals a distinct pharmacological profile. *Molecular Pharmacology*, 51(1):119–125.

Savell, K.E., et al. (2020). A dopamine-induced gene expression signature regulates neuronal function and cocaine response. *Science Advances*, 6(26).

Schachter, H.M., Pham, B., King, J., Langford, S., and Moher, D. (2001). How efficacious and safe is short-acting methylphenidate for the treatment of attention-deficit disorder in children and adolescents? A meta-analysis. *Canadian Medical Association Journal*, 165(11):1475–1488.

Schain, R.J. (1975). Minimal brain dysfunction. *Current Problems in Pediatrics*, 5(10):3–30.

Scherer, S.W., et al. (1996). Localization of two metabotropic glutamate receptor genes, *GRM3* and *GRM8*, to human chromosome 7q. *Genomics*, 31(2):230–233.

Scheres, A., Milham, M.P., Knutson, B., and Castellanos, F.X. (2007). Ventral striatal hyporesponsiveness during reward anticipation in attention-deficit/hyperactivity disorder. *Biological Psychiatry*, 61(5):720–724.

Schindelin, J., et al. (2012). Fiji: An open-source platform for biological-image analysis. *Nature Methods*, 9(7):676–682.

Schmid, S. and Fendt, M. (2006). Effects of the mGluR8 agonist (*S*)-3,4-DCPG in the lateral amygdala on acquisition/expression of fear-potentiated startle, synaptic transmission, and plasticity. *Neuropharmacology*, 50(2):154–164.

Schoepp, D.D. (2001). Unveiling the functions of presynaptic metabotropic glutamate receptors in the central nervous system. *The Journal of Pharmacology and Experimental Therapeutics*, 299(1):12–20.

Schoepp, D.D., Jane, D.E., and Monn, J.A. (1999). Pharmacological agents acting at subtypes of metabotropic glutamate receptors. *Neuropharmacology*, 38(10):1431–1476.

Schön, C., Wochnik, A., Rössner, A., Donow, C., and Knöchel, W. (2006). The FoxP subclass in *Xenopus laevis* development. *Development Genes and Evolution*, 216(10):641–646.

Schultz, M.R., Rabi, K., Faraone, S.V., Kremen, W., and Lyons, M.J. (2006). Efficacy of retrospective recall of attention-deficit hyperactivity disorder symptoms: A twin study. *Twin Research and Human Genetics*, 9(2):220–232.

Schulz, S.B., Haesler, S., Scharff, C., and Rochefort, C. (2010). Knockdown of FoxP2 alters spine density in Area X of the zebra finch. *Genes, Brain, and Behavior*, 9(7):732–740.

Segal, D.S. and Kuczenski, R. (1999). Escalating dose-binge treatment with methylphenidate: Role of serotonin in the emergent behavioral profile. *Journal of Pharmacology and Experimental Therapeutics*, 291(1):19–30.

Segebarth, D., et al. (2020). On the objectivity, reliability, and validity of deep learning enabled bioimage analyses. *eLife*, 9:e59780.

Sehested, L.T., et al. (2010). Deletion of 7q34–q36.2 in two siblings with mental retardation, language delay, primary amenorrhea, and dysmorphic features. *American Journal of Medical Genetics Part A*, 152A(12):3115–3119.

Seidman, L.J., et al. (2006). Dorsolateral prefrontal and anterior cingulate cortex volumetric abnormalities in adults with attention-deficit/hyperactivity disorder identified by magnetic resonance imaging. *Biological Psychiatry*, 60(10):1071–1080.

Seidman, L.J., et al. (2011). Gray matter alterations in adults with attention-deficit/hyperactivity disorder identified by voxel based morphometry. *Biological Psychiatry*, 69(9):857–866.

Semeijn, E.J., et al. (2016). Lifetime stability of ADHD symptoms in older adults. *Attention Deficit and Hyperactivity Disorders*, 8(1):13–20.

Serajee, F.J., Zhong, H., Nabi, R., and Huq, A.H.M.M. (2003). The metabotropic glutamate receptor 8 gene at 7q31: Partial duplication and possible association with autism. *Journal of Medical Genetics*, 40(4):e42–e42.

Shah, R., Medina-Martinez, O., Chu, L.F., Samaco, R.C., and Jamrich, M. (2004). Expression of *FoxP2* during zebrafish development and in the adult brain. *International Journal of Developmental Biology*, 50(4):435–438.

Shaw, P., Stringaris, A., Nigg, J., and Leibenluft, E. (2014). Emotional dysregulation and attention-deficit/hyperactivity disorder. *The American Journal of Psychiatry*, 171(3):276–293.

Shaw, P., et al. (2007). Attention-deficit/hyperactivity disorder is characterized by a delay in cortical maturation. *Proceedings of the National Academy of Sciences of the United States of America*, 104(49):19649–19654.

Shaw, P., et al. (2009). Psychostimulant treatment and the developing cortex in attention-deficit/hyperactivity disorder. *The American Journal of Psychiatry*, 166(1):58–63.

Shaw, P., et al. (2012). Development of cortical surface area and gyrification in attention-deficit/hyperactivity disorder. *Biological Psychiatry*, 72(3):191–197.

Shaywitz, B.A., Klopper, J.H., and Gordon, J.W. (1978). Methylphenidate in 6-hydroxydopamine-treated developing rat pups: Effects on activity and maze performance. *Archives of Neurology*, 35(7):463–469.

Sherman, D.K., McGue, M.K., and Iacono, W.G. (1997). Twin concordance for attention-deficit hyperactivity disorder: A comparison of teachers' and mothers' reports. *The American Journal of Psychiatry*, 154(4):532–535.

Shigemoto, R., et al. (1996). Target-cell-specific concentration of a metabotropic glutamate receptor in the presynaptic active zone. *Nature*, 381(6582):523–525.

Shigemoto, R., et al. (1997). Differential presynaptic localization of metabotropic glutamate receptor subtypes in the rat hippocampus. *Journal of Neuroscience*, 17(19):7503–7522.

Shinwari, J.M.A., et al. (2017). Analysis of shared homozygosity regions in Saudi siblings with attention-deficit hyperactivity disorder. *Psychiatric Genetics*, 27(4):131–138.

Shu, W., Yang, H., Zhang, L., Lu, M.M., and Morrisey, E.E. (2001). Characterization of a new subfamily of winged-helix/forkhead (*Fox*) genes that are expressed in the lung and act as transcriptional repressors. *The Journal of Biological Chemistry*, 276(29):27488–27497.

Shu, W., et al. (2005). Altered ultrasonic vocalization in mice with a disruption in the *Foxp2* gene. *Proceedings of the National Academy of Sciences of the United States of America*, 102(27):9643–9648.

Shumay, E., Fowler, J.S., and Volkow, N.D. (2010). Genomic features of the human dopamine transporter gene and its potential epigenetic states: Implications for phenotypic diversity. *PLOS ONE*, 5(6):e11067.

Silk, T.J., Vance, A., Rinehart, N., Bradshaw, J.L., and Cunnington, R. (2009). Structural development of the basal ganglia in attention-deficit hyperactivity disorder: A diffusion tensor imaging study. *Psychiatry Research*, 172(3):220–225.

Silk, T.J., et al. (2016). Cortical morphometry in attention-deficit/hyperactivity disorder: Contribution of thickness and surface area to volume. *Cortex*, 82:1–10.

Silva, D., Colvin, L., Hagemann, E., and Bower, C. (2014). Environmental risk factors by gender associated with attention-deficit/hyperactivity disorder. *Pediatrics*, 133(1):e14–22.

Silveri, M.M., et al. (2013). Frontal lobe gamma-Aminobutyric acid levels during adolescence: Associations with impulsivity and response inhibition. *Biological Psychiatry*, 74(4):296–304.

Simone, B.W., Martínez-Gálvez, G., WareJoncas, Z., and Ekker, S.C. (2018). Fishing for understanding: Unlocking the zebrafish gene editor's toolbox. *Methods*, 150:3–10.

Sin, C., Li, H., and Crawford, D.A. (2015). Transcriptional regulation by FOXP1, FOXP2, and FOXP4 dimerization. *Journal of Molecular Neuroscience*, 55(2):437–448.

Siper, P.M., et al. (2017). Prospective investigation of FOXP1 syndrome. *Molecular Autism*, 8:57.

Skoglund, C., Chen, Q., D'Onofrio, B.M., Lichtenstein, P., and Larsson, H. (2014). Familial confounding of the association between maternal smoking during pregnancy and ADHD in offspring. *Journal of Child Psychology and Psychiatry, and Allied Disciplines*, 55(1):61–68.

Smith, K.M. (2018). Hyperactivity in mice lacking one allele of the glutamic acid decarboxylase 67 gene. *Attention Deficit and Hyperactivity Disorders*, 10(4):267–271.

Smith, E., et al. (2016). Cortical thickness change in autism during early childhood. *Human Brain Mapping*, 37(7):2616–2629.

Solleveld, M.M., Schrantee, A., Puts, N.A.J., Reneman, L., and Lucassen, P.J. (2017). Age-dependent, lasting effects of methylphenidate on the GABAergic system of ADHD patients. *NeuroImage. Clinical*, 15:812–818.

Somogyi, P., et al. (2003). High level of mGluR7 in the presynaptic active zones of select populations of GABAergic terminals innervating interneurons in the rat hippocampus. *The European Journal of Neuroscience*, 17(12):2503–2520.

Song, X., Wang, Y., and Tang, Y. (2013). Rapid diversification of *FoxP2* in teleosts through gene duplication in the teleost-specific whole genome duplication event. *PLoS ONE*, 8(12).

Song, Y., et al. (2017). GABAergic neurons and their modulatory effects on GnRH3 in zebrafish. *Endocrinology*, 158(4):874–886.

Souza, B.R., Romano-Silva, M.A., and Tropepe, V. (2011). Dopamine D2 receptor activity modulates Akt signaling and alters GABAergic neuron development and motor behavior in zebrafish larvae. *Journal of Neuroscience*, 31(14):5512–5525.

Sowell, E.R., et al. (2003). Cortical abnormalities in children and adolescents with attention-deficit hyperactivity disorder. *The Lancet*, 362(9397):1699–1707.

Spencer, T., et al. (1996). Pharmacotherapy of attention-deficit hyperactivity disorder across the life cycle. *Journal of the American Academy of Child & Adolescent Psychiatry*, 35(4):409–432.

Spencer, T.J., et al. (2005). *In vivo* neuroreceptor imaging in attention-deficit/hyperactivity disorder: A focus on the dopamine transporter. *Biological Psychiatry*, 57(11):1293–1300.

Spencer, T.J., et al. (2007). Further evidence of dopamine transporter receptor dysregulation in ADHD: A controlled PET imaging study using altropane. *Biological Psychiatry*, 62(9):1059–1061.

Spiteri, E., et al. (2007). Identification of the transcriptional targets of *FOXP2*, a gene linked to speech and language, in developing human brain. *American Journal of Human Genetics*, 81(6):1144–1157.

Sprich, S., Biederman, J., Crawford, M.H., Mundy, E., and Faraone, S.V. (2000). Adoptive and biological families of children and adolescents with ADHD. *Journal of the American Academy of Child and Adolescent Psychiatry*, 39(11):1432–1437.

Spulber, S., et al. (2014). PFOS induces behavioral alterations, including spontaneous hyperactivity that is corrected by dexamfetamine in zebrafish larvae. *PLOS ONE*, 9(4):e94227.

Sripada, C.S., Kessler, D., and Angstadt, M. (2014). Lag in maturation of the brain's intrinsic functional architecture in attention-deficit/hyperactivity disorder. *Proceedings of the National Academy of Sciences*, 111(39):14259–14264.

Stawicki, J.A., Nigg, J.T., and Eye, A.V. (2006). Family psychiatric history evidence on the nosological relations of DSM-IV ADHD combined and inattentive subtypes: New data and meta-analysis. *Journal of Child Psychology and Psychiatry*, 47(9):935–945.

Stehr, C.M., Linbo, T.L., Incardona, J.P., and Scholz, N.L. (2006). The developmental neurotoxicity of fipronil: Notochord degeneration and locomotor defects in zebrafish embryos and larvae. *Toxicological Sciences*, 92(1):270–278.

Stephenson-Jones, M., Ericsson, J., Robertson, B., and Grillner, S. (2012). Evolution of the basal ganglia: Dual-output pathways conserved throughout vertebrate phylogeny. *The Journal of Comparative Neurology*, 520(13):2957–2973.

Stephenson-Jones, M., Samuelsson, E., Ericsson, J., Robertson, B., and Grillner, S. (2011). Evolutionary conservation of the basal ganglia as a common vertebrate mechanism for action selection. *Current Biology*, 21(13):1081–1091.

Stergiakouli, E., et al. (2012). Investigating the contribution of common genetic variants to the risk and pathogenesis of ADHD. *The American Journal of Psychiatry*, 169(2):186–194.

Sternberg (1983). Biomedical image processing. *Computer*, 16(1):22–34.

Still, G.F. (2006). Some abnormal psychical conditions in children: Excerpts from three lectures. *Journal of Attention Disorders*, 10(2):126–136.

Straub, R.E., et al. (2007). Allelic variation in *GAD1* (GAD_{67}) is associated with schizophrenia and influences cortical function and gene expression. *Molecular Psychiatry*, 12(9):854–869.

Strauss, A.A. and Lehtinen, L.E. (1947). *Psychopathology and Education of the Brain-Injured Child*. Grune & Stratton, Oxford, England.

Strauss, K.A., et al. (2006). Recessive symptomatic focal epilepsy and mutant contactin-associated protein-like 2. *The New England Journal of Medicine*, 354(13):1370–1377.

Ströhle, A., et al. (2008). Reward anticipation and outcomes in adult males with attention-deficit/hyperactivity disorder. *NeuroImage*, 39(3):966–972.

Sun, L., et al. (2012). Abnormal functional connectivity between the anterior cingulate and the default mode network in drug-naïve boys with attention-deficit hyperactivity disorder. *Psychiatry Research: Neuroimaging*, 201(2):120–127.

Sundararajan, T., Manzardo, A.M., and Butler, M.G. (2018). Functional analysis of schizophrenia genes using GeneAnalytics program and integrated databases. *Gene*, 641:25–34.

Sundquist, J., Sundquist, K., and Ji, J. (2014). Autism and attention-deficit/hyperactivity disorder among individuals with a family history of alcohol use disorders. *eLife*, 3:e02917.

Swanson, C.J., et al. (2005). Metabotropic glutamate receptors as novel targets for anxiety and stress disorders. *Nature Reviews Drug Discovery*, 4(2):131–144.

Sykes, D.H., Douglas, V.I., and Morgenstern, G. (1973). Sustained attention in hyperactive children. *Journal of Child Psychology and Psychiatry*, 14(3):213–220.

Tabor, H.K., Risch, N.J., and Myers, R.M. (2002). Candidate-gene approaches for studying complex genetic traits: Practical considerations. *Nature Reviews Genetics*, 3(5):391–397.

Takahashi, K., Liu, F.C., Hirokawa, K., and Takahashi, H. (2003). Expression of *Foxp2*, a gene involved in speech and language, in the developing and adult striatum. *Journal of Neuroscience Research*, 73(1):61–72.

Takahashi, K., et al. (2008). Expression of *FOXP2* in the developing monkey forebrain: Comparison with the expression of the genes *FOXP1, PBX3*, and *MEIS2*. *The Journal of Comparative Neurology*, 509(2):180–189.

Takaki, H., et al. (2004). Positive associations of polymorphisms in the metabotropic glutamate receptor type 8 gene (*GRM8*) with schizophrenia. *American Journal of Medical Genetics. Part B, Neuropsychiatric Genetics*, 128B(1):6–14.

Tavakkoly-Bazzaz, J., et al. (2018). *TCF4* and *GRM8* gene polymorphisms and risk of schizophrenia in an Iranian population: A case-control study. *Molecular Biology Reports*, 45(6):2403–2409.

Tay, T.L., Ronneberger, O., Ryu, S., Nitschke, R., and Driever, W. (2011). Comprehensive catecholaminergic projectome analysis reveals single-neuron integration of zebrafish ascending and descending dopaminergic systems. *Nature Communications*, 2:171.

Taylor, J.S., Braasch, I., Frickey, T., Meyer, A., and de Peer, Y.V. (2003). Genome duplication, a trait shared by 22,000 species of ray-finned fish. *Genome Research*, 13(3):382–390.

Teramitsu, I., Kudo, L.C., London, S.E., Geschwind, D.H., and White, S.A. (2004). Parallel *FoxP1* and *FoxP2* expression in songbird and human brain predicts functional interaction. *Journal of Neuroscience*, 24(13):3152–3163.

Terracciano, A., et al. (2010). Genome-wide association scan of trait depression. *Biological Psychiatry*, 68(9):811–817.

Teufel, A., Wong, E.A., Mukhopadhyay, M., Malik, N., and Westphal, H. (2003). *FoxP4*, a novel forkhead transcription factor. *Biochimica Et Biophysica Acta*, 1627(2-3):147–152.

Thakur, G.A., et al. (2013). Maternal smoking during pregnancy and ADHD: A comprehensive clinical and neurocognitive characterization. *Nicotine & Tobacco Research*, 15(1):149–157.

Thisse, C. and Thisse, B. (2008). High-resolution *in situ* hybridization to whole-mount zebrafish embryos. *Nature Protocols*, 3(1):59–69.

Thompson, P.D., et al. (1988). The coexistence of bradykinesia and chorea in Huntington's disease and its implications for theories of basal ganglia control of movement. *Brain*, 111.2:223–244.

Thompson, J.M.D., et al. (2014). Associations between acetaminophen use during pregnancy and ADHD symptoms measured at ages 7 and 11 years. *PloS One*, 9(9):e108210.

Thyme, S.B., et al. (2019). Phenotypic landscape of schizophrenia-associated genes defines candidates and their shared functions. *Cell*, 177(2):478–491.e20.

Tiemeier, H., et al. (2010). Cerebellum development during childhood and adolescence: A longitudinal morphometric MRI study. *NeuroImage*, 49(1):63–70.

Todd, R.D., et al. (2008). Predictors of stability of attention-deficit/hyperactivity disorder subtypes from childhood to young adulthood. *Journal of the American Academy of Child and Adolescent Psychiatry*, 47(1):76–85.

Trifonov, S., Yamashita, Y., Kase, M., Maruyama, M., and Sugimoto, T. (2014). Glutamic acid decarboxylase 1 alternative splicing isoforms: Characterization, expression and quantification in the mouse brain. *BMC Neuroscience*, 15(1):114.

Tsuchiya, D., Kunishima, N., Kamiya, N., Jingami, H., and Morikawa, K. (2002). Structural views of the ligand-binding cores of a metabotropic glutamate receptor complexed with an antagonist and both glutamate and Gd^{3+}. *Proceedings of the National Academy of Sciences of the United States of America*, 99(5):2660–2665.

Tsui, D., Vessey, J.P., Tomita, H., Kaplan, D.R., and Miller, F.D. (2013). FoxP2 regulates neurogenesis during embryonic cortical development. *Journal of Neuroscience*, 33(1):244–258.

Tung, I., et al. (2016). Patterns of comorbidity among girls with ADHD: A meta-analysis. *Pediatrics*, 138(4).

Ulke, C., et al. (2019). Adult attention-deficit/hyperactivity disorder is associated with reduced norepinephrine transporter availability in right attention networks: A (S,S)-O-[^{11}C]methylreboxetine positron emission tomography study. *Translational Psychiatry*, 9(1):301.

Usui, N., et al. (2017). Sumoylation of FOXP2 regulates motor function and vocal communication through Purkinje cell development. *Biological Psychiatry*, 81(3):220–230.

Vaidya, C.J., et al. (1998). Selective effects of methylphenidate in attention-deficit hyperactivity disorder: A functional magnetic resonance study. *Proceedings of the National Academy of Sciences of the United States of America*, 95(24):14494–14499.

Vaidya, C.J., et al. (2005). Altered neural substrates of cognitive control in childhood ADHD: Evidence from functional magnetic resonance imaging. *The American Journal of Psychiatry*, 162(9):1605–1613.

Valera, E.M., Faraone, S.V., Murray, K.E., and Seidman, L.J. (2007). Meta-analysis of structural imaging findings in attention-deficit/hyperactivity disorder. *Biological Psychiatry*, 61(12):1361–1369.

van den Berg, S.M., Willemsen, G., de Geus, E.J.C., and Boomsma, D.I. (2006). Genetic etiology of stability of attention problems in young adulthood. *American Journal of Medical Genetics. Part B, Neuropsychiatric Genetics*, 141B(1):55–60.

van Rhijn, J.R., Fisher, S.E., Vernes, S.C., and Nadif Kasri, N. (2018). Foxp2 loss of function increases striatal direct pathway inhibition via increased GABA release. *Brain Structure & Function*.

Vargha, A. and Delaney, H.D. (2000). A critique and improvement of the *CL* common language effect size statistics of McGraw and Wong. *Journal of Educational and Behavioral Statistics*, 25(2):101–132.

Vargha-Khadem, F., Gadian, D.G., Copp, A., and Mishkin, M. (2005). *FOXP2* and the neuroanatomy of speech and language. *Nature Reviews. Neuroscience*, 6(2):131–138.

Verbeeck, W., Bekkering, G.E., Van den Noortgate, W., and Kramers, C. (2017). Bupropion for attention-deficit hyperactivity disorder (ADHD) in adults. *The Cochrane Database of Systematic Reviews*, 10:CD009504.

Verkerk, A.J.M.H., et al. (2003). *CNTNAP2* is disrupted in a family with Gilles de la Tourette syndrome and obsessive compulsive disorder. *Genomics*, 82(1):1–9.

Vernes, S.C., et al. (2006). Functional genetic analysis of mutations implicated in a human speech and language disorder. *Human Molecular Genetics*, 15(21):3154–3167.

Vernes, S.C., et al. (2007). High-throughput analysis of promoter occupancy reveals direct neural targets of *FOXP2*, a gene mutated in speech and language disorders. *American Journal of Human Genetics*, 81(6):1232–1250.

Vernes, S.C., et al. (2008). A functional genetic link between distinct developmental language disorders. *New England Journal of Medicine*, 359(22):2337–2345.

Vernes, S.C., et al. (2011). Foxp2 regulates gene networks implicated in neurite outgrowth in the developing brain. *PLoS Genetics*, 7(7).

Viggiano, D., Vallone, D., Welzl, H., and Sadile, A.G. (2002). The Naples High- and Low-Excitability rats: Selective breeding, behavioral profile, morphometry, and molecular biology of the mesocortical dopamine system. *Behavior Genetics*, 32(5):315–333.

Vilar-Ribó, L., et al. (2020). Genetic overlap and causality between substance use disorder and attention-deficit and hyperactivity disorder. *American Journal of Medical Genetics. Part B, Neuropsychiatric Genetics*.

Volkow, N.D., Fowler, J.S., Wang, G.J., Ding, Y.S., and Gatley, S.J. (2002). Role of dopamine in the therapeutic and reinforcing effects of methylphenidate in humans: Results from imaging studies. *European Neuropsychopharmacology*, 12(6):557–566.

Volkow, N.D., Wang, G.J., Fowler, J.S., and Ding, Y.S. (2005). Imaging the effects of methylphenidate on brain dopamine: New model on its therapeutic actions for attention-deficit/hyperactivity disorder. *Biological Psychiatry*, 57(11):1410–1415.

Volkow, N.D., et al. (2001). Therapeutic doses of oral methylphenidate significantly increase extracellular dopamine in the human brain. *Journal of Neuroscience*, 21(2):RC121–RC121.

Volkow, N.D., et al. (2007a). Brain dopamine transporter levels in treatment and drug naïve adults with ADHD. *NeuroImage*, 34(3):1182–1190.

Volkow, N.D., et al. (2007b). Depressed dopamine activity in caudate and preliminary evidence of limbic involvement in adults with attention-deficit/hyperactivity disorder. *Archives of General Psychiatry*, 64(8):932–940.

Volkow, N.D., et al. (2009). Evaluating dopamine reward pathway in ADHD: Clinical implications. *JAMA*, 302(10):1084–1091.

Walton, E., et al. (2017). Epigenetic profiling of ADHD symptoms trajectories: A prospective, methylome-wide study. *Molecular Psychiatry*, 22(2):250–256.

Wang, G.J., et al. (2009). Chronic treatment with methylphenidate increases dopamine transporter density in patients with attention-deficit hyperactive disorder. *Journal of Nuclear Medicine*, 50:1283–1283.

Wang, Y., et al. (2010). *Dlx5* and *Dlx6* regulate the development of parvalbumin-expressing cortical interneurons. *Journal of Neuroscience*, 30(15):5334–5345.

Wang, S.M., et al. (2017). Modafinil for the treatment of attention-deficit/hyperactivity disorder: A meta-analysis. *Journal of Psychiatric Research*, 84:292–300.

Wang, Z., et al. (2018). Axon guidance pathway genes are associated with schizophrenia risk. *Experimental and Therapeutic Medicine*, 16(6):4519–4526.

Wang, H.L., et al. (2019). Adolescent stress increases depression-like behaviors and alters the excitatory-inhibitory balance in aged mice. *Chinese Medical Journal*, 132(14):1689–1699.

Weissman, D.H., Roberts, K.C., Visscher, K.M., and Woldorff, M.G. (2006). The neural bases of momentary lapses in attention. *Nature Neuroscience*, 9(7):971–978.

Wells, M.F., Wimmer, R.D., Schmitt, L.I., Feng, G., and Halassa, M.M. (2016). Thalamic reticular impairment underlies attention-deficit in *Ptchd1*$^{Y/-}$ mice. *Nature*, 532(7597):58–63.

Wen, L., et al. (2008). Visualization of monoaminergic neurons and neurotoxicity of MPTP in live transgenic zebrafish. *Developmental Biology*, 314(1):84–92.

Weyandt, L.L., et al. (2003). The internal restlessness scale: Performance of college students with and without ADHD. *Journal of Learning Disabilities*, 36(4):382–389.

Wigal, T.L., et al. (2018). A double-blind, placebo-controlled, phase II study to determine the efficacy, safety, tolerability and pharmacokinetics of a controlled release (CR) formulation of mazindol in adults with DSM-5 attention-deficit/hyperactivity disorder (ADHD). *CNS Drugs*, 32(3):289–301.

Wilens, T.E. (2008). Effects of methylphenidate on the catecholaminergic system in attention-deficit/hyperactivity disorder. *Journal of Clinical Psychopharmacology*, 28(3 Suppl 2):46–53.

Willard, S.S. and Koochekpour, S. (2013). Glutamate, glutamate receptors, and downstream signaling pathways. *International Journal of Biological Sciences*, 9(9):948–959.

Willcutt, E.G. (2012). The prevalence of DSM-IV attention-deficit/hyperactivity disorder: A meta-analytic review. *Neurotherapeutics*, 9(3):490–499.

Willcutt, E.G., Doyle, A.E., Nigg, J.T., Faraone, S.V., and Pennington, B.F. (2005). Validity of the executive function theory of attention-deficit/hyperactivity disorder: A meta-analytic review. *Biological Psychiatry*, 57(11):1336–1346.

Williams, N.M., et al. (2010). Rare chromosomal deletions and duplications in attention-deficit hyperactivity disorder: A genome-wide analysis. *The Lancet*, 376(9750):1401–1408.

Williams, N.M., et al. (2012). Genome-wide analysis of copy number variants in attention-deficit hyperactivity disorder: The role of rare variants and duplications at 15q13.3. *The American Journal of Psychiatry*, 169(2):195–204.

Wolff, J.R., Joó, F., and Dames, W. (1978). Plasticity in dendrites shown by continuous GABA administration in superior cervical ganglion of adult rat. *Nature*, 274(5666):72–74.

Wolman, M. and Granato, M. (2012). Behavioral genetics in larval zebrafish: Learning from the young. *Developmental Neurobiology*, 72(3):366–372.

Wolosin, S.M., Richardson, M.E., Hennessey, J.G., Denckla, M.B., and Mostofsky, S.H. (2009). Abnormal cerebral cortex structure in children with ADHD. *Human Brain Mapping*, 30(1):175–184.

Won, H., et al. (2011). *GIT1* is associated with ADHD in humans and ADHD-like behaviors in mice. *Nature Medicine*, 17(5):566–572.

Woo, M.S., et al. (2021). Neuronal metabotropic glutamate receptor 8 protects against neurodegeneration in CNS inflammation. *The Journal of Experimental Medicine*, 218(5).

Woods, D.L. and Knight, R.T. (1986). Electrophysiologic evidence of increased distractibility after dorsolateral prefrontal lesions. *Neurology*, 36(2):212–216.

World Health Organization (WHO), editor (2004). *ICD-10: International Statistical Classification of Diseases and Related Health Problems*. World Health Organization, Geneva.

Wu, C. and Sun, D. (2015). GABA receptors in brain development, function, and injury. *Metabolic Brain Disease*, 30(2):367–379.

Wullimann, M.F. (2014). Ancestry of basal ganglia circuits: New evidence in teleosts. *Journal of Comparative Neurology*, 522(9):2013–2018.

Wullimann, M.F. and Umeasalugo, K.E. (2020). Sonic hedgehog expression in zebrafish forebrain identifies the teleostean pallidal signaling center and shows preglomerular complex and posterior tubercular dopamine cells to arise from *shh* cells. *Journal of Comparative Neurology*, 528(8):1321–1348.

Xiao, L., et al. (2021). Expression of *FoxP2* in the basal ganglia regulates vocal motor sequences in the adult songbird. *Nature Communications*, 12(1):2617.

Xing, L., et al. (2012). Zebrafish *foxP2* zinc finger nuclease mutant has normal axon pathfinding. *PloS One*, 7(8):e43968.

Xu, Y., et al. (2015). Multiple epigenetic factors predict the attention-deficit/hyperactivity disorder among the Chinese Han children. *Journal of Psychiatric Research*, 64:40–50.

Yamashita, M., et al. (2013). Impaired cliff avoidance reaction in dopamine transporter knockout mice. *Psychopharmacology*, 227(4):741–749.

Yang, P., Cai, G., Cai, Y., Fei, J., and Liu, G. (2013a). Gamma-Aminobutyric acid transporter subtype 1 gene knockout mice: A new model for attention-deficit/hyperactivity disorder. *Acta Biochimica Et Biophysica Sinica*, 45(7):578–585.

Yang, L., et al. (2013b). Polygenic transmission and complex neuro-developmental network for attention-deficit hyperactivity disorder: Genome-wide association study of both common and rare variants. *American Journal of Medical Genetics. Part B, Neuropsychiatric Genetics*, 162B(5):419–430.

Yang, L., et al. (2018). A new locus regulating *MICALL2* expression was identified for association with executive inhibition in children with attention-deficit hyperactivity disorder. *Molecular Psychiatry*, 23(4):1014–1020.

Yano, M. and Steiner, H. (2005). Topography of methylphenidate (Ritalin)-induced gene regulation in the striatum: Differential effects on *c-Fos* , Substance P and opioid peptides. *Neuropsychopharmacology*, 30(5):901–915.

Yates, J.R., Darna, M., Beckmann, J.S., Dwoskin, L.P., and Bardo, M.T. (2016). Individual differences in impulsive action and dopamine transporter function in rat orbitofrontal cortex. *Neuroscience*, 313:122–129.

Yates, A.D., et al. (2020). Ensembl 2020. *Nucleic Acids Research*, 48(D1):D682–D688.

Yauy, K., et al. (2019). Disruption of chromatin organisation causes *MEF2C* gene overexpression in intellectual disability: A case report. *BMC Medical Genomics*, 12(1):116.

Yip, J., Soghomonian, J.J., and Blatt, G.J. (2007). Decreased GAD67 mRNA levels in cerebellar Purkinje cells in autism: Pathophysiological implications. *Acta Neuropathologica*, 113(5):559–568.

Yizhar, O., et al. (2011). Neocortical excitation/inhibition balance in information processing and social dysfunction. *Nature*, 477(7363):171–178.

Yoon, S.H., et al. (2020). Shifting hippocampal excitation/inhibition balance modifies despair-like behavior in mice. *bioRxiv*, page 2020.02.18.953786.

Yoshimasu, K., Kiyohara, C., Takemura, S., and Nakai, K. (2014). A meta-analysis of the evidence on the impact of prenatal and early infancy exposures to mercury on autism and attention-deficit/hyperactivity disorder in the childhood. *Neurotoxicology*, 44:121–131.

Young, J.W., van Enkhuizen, J., Winstanley, C.A., and Geyer, M.A. (2011). Increased risk-taking behavior in dopamine transporter knockdown mice: Further support for a mouse model of mania. *Journal of Psychopharmacology*, 25(7):934–943.

Yuan, F.F., Gu, X., Huang, X., Zhong, Y., and Wu, J. (2017). *SLC6A1* gene involvement in susceptibility to attention-deficit/hyperactivity disorder: A case-control study and gene-environment interaction. *Progress in Neuro-Psychopharmacology & Biological Psychiatry*, 77:202–208.

Zagar, R. and Bowers, N.D. (1983). The effect of time of day on problem solving and classroom behavior. *Psychology in the Schools*, 20(3):337–345.

Zametkin, A.J., et al. (1990). Cerebral glucose metabolism in adults with hyperactivity of childhood onset. *New England Journal of Medicine*, 323(20):1361–1366.

Zangrossi, H., Viana, M.B., and Graeff, F.G. (1999). Anxiolytic effect of intra-amygdala injection of midazolam and 8-hydroxy-2-(di-*n*-propylamino)tetralin in the elevated T-maze. *European Journal of Pharmacology*, 369(3):267–270.

Zhang, K., Davids, E., Tarazi, F.I., and Baldessarini, R.J. (2002). Effects of dopamine D$_4$ receptor-selective antagonists on motor hyperactivity in rats with neonatal 6-hydroxydopamine lesions. *Psychopharmacology*, 161(1):100–106.

Zhang, L., et al. (2014). Association analysis of the *GRM8* gene with schizophrenia in the Uygur Chinese population. *Hereditas*, 151(6):140–144.

Zhang, P., et al. (2019). Genomic sequencing and editing revealed the GRM8 signaling pathway as potential therapeutic targets of squamous cell lung cancer. *Cancer Letters*, 442:53–67.

Zhao, Y., et al. (2018). A large-scale integrative analysis of GWAS and common meQTLs across whole life course identifies genes, pathways and tissue/cell types for three major psychiatric disorders. *Neuroscience & Biobehavioral Reviews*, 95:347–352.

Zhu, J.L., et al. (2014). Parental smoking during pregnancy and ADHD in children: The Danish national birth cohort. *Pediatrics*, 134(2):e382–388.

Zhuang, X., et al. (2001). Hyperactivity and impaired response habituation in hyperdopaminergic mice. *Proceedings of the National Academy of Sciences of the United States of America*, 98(4):1982–1987.

Zweier, C., et al. (2009). *CNTNAP2* and *NRXN1* are mutated in autosomal-recessive Pitt-Hopkins-like mental retardation and determine the level of a common synaptic protein in *Drosophila*. *American Journal of Human Genetics*, 85(5):655–666.

Zweier, M., et al. (2010). Mutations in *MEF2C* from the 5q14.3q15 microdeletion syndrome region are a frequent cause of severe mental retardation and diminish *MECP2* and *CDKL5* expression. *Human Mutation*, 31(6):722–733.

Appendix

Abbreviations

Table 12: **List of general abbreviations.**

Abbreviation	Meaning	Abbreviation	Meaning
ACC	anterior cingulate cortex	*L3MBTL3*	histone methyl-lysine binding protein 3
actb1/β-actin	actin, beta 1	*lbx1a*	ladybird homeobox 1a
AcTub	acetylated tubulin	LPHN3	latrophilin 3
ADD	attention-deficit disorder	MAO-A	monoamine oxidase A
ADHD	attention-deficit/hyperactivity disorder	MAPK	mitogen-activated protein kinase
ADHS	Aufmerksamkeitsdefizit-/Hyperaktivitätsstörung	MBD	minimal brain damage
AMP	amphetamines	MDD	major depressive disorder
AMPA	alpha-amino-3-hydroxy-5-methyl-4-isoxazolepropionic acid (receptor)	*mef2c*	myocyte enhancer factor 2
AN	affective network	MeOH	methanol
AP	Alkaline Phophatase	mGluR III	type III metabotropic glutamate receptor
APA	American Psychiatric Association	MO	splice-inhibiting morpholino
APOPT1/COA8	cytochrome c oxidase assembly factor 8	mPFC	medial prefrontal cortex
BG	basal ganglia	MPH	methylphenidate
BSA	bovine serum albumin	MR	master regulator
cAMP	cyclic adenosine monophosphate	*MRPS33*	mitochondrial ribosomal protein S33
CC	corpus callosum	MS-222	tricaine methanesulfonate
cCasp3	cleaved caspase 3	MSN	medium spiny neurons
CD	conduct disorder	NAc	nucleus accumbens
cDNA	complementary DNA	NBT/BCIP	nitroblue tetrazolium/5-bromo-4-chloro-3-indolylphosphate
CNS	central nervous system	NDD	neurodevelopmental disorder
cntnap2	contactin associated protein 2	*NEGR1*	neuronal growth regulator 1
CNV	copy number variation	NET/*NET(1)*	norepinephrine transporter (1)
CtBP1	C-terminal binding protein 1	NMDA	N-methyl-D-aspartate (receptor)
CTNND1	catenin delta 1	NSS	normal sheep serum
D1R/DRD1	dopamine D1 receptor	OCD	obsessive-compulsive disorder
D2R/DRD2	dopamine D2 receptor	ODD	oppositional defiant disorder
dACC	dorsal anterior cingulate cortex	OFC	orbitofrontal prefrontal cortex
DAN	dorsal attention network	PAM	protospacer adjacent motif
DARPP-32	dopamine- and cAMP-regulated neuronal phosphoprotein	PBS	phosphate-buffered saline
DAT1	dopamine transporter 1	PBST	phosphate-buffered saline + 0.1 % tween-20
DIG	digoxigenin	PCC	posterior cingulate cortex
DLPFC	dorso-lateral prefrontal cortex	p-ERK	extracellular-signal regulated kinases (phosphorylated)
DLX5-6	distal-less homeobox 5-6	PET	positron emission tomography
DMN	default mode network	PFA	paraformaldehyde
dpf	days post fertilization	PFC	prefrontal cortex
DRD2-5	dopamine receptor D2-5	PG	precentral gyrus
DSM	Diagnostic and Statistical Manual of Mental Disorders	PLP	pyridoxal phosphate
DTI	diffusion tensor imaging	*ppp1r1b*	protein phosphatase 1 regulatory subunit 1B
E. coli	*Escherichia coli*	qPCR	real-time quantitative PCR
E/I imbalance	excitatory/inhibitory imbalance	*RBFOX1*	RNA binding protein, Fox-1 homolog 1
ER	endoplasmatic reticulum	RDoC	Research Domain Criteria
FB/MB	forebrain/midbrain	rev.	reverse
FLUO	fluorescein	ROI	region of interest
fMRI	functional magnetic resonance imaging	RT	room temperature
FOXP	forkhead-box transcription factor, subfamily P	RT-PCR	reverse transcriptase PCR
FOXP2	forkhead-box transcription factor P2	SERT	sodium-dependent serotonin transporter
FPN	fronto-parietal network	sgRNA	single guide RNA
fwd.	forward	*Shhrs/Dlx6os1*	distal-less homeobox 6, opposite strand 1
GABA	gamma-Aminobutyric-acid	*SLC30A9*	solute carrier family 30 member 9
GABA-A-R	GABA-A-receptor	sMRI	structural magnetic resonance imaging
GABA-B-R	GABA-B-receptor	SN	substantia nigra
GAD1/GAD67	glutamate decarboxylase 1 (67 kDa)	SNP	single nucleotide polymorphism
GAD2/GAD65	glutamate decarboxylase 2 (65 kDa)	*SOX5*	SRY-box transcription factor 5
GAT1	GABA transporter 1	SPECT	single photon emission computed tomography
gDNA	genomic DNA	SSC	saline-sodium-citrate
GPi	internal segment of the globus pallidus	SSN	somatosensory network
GRM	metabotropic glutamate receptor	SUD	substance use disorder
GRM8	metabotropic glutamate receptor 8	TALEN	transcription activator-like effector nuclease
GWAS	genome-wide association study	TH	tyrosine hydroxylase
HB	hindbrain	TPH1-2	tryptophan hydroxylase 1-2
hpf	hours post fertilization	TRN	thalamic reticular nucleus
ICD	International Statistical Classification of Diseases and Related Health Problems	VAN	ventral attention network
IHC	immunohistochemistry	VFD	venus flytrap domain
indel	insertion/deletion	VMAT2	vesicular monoamine transporter 2
ISH	*in situ* hybridization	vmPFC	ventromedial prefrontal cortex
KCNB1	potassium voltage-gated channel subfamily B member 1	w/o	without
KCNQ5	potassium voltage-gated channel subfamily Q member 5	WT	wildtype

Table 13: **List of anatomical abbreviations.**

Abbreviation	Anatomical structure	Abbreviation	Anatomical structure
AC	anterior commissure	OB	olfactory bulb
ATN	anterior tuberal nucleus	OC	optic commissure
CC	cerebellar crest	ORR	optic recess region
CCe	cerebellar corpus	OT	optic tract
CeP	cerebellar plate	OTC	otic capsule
CIL	central nucleus of the inferior lobe	P	pallium
Cpost	posterior commissure	Pc	pretectal complex
DIL	diffuse nucleus of the inferior lobe	PG	preglomerular nuclei
DON	descending octaval nucleus	PGZ	periventricular gray zone of optic tectum
DT	dorsal thalamus	Po	preoptic region
DTN	dorsal tegmental nucleus	POC	post-optic commissure
EG	granular eminence	PP	periventricular pretectal nucleus
EN	entopeduncular nucleus	PT	posterior tuberculum
GCL	ganglion cell layer	PTN	posterior tuberal nucleus
H	hypothalamus	PVO	paraventricular organ
Ha	habenula	RF	reticular formation
Hc	caudal zone of the periventricular hypothalamus	RV	rhombencephalic ventricle
Hd	dorsal zone of periventricular hypothalamus	S	subpallium
Hv	ventral zone of periventricular hypothalamus	SC	spinal cord
INL	inner nuclear layer	SOT	supra-optic tract
IO	inferior olive	Tel	telencephalon
LCa	caudal lobe of cerebellum	TeO	optic tectum
LH	lateral hypothalamic nucleus	TeV	tectal ventricle
LIX	glossopharyngeal lobe	Tg	tegmentum
LLF	lateral longitudinal fascicle	Th	thalamus
LRL	lower rhombic lip	TL	longitudinal torus
LVII	facial lobe	TLa	lateral torus
LX	vagal lobe	TPp	periventricular nucleus of posterior tuberculum
MFN	medial funicular nucleus	TS	torus semicularis
MLF	medial longitudinal fascicle	TTB	tractus tectobulbaris
MO	medulla oblongata	Va	valvular cerebelli
MON	medial octavolateralis nucleus	VT	ventral thalamus
NLV	lateral valvular nucleus	vTg	ventral tegmentum
NIII/IV	oculomotor/trochlear nucleus	X	vagal nerve
NXm	vagal motor nucleus	Y	yolk sac

Result summary

Table 14: **Summary of morphological and behavioral phenotypes for *grm8a*, *grm8b*, and *gad1b* splice-morphants (MO) and *grm8a*, *grm8b*, and *foxp2* CRISPR/Cas9 mutants (CRISPR).** FB/MB: forebrain/midbrain, HB: hindbrain.

	grm8a MO	*grm8a* CRISPR	*grm8b* MO	*grm8b* CRISPR	*foxp2* CRISPR	*gad1b* MO
morphology	unchanged	unchanged	unchanged	unchanged	swim bladder	unchanged
body length	decreased	unchanged	increased	tend. decreased	unchanged	decreased
head size	unchanged	unchanged	unchanged	unchanged	unchanged	unchanged
yolk diameter	unchanged	unchanged	unchanged	unchanged	unchanged	unchanged
apoptosis	unchanged	unchanged	unchanged	unchanged	unchanged	increased
FB/MB cell number	decreased	unchanged	x	x	unchanged	x
HB cell number	increased	increased	x	x	tend. decreased	decreased
locomotor behavior	increased	decreased	increased	unchanged	increased	increased
thigmotaxis behavior	increased	tend. increased	unchanged	increased	unchanged	increased

Recipes and protocols

Danieau's solution:
(*with methylene blue*)

17.4 ml	NaCl (1M)
210 μl	KCl (1M)
120 μl	MgSO$_4$ (1M)
180 μl	Ca(NO$_3$)$_2$ (1M)
1.5 ml	HEPES (1M, pH 7.4)
1 ml	methylene blue (0.1 %)
up to 1 l	with H$_2$O

Danieau's solution:
(*w.o. methylene blue*)

17.4 ml	NaCl (1M)
210 μl	KCl (1M)
120 μl	MgSO$_4$ (1M)
180 μl	Ca(NO$_3$)$_2$ (1M)
1.5 ml	HEPES (1M, pH 7.4)
up to 1 l	with H$_2$O

Hybridization buffer (for RNA ISH):
(*with torula yeast RNA and heparin*)

32.5 ml	formamide (100 %)
12.5 ml	SSC (20 %)
100 μl	heparin (5000 U/ml)
250 mg	torula yeast RNA
250 μl	tween-20 (20 %)
250 μl	citric acid (0.5 M, pH: 6.0)
up to 50 ml	with H$_2$O

Hybridization buffer (for RNA ISH):
(*w.o. tRNA and heparin*)

32.5 ml	formamide (100 %)
12.5 ml	SSC (20 %)
250 μl	tween-20 (20 %)
250 μl	citric acid (0.5 M, pH 6.0)
up to 50 ml	with H$_2$O

Blocking buffer (for RNA ISH):

1 ml	NSS
100 mg	BSA (albumin fraction V)
up to 50 ml	with PBST

Alkaline tris-buffer (pH 9.5):

5 ml	Tris-HCl (1 M, pH 9.5)
2.5 ml	MgCl$_2$ (1 M)
1 ml	NaCl (5 M)
250 μl	tween-20 (20 %)
up to 50 ml	with H$_2$O

Tris-buffer (pH 8.2):

5ml ml	Tris-HCl (1M, pH 8.2)
250 μl	tween-20 (20 %)
up to 50 ml	with H$_2$O

10 % Blocking buffer (for IHC):

5 ml	NSS
100 mg	BSA (albumin fraction V)
up to 50 ml	with PBST

2 % Blocking buffer (for IHC):

1 ml	NSS
100 mg	BSA (albumin fraction V)
up to 50 ml	with PBST

DMSO Blocking buffer (for IHC):

5 ml	NSS
100 mg	BSA (albumin fraction V)
500 μl	DMSO
up to 50 ml	with PBST

TE buffer (pH 8.0):
(for fin clipping and gDNA extraction)

400 μl	EDTA (0.5 M, pH 8.0)
200 μl	Tris-HCl (1 M, pH 8.0)
4 ml	NaCl (1M)
up to 20 ml	with ddH$_2$O

LiCl and ethanol precipitation:

Add to 20 μl reaction mix

30 μl	TE buffer (pH 8.0)
5 μl	LiCl (4M)
150 μl	ethanol (100 %)

- precipitate at -20 °C for >1 h

- centrifuge (15 min, 4 °C, max. speed)

- remove supernatant

- add 100 μl ethanol (75 %)

- centrifuge (15 min, 4 °C, max. speed)

- remove supernatant

- dry pellet at RT

- resuspend pellet in 40 μl H_2O (RNase-free)

- store at -80 °C

Genomic DNA (gDNA) extraction:

(on fraction or total tissue)

- Add 12.5 μl TE buffer + 200 μg/ml PK

- Add tissue/ euthanized (ice) larvae/embryo

- Incubate for 4 hours at 55 °C

- Inactivate PK for 10 min at 95 °C

- Use 2 μl for a 25 μl genotyping PCR mix

- Store at -20 °C

Phenol/chloroform/isoamylalcohol (P:C:I) precipitation:

Add to 20 μl reaction mix

30 μl	H_2O (RNase-free)
50 μl	P:C:I (in water, pH 4.5)

- mix vigorously

- centrifuge (5 min, max. speed)

- transfer aqueous phase to new Eppi

- add 50 μl chloroform

- mix vigorously

- centrifuge (5 min, max. speed)

- transfer aqueous phase to new Eppi

- add 50 μl isopropanol (100 %)

- mix vigorously

- precipitate at -20 °C for 1 h

- centrifuge (15 min, 4 °C, max. speed)

- remove supernatant

- add 50 μl ethanol (100 %)

- centrifuge (10 min, 4 °C, max. speed)

- remove supernatant

- dry pellet at RT

- resuspend pellet in 25 μl H_2O (RNase-free)

- store at -80 °C

TRIZOL/chloroform precipitation:

Pool 5 embryos of the same stage/condition in an Eppi and remove all Danieau's solution

- add 500 μl TRIZOL reagent

- incubate for 5 min at RT

- if possible, homogenize the tissue directly using a syringe plus needle (BD Discardit II 2ml + BD Microlance 23G 1 1/4 0.6 x 30 mm), otherwise store at - 20 °C

- add 100 μl chloroform (99.9 %) and vortex for 15 sec.

- incubate for another 2-3 min at RT

- centrifuge (15 min, 4 °C, 12.000 g)

- transfer the aqueous (upper) phase to a new Eppi

- add 500 μl isopropanol (100 %) mix by inverting and incubate for 10 min at RT

- centrifuge (10 min, 4 °C, 12.000 g)

- remove the supernatant and wash the pellet with 500 μl ethanol (100 %)

- centrifuge (5 min, 4 °C, 12.000 g)

- remove the supernatant and wash the pellet with 500 μl ethanol (75 % in H_2O)

- centrifuge (5 min, 4 °C, 12.000 g)
- repeat the last two steps
- remove the ethanol and let the pellet air dry /instead at 40 °C for a maximum of 10 min
- dissolve the pellet in 20 μl H_2O
- if the nanodrop peaks too high at 230, perform a LiCl and ethanol precipitation
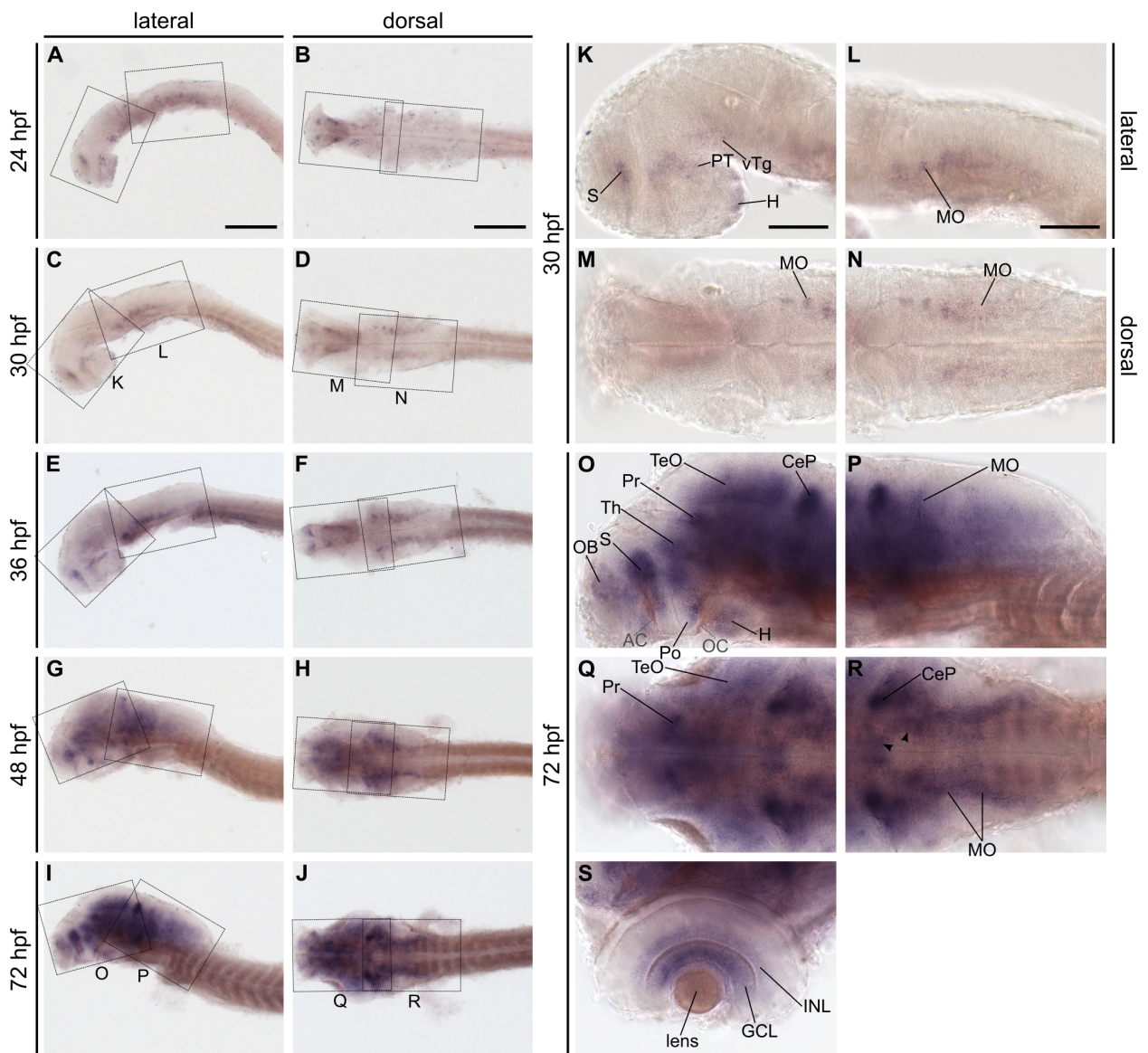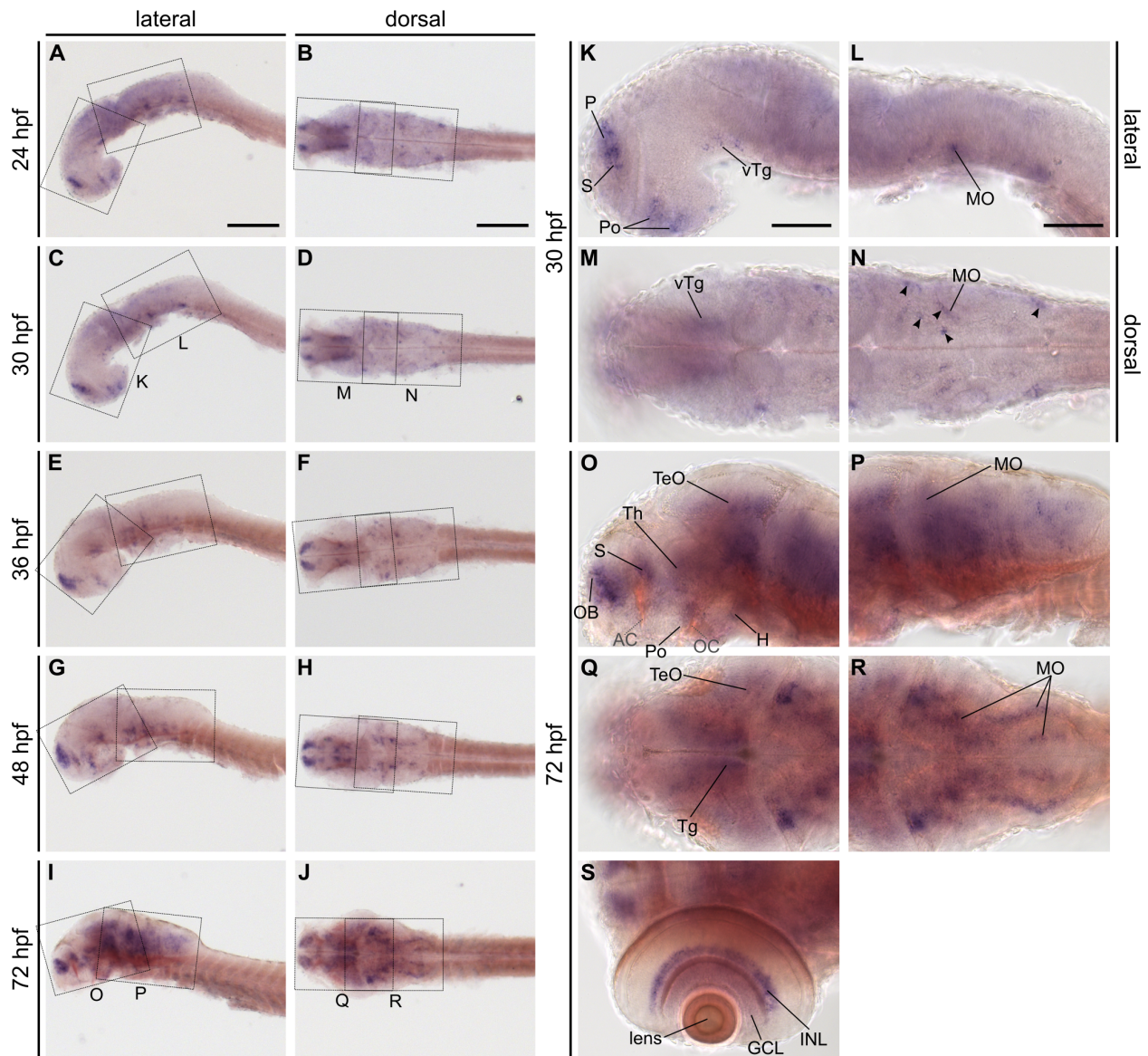- store the RNA at -80 °C

Supplementary figures and tables

Figure 31: **Spatio-temporal gene expression pattern of *grm8a* in the developing zebrafish revealed by whole-mount RNA *in situ* hybridization.** Lateral (A, C, E, G, I) and dorsal overview (B, D, F, H, J) of *grm8a* transcript labeling in 24 hpf, 30 hpf, 36 hpf, 48 hpf, and 72 hpf old wildtype zebrafish. Developmental stage increases from top to bottom. Magnifications of boxed regions in C, D and I, J are presented in K-N and O-R, respectively. Remaining magnifications of boxed regions in A-B, E-F, and G-H are displayed in Fig. 8. (S) *grm8a* expression in the eye from dorsal view. Details on *grm8a* expression are described in the main text and summarized in Table 11. All images are oriented with anterior to the left. For anatomical abbreviations, see Table 13. Scale bars represent 200 μm for overview (left panel) and 100 μm for magnified images (right panel). Adjusted from Lueffe et al. 2021b.

Figure 32: **Spatio-temporal gene expression pattern of *grm8b* in the developing zebrafish revealed by whole-mount RNA *in situ* hybridization.** Lateral (A, C, E, G, I) and dorsal overview (B, D, F, H, J) of *grm8b* transcript labeling in 24 hpf, 30 hpf, 36 hpf, 48 hpf, and 72 hpf old wildtype zebrafish. Developmental stage increases from top to bottom. Magnifications of boxed regions in C, D and I, J are presented in K-N and O-R, respectively. Remaining magnifications of boxed regions in A-B, E-F, and G-H are displayed in Fig. 8. (S) *grm8b* expression in the eye from dorsal view. Details on *grm8b* expression are described in the main text and summarized in Table 11. All images are oriented with anterior to the left. For anatomical abbreviations, see Table 13. Scale bars represent 200 μm for overview (left panel) and 100 μm for magnified images (right panel). Adjusted from Lueffe et al. 2021b.
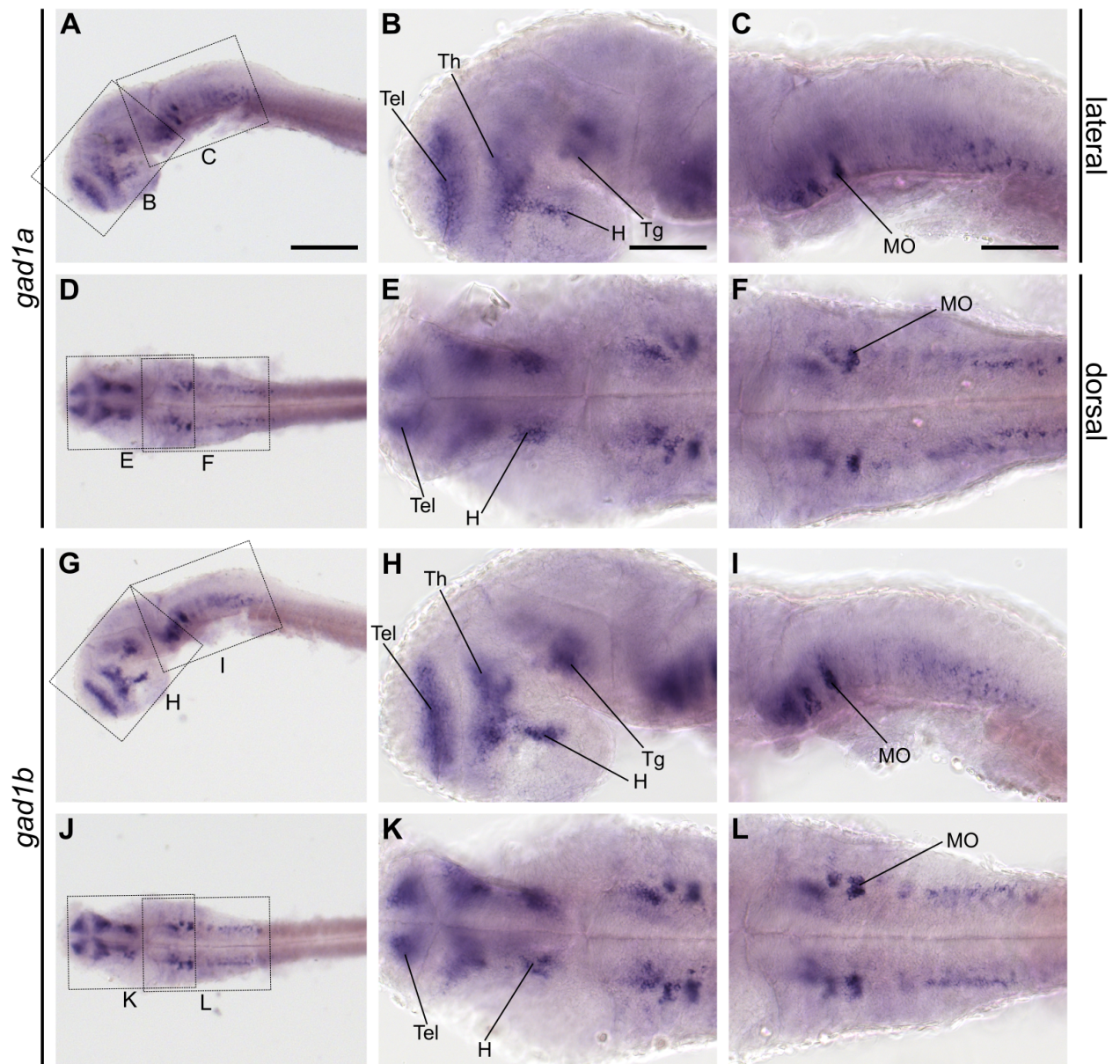
Figure 33: **Whole-mount RNA *in situ* hybridization reveals similar patterns for *gad1a* and *gad1b* expression in 36 hpf old wildtype embryos.** *gad1a* (A-F) and *gad1b* (G-L) transcript labeling displayed as lateral and dorsal overviews (A, G and D, J) and corresponding magnifications (B-C, H-I and E-F, K-L) with anterior directed to the left. For anatomical abbreviations, see Table 13. Scale bars represent 200 μm in overview and 100 μm in magnified images. Adjusted from Lueffe et al. 2021a.
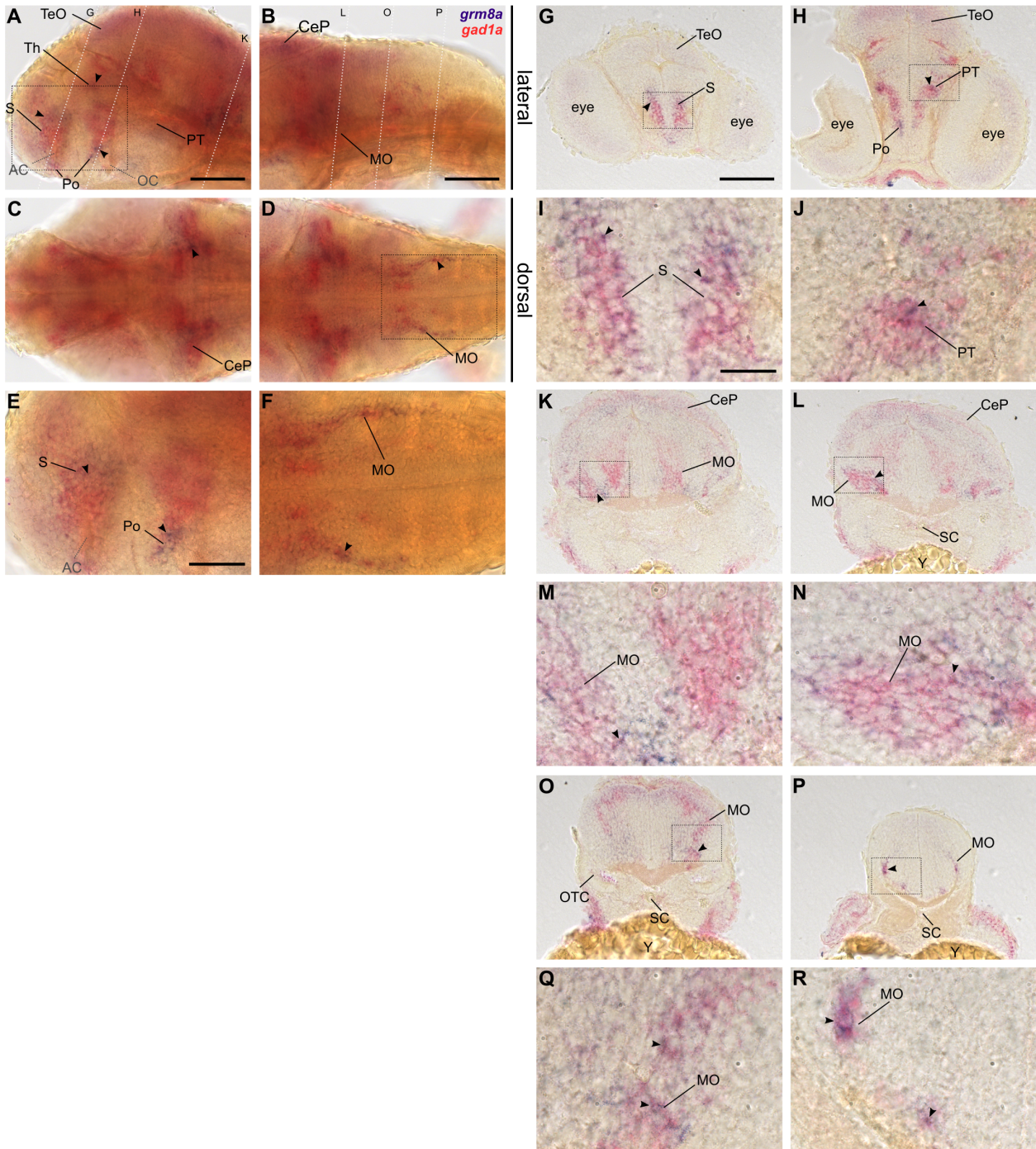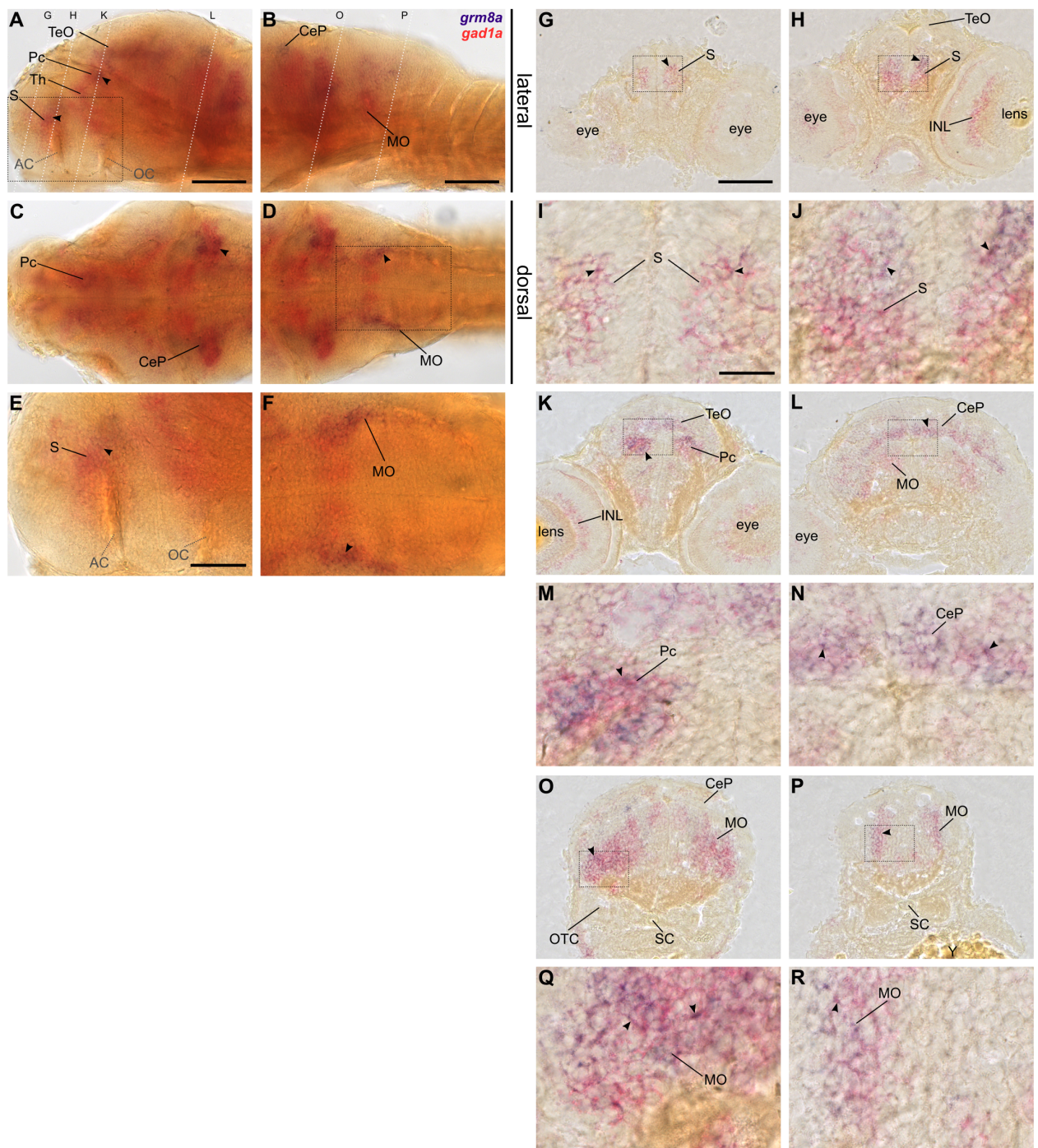
Figure 34: **Double-labeling of *grm8a* and *gad1a* transcripts in 48 hpf old wildtype zebrafish embryos.** (A-F) Whole-mount two-color RNA *in situ* hybridization for *grm8a* (blue) and *gad1a* (red) shown from lateral (A, B, E) and dorsal views (C, D, F) with anterior displayed to the left. Boxed regions in A, D are magnified in E, F. Dashed, white lines illustrate cutting sites for cross-sections displayed in G-R. Magnifications of boxed regions in G, H, K, L, O, and P are shown in I, J, M, N, Q, and R, respectively. Arrows point out regions with apparent colocalization of both expression patterns. A detailed description of regions with common and distinct expression is given in the main text and summarized in Table 11. For anatomical abbreviations, see Table 13. Scale bar represents 100 μm in overview and 50 μm in magnified images. Adjusted from Lueffe et al. 2021b.

Figure 35: **Double-labeling of *grm8a* and *gad1a* transcripts in 72 hpf old wildtype zebrafish larvae.** (A-F) Two-color RNA *in situ* hybridization for *foxp2* (blue) and *gad1a* (red) on whole-mount preparations shown from lateral and dorsal views with anterior displayed to the left. Boxed regions in A, D are magnified in E, F. Dashed, white lines illustrate cutting sites for cross-sections displayed in G-R. Boxed regions in G, H, K, L, O, and P are magnified in I, J, M, N, Q, and R, respectively. Arrows point out regions with apparent *grm8a* and *gad1a* expression colocalization. Details on expression colocalization are described in the main text and summarized in Table 11. For anatomical abbreviations, see Table 13. Scale bars represent 100 μm in overview and 50 μm in magnified images. Adjusted from Lueffe et al. 2021b.
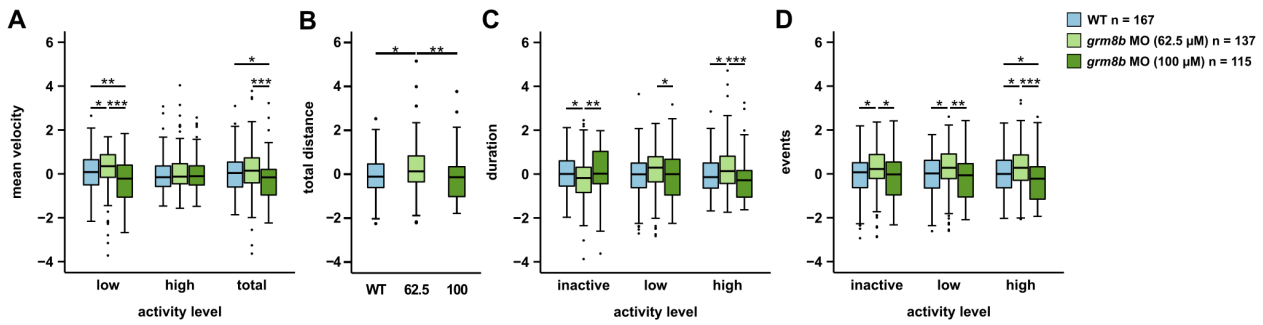
Figure 36: **Behavioral assessment of locomotor activity in *grm8b* splice-morphants of two injection concentrations.** Comparative analysis of locomotor activity determined by (A) mean velocity during low, high or both (total) activity (levels), (B) total distance swum and (C) duration or (D) events of inactivity, low and high activity. Two different grm8b splice-morpholino (MO) concentrations were injected: 62.5 μM (light green) and 100 μM (dark green) and compared to uninjected wildtype larvae (WT, light blue). Z-score transformation was applied to standardize raw datasets. The sample sizes are given by n. *P<0.05, **P<0.01, ***P<0.001.
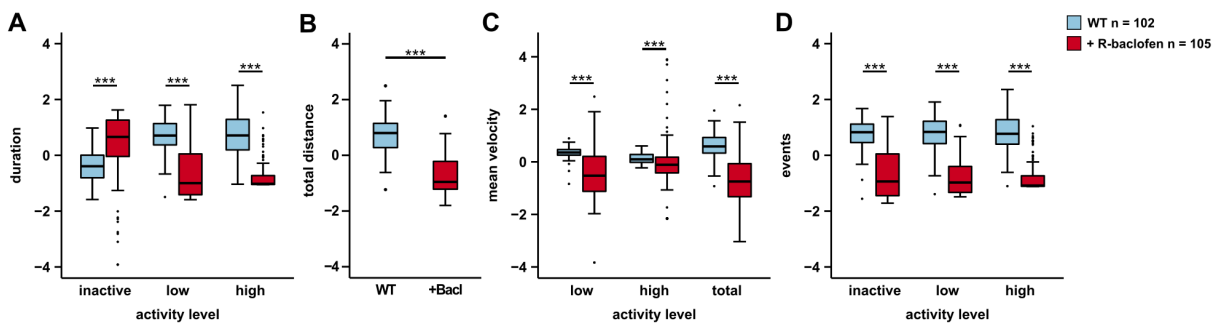
Figure 37: **Behavioral assessment of 5 dpf old wildtype larvae exposed to R-baclofen.** Locomotor activity of treated (0.1 mM for 48 hours, red) and untreated (Danieau's solution, light blue) 5 dpf old wildtype larvae. Locomotor activity was determined by (A) mean velocity during low, high or both (total) activity (levels), (B) total distance swum and (C) duration or (D) events of inactivity, low and high activity. Z-score transformation was applied to standardize raw datasets. The sample sizes are given by n. ***P<0.001.
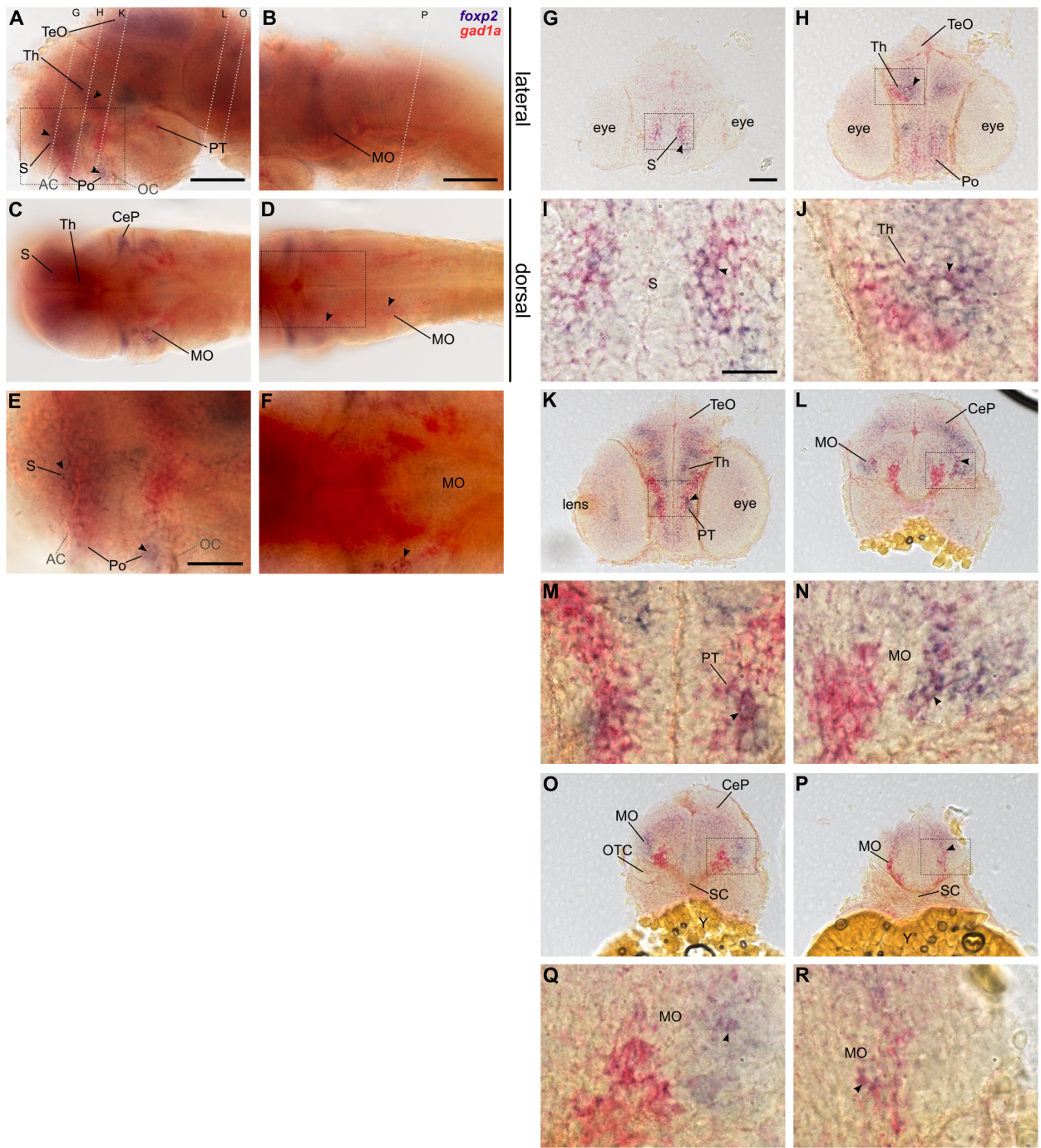
Figure 38: **Double-labeling of *foxp2* and *gad1a* transcripts in 36 hpf old wildtype zebrafish embryos.** (A-F) Two-color RNA *in situ* hybridization for *foxp2* (blue) and *gad1a* (red) on whole-mount preparations shown from lateral (A, B, E) and dorsal views (C, D, F) with anterior displayed to the left. Magnifications of boxed regions in A, D are displayed in E, F. Dashed, white lines illustrate cutting sites for cross-sections displayed in G-R. Boxed regions in G, H, K, L, O, and P are magnified in I, J, M, N, Q, and R, respectively. Arrows point out regions with apparent colocalization of both expression patterns. A detailed description of regions with common and distinct expression is given in the main text. For anatomical abbreviations, see Table 13. Scale bar represents 100 μm in overview and 50 μm in magnified images. Adjusted from Lueffe et al. 2021a.
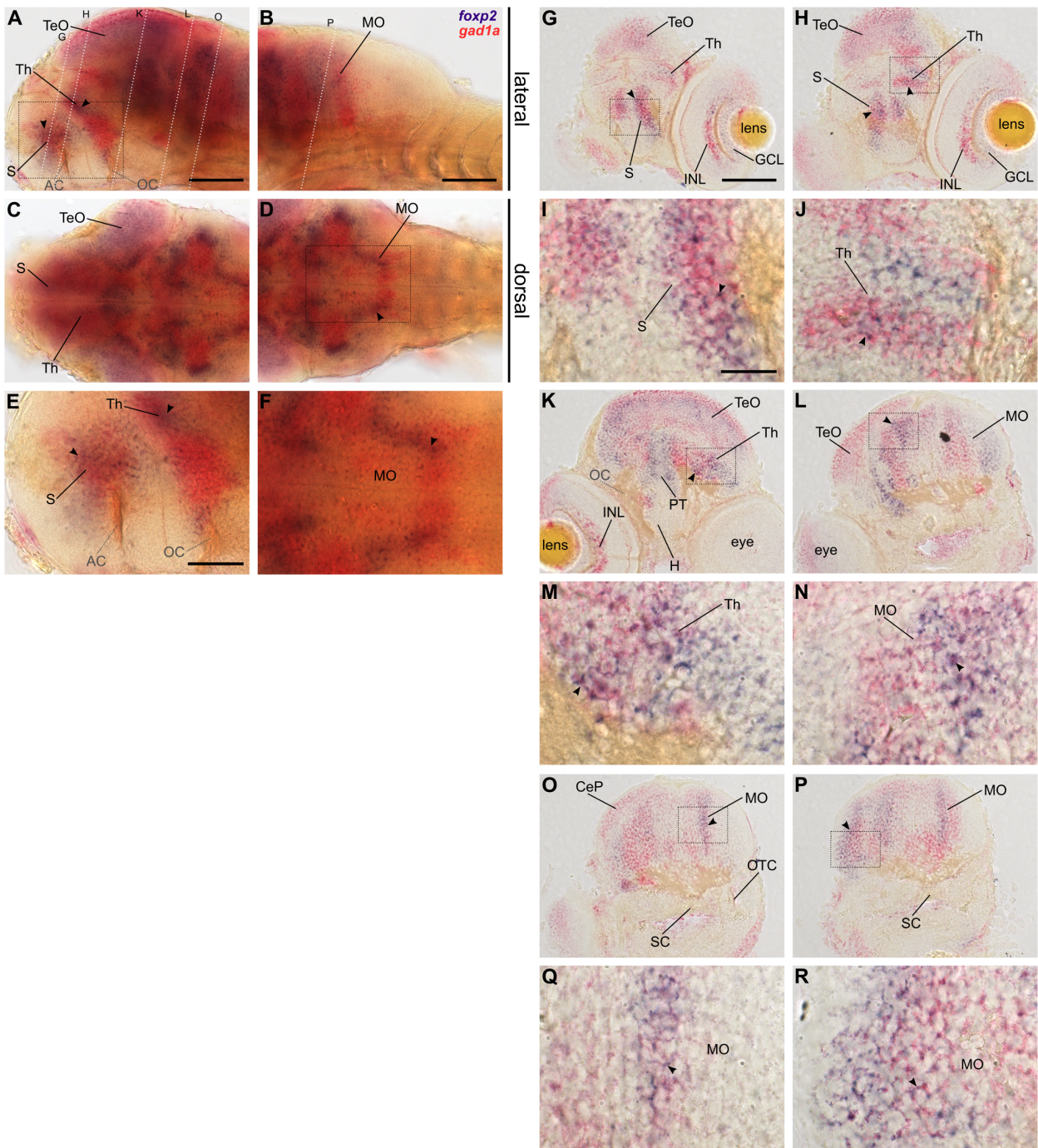
Figure 39: **Double-labeling of *foxp2* and *gad1a* transcripts in 72 hpf old wildtype zebrafish larvae.** (A–F) Whole-mount two-color RNA *in situ* hybridization for *foxp2* (blue) and *gad1a* (red) shown from lateral and dorsal views with anterior displayed to the left. Boxed regions in A, D are magnified in E, F. Dashed, white lines illustrate cutting sites for cross-sections displayed in G-R. Magnifications of boxed regions in G, H, K, L, O, and P are shown in I, J, M, N, Q, and R, respectively. Arrows point out regions with apparent *foxp2* and *gad1a* expression colocalization. Details on expression colocalization are described in the main text. For anatomical abbreviations, see Table 13. Scale bars represent 100 μm in overview and 50 μm in magnified images. Adjusted from Lueffe et al. 2021a.
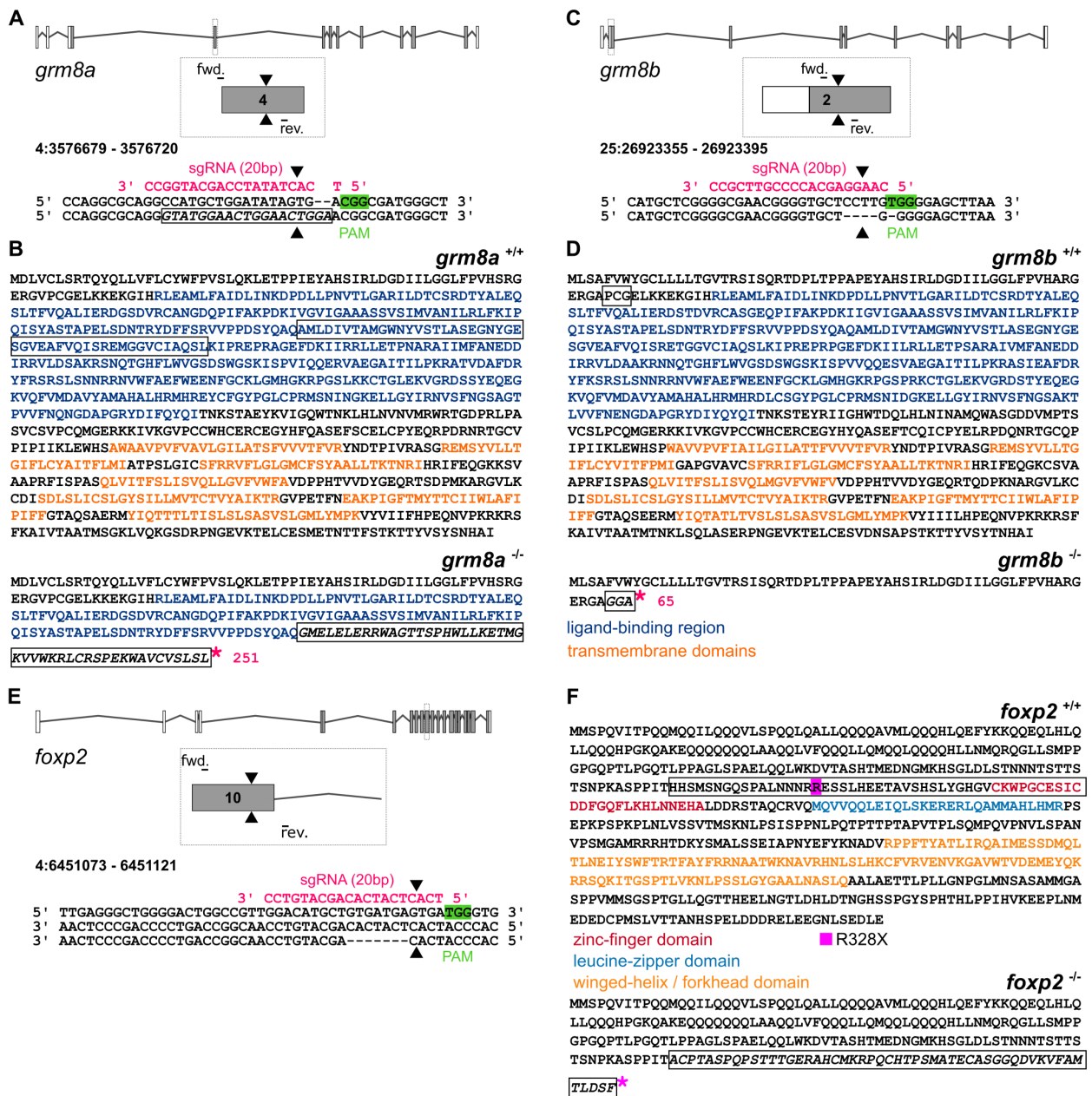
Figure 40: **Genetic description of remaining *grm8a*, *grm8b*, and *foxp2* CRISPR/Cas9 mutant lines.** (A, C, E) Schematic illustrating exon-intron structure of *grm8a* (A), *grm8b* (C), and *foxp2* (E) indicating sgRNA binding site (pink), Cas9-induced double-strand break (black triangle), and primer binding sites for genotyping PCR. Coding and non-coding exons are marked in grey and white, respectively. (B, D, F) Predicted amino acid sequence of wildtype (top) and mutated allele (bottom) for *grm8a* (B), *grm8b* (D), and *foxp2* (F). Boxed sequence indicates region affected by the induced frame shift, interrupted by a premature stop codon (pink asterisk). Functional domains are colored. The location of the human *foxp2* gene variant R328X is boxed in pink. Generation and injection of the respective sgRNAs was performed by M. Bauer.

Table 15: **Mean relative normalized expression of putative Foxp2 target genes in hetero- ($^{+/-}$) and homozygous ($^{-/-}$) *foxp2* mutants and wildtype siblings and corresponding statistics.** For raw data normalization, the housekeeping genes actin, beta 1 (*actb1*), and glyceraldehyde-3-phosphate dehydrogenase (*gapdh*) were used. Wildtype siblings (*foxp2$^{+/+}$*) served as controls. From Lueffe et al. 2021a.

Gene symbol / ID (Ensembl)	Gene name	Genotype	Mean	Lower limit	Upper limit	P-value
adgrl3.1 / ENSDARG00000061121	adhesion G protein-coupled receptor L3.1					
		+/+	1.0000	0.8610	1.3511	
		+/-	1.0786	0.8735	1.3533	0.5976
		-/-	1.0873	0.9605	1.0412	0.5504
adgrl3(.2) / ENSDARG00000090624	adhesion G protein-coupled receptor L3(.2)					
		+/+	1.0000	0.7926	1.2617	
		+/-	1.4745	0.8762	2.4815	0.3034
		-/-	2.1122	1.4202	3.1413	0.0480
cntnap2a / ENSDARG00000058969	contactin associated protein 2a					
		+/+	1.0000	0.5231	1.9117	
		+/-	0.9473	0.3745	2.3964	0.9380
		-/-	1.3591	0.3321	5.5626	0.7491
cntnap2b / ENSDARG00000074558	contactin associated protein 2b					
		+/+	1.0000	0.7434	1.3452	
		+/-	1.8448	1.6024	2.1238	0.0320
		-/-	1.8035	1.5166	2.1446	0.0410
dusp6 / ENSDARG00000070914	dual specificity phosphatase 6					
		+/+	1.0000	0.8599	1.1630	
		+/-	1.2848	1.0960	1.5060	0.1188
		-/-	1.4903	1.1367	1.9540	0.0898
foxp1a / ENSDARG00000004843	forkhead box P1a					
		+/+	1.0000	0.9120	1.0965	
		+/-	1.0907	0.9314	1.2773	0.4570
		-/-	1.5366	1.2419	1.9011	0.0327
foxp1b / ENSDARG00000014181	forkhead box P1b					
		+/+	1.0000	0.8167	1.2244	
		+/-	1.0581	0.9188	1.2184	0.7123
		-/-	1.2072	0.9285	1.5696	0.3810
foxp2 / ENSDARG00000005453	forkhead box P2					
		+/+	1.0000	0.7706	1.2977	
		+/-	0.5842	0.5468	0.6241	0.0257
		-/-	0.3410	0.2046	0.5684	0.0314
gad1a / ENSDARG00000093411	glutamate decarboxylase 1a					
		+/+	1.0000	0.8081	1.2374	
		+/-	1.1613	1.0548	1.2785	0.3299
		-/-	0.9543	0.5246	1.7361	0.9048
gad1b / ENSDARG00000027419	glutamate decarboxylase 1b					
		+/+	1.0000	0.9736	1.0271	
		+/-	0.8777	0.8381	0.9192	0.0133
		-/-	1.0470	0.7766	1.4115	0.8041
gad2 / ENSDARG00000015537	glutamate decarboxylase 2					
		+/+	1.0000	0.8149	1.2272	
		+/-	1.3036	1.2910	1.3164	0.0885
		-/-	1.1004	0.7116	1.7015	0.7481
grm3 / ENSDARG00000031712	glutamate receptor, metabotropic 3					
		+/+	1.0000	0.7406	1.3503	
		+/-	0.9616	0.8725	1.0598	0.8402
		-/-	1.1090	0.7275	1.6905	0.7467
lrrn1 / ENSDARG00000060115	leucine rich repeat neuronal 1					
		+/+	1.0000	0.9295	1.0758	
		+/-	1.0356	0.9252	1.1593	0.6751
		-/-	1.0123	0.8856	1.1571	0.8962
mef2ca / ENSDARG00000029764	myocyte enhancer factor 2ca					
		+/+	1.0000	0.8500	1.1764	
		+/-	1.4037	1.0165	1.9384	0.1794
		-/-	1.5511	1.1090	2.1695	0.1110
mef2cb / ENSDARG00000009418	myocyte enhancer factor 2cb					
		+/+	1.0000	0.8606	1.1620	
		+/-	1.5804	1.2971	1.9254	0.0331
		-/-	1.5937	1.2113	2.0969	0.0613
ntrk2b / ENSDARG00000098511	neurotrophic tyrosine kinase, receptor, type 2b					
		+/+	1.0000	0.7235	1.3822	
		+/-	1.2195	1.0197	1.4583	0.4053
		-/-	1.3931	0.8530	2.2752	0.3839
pcdh7a / ENSDARG00000078898	protocadherin 7a					
		+/+	1.0000	0.7146	1.3993	
		+/-	1.1458	0.7745	1.6952	0.6714
		-/-	1.8968	1.0962	3.2821	0.1597
pcdh7b / ENSDARG00000060610	protocadherin 7ab					
		+/+	1.0000	0.7713	1.2964	
		+/-	0.9461	0.8512	1.0516	0.7493
		-/-	1.0257	0.7941	1.3247	0.9099
ppp1r1b / ENSDARG00000076280	protein phosphatase 1, regulatory (inhibitor) subunit 1B					
		+/+	1.0000	0.7593	1.3169	
		+/-	1.4334	1.0936	1.8789	0.1815
		-/-	1.3813	1.1286	1.6906	0.1767
sema6d / ENSDARG00000002748	semaphorin 6D					
		+/+	1.0000	0.8385	1.1926	
		+/-	1.0700	0.9111	1.2567	0.6488
		-/-	1.2786	0.9445	1.7309	0.2912
slitrk2 / ENSDARG00000006636	SLIT and NTRK-like family, member 2					
		+/+	1.0000	0.5652	1.7694	
		+/-	1.8939	1.5606	2.2983	0.1403
		-/-	2.1248	1.3995	3.2259	0.1386

Author contribution statement

The present thesis partly contains experimental work conducted during Bachelor- (Moritz Bauer (M.B.)), Master- (Victoria Schöffler (V.S.), Zoi Gioga (Z.G.)) or Medical Ph.D.- (Andrea D'Orazio (A.D.)) project(s) and, thus, has already been presented in parts in the following theses:

- *CRISPR/Cas9-Based Knock-Out of ADHD Candidate Genes in Zebrafish* (M.B.)

- *Morphological and behavioural analyses of zebrafish larvae after impairment of GABAergic components* (V.S.)

- *Expression analysis in zebrafish models of psychiatric disorders* (Z.G.)

The individual contribution to the present work is described in detail below.

A.D. determined the appropriate concentration of the applied *gad1b* splice-inhibiting morpholino by performing a titration experiment. Further, A.D. monitored the locomotor activity of 114 out of 287 *gad1b* splice-morphant/uninjected control individuals. In addition, A.D. behaviorally assessed the effect of injected SR-95531 on the locomotor activity of wildtype larvae. Like Teresa M. Lüffe (T.L.) and Dr. Carsten Drepper, A.D. manually counted GABA-positive cells in heterozygous *foxp2* mutants and wildtype siblings.

Under the supervision of T.L., M.B. generated, injected, and determined the appropriate injection concentration for the applied CRISPR/Cas9 sgRNAs.

Under the supervision of T.L., V.S. performed anti-GABA and anti-Gad1b immunostainings and subsequent confocal imaging to obtain images for manual cell quantifications. Further, like T.L. and PD Dr. Christina Lillesaar, V.S. manually quantified GABA-positive cells in *gad1b* splice-morphants and corresponding controls. In addition, V.S. performed the MPH rescue experiment on heteroallelic *foxp2* CRISPR/Cas9 mutants and wildtype siblings.

Z.G. established and performed the qPCR experiment on collected and genotyped (T.L.) *foxp2* CRISPR/Cas9 mutants and wildtype siblings.

PD Dr. Christina Lillesaar dissected and cut adult brain sections, applied for RNA ISH by T.L..

Besides foreign contributions to the present work, the author (T.L.) has likewise contributed to the work of others of which parts have already been published in two manuscripts of peer-reviewed journals (for details, see the following publications list):

For the publication of Lechermeier et al. (2019), T.L. established a two-color RNA ISH protocol for whole-mount zebrafish specimens, generated the DIG-labeled RNA ISH probe for the GABAergic marker gene *gad1b* and performed the corresponding RNA ISH on 24 hpf and 36 hpf old wildtype zebrafish embryos.

For the publication of Segebarth et al. (2020), T.L. generated *gad1b* splice-morphants through microinjections, confirmed missplicing by RT-PCR and performed manual cell quantifications on immunohistochemically stained and imaged *gad1b* splice-morphants and uninjected controls.

The practical contribution also comprises the generation and genotyping of adult *grm8a*, *grm8b*, and *foxp2* CRISPR/Cas9 mutants which are currently monitored for behavioral phenotypes by Kim Kessler.

Publications list

Lueffe, T.M., et al. (2018). Seasonal variation and an "outbreak" of frog predation by tamarins. *Primates*, 59(6):549–552.

Lechermeier, C.G., et al. (2019). Transcript analysis of zebrafish GLUT3 genes, *slc2a3a* and *slc2a3b*, define overlapping as well as distinct expression domains in the zebrafish (*Danio rerio*) central nervous system. *Frontiers in Molecular Neuroscience*, 12:199.

Souza-Alves, J.P., et al. (2019). Terrestrial behavior in titi monkeys (Callicebus, Cheracebus, and Plecturocebus): Potential correlates, patterns, and differences between genera. *International Journal of Primatology*, 40(4):553–572.

Segebarth, D., et al. (2020). On the objectivity, reliability, and validity of deep learning enabled bioimage analyses. *eLife*, 9:e59780.

Lueffe, T.M., et al. (2021a). Increased locomotor activity via regulation of GABAergic signalling in *foxp2* mutant zebrafish – implications for neurodevelopmental disorders. *Translational Psychiatry*, (accepted).

Lueffe, T.M., et al. (2021b). (in preparation).

Curriculum vitae

Acknowledgments

Bedanken möchte ich mich außerdem bei allen aktuellen und bisherigen Mitarbeitenden der Physiologischen Chemie und der AG Klopocki. Dabei gilt mein besonderer Dank Benedikt, Angela und vor allem Daniel, die immer ein offenes Ohr, helfende Hände und wertvolle Ratschläge für mich hatten.

Danken möchte ich auch allen aktuellen und bisherigen Mitarbeitenden der AG Lillesaar und der AG Drepper. Besonders Andrea, Moritz, Victoria und Zoi, die mit ihren Abschlussarbeiten einen wichtigen Beitrag zu dieser Arbeit geleistet haben.

Aus der Ferne danke ich außerdem David Gustav, Nicholas Kirkerud, Christoph Kleineidam, Florian Bilz und Marion Silies, die meine Begeisterung für die Wissenschaft entfacht und die Grundlage für das Gelingen dieser Arbeit geschaffen haben.

Besonders bedanken möchte ich mich zudem bei Isabel, Carina, Lina, Frederick, Anna-Maria, Jana, Andrea, Zoi, Moritz und Victoria für Motivation und Zuspruch während schwieriger Phasen dieser Arbeit, für Philosophieren und Diskutieren über Wissenschaft und Nicht-Wissenschaft, für die Portion Kaffee zwischendurch, für gemeinsame Freizeit und das Bejubeln von kleinen und großen Erfolgen. Ihr habt Hindernisse überwindbar und Erfolge zu Festen gemacht. Danken möchte ich außerdem allen anderen, nicht namentlich genannten Konstanzern, Göttingern und Würzburgern, die mich seit Beginn meines Studiums begleiten und unterstützen und insbesondere in den letzten Monaten für den nötigen Ausgleich gesorgt haben.

Mein besonderer Dank geht dabei an Tim. Danke für dein Verständnis, deinen Zuspruch, deine Gelassenheit und deinen bedingungslosen Rückhalt in jeder Lebenslage.

Zu guter Letzt gebührt mein tiefster Dank meiner Familie. Danke, dass ihr mich stets in meinem Weg bestärkt und unterstützt habt. Euch an meiner Seite zu wissen, macht mich stärker, als ich es je allein sein könnte.

Danke!

Affidavit

I hereby confirm that my thesis entitled "Behavioral and pharmacological validation of genetic zebrafish models for ADHD" is the result of my own work. I did not receive any help or support from commercial consultants. All sources and/or materials applied are listed and specified in the thesis.

Furthermore, I confirm that this thesis has not yet been submitted as part of another examination process neither in identical nor in similar form.

Place, Date   Signature

Eidesstattliche Erklärung

Hiermit erkläre ich an Eides statt, die Dissertation "Pharmakologische und verhaltensbasierte Validierung genetischer Zebrafischmodelle für ADHS" eigenständig, d.h. insbesondere selbständig und ohne Hilfe eines kommerziellen Promotionsberaters, angefertigt und keine anderen als die von mir angegebenen Quellen und Hilfsmittel verwendet zu haben.

Ich erkläre außerdem, dass die Dissertation weder in gleicher noch in ähnlicher Form bereits in einem anderen Prüfungsverfahren vorgelegen hat.

Ort, Datum   Unterschrift